

## ABSTRACT

FAHEY, PATRICK JOHN. Alcohol and Saccharide Model-Compound Pyrolysis Experiments to Improve Understanding of Cellulose Pyrolysis. (Under the direction of Phillip R. Westmoreland.)

The pyrolysis of model compounds was investigated for improved understanding of cellulose pyrolysis. These alcohol and saccharide/saccharide-like model-compound comparisons are important to the progress of obtaining organic chemicals from renewable biomass resources via pyrolysis. Understanding the reaction mechanisms of cellulose will enable vital modifications to biomass-pyrolysis processes. These vital process modifications should not simply be optimized reaction temperatures and residence times, but instead should be catalysts and co-reagents designed to augment cellulose's inherent reaction network.

The two main sets of model compounds employed were alcohols and saccharide/saccharide-like molecules. The set of alcohols included nine monols (methanol, ethanol, propan-1-ol, 2,2-dimethylpropan-1-ol, 5-hydroxymethylfurfural, propan-2-ol, butan-2-ol, 2-methylpropan-2-ol, and phenol) three diols (ethan-1,2-diol, propan-1,2-diol, and propan-1,3-diol), and one triol (propan-1,2,3-triol), pyrolyzed in a pulse-injected gas-phase reactor operating at 200-400°C. Primary and secondary monols preferentially dehydrogenated to their respective aldehyde and ketone, but they also dehydrated to a very small extent. Phenol was the main exception, as it provided no reaction products. Tertiary monols dehydrated and showed no dehydrogenation. Products of carbon-carbon fragmentation were either undetected or provided only trace product quantities for all monols, with the exception being 5-hydroxymethylfurfural, which deformylated to a significant degree. Diols and triols dehydrogenated, dehydrated, and fragmented carbon-carbon bonds but still did not combine to form larger products. Concerted mechanisms were proposed for dehydrogenation and dehydration based upon their success with previous studies [1], [2], and [3], and four- and six-center cyclic transition states were evaluated.

The set of saccharide/saccharide-like model compounds were tested by TGA/DSC, and they consisted of five D-aldohexoses (D-allose, D-altrose, D-galactose, D-glucose, and D-mannose), two D-aldohexitols (D-glucitol and D-mannitol), two deoxy-aldohexoses (2-

deoxy-D-glucose and 6-deoxy-L-galactose), three aldopentoses (D-arabinose, L-arabinose, and D-xylose), two ketohexoses (D-fructose and D-tagatose), two D-glucose dimers (D-cellobiose and D-trehalose dihydrate), and two pyranose-based polymers (cellulose and xylan). Observation of the effects of structural changes focused upon explaining the presence of two maxima in the mass-loss rate. Comparisons among these model compounds revealed that the cause of the separate maxima is not solely any of the following structural aspects of saccharides:

- The stereochemistry of hydroxyl groups on a pentose or hexose
- The saccharide being an aldose versus a ketose
- The presence of a carbon 6 (i.e., pentose vs. hexose)
- The presence of a hydroxyl group on carbon 6 (i.e., a 6-deoxy-hexose)
- The presence of a hydroxyl group on carbon 2 (i.e., a 2-deoxy-hexose)
- The saccharide being dimerized or polymerized

These structural aspects also reveal that the two-stage mass loss is not due to the combination of 1,6-bicyclic formation and dehydration activity favored at different temperatures. Additionally, comparisons among the model compounds revealed that a single maximum occurs if the reactant may be described by:

- Hydrogenating the sugar to a sugar alcohol
- Dimerizing D-glucose with an  $\alpha(1-1)$  glycosidic bond
- Polymerizing D-glucose with  $\beta(1-4)$  glycosidic bonds

Several stationary-phase pairs for GCxGC separations were also evaluated for application to carbohydrate pyrolysis vapors and hydrolysis oils. These stationary-phase pairs were poly(trifluoropropylmethylsiloxane) to 1,4-bis(dimethylsiloxy)phenylene, poly(trifluoropropylmethylsiloxane) to poly(ethylene glycol), and poly(bis(cyanopropylsiloxane)) to poly(ethylene glycol). Tabulated McReynolds constants provide precise descriptions of the interaction types available to stationary-phase materials, but selecting stationary phases based solely upon stationary phases having different McReynolds constants was not sufficient to ensure orthogonal separations. Additionally,

thermal modulation proves to be a vital aspect when separating a mixture with analytes covering a broad range of volatilities. Compounds like levoglucosan and 2,3-dihydroxypropanal provided severely tailing peaks when thermal modulation was tailored to compounds like alkylbenzene homologues and furan homologues.

© Copyright 2015 Patrick John Fahey

All Rights Reserved

Alcohol and Saccharide Model-Compound Pyrolysis Experiments to Improve  
Understanding of Cellulose Pyrolysis

by  
Patrick John Fahey

A dissertation submitted to the Graduate Faculty of  
North Carolina State University  
in partial fulfillment of the  
requirements for the degree of  
Doctor of Philosophy

Chemical Engineering

Raleigh, North Carolina

2015

APPROVED BY:

---

Professor Phillip R. Westmoreland  
Committee Chair

---

Professor H. Henry Lamb

---

Professor Sunky Park

---

Professor Steven W. Peretti

## **DEDICATION**

I dedicate this achievement, along with all of the achievements which lead me here, to my parents. Any success I earned in my education and research is due to their emphasizing hard work in school. Their support and encouragement was tireless, and luckily their priority on scholastics took hold in my stubborn mind. All of my successes resulted from the drive and discipline instilled by them, and not to mention the sacrifices they made to provide a strong, well-rounded education to my brother and me.

I also dedicate this work to anyone who wishes or ever wished to be in my shoes along my way here. I have had a very fortunate life. I had access to excellent K-12 schools, college, and graduate school. I had excellent people surrounding me along the entire way. I consider myself very lucky to be given the opportunities which led me here. I know a lot of very smart, very hard-working people were not given access to the opportunities I had. I try to be mindful of this fact every day. I hope my performance was adequate in the eyes of anyone who envies my lucky circumstances.

## BIOGRAPHY

I like the many amazing things made available by cheaper energy, organic chemicals, and electricity. To name a few, there are (1) living comfortably with modern conveniences, (2) travelling to see family, friends, and interesting places, (3) the ability to purchase products made around the world, and (4) obnoxiously fast and loud machines like Formula-1 cars and MotoGP motorcycles. Another thing I like very much is the astounding beauty of Earth's natural environment. Often people think there is a compromise between having a modern 21<sup>st</sup>-century society and environmental quality. From a young age I wanted to invent things to make it possible so society can have all of its modern conveniences and entertainment without compromising environmental quality.

Obviously, I studied chemical engineering in college. Everyone bothering to read this document knows it already. However, what many of these readers might not know is that I also took a liking to economics. I wish more engineers and scientists would study economics because it analyzes compromises and trade-offs to determine how resources should be allocated. Thinking critically about compromises and trade-offs is vital to effective problem solving.

One subtopic of economics I found particularly fascinating was environmental economics. This topic centers around how externalities affect society, and how they should be treated to obtain the outcome valued most by society. A classic example of an externality is a producer of a good who emits pollution. Society as a whole often must bear the burden of the emitted pollution, yet they cannot influence the decision on the quantity exchanged made privately between the producer and consumer. Economists devise systems of pollution taxes and cap-and-trade systems to create an incentive on producers to emit less pollution without mandating how much good should be produced. Such incentives drive producers to create new processes which reduce the pollution emitted per unit of manufactured good, so valuable markets may exist with less external damage to a third party. Here is where it comes back to my chemical-engineering research: I want to invent those methods of making these products

we want while also decreasing pollution. I want people to enjoy their modern conveniences and entertainment without doing harm to this beautiful place we call Earth. Research engineers can do it, and it needs to be done. What can you do to help?

## ACKNOWLEDGMENTS

First I must acknowledge several funding resources which made this research possible. First was the U.S. Department of Energy Award DE-SC0001004 to its Catalysis Center for Energy Innovation (CCEI) led by the University of Delaware, provided through subcontract 23879 from 2011 through 2012.<sup>1</sup> Next was subcontract 1-340-0212662 from RTI International, who led the hydrolysis-process project within the National Advanced Biofuel Consortium.<sup>2</sup> Lastly was a discretionary account and the startup funds of my advisor. These three sources provided the necessary support for brand-new laboratory equipment and consumables, tuition, and a stipend. While it was a surprising amount of work just to acquire, install, maintain, troubleshoot, and optimize these instruments, this process taught me very much about engineering research which isn't known to many graduate students. Being the one to develop a laboratory gave me an added understanding and appreciation of management and funding resources.

Funding aside, there are a lot of people who allowed me to get here. I have loosely categorized them into fellow researchers, mentors, and friends. (Obviously many people fall into more than one category, but this system of organization will have to do.) I know there are some who helped me and I didn't realize it or I forgot to mention them here. I will do my best try to realize, remember, and appreciate everyone.

For fellow researchers, I first must thank my entire group. Professor Phillip Westmoreland has been an excellent advisor. He has an exceptional ability to draw from many areas (both scientific and non-scientific) and simplify complicated concepts like kinetic phenomena and chemical reactions. His patience and positive outlook on research was practically inexhaustible. I have met very few people who maintain such a positive attitude.

---

<sup>1</sup> The CCEI is one of 32 Energy Frontier Research Centers supported by the US Department of Energy's Office of Science.

<sup>2</sup> The NABC is an organization of 17 partners from industry, national laboratories, and universities. It is supported by the US Department of Energy's Bioenergy Technology Office.

Dr. Vikram Seshadri was an excellent older graduate student to have. While we often did not work on the same project (or even in the same building), he was always happy to explain complex physical and mathematical concepts and propose ways to improve my experiments. He is another rare person who always whose patience, positive outlook, and kindness is practically inexhaustible. He brought a calm, appreciative, and friendly attitude to research along with his strong work ethic and impressive analytical thinking.

As noted with Dr. Seshadri, having my lab off in another building kept me from daily, in-person interaction with other group members. They are Dr. Wenjun Li, Dr. Nicole Labbe, Craig Needham, Sara Jo Taylor, and Scott Crymble. You have all put up with my ramblings on many occasions during group meetings, and you have all undoubtedly helped me get to this point.

Outside of my research group there were many co-workers at the Integrated Biomass Research Initiative (IBRI). Some of them were instrumental in helping me to establish my small laboratory. Professor Steven Peretti continually provided permission to mess around in his lab module, occasional advice on research, and thoughts on small research proposals. Dr. Dhana Savithri was tireless in her management of support equipment around the IBRI. She and Dr. Debra Clare always offered support and a kind voice. Cari Furiness also helped with countless office and building support systems. Al Springer was an excellent resource for constructing equipment, and he allowed me to raid his personal tool closet on a weekly to daily basis. Without his help (and willingness to share tools), practically none of my lab in the Varsity Research Building could get the basic utilities they needed like electrical power and gas-cylinder storage.

Outside of the IBRI, and even outside of the Department of Chemical & Biomolecular Engineering, came some vital help from Professor David Tilotta. He was one of the few people to actually sit down with me and tell me practical things to look for in instruments like a GC-MS or Pyroprobe®. I had no older group members with experience in these instruments, but Professor Tilotta met me over coffee several times to get me started in

the right direction on instrument know how. An outgoing nature coupled with real know-how is gravely underappreciated by those in big research groups with older graduate students to teach younger graduate students who to operate complicated equipment and experiments.

I had continual help from the technical-support team at LECO Corporation for the GCxGC-TOFMS. Their help was always quite thorough, and they were never difficult to reach. I am especially grateful for the repeated help from Ken Kite, Erin Barkel, Chris Immoos, and James Paulaski. I almost must thank Ray Clifford of LECO Corp's field-service unit for a painless and instructive installation process.

I received excellent help from the technical-support team for the chemical-analysis section of Agilent Technologies. They answered countless, highly-detailed (i.e., rather annoyingly complicated) questions on exactly how gas flows in the 7890A gas chromatograph work – and how many users misunderstand how these gas flows work.

One vital set of experiments was made possible by Professor Fanxing Li's laboratory. Arya Shafiefarhood made accommodations for me to use their pulse-injected quartz-reactor system on several occasions, collectively taking several hours to show me proper use of the various pieces of equipment and software. His willingness to help directly enabled results very important to my work on alcohol pyrolysis.

The oven and balance in Professor Peter Fedkiw's laboratory was crucial to a set of experiments with the Pyroprobe®. Marty Dufficy and Shangyang Huang were very accommodating to the many hours I spent occupying their oven and balance.

An absolutely vital set of saccharide materials was given to me by Andrew Loder of Professor Robert Kelly's laboratory. When searching for a particular compound, Andrew offered the very small quantity (~20 mg) required for our purposes. While picking up the sample, Andrew offered samples of other rare sugars. Not only did this offering save the Westmoreland Group having to purchase much larger quantities than we could possibly use, it enlightened us to several other useful model compounds which hadn't been discussed in

the saccharide textbooks or the pyrolysis literature. Several model compounds were also obtained from William “Billy” Kish of Professor Ruben Carbonell’s laboratory and Dr. Dennis McOwen of Professor Wesley Henderson’s laboratory. Without all of these donated samples, the “glucopyranose-like model-compound set” would have never been conceived.

Dr. Jiajia (“August”) Meng let Dr. Seshadri and I come to his lab several times to both watch him run his reactor and to show us how to run Pyroprobe® experiments. His willingness to familiarize me with the Pyroprobe® allowed me to see first hand what my laboratory would soon purchase. In addition, Dr. Meng made a lasting impression on me when he was willing to challenge professionals to make biofuels work during the 2012 National Meeting of AIChE.

Aside from the direct help on my research work, I also received important mentoring advice on the research world. Professor Matthew Cooper gave me a lot of professional advice sprinkled over the better lunch spots surrounding Centennial Campus. He always offered his view of the big picture, which sometimes gets left behind by most people absorbed into their day-to-day research projects. We share a passion for figuring out how to make things better, with a particular fascination with catalytic and thermal processes. He also showed that even very, very busy people can make time to share a nice lunch.

A person I met around the same time as Professor Cooper is Professor Jason Trembly. He has been a great example of what a Ph.D. in chemical engineering (and some hard work) can do, as he managed me under some very interesting projects at RTI International. These projects showed me that I did, in fact, really need to get a Ph.D. to have a shot at working with the cool, advanced stuff. He continues to offer professional advice and opportunity.

During my undergraduate experience I had many superb instructors, advisors, and mentors. One that immediately stands out is Professor Valerie Young, my undergraduate academic advisor. In addition to advising me through the courses, she was a constant source of professional opportunity and career advice. Another standout influence is Professor David Bayless. Not only did he run the research laboratory which eventually put me into contact

with Professor Jason Trembly, but he exposed me to the amazing examples of leadership in the Robe Leadership Institute. Others who have inspired me greatly are Professor David Young, who always had a fascination and zest for teaching the amazing world of chemistry, Professor Ariaster Chimeli, who's instruction and lecture style to this day is the best I have ever seen, and Professor Klaus Himmeldirk, who was the kindest-yet-hardest-grading organic chemistry lab professor someone has the luck to have.

An amazing group of friends helped me stay happy and sane while in the graduate school game. Their contributions, while less direct than fellow researchers, were invaluable. The first to come to mind is Tyler Hanak. He was a constant source of stability, both in graduate and undergraduate school. He provided endless entertainment, mischief, professional inspiration, kind support, and not to mention great driving adventures and a few much needed vacations in Salt Lake City. I'm not sure where I would be if we didn't share music interests over breakfast in Jeff Hall back in 2005.

Along with Tyler would be Nick Brokaw, who's amazing sense of humor was endless. He also showed me that great work in sustainability does not have to come from corporate R&D labs and academic institutions. (Naturally, along with Tyler and Nick would be Bill Brasky, who has always been a source of great inspiration through his triumphant tales of adventure, friendship, love, and yes, sales.)

Billy Kish, Edwin Walker, and I often helped each other muscle through homework assignments during the first semester of graduate school. Together, we never settled for artificial understanding. As punishing as it was to our schedules, we wanted to truly understand the material we needed to regurgitate. This commiserating started a great friendship between us. To this day, these are two of the most stand-up guys I've ever known.

There were also some good friends I had through all of graduate school, and they really helped me out during some frustrating moments in my last year of study. They stuck around and gave me friendship and support at a rather crucial time, and some of them people might not understand exactly how much their supportive conversations mattered. They are

Cathy Semones, Dennis McOwen, Taylor Schulz, Sophie Carrell, Rachel Turner, Sueji Smith, and Lauren Ridge. Special thanks also goes to Simon Thompson for moving into the House of Avent Fairies and breathing some life into me during the last year of graduate school. He worked hard and showed me there are still researchers in academia who appreciate heavy reaction science. He also got me off my rear end to exercise regularly, and reminded me what it's like to live with a close friend again.

Lastly, I need to acknowledge the tremendous amount of good luck I have been granted. Hard work is important, and I have worked very hard to get here. Still, to claim my hard work alone got me here would be an insult to many, many people helping me along the way (especially my parents' constant pushing and support). I want to thank all of these people for giving a stubborn kid the chance to study the cool, heavy reaction sciences. If he plays his cards right, then maybe he can work the reactions science right and make those fascinating hot, loud machines like power plants and jet engines keep going with a smaller impact on Earth.

## TABLE OF CONTENTS

LIST OF TABLES .....	xviii
LIST OF FIGURES .....	xxi
LIST OF NOMENCLATURE.....	xxix
IUPAC SYSTEMATIC DESCRIPTION OF CHEMICAL COMMON NAMES.....	xxx
LIST OF ABBREVIATIONS AND SHORTENED WORDS .....	xxxii
<b>CHAPTER 1. INTRODUCTION .....</b>	<b>1</b>
1.1. <i>Biomass pyrolysis is a potential route to renewable organic chemicals ...</i>	1
1.2. <i>Understanding Cellulose Pyrolysis Is Important to Improving Biomass Pyrolysis</i>	3
1.3. <i>Elementary Pyrolysis Chemistry Is Important for Desirable Reaction Products</i>	3
1.4. <i>Past Progress with Reaction Models for Cellulose Pyrolysis .....</i>	5
1.5. <i>Elementary Reactions Are Vital for Producing Less Oxygenated Bio-oils</i>	6
<b>CHAPTER 2. EQUIPMENT AND PROCEDURES .....</b>	<b>7</b>
2.1. <i>Abstract .....</i>	7
2.2. <i>Combined Thermogravimetric Analyzer and Differential Scanning Calorimeter</i>	7
2.2.1. <i>TGA/DSC experimental procedures .....</i>	8
2.2.2. <i>Char and tar removal from pans and furnace .....</i>	11
2.3. <i>TGA/DSC Transfer-Line Sampling System(s) .....</i>	15
2.4. <i>Cold-Needle Sampling of TGA/DSC Effluent .....</i>	19
2.5. <i>Pyroprobe® Micropyrolyzer .....</i>	26

2.5.1.	<i>Basic Pyroprobe® instrument description</i>	26
2.5.2.	<i>Pyrolysis-method parameters for the Pyroprobe®</i>	33
2.5.3.	<i>Experimental shortcomings of the Pyroprobe®</i>	35
2.5.4.	<i>Cumulative-sampling technique to match TGA/DSC temperature intervals</i>	41
2.5.5.	<i>Matching total-mass differences between TGA/DSC and Pyroprobe® experiments</i>	42
2.5.6.	<i>Loading Pyroprobe® sample tubes</i>	44
2.6.	<i>Pulse-Injected Deactivated Stainless-Steel Reactor</i>	48
2.6.1.	<i>PIDSSR construction</i>	49
2.6.2.	<i>Operating the PIDSSR</i>	55
2.7.	<i>Comprehensive Two-Dimensional Gas Chromatograph Time-of-Flight Mass Spectrometer</i>	56
2.8.	<i>Pulse-Injected Quartz Reactor</i>	57
2.8.1.	<i>PIQR construction</i>	58
2.8.2.	<i>Quadrupole mass spectrometer</i>	62
2.8.3.	<i>Evaluation of the reactant pulse and the reaction products</i>	63
2.9.	<i>Balances</i>	63
2.10.	<i>Gaussian 09</i>	64
<b>CHAPTER 3. USE OF MCREYNOLDS CONSTANTS FOR ORTHOGONAL GCxGC COLUMN CONFIGURATIONS</b>		65
3.1.	<i>Abstract</i>	65
3.2.	<i>Introduction: The Benefit of GCxGC</i>	66
3.3.	<i>Characterizing Stationary Phases</i>	67

3.3.1. <i>Describing specific interaction types</i> .....	67
3.3.2. <i>McReynolds constants describe retention with groups of specific interactions</i>	70
3.3.3. <i>Using McReynolds constants to select stationary-phase pairs in GCxGC</i>	78
3.4. <i>Methods of Comparing GCxGC Column Configurations</i> .....	78
3.5. <i>Results</i> .....	79
3.5.1. <i>p(DPS-co-DMS)5/95-p(DPS-co-DMS)50/50 showed the expected orthogonality</i>	79
3.5.2. <i>PTFPMS-p(BDMSP-co-DMS)5/95 stationary-phase pairs show orthogonality and analyte grouping</i> .....	86
3.5.3. <i>PTFPMS-PEG stationary-phase pairs show orthogonality but no grouping</i>	92
3.5.4. <i>p(BCPS-co-CPPS)90/10-PEG stationary-phase pair showed analyte correlation</i>	95
3.6. <i>Discussion</i> .....	98
3.6.1. <i>Analysis of stationary-phase pairs by analysis of McReynolds constants</i>	98
3.6.2. <i>The importance of London dispersion forces for separating oxygenated analytes</i>	115
3.6.3. <i>Overloading primary columns by carbohydrate pyrolysis vapors</i> .....	116
3.6.4. <i>PEG and separation of carbonyl and alcohol groups</i> .....	117
3.6.5. <i>TFPMS and separation by differences in oxygen-atom content</i> .....	119
3.6.6. <i>Secondary-oven limitation on stationary-phase pairs in the Pegasus 4D</i>	122

3.6.7.	<i>Secondary column and thermal modulation</i>	123
3.6.8.	<i>Obtaining orthogonality is important to simpler comparisons of analyte mixtures</i>	127
3.7.	<i>Conclusion</i>	128
<b>CHAPTER 4.</b>	<b>DEHYDRATIONS AND DEHYDROGENATIONS OF ALCOHOLS</b>	
	130	
4.1.	<i>Abstract</i>	130
4.2.	<i>Introduction</i>	131
4.2.1.	<i>Model compounds effectively test hypothesized reactions</i>	132
4.2.2.	<i>Alcohols form model compound sets for cellulose's reaction-pattern hypotheses</i>	133
4.3.	<i>Methods and Procedures</i>	138
4.3.1.	<i>Selection of alcohols for members of model-compound sets</i>	138
4.3.2.	<i>Materials</i>	143
4.3.3.	<i>Pyrolysis reactors and chemical analyses</i>	144
4.3.4.	<i>Computational-quantum-chemistry simulations</i>	147
4.4.	<i>Results</i>	147
4.4.1.	<i>Most monols dehydrogenated in the PIDSSR-GCxGC-TOFMS</i>	147
4.4.2.	<i>The butan-2-ol impurity became an useful model compound</i>	149
4.4.3.	<i>Hydrogen was observed as a monol pyrolysis product with the PIQR-QMS</i>	150
4.4.4.	<i>Reaction products of the diols-and-triol set</i>	159
4.5.	<i>Discussion</i>	160

4.5.1. <i>Proposed mechanistic explanation of dehydrogenation with concerted reactions</i>	161
4.5.2. <i>Deuterated alcohols didn't provide conclusive evidence for the six-center, bimolecular dehydrogenations</i> .....	169
4.5.3. <i>Past evidence of hydrogen formation during cellulose pyrolysis</i> .....	180
4.5.4. <i>Why is the small quantity of hydrogen rarely mentioned in most biomass-pyrolysis studies?</i> .....	181
4.5.5. <i>Proposed mechanistic explanation of dehydration with concerted reactions</i>	182
4.5.6. <i>Other studies focused upon dehydrations including the 1,2-elimination dehydration</i>	189
4.5.7. <i>Comparing the products obtained by experiment to those predicted by the elementary mechanisms</i> .....	190
4.5.8. <i>Dehydrogenation inhibits some subsequent adjacent 1,2-dehydrations</i>	201
4.5.9. <i>Recommended future research</i> .....	202
4.6. <i>Conclusion</i> .....	203
<b>CHAPTER 5. PYROLYSIS OF D-GLUCOSE-LIKE MODEL COMPOUNDS FOR ELUCIDATING D-GLUCOSE PYROLYSIS REACTIONS</b> .....	205
5.1. <i>Abstract</i> .....	205
5.2. <i>Introduction</i> .....	206
5.2.1. <i>Understanding cellulose pyrolysis requires more than just cellulose experiments</i>	206
5.2.2. <i>Model compounds, revisited</i> .....	208
5.2.3. <i>The selection of D-glucose-like model compounds</i> .....	209

5.2.4.	<i>The complication of isomerism with saccharides like aldohexoses and aldopentoses</i>	212
5.3.	<i>Review of Structural Concepts in D-Aldohexoses and D-Aldopentoses</i>	212
5.4.	<i>Methods and Procedures</i>	214
5.4.1.	<i>Materials</i>	214
5.4.2.	<i>Pyrolysis reactors</i>	215
5.5.	<i>Results</i>	216
5.5.1.	<i>Results for D-aldohexoses – effect of stereochemistry</i>	216
5.5.2.	<i>Results for D-alditols</i>	224
5.5.3.	<i>Results for deoxy-D-aldohexoses</i>	227
5.5.4.	<i>Results for D-aldopentoses and L-aldopentose</i>	229
5.5.5.	<i>Results for D-ketohexoses</i>	232
5.5.6.	<i>Results for dimers of D-glucose</i>	235
5.5.7.	<i>Results for pyranose-based polymers</i>	238
5.6.	<i>Discussion</i>	241
5.6.1.	<i>Understanding differences between mass-loss behavior of D-glucopyranose’s D-aldohexose stereoisomers</i>	241
5.6.2.	<i>The leading explanation for two maxima in mass-loss rate</i>	267
5.6.3.	<i>Comparison between D-aldohexoses and D-alditols</i>	268
5.6.4.	<i>Comparison of 2-deoxy-glucose to D-glucose</i>	272
5.6.5.	<i>Comparison between D-aldopentoses and D-aldohexoses</i>	273
5.6.6.	<i>Comparison between enantiomers and implication for comparing D-galactose to 6-deoxy-D-galactose comparisons</i>	277
5.6.7.	<i>Comparison of D-trehalose dihydrate and D-cellobiose</i>	280

5.6.8. <i>Recommended future research</i> .....	282
5.7. <i>Conclusions</i> .....	284
5.8. <i>Special Acknowledgements</i> .....	285
<b>CHAPTER 6. RECOMMENDATIONS</b> .....	286
6.1. <i>PIQR-QMS experiments are needed for more alcohols and ethers</i> .....	286
6.2. <i>Evaluate the Frontier Pyrolyzer for simpler experiments to match TGA/DSC experiments</i> .....	286
6.3. <i>Operate reactors independently of GC carrier-gas flow</i> .....	289
6.4. <i>Reactors should operate above atmospheric pressure</i> .....	289
6.5. <i>Construct a reactor to mimic TGA/DSC heating rates but employ shorter residence times</i> .....	290
6.6. <i>Recognize that GCxGC cannot separate highly polar pyrolysis products</i> .....	291
6.7. <i>Derivatize oxygenated functional groups to allow sharper peaks in gas chromatography</i> .....	292
6.8. <i>Preserve and analyze hypothesized monosaccharide and oligomer cellulose-pyrolysis intermediates as volatile silylated compounds</i> .....	293
6.9. <i>The adhesion and expansion of chars may provide vital clues to the intermolecular attractions of saccharides and polysaccharides during pyrolysis</i> .....	294
6.10. <i>Experimental evidence of reactive intermediates or transition states can guide iterative computational evaluations of elementary chemistry</i> .....	295
6.11. <i>Increase research on the catalytic chemistry of inorganic salts on cellulose-pyrolysis products</i> .....	299
<b>CHAPTER 7. CONCLUSIONS</b> .....	301
<b>REFERENCES</b>	304

## LIST OF TABLES

Table 1. The chemical structures of repeating units for common GC stationary phases. (The monomer units typically copolymerized purposefully do not contain the “poly” prefix, as doing so implies they are a homopolymer. While all of the repeating units carry the subscript “n” for degree of polymerization, it is not implied that n is equal for all of these different polymeric materials.) .....	69
Table 2. Types of intermolecular interactions described by Rotzsche, Barry and Grob, and Kaliszan are matched by the molecular cause of attraction.....	70
Table 3. McReynolds test analytes and their associated selectivities. (Recreated from Table 9, page 92 of [36] and Table 2.9, page 40 of Barry and Grob [38]) .....	72
Table 4. McReynolds constants measured for commercially available stationary-phase materials.....	73
Table 5. A collection of GCxGC analyses showing the importance of stationary-phase pairs. ....	99
Table 6. Fractional retention differences from squalane to a particular stationary-phase material. ....	107
Table 7. Fractional retention differences from squalane to a particular stationary-phase material, continued.....	108
Table 8. The presence of alcohol functional groups in cellulose lend themselves to representation by monol, diol, and triol systems. (The oxygen atoms are numbered according to the carbon number to which they are bonded.).....	136
Table 9. The monols group can be divided into subgroups describing the substitution of the $\alpha$ carbon.....	139
Table 10. List of reagents used in the study of alcohol model compounds, ordered alphabetically. ....	144
Table 11. Reaction products observed from pyrolyzing monols in the PIDSSR at 400°C...	148
Table 12. The reaction products observed from pyrolyzing three diols and a triol in the PIDSSR.....	160
Table 13. The computed enthalpy of activation for hypothesized dehydrogenation transition states for monols. ....	164

Table 14. The computed enthalpy of activation for hypothesized dehydration transition states for monols. ....	185
Table 15. Materials used for the D-glucopyranose-like model-compound set. ....	215
Table 16. Summary of mass-loss character for five D-aldohexoses pyrolyzed at 50°C min <sup>-1</sup> . ....	218
Table 17. Summary of mass-loss rates for five D-aldohexoses pyrolyzed at 50°C min <sup>-1</sup> . ...	218
Table 18. Summary of mass-loss and heat-flow character for D-aldohexoses pyrolyzed at 50°C min <sup>-1</sup> . ....	224
Table 19. Summary of mass-loss character for deoxy-D-aldohexoses pyrolyzed at 50°C min <sup>-1</sup> . ....	227
Table 20. Summary of mass-loss rates for deoxy-D-aldohexoses pyrolyzed at 50°C min <sup>-1</sup> . 227	
Table 21. Summary of mass-loss character for three D-aldopentoses pyrolyzed at 50°C min <sup>-1</sup> . ....	230
Table 22. Summary of mass-loss rates for three D-aldopentoses pyrolyzed at 50°C min <sup>-1</sup> . 230	
Table 23. Summary of mass-loss character for D-ketoses pyrolyzed at 50°C min <sup>-1</sup> . ....	233
Table 24. Summary of mass-loss rates for D-ketoses pyrolyzed at 50°C min <sup>-1</sup> . ....	233
Table 25. Summary of mass-loss character for D-glucose dimers pyrolyzed at 50°C min <sup>-1</sup> . 236	
Table 26. Summary of mass-loss rates for D-glucose dimers pyrolyzed at 50°C min <sup>-1</sup> . ....	236
Table 27. Summary of mass-loss character for the two pyranose-based polymers cellulose and xylan. ....	239
Table 28. Summary of mass-loss rates for the two pyranose-based polymers cellulose and xylan. ....	239
Table 29. The equilibrium composition of saccharides in aqueous solution. (Recreated from Table 2.1 in Levy and Fügedi [58, p. 36]. The sum of the percentages was not present in the original Table 2.1.).....	245
Table 30. The equilibrium composition of saccharides in aqueous solution. (Recreated from data in Table 2.4 in Collins and Ferrier [55, p. 41]. The sum of the percentages was not present in the original Table 2.4.).....	245

Table 31. Equilibrium composition of methyl glycoside mixtures in methanol at 35°C. (Recreated from data in Table 3.1 in Collins and Ferrier [55, p. 63].) .....	246
Table 32. Newman projections show the three conformations evaluated for D-allopyranose rings.....	249
Table 33. Newman projections show the three conformations evaluated for D-altropyranose rings.....	250
Table 34. Newman projections show the three conformations evaluated for D-glucopyranose rings.....	251
Table 35. Newman projections show the three conformations evaluated for D-galactopyranose rings.....	252
Table 36. Newman projections show the three conformations evaluated for D-mannopyranose rings. ....	253
Table 37. Comparison of <i>quasi-cis</i> hydrogen-hydroxyl pairs present in five D-aldohexoses viewed in their <sup>4</sup> C <sub>1</sub> Reeves projection. ....	258
Table 38, continued. Comparing of <i>quasi-cis</i> hydrogen-hydroxyl pairs present in five D-aldohexoses viewed in their <sup>4</sup> C <sub>1</sub> Reeves projection.....	259
Table 39. The specific arrangements of adjacent H-OH pairs for carbons 1 through 5 of D-allopyranose. ....	262
Table 40. The specific arrangements of adjacent H-OH pairs for carbons 1 through 5 of D-altropyranose.....	263
Table 41. The specific arrangements of adjacent H-OH pairs for carbons 1 through 5 of D-galactopyranose.....	264
Table 42. The specific arrangements of adjacent H-OH pairs for carbons 1 through 5 of D-glucopyranose. ....	265
Table 43. The specific arrangements of adjacent H-OH pairs for carbons 1 through 5 of D-mannopyranose. ....	266

## LIST OF FIGURES

- Figure 1. The beams have metallic, circular platforms with a surrounding lip (left), and the pans were positioned to rest against the platform's lip on the downstream side. .... 10
- Figure 2. Positioning the TGA/DSC pans at the exterior edge of the outer diffusion flame removed char fastest, potentially due to higher local oxygen concentration and temperatures still hot enough to make the pans glow with an orange color. Quartz Pyroprobe® tubes prevented contact between the alumina TGA/DSC pans and the stainless-steel tubes clamped to the ring stand. .... 12
- Figure 3. Dark brown and black residue, most likely condensed and solidified tars, accumulated on the inner surfaces of the alumina furnace tube. Routine furnace cleaning with high temperatures and air flow did not remove residue from the furnace tube's outlet. .... 14
- Figure 4. The interface is the stainless-steel tube which houses the tip of the probe assembly. This top view shows the interface as the large, horizontal tube. The interface's left side is encased in its heating element, and the right side is exposed stainless steel. .... 28
- Figure 5. The interface is the stainless-steel tube which houses the tip of the probe assembly. This side view shows the empty interface as the left tube. .... 29
- Figure 6. The probe assembly has a platinum coil which mechanically holds the quartz sample tubes. The end with the platinum coil and quartz sample tube probe is inserted into the interface. .... 29
- Figure 7. Schematic of the GC carrier- and purge-gas flows for the Pyroprobe® 5200 during the interface's rest and initial phases while set to Py-GC mode. (This image is from page 3.14 of CDS Analytical's manual for the Pyroprobe® instrument series. It is copied here with permission.) .... 31
- Figure 8. Schematic of the GC carrier- and purge-gas flows for the Pyroprobe® 5200 during the interface's ramp and final phases while set to Py-GC mode. (This image is from page 3.15 of CDS Analytical's manual for the Pyroprobe® instrument series. It is copied here with permission.) .... 32
- Figure 9. Residence times of the quartz tube as a function of fraction of carrier gas blowing through each zone. A flow fraction of 0.176 is the upper bound of possible fractions, as it represents zero flow restriction caused by quartz wool and sample material. .... 39
- Figure 10. Residence times of the annular region as a function of fraction of carrier gas blowing through each zone. .... 40

Figure 11. The exploded view of the PIDSSR inlet shows how the orange GC septum is secured in the 1/4-inch-to-3/8-inch union. The short length of ferruled tubing (second from right) presses the septum into the 3/8-inch cavity. A washer (third from right) was carefully filed down to fit into the 3/8-inch cavity and evenly apply pressure to the septum. .... 51

Figure 12. The partially assembled PIDSSR shows its components most easily. Here it has heating elements fixed in place, but it is yet to be wrapped with insulation. In this image, the carrier gas flow enters the inlet from the right. The sample is injected to the inlet through the open tube, where the septum is accessed. The reactor tube is shown on the far side of the 1/4-inch tee (not visible due to heating elements)..... 54

Figure 13. The U-shaped quartz tube with a US 25-cent coin for size reference. .... 59

Figure 14. Approximately 8 cm of the U-tube extended out of the furnace cavity. Part of the 8 cm was covered by the white insulation used to cover the furnace cavity. .... 60

Figure 15. The stainless-steel bubbler was used during the methanol experiments. A similar bubbler using an Erlenmeyer flask was used for propan-1-ol experiments..... 61

Figure 16. The p(DPS-co-DMS)5/95-p(DPS-DMS)50/50 stationary-phase pair only separated alkanes into a distinguished analyte-homologue group, seen as the peaks at lower secondary retention times than the bulk of the peaks. .... 80

Figure 17. Annotated chromatogram highlighting general regions of analyte homologues. Only the alkanes are grouped and well separated by p(DPS-co-DMS)5/95-p(DPS-DMS)50/50. .... 81

Figure 18. A closer view of the earlier primary-retention-time segment shows how the alkane analyte-homologue group separates from the remaining alkylbenzenes and ketone group. .. 82

Figure 19. A closer view of the mid primary-retention-time segment shows the alkane peaks well separated from the remaining analytes. There is some slight separation of alkylbenzenes and alkylphenols. .... 83

Figure 20. A closer view of the higher secondary retention-time segment shows some slight grouping of the alkylbenzenes, alkyl-naphthalenes, and alkylphenols, but no large separation between groups. .... 84

Figure 21. A closer view of the later primary retention-time segment shows the alkyl-naphthalenes and alkylPAHs, but no clear grouping or separation between groups. .... 85

Figure 22. Rtx-200 primary column and Rxi-5SiIMS secondary column performed a very different separation than the apolar-polar configurations. The alkanes are at higher secondary

retention times than the aromatics, and the aromatics are at higher secondary retention times than the oxygenates. ....	87
Figure 23. Annotated version of the separation showing the grouping and separation by the PTFPMS-P(5%BDMSP/95%DMS). ....	88
Figure 24. The chemical structures help display the analyte-homologue groups annotated in Figure 23. ....	89
Figure 25. The ketones were not only grouped into a specific region, but their region was well separated in retention time form the other analyte-homologue groups. ....	90
Figure 26. The alkylbenzenes and alkylphenols were grouped into regions, and these regions were well separated in retention time. ....	91
Figure 27. The PTFPMS-PEG stationary-phase pair spread the oxygenated organics into peaks with no correlation of retention time. ....	93
Figure 28. A closer view shows the orthogonal nature and the ability to avoid column flooding with a highly polar mixture of analytes. ....	94
Figure 29. The full chromatogram view shows a strong retention-time correlation. Dimethylformamide is observed to “wrap around” due to the strong affinity in the second dimension. ....	96
Figure 30. A closer view of the analyte peaks shows their chemical structures more easily at the expense of eliminating pyridine and dimethylformamide. ....	97
Figure 31. The retention of analytes subject to hydrogen-bridge bonds decreases as PEG’s molecular weight (or DOP) increases. This decrease in retention is likely due to the decreasing presence of terminal chain units which possess hydroxyl groups. ....	119
Figure 32. The large differences in primary retention time of furan-like molecules. ....	121
Figure 33. Hydroxyl groups are predominant in cellulose. The numbering scheme of D-glucose is kept for each unit to describe the location of functional groups specifically. (Hydrogen atoms bonded to carbon are not shown for simplicity.) ....	135
Figure 34. Examples of extracting alcohol model compounds from the cellulose chain. ....	138
Figure 35. Comparison of the diols and triol to some of the monols. Lines indicate the simplest possible structural change between stable molecules. ....	141

Figure 36. 2-Methylpropan-2-ol contained butan-2-ol as an impurity. Its pyrolysis in the 400°C PIDSSR-GCxGC-TOFMS revealed how the butan-2-ol impurity mainly dehydrogenated to butanol but also dehydrated to but-2-ene. .... 150

Figure 37. Spectra of H<sub>2</sub> from NIST MS 2.0 Database (70 eV ionization energy). .... 152

Figure 38. Spectra of methanol from NIST MS 2.0 Database (70 eV ionization energy).... 152

Figure 39. Spectra of methanal from NIST MS 2.0 Database (70 eV ionization energy).... 152

Figure 40. Spectra of carbon monoxide from NIST MS 2.0 Database (70 eV ionization energy). .... 153

Figure 41. Mean, baseline-corrected peak areas for ion spectra observed from methanol pyrolysis in the PIQR-QMS system. Note the 2 Da e<sup>-1</sup> peaks likely represent H<sub>2</sub> dehydrogenation product. Spectra below 5 Da e<sup>-1</sup> could not be detected by the TOFMS, and therefore H<sub>2</sub> is not seen with the PIDSSR-GCxGC-TOFMS experiments..... 155

Figure 42. Peak areas of 2 and 30 Da e<sup>-1</sup> to highlight the formation of H<sub>2</sub> and methanal (with some slight addition of a 30 Da e<sup>-1</sup> methanol fragment) in the PIQR-QMS system. .... 156

Figure 43. The injected quantity for argon was different between the propan-1-ol series and the methanol series. However, the standard deviations of argon-injected quantities were very similar in magnitude: the propan-1-ol series' argon-quantity standard deviation was 69.2 units, and the methanol series' argon-quantity standard deviation was 63.1 units..... 158

Figure 44. The injected quantity of propan-1-ol varied much more than the injected quantity of methanol. This caused poor repeatability for the propan-1-ol series of experiments in the PIQR-QMS. .... 158

Figure 45. The three hypothesized cyclic transition-state structures for dehydrogenation applied to generic alcohols..... 163

Figure 46. The hypothesized four-centered unimolecular dehydrogenation transition-state structure was evaluated for each of the four evaluated monols. .... 165

Figure 47. The hypothesized meta-oxygen, six-centered, bimolecular dehydrogenation transition-state structure was evaluated for each of the four evaluated monols. .... 166

Figure 48. The hypothesized para-oxygen, six-centered, bimolecular dehydrogenation transition-state structure was evaluated for each of the four evaluated monols. .... 167

Figure 49. If monol dehydrogenation proceeded via the concerted “meta-oxygen” bimolecular transition state, then co-pyrolysis of non-deuterated propan-1-ol and fully

deuterated propan-2-ol would provide a fraction of its hydrogen product as H-D and a fraction of its assisting alcohols as partially deuterated alcohols. ....	171
Figure 50. If monol dehydrogenation proceeded via the concerted “para-oxygen” bimolecular transition state, then co-pyrolysis of non-deuterated propan-1-ol and fully deuterated propan-2-ol would provide a fraction of its hydrogen product as H-D and a fraction of its assisting alcohols as partially deuterated alcohols.....	172
Figure 51. Using the ChromaTOF software’s spectral observation (“Caliper” at top) and spectral deconvolution (“Peak True” in middle) both show no significant spectral lines with additional masses compared to the spectral-library identification of propan-1-ol (“Library Hit” at bottom). ....	174
Figure 52. ChromaTOF’s spectral observation (“Caliper” at top) and spectral deconvolution (“Peak True” in middle) both show no significant spectral lines with additional or fewer masses compared to the spectral-library identification of propanal (“Library Hit” at bottom). ....	176
Figure 53. ChromaTOF’s spectral observation (“Caliper” at top) and spectral deconvolution (“Peak True” in middle) both show no significant spectral lines with additional or fewer masses compared to the spectral-library identification of fully-deuterated propanone “Acetone-D6” (“Library Hit” at bottom). ....	177
Figure 54. ChromaTOF’s spectral observation (“Caliper” at top) and spectral deconvolution (“Peak True” in middle) both show no significant spectral lines with additional masses compared to the spectral-library identification of ethanal (“Library Hit” at bottom).....	178
Figure 55. ChromaTOF’s spectral observation (“Caliper” at top) and spectral deconvolution (“Peak True” in middle) both show no significant spectral lines with madditional masses compared to the spectral-library identification of ethanal (“Library Hit” at bottom).....	179
Figure 56. The two hypothesized cyclic transition-state structures for dehydration applied to generic alcohols. ....	184
Figure 57. The hypothesized four-centered unimolecular dehydration transition-state structure was evaluated for each of the three evaluated monols.....	187
Figure 58. The hypothesized four-centered unimolecular dehydration transition-state structure was evaluated for each of the three evaluated monols.....	188
Figure 59. The reaction scheme for low-temperature pyrolysis of methanol. ....	192
Figure 60. The reaction scheme for low-temperature pyrolysis of ethanol (left) and generic saturated primary monols (right). ....	192

Figure 61. The reaction scheme for low-temperature pyrolysis of propan-2-ol (left) and generic saturated secondary monols (right). .....	193
Figure 62. The reaction scheme for low-temperature pyrolysis of 2-methylpropan-2-ol (left) and generic saturated tertiary monols (right). .....	193
Figure 63. The reaction scheme for pyrolysis of ethan-1,2-diol when considering only the concerted alcohol dehydrogenation, concerted 1,2-elimination of water, and an undetermined fragmentation route. ....	196
Figure 64. The reaction scheme for pyrolysis of propan-1,2-diol when considering only the concerted alcohol dehydrogenation, the concerted 1,2-elimination of water, the concerted hydroxyketone-hydroxyaldehyde isomerization, and a necessary undetermined fragmentation reaction. ....	197
Figure 65. The reaction scheme for pyrolysis of propan-1,3-diol when considering only the cyclic Grob fragmentation, concerted alcohol dehydrogenation, and concerted 1,2-elimination of water. ....	198
Figure 66. The reaction scheme for pyrolysis of propan-1,2,3-triol when considering only the concerted alcohol dehydrogenation, the concerted 1,2-elimination of water, and enol-aldehyde and hydroxyketone-hydroxyaldehyde isomerizations. ....	199
Figure 67. The reaction scheme for pyrolysis of propan-1,2,3-triol when considering only the cyclic Grob fragmentation, enol-aldehyde tautomerization, and an unidentified fragmentation. ....	200
Figure 68. The D-glucose-like model compounds used to probe the chemistry of cellulose pyrolysis. Only the $\alpha$ anomers are shown in this image. The line types connecting model compounds depict the differences between chemical structures. Aldopentose and aldohexose structures are obtained from Collins and Ferrier [55, pp. 16, 18] and Shallenberger [56, pp. 81, 103-105]. ....	211
Figure 69. Pyrolysis of D-allose at $50^{\circ}\text{C min}^{-1}$ . ....	219
Figure 70. The comparison of three pyrolyses of D-altrose at $50^{\circ}\text{C min}^{-1}$ shows the mass-loss behavior is very repeatable. ....	220
Figure 71. The comparison of three pyrolyses of D-galactose at $50^{\circ}\text{C min}^{-1}$ shows the mass-loss behavior is very repeatable. ....	221
Figure 72. The comparison of three pyrolyses of D-glucose at $50^{\circ}\text{C min}^{-1}$ shows the mass-loss behavior is very repeatable. ....	222

Figure 73. The comparison of two pyrolyses of D-mannose at 50°C min <sup>-1</sup> shows that this D-aldoheptoses is somewhat less repeatable than the others. ....	223
Figure 74. The comparison of three pyrolyses of D-glucitol at 50°C min <sup>-1</sup> show a repeatable mass-loss and heat-flow behavior. ....	225
Figure 75. The comparison of three pyrolyses of D-mannitol at 50°C min <sup>-1</sup> show a repeatable mass-loss and heat-flow behavior. ....	226
Figure 76. The comparison of three pyrolyses of 2-deoxy-D-glucose at 50°C min <sup>-1</sup> . ....	228
Figure 77. Three pyrolyses of three 6-deoxy-L-galactose (also known as “L-fucose”) is uniform at 50°C min <sup>-1</sup> . ....	229
Figure 78. The comparison of three identical pyrolyses of D-xylose at 50°C min <sup>-1</sup> . ....	231
Figure 79. The comparison of three identical pyrolyses of D-arabinose at 50°C min <sup>-1</sup> . ....	232
Figure 80. The comparison of three pyrolyses of D-fructose at 50°C min <sup>-1</sup> . ....	234
Figure 81. The comparison of three pyrolyses of D-tagatose at 50°C min <sup>-1</sup> . ....	235
Figure 82. The comparison of three pyrolyses of D-cellobiose at 50°C min <sup>-1</sup> . ....	237
Figure 83. The comparison of three pyrolyses of D-trehalose dihydrate at 50°C min <sup>-1</sup> . ....	238
Figure 84. The comparison of three pyrolyses of cellulose at 50°C min <sup>-1</sup> . ....	240
Figure 85. The pyrolysis of xylan at 50°C min <sup>-1</sup> . ....	241
Figure 86. Reeves projections (in the <sup>4</sup> C <sub>1</sub> conformation) of the five D-aldopyranoses for structural comparison. ....	247
Figure 87. The Newman projection (left) for the anti-periplanar geometry in the E2 reaction (right). This E2 reaction differs from the concerted, cyclic 1,2-dehydrations due to non-cyclic nature, ionic reactants and products, and its not forming a single co-product. (After Hornback [57, pp. 316-319].) ....	254
Figure 88. The Newman projection (left) for the syn-periplanar geometry in the E2 reaction (right). This E2 reaction differs from the concerted, cyclic 1,2-dehydrations due to non-cyclic nature, ionic reactants and products, and its not forming a single co-product. (After Hornback [57, pp. 316-319].) ....	254

Figure 89. The derivatives of mass-vs-time show that the mass-loss onset of D-galactose leads D-glucose. In fact, both D-galactose's two peak rates of mass loss lead the two respective peak rates of mass loss for D-glucose. Heat flow suggests D-glucose melts at a lower temperature in the onset of pyrolysis for both maxima in the derivative. ....	267
Figure 90. The comparison of D-glucose and D-glucitol at 50°C min <sup>-1</sup> .....	269
Figure 91. The comparison of D-mannose and D-mannitol at 50°C min <sup>-1</sup> .....	270
Figure 92. The comparison of one D-glucose pyrolysis experiment to one 2-deoxy-D-glucose experiment at 50°C min <sup>-1</sup> .....	272
Figure 93. Reeves projections in the <sup>4</sup> C <sub>1</sub> conformation of D-glucopyranose and D-xylopyranose for structural comparison.....	274
Figure 94. The two-stage mass-loss phenomena is seen with both D-glucose and D-xylose, suggesting the formation of levoglucosan is not responsible for the initial mass-loss phase in D-glucose. ....	275
Figure 95. The two-stage mass-loss phenomena is seen with both D-glucose and D-arabinose, suggesting the formation of levoglucosan is not responsible for the initial mass-loss phase in D-glucose. ....	276
Figure 96. The mass and heat-flow signals of three D-arabinose and three L-arabinose experiments at 50°C min <sup>-1</sup> .....	279
Figure 97. The comparison of D-galactose and L-fucose (6-deoxy-L-galactose). ....	280
Figure 98. The comparison of D-trehalose dihydrate to cellobiose.....	282
Figure 99. The iterative method of determining elementary chemistry based upon comparing a reactor model with theory-based rates to performance data from a physical reactor. ....	296

## LIST OF NOMENCLATURE

Bio-oil: Liquid product made by biomass pyrolysis. Its composition varies by biomass type and processing conditions.

Deoxygenation: A general process step to remove oxygen atoms from organic molecules within bio-oils.

Reaction Mechanism: A chemical reaction explained by several elementary reaction steps. For example, a simple substitution may proceed via two mechanisms, which are bimolecular nucleophilic substitution ( $S_N2$ ) and unimolecular nucleophilic substitution ( $S_N1$ ). Both  $S_N2$  and  $S_N1$  execute the substitution, but they involve different elementary reaction steps. In this work “reaction mechanism” does not refer to a reaction network as it often does in combustion research.

Reaction Network: A collection of many chemical reactions, often creating many different reaction products. Reaction network often applies to reactions that proceed in both series and parallel.

Upgrading: A general process to modify bio-oils by chemically reacting them to make more desirable products. Often upgrading refers to some form of deoxygenation chemistry so that bio-oil may become more useful to hydrocarbon processing.

## IUPAC SYSTEMATIC DESCRIPTION OF CHEMICAL COMMON NAMES

Common Name	IUPAC Systematic Name
Acetaldehyde	Ethanal
Dihydroxyacetone	1,3-Dihydroxypropanone
Ethylene glycol	Ethan-1,2-diol
Formaldehyde	Methanal
Furfural	Furfural
Glycolaldehyde	2-Hydroxyethanal
Glyceraldehyde	2,3-Dihydroxypropanal
Glycerol	Propan-1,2,3-triol
Hydroxyacetone	1-Hydroxypropanone
Isopropanol	Propan-2-ol
Levoglucosan	1,6-anhydro- $\beta$ -D-glucopyranose
Methylglyoxal	2-Oxopropanal
Propanol	Ambiguous: Propan-1-ol or Propan-2-ol
Propylene glycol	Propan-1,2-diol

## LIST OF ABBREVIATIONS AND SHORTENED WORDS

Abbreviation	Full Name
CQC	Computational quantum chemistry
EPC	Electronic pressure control
EPR	Electron paramagnetic resonance
FID	Flame-ionization detector
GC	Gas chromatography
GCxGC	Comprehensive, two-dimensional gas chromatotgraphy
GC-MS	Gas chromatography-mass spectrometry
GLC	Gas-liquid chromatography
HDO	Hydrodeoxygenation
m	Meter (unit of displacement)
min	Minute (time, not angular displacement)
mm	Millimeter
MS	Mass spectrometry
MSD	Mass-selective detector
PIDSSR	Pulse-injected deactivated-stainless-steel reactor
PIQR	Pulse-injected quartz reactor

Py-GC-MS	Pyrolysis coupled directly to GC-MS
QMS	Quadrupole mass spectrometer
R&D	Research and development
TOFMS	Time-of-flight mass spectrometer

## CHAPTER 1. INTRODUCTION

### *1.1. Biomass pyrolysis is a potential route to renewable organic chemicals*

Biomass pyrolysis is a general process for transforming plant materials into a range of organic chemicals with heat and an absence of oxygen.<sup>3</sup> Reaction conditions for biomass pyrolysis vary upon application and are not defined uniformly with clear thresholds. The temperatures, residence times, and heating rates vary greatly in order to influence the major products obtained. Longer residence times (order of minutes) and slower temperature rates favor formation of solid char and light gases. Shorter residence times (order of seconds or less) and faster temperature rates (order of 10 to above 1000°C s<sup>-1</sup>), often called “fast pyrolysis,” provide higher yields of a condensable organic liquid called “bio-oil” [4]. Fast pyrolysis can transform up to roughly 75 weight % of the biomass to bio-oil product, with the balance consisting of gases and char. Temperature rates and residence times are often considered the most vital parameters because applied biomass pyrolysis is interested in maximizing the yield of bio-oil. However, the reaction temperature itself has a profound effect on the chemical composition of this bio-oil as well as the accompanying solid and gas phases. Reaction temperatures closer to 400°C favor highly oxygenated organic chemicals like hydroxyaldehydes and hydroxyketones, organic acids, anhydrosugars, and substituted phenolic compounds. Increasing the reaction temperature towards 700°C and beyond causes the formation of increased CO, CO<sub>2</sub>, H<sub>2</sub>, light olefins, aromatics, and coke due to rising thermal-cracking activity [5]. The variability in reaction products allows biomass pyrolysis to be involved in many hypothetical processes for making renewable organic compounds.

Biomass fast pyrolysis has attracted research attention for several decades due to interest in using bio-oils to make renewable organic chemicals, particularly carbon-neutral

---

<sup>3</sup> The root word “pyro” comes from the Greek word for fire, and hence oxidative combustion. However, pyrolysis processes carry the connotation that air or oxygen is purposefully excluded in order to prevent oxidative combustion.

transportation fuels. However, raw bio-oils aren't useful fuels because of practical issues which would greatly complicate the ability to store, inject, and completely burn them in existing engine and furnace equipment. These practical issues are bio-oils' low heating value, high viscosity, hydrophilicity, and slight acidity in comparison to hydrocarbon<sup>4</sup> mixtures. In addition to inadequate performance for most direct applications as a fuel, bio-oils are also difficult to manufacture into chemicals due to reactions occurring while approaching temperatures necessary for subsequent vaporization. In fact, distillation often results in forming solid residue in yields of 30-50%. Most of these combustion and separation problems are because the most organic compounds in bio-oils contain alcohol and carbonyl functional groups. These oxygen-containing functional groups make bio-oils more problematic<sup>5</sup> than hydrocarbon mixtures (such as petroleum) during either direct fuel applications or downstream chemical processing [6].

To enable industrial processing of bio-oils into renewable organic chemicals, much research focuses on removing the oxygenated functional groups which ultimately preclude bio-oils from common refining operations like distillation. This process of removing oxygenated functional groups is usually called "upgrading." Upgrading works by removing oxygen atoms from the bio-oil molecules through the formation of CO<sub>2</sub> and H<sub>2</sub>O byproducts. Upgrading is often subdivided into "deoxygenation,"<sup>6</sup> which employs acidic cracking catalysts like zeolites, and "hydrodeoxygenation," which employs reagent hydrogen and various supported-metal catalysts [7] [8]. Some work has even experimented with integrating these catalytic-upgrading methods within the pyrolysis reactor itself [9], [10], [11], [12]). Ultimately, this upgrading research strives to create catalysts with improved deoxygenation

---

<sup>4</sup> Throughout this dissertation, the term "hydrocarbon" is reserved for molecules containing only hydrogen and carbon. This term is used in such a literal fashion to distinguish it from heteroatom-containing organic chemicals like oxygenates found throughout bio-oils.

<sup>5</sup> Throughout this dissertation, the term "problematic" in the context of bio-oil components refers to the compounds responsible for the hydrophilicity, slight acidity, and poor vaporization.

<sup>6</sup> Deoxygenation could be used by some researchers as an umbrella term to cover all methods of removing oxygenated function groups, as its name merely implies removing oxygen. However, most researchers currently use it in a way which implies acidic cracking catalysts and not hydrodeoxygenation.

activity, crucial resistance to deactivation, and minimizing the need for additional reagents like hydrogen.<sup>7</sup> More effective and efficient catalytic upgrading is vital to improving economics of manufacturing renewable organic chemicals via biomass pyrolysis.

### ***1.2. Understanding Cellulose Pyrolysis Is Important to Improving Biomass Pyrolysis***

It is very difficult to hypothesize and experimentally test elementary pyrolysis chemistry of real biomass because biomass is a composite of many individual materials. Cellulose, hemicellulose, and lignin are often the major components, but many other organic chemicals and minerals also contribute non-negligible mass fractions. These many individual components create a large, complicated reaction network. Model compounds can be used as surrogates for biomass to reduce the complexity of chemical reaction networks, making hypothesis generation and testing much simpler. Cellulose is used for this purpose because it often contributes the largest mass fraction to woody biomass, sometimes up to 50% of the dry mass [13], [14], [15]. In addition to being present in the largest quantity, cellulose is the only major component of plant materials which is a simple and well-defined polymer.<sup>8</sup> Being the most prevalent and most well characterized component in woody biomasses, cellulose pyrolysis has helped elucidate biomass pyrolysis for several decades [16].

### ***1.3. Elementary Pyrolysis Chemistry Is Important for Desirable Reaction Products***

Understanding the elementary chemical reactions is beneficial to designing a reaction process because it allows designers to predict reaction products accurately. An elementary model will find value in predicting bio-oil composition of conventional fast pyrolysis processes. Accurate product predictions lead to more accurate economic analyses, which are

---

<sup>7</sup> It is vital to consider all inputs required for transforming biomass to upgraded bio-oils. Hydrolysis is often claimed to have a higher yield of biomass' carbon remaining in the upgraded bio-oils, but rarely are the additional necessary resources for renewable hydrogen (like biomass fed to gasification processes or area occupied by photovoltaic-powered electrolysis) addressed quantitatively in these yield arguments.

<sup>8</sup> Hemicellulose and lignin can be represented by combinations of model compounds, but their exact structures are not properly represented as uniform and predictable co-polymers.

necessary to justify investment in continued research and development (R&D). However, obtaining an extensive elementary reaction set (as well as the associated kinetic, thermophysical, and transport-phenomena data necessary for a real-world reactor model) is expensive in terms of research resources. Once obtained, having such an elementary reactor model will not change the fact that conventional biomass-pyrolysis processes will still produce undesirable bio-oils. In addition, this accurate elementary reactor model will likely be no more precise than using the accumulated empirical data to determine what bio-oil compositions will be made by certain reaction conditions and reactor types. One should seriously question the merits of spending great research resources on developing elementary-chemistry reactor models to make marginal gains in composition prediction for inherently low-value bio-oils.

Some understanding of elementary reactions is vital to the success of making higher-value bio-oils, although determining full elementary-reaction networks is very research-resource-intensive for its marginal benefits to predicting typical bio-oil composition. The reason is that elementary-reaction knowledge allows R&D engineers to take advantage of intermediate chemical species for the promotion of desired final products (and inhibition of undesired final products). Strategically elucidating small, specific portions of the cellulose-pyrolysis network can guide future investigations into non-conventional biomass pyrolysis processes like in-situ catalytic upgrading. An example is to determine which intermediate chemical species form the most problematic final oxygenated species in bio-oils, and then to test catalysts with pore sizes tailored to these intermediates or acid strengths tailored to these intermediates' oxygenated functional groups (instead of alkenes). Reserving limited R&D resources for chemistry directly related to eliminating problematic oxygenated compounds is vital to continued industrial interest and any potential success with making renewable chemicals via biomass pyrolysis. Spending renewables research resources wisely is especially important with such strong growth in and competition from manufacturing chemicals from shale gas in North America [17].

#### ***1.4. Past Progress with Reaction Models for Cellulose Pyrolysis***

The chemistry of cellulose pyrolysis has been investigated for several decades. Much of the earlier work obtained vapor-formation rates via mass-loss studies with thermogravimetric analysis. Their resulting kinetic models distinguished the pyrolysis products into broad pseudospecies categories like light gases, condensable vapors (like “volatiles” and “tar”), and char instead of specific chemical species. These studies did, however, initiate a valuable discussion on the fundamental phenomena involved when cellulose begins pyrolyzing. This discussion was often based around how observed mass-loss rates and energy flows were influenced by sample size and vapor residence time. These parameters were particularly important because they affected gas-solid reactions. Another key issue of discussion was whether to include an initiation component, often called “active cellulose,” in the simplified kinetic models, and what, if anything, active cellulose physically represented [18] [19]. It is easy to overlook these earlier studies due to their use of vague products, but their “macroscopic” findings on overall enthalpies and complex gas-solid reactions are still excellent clues to elucidating the fundamental phenomena of cellulose and biomass pyrolysis.

In the last several decades, research has put more emphasis upon detailed speciation of products in the gas and condensable-vapor phases. Such focus upon individual chemicals is obviously necessary for hypothesizing the detailed reaction phenomena of cellulose pyrolysis, especially at an elementary level of detail. A remaining difficulty of assembling reaction networks is the lack of accurate chemical speciation of the char products. Without accurate knowledge of the chars’ molecular structures, the chemistry of vital gas-solid reactions is impossible to hypothesize and test at an elementary level. To further increase the accuracy of reactor models designed to predict biomass pyrolysis products outside the conditions of low pressure and very small particle size, researchers must find a way to analyze solid products to the same detail as gases and volatiles.

### ***1.5. Elementary Reactions Are Vital for Producing Less Oxygenated Bio-oils***

This study differed from typical elementary cellulose-pyrolysis studies because it focused upon identifying elementary reaction patterns with the help of model compounds other than D-glucose and its various oligomers and polymers. These model compounds were categorized into two main groups.

- Alcohols, including monols, diols and triol
- Glucopyranose-like molecules

Differences in reaction behavior among members of these groups helped elucidate reaction patterns which were at an elementary or near-elementary level of detail. Such patterns are difficult or impossible to observe in the much larger reaction networks of D-glucose oligomers and polymers. The volatility of the alcohol model-compound group precluded the gas-solid reactions which greatly complicate the elementary networks of solids like cellulose and glucopyranose-like molecules. The elementary-reaction patterns learned from the model-compound sets can then improve the elemental-level understanding of cellulose pyrolysis.

Finally, it is worth repeating that this study also differed from most other cellulose-pyrolysis studies because its elementary-level focus was primarily meant to highlight exactly how problematic oxygenated species form. Understanding these elementary formation patterns was meant to guide research thrusts for modified pyrolysis processes meant to make industrially relevant bio-oils by inhibiting these most problematic oxygenated species.

## CHAPTER 2. EQUIPMENT AND PROCEDURES

### *2.1. Abstract*

Equipment and procedures described in this chapter were mostly for physical experiments, but there is also information for several important sets of computational simulations. The physical experimental equipment used was a suite of four small chemical reactors and a gas chromatograph-mass spectrometer (GC-MS<sup>9</sup>). A suite of reactors was necessary because each reactor had experimental advantages and disadvantages for the different model-compound groups tested. The GC-MS separated and identified the volatile chemical reaction products from two of these four reactors. The principal computational code was Gaussian 09, which was used to compute thermochemical properties of molecules and transition states. The results of the physical experiments and computational simulations complemented one another by iteratively stimulating hypotheses and providing support for or against elementary reactions.

### *2.2. Combined Thermogravimetric Analyzer and Differential Scanning Calorimeter*

The combined thermogravimetric analyzer/differential-scanning calorimeter (TGA/DSC) was a SDT Q600 model (TA Instruments, New Castle, Delaware, USA). Alumina pans were used for the experiments because the only alternative pan material available from TA Instruments was platinum, and platinum carried concerns of (undesired) heterogeneous catalytic effects. The main purpose of the TGA/DSC was to obtain quantitative mass-loss and heat-flow data which would be used to determine rates and enthalpies of reactions. These mass-loss and heat-flow data would be matched to vapor-product analyses from similar experiments in a different reactor.

---

<sup>9</sup> Gas chromatography-mass spectrometry is frequently abbreviated as “GC/MS.” This forward-slash convention is not followed here. Instead, a hyphen is used because instrument combinations are typically called “hyphenated methods” and we wish to remain consistent by using a hyphen instead of a forward slash.

### ***2.2.1. TGA/DSC experimental procedures***

The collection of controlled furnace parameters used for a TGA/DSC test, namely the time-temperature program and purge-gas flowrate, was called a “TGA/DSC method.” These TGA/DSC methods varied depending on the experiment’s objective, but most were identical or quite similar. All methods started at ambient temperature, which was between 20 and 25°C for Room 1008, Module 2 of the Varsity Research Building.<sup>10</sup> The final temperature was usually chosen to be 500°C<sup>11</sup> because conversion was high and weight loss became very small by the time this temperature was reached for saccharide and polysaccharide materials. Most TGA/DSC methods used constant time-temperature rates for the entire test, almost always 10 and 50°C min<sup>-1</sup>. Some different methods were used to isolate specific behavior, such as polymerization and evaporation of 1,6-anhydro-β-D-glucopyranose (levoglucosan), and these methods brought the pan to a desired temperature and held it constant for a specific duration of time. Atypical TGA/DSC methods used are further explained as necessary with their results and discussion in the subsequent chapters.

The beginning of each TGA/DSC test followed the same sample-loading procedure. The purge-gas flowrate was checked to be flowing at the specified value before any weight measurements.<sup>12</sup> The furnace was opened, and the sample pan and the reference pan were placed on their respective beam’s platforms. Next the furnace was closed and the sample weight and reference weight were checked to be stable. After the weight signals stabilized, which took about five seconds, the pans were tared. After the tare function was executed, the weight signals were checked to have stabilized at a value very close to zero (typically the magnitude stabilized to less than 0.0010 mg), again taking about five seconds to stabilize.

---

<sup>10</sup> The Varsity Research Building (1575 Varsity Drive, Raleigh, NC 27606) was formerly known as the “Flex Building.”

<sup>11</sup> The final-temperature set point was more of a nominal parameter: the true recorded final temperature was actually below the set point. For example, the final furnace temperature was actually recorded as ~478°C when the final-temperature set point was 500°C and the temperature ramp rate was 50°C min<sup>-1</sup>.

<sup>12</sup> This flowrate was checked because the purge gas is stopped when the TGA/DSC is not in use to conserve the high-purity nitrogen. The TGA/DSC never had issues or anomalies controlling its purge-gas flowrate.

The furnace was then opened again and only the sample pan was removed. (The reference pan was left carefully untouched.) The sample pan was loaded with the desired quantity of reactant, which was between 4 and 6 mg for almost all experiments. Keeping the mass within this range was reported to reduce or eliminate transport effects and keep experiments more reproducible [20]. After the sample material was loaded, the sample pan was placed back on the sample beam's platform very gently, and the furnace was closed again. After the beams were allowed to restabilize, which took around 20 seconds after closing the furnace, the TGA/DSC method was started.

Cleanliness was vital while loading the TGA/DSC pans. Tweezers and a metal tray were used to hold and transport the pans between the furnace and their cleaning and loading locations across the laboratory benchtop. The loading procedures were done with special care in regards to keeping all surfaces clean of contaminants like dust. The countertops were continually wiped clean with wet paper towels to remove any dust or traces of previously loaded starting materials in order to prevent trace contamination of subsequent experiments. Gloves were worn to prevent finger oils from touching the pans or any tools which may touch pans; i.e., the tweezers, scoopula, or the metal tray. Cleanliness boosts confidence in pyrolysis experiments when trace inorganic materials are known to have an effect on reaction behavior [21].

This TGA/DSC operates with the pans resting on circular platforms at the downstream end of the beams. (These circular platforms contain the thermocouples which gathered temperature data.) These circular platforms have a metallic top surface and a slightly elevated alumina lip to ensure the pan is seated entirely on the inner-top surface. The inner diameter of the platform (the metallic portion) has a diameter roughly 1 mm larger than the pans' outer diameter. Because the pans could be put in slightly different positions within the circular platforms, care was taken to put the pans in the same position every time, as instructed by TA Instruments technical support. Cleaned pans were always set on the pan platforms in the furthest possible downstream position as a simple way to use the same pan position repetitively. Doing so was meant to do two things. First, it was to ensure the

instrument's perceived difference in mass between the tared, empty sample pan and the newly loaded and replaced sample pan is due only to the added sample mass.<sup>13</sup> Second, it was to ensure minimal experiment-to-experiment differences in TGA/DSC response. For example, a slight change in pan position may cause a slightly different response from the thermocouples below the pans. After seating on the platforms, the pans were gently pushed against the platform's lip on the downstream side to ensure they were always positioned in the same way. The beam's metallic, circular platforms and the positioning of the pans on these platforms are displayed in Figure 1.

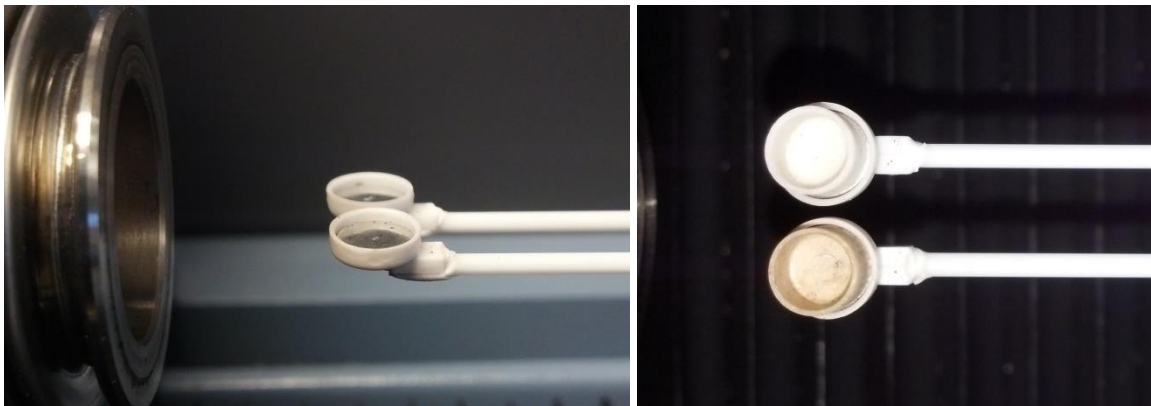


Figure 1. The beams have metallic, circular platforms with a surrounding lip (left), and the pans were positioned to rest against the platform's lip on the downstream side.

---

<sup>13</sup> Because the beams sense weight by the torque exerted upon them, changing either the suspended mass or its radial position affects the torque, and hence, perceived weight. Possible changes in torque are explained by the simple relationship  $\tau = r_{\text{pan}} \times m_{\text{sample}} \alpha_{\text{g}}$ , where  $\tau$  in this equation is torque (not residence time) and  $r$  is radial position (not reaction rate). Replacing the loaded sample pan in a different radial position from the empty sample pan when it was tared will cause an incorrect perceived sample mass.

### 2.2.2. *Char and tar removal from pans and furnace*

Both the sample and the reference pans were cleaned between each experiment by shaking or scraping<sup>14</sup> the bulk of the char out of them and then burning the residual char in the flame of a Meker burner.<sup>15</sup> The Meker burner was fueled by natural gas, and its air feed's aperture was set to provide the maximum air flow to ensure the lowest possible fuel-air equivalence ratio. This "premixed" flame actually had two parts: there was a small light-blue, conical flame (the true-premixed-flame region) inside a larger pale-violet conical flame (the diffusion-flame region). The Meker burner was positioned so the pans were only partially touching the exterior edge of the pale-violet diffusion flame. This position was observed to remove char faster than positioning the pan anywhere else within either the diffusion-flame region or even the hotter true-premixed region. Even though the outside edge of the diffusion-flame region may be much cooler than the true-premixed-flame region, it is surmised that partially exposing the pan to the air surrounding the diffusion-flame region allowed oxygen better access to the pan surfaces in order to oxidize the char more rapidly. After the pans lost any visual indication of char, they were allowed to cool in air for roughly 1 minute.

The two pans were held together in the flame by being hung upside down on the ends of thin quartz tubes fixed to a ring stand (Figure 2). These quartz tubes, which were sample tubes for use in a Pyroprobe® instrument, were held in place by being inserted over the ends of 1/16-inch outer-diameter stainless-steel tubes. The stainless-steel tubes were fixed to the ring stand by a clamp. (Tweezers could not safely hold the pan in the flame because they transferred heat to the user's hands too easily and the tweezers' tips warped in the flame.) Before the series of experiments used for data in this work, the pans were held directly by the

---

<sup>14</sup> Monosaccharides, disaccharides, and starches left porous solidified pools of char adhered to the pan's interior surface. Cellulose and xylan char did not adhere to the pan, and its char could be removed as a single piece by simply inverting the pan and letting the char fall by gravity.

<sup>15</sup> A Meker burner looks almost identical to Bunsen burner. The difference is that a Meker burner has a larger diameter burner and also has a grid pattern set into its burner where fuel and air exit the premixing section.

stainless-steel tubes. On 29 August 2014, the pan-cleaning protocol was changed by adding the quartz tubes over the ends of the stainless-steel tubes. This modification was introduced so the alumina pans only contacted quartz as they were burned, preventing contact with any metal which may continually contaminate the pan surface and contribute cumulatively to some form of catalytic effect or altered thermal conductivity over the course of many experiments.



Figure 2. Positioning the TGA/DSC pans at the exterior edge of the outer diffusion flame removed char fastest, potentially due to higher local oxygen concentration and temperatures still hot enough to make the pans glow with an orange color. Quartz Pyroprobe® tubes

prevented contact between the alumina TGA/DSC pans and the stainless-steel tubes clamped to the ring stand.

Tars accumulated at the outlet of the TGA/DSC's alumina furnace tube over time, as evidenced by the dark residue on the interior surfaces of the white alumina (Figure 3). This dark residue was assumed to be deposited tars from pyrolysis reactions, but their exact makeup could not be determined because a sample could not be scraped from the hardened tars, dissolved in a solvent, and injected to GC-MS. The full extent of tar accumulation was not known because the inside of the alumina furnace tube is difficult to inspect due to its narrow 0.4-cm downstream opening and its obstructed view of the upstream opening. It is likely that significant tar accumulation was only present near the furnace tube's downstream end because this portion of the furnace tube lies outside of the coaxial furnace.<sup>16</sup> The outlet side of the alumina furnace tube is usually cooler than the portion of the alumina furnace tube within the furnace.<sup>17</sup> The lack of residue accumulation in the visible, far upstream portion of the alumina furnace tube and the beams suggests these locations were hot enough to prevent condensation and deposition of pyrolysis vapors. In addition, the lack of residue accumulation on the beams suggests weight-loss and heat-flow measurements were not affected by gradual tar accumulation over the course of many experiments.

---

<sup>16</sup> The term "furnace" refers to the assembly of heat-generating components which surrounding the "alumina furnace tube." The furnace does not extend over the entire length of the alumina furnace tube, and hence not all locations of the alumina furnace tube were heated to the furnace set-point temperatures. Care was taken in this dissertation to refer specifically to either the furnace or the alumina furnace tube when a distinction was necessary.

<sup>17</sup> This difference in temperature is especially obvious when burning out the TGA/DSC, as the portion of the alumina furnace tube near the furnace glows bright orange while the outlet does not.



Figure 3. Dark brown and black residue, most likely condensed and solidified tars, accumulated on the inner surfaces of the alumina furnace tube. Routine furnace cleaning with high temperatures and air flow did not remove residue from the furnace tube's outlet.

Some of the accumulated tar was removed from the furnace tube by periodic oxidation procedures, which were done by switching the purge gas from nitrogen to air and ramping the furnace temperature to 1200°C. The beams appeared slightly brighter after “burning out” the furnace, but it was difficult to tell if the marginal color difference was imagined. The interior surface of the alumina furnace tube's outlet always retained a dark discoloration, which was assumed to be accumulated tars hardened into a coke-like material from repeated heating programs. It is suspected the tars remained on the furnace tube's outlet because alumina is a poor thermal conductor, and the outlet lies several centimeters outside of the furnace. This outlet region remaining cooler than the furnace set-point temperature is likely why the tars condensed during experiments and subsequently were not fully oxidized and removed during furnace cleaning procedures.

After burning out the TGA/DSC's alumina furnace tube, the TGA/DSC was recalibrated by the procedure detailed by the SDT Q600 instructions.<sup>18</sup> The calibration procedure was a series of weight (empty beams and reference weight), temperature (lead standard), and heat-flow (empty pan, sapphire standard, and lead standard) "calibration methods." These calibration methods required roughly one to two days of instrument downtime. TA Instruments suggested these calibrations methods use the exact same purge-gas flow rates and temperature-ramp rates as to be used in the subsequent set of experiments. This advice was followed, but a notable exception was the series of TGA/DSC experiments which used a temperature-ramp rate of 50°C min<sup>-1</sup>. This series of experiments was interspersed with a series of experiments at 10°C min<sup>-1</sup>. Instead of continually recalibrating the TGA/DSC back and forth between the temperature-ramp rates, the same calibration method, run at 20°C min<sup>-1</sup>, was used for both sets of experiments. The same calibration method was used for both sets to avoid excessive time in recalibrating the instrument. The results of the two experiment series were compared by "blank" runs with empty pans and with inert weight standards to ensure gravimetric responses were very similar at both 10 and 50°C min<sup>-1</sup>.

### ***2.3. TGA/DSC Transfer-Line Sampling System(s)***

A series of transfer-line sampling systems were constructed to carry a sample of reaction products from the TGA/DSC to the GC's inlet. These sampling systems had the fundamental task of delivering a short pulse of reaction products from a continuous stream of reactor effluent. A short pulse of sample is necessary for GC because it is a non-steady-state separation technique, and it cannot function with a steady flow of sample to its inlet. In addition, the reactor effluent's composition is not steady in time, and therefore short sample

---

<sup>18</sup> There are two sets of instructions offered on the SDT Q600. One is the stand-alone SDT Q600 manual on CD-ROM, and the other is built into the help features within the Thermal Analysis software used to control the TGA/DSC. The help features within Thermal Analysis are substantially more instructive than the stand-alone manual when describing the calibration procedures. Knowing the help features within Thermal Analysis will save countless time and e-mail conversations with TA Instruments personnel when calibrating the SDT Q600.

pulses are needed to approach an instantaneous reactor composition at a desired reaction time.

The transfer-line sampling systems were not successful for providing reaction product analyses for TGA/DSC experiments. The transfer-line sampling systems were able to detect volatile solvents like methanol and hexanes evaporating in the TGA/DSC pans in troubleshooting experiments, yet they could not detect major pyrolysis products during cellulose pyrolysis experiments, even during maximum rates of weight loss. Ultimately it was determined that the pyrolysis vapors are too dilute in the TGA/DSC purge gas given the volume of the sampling loop. To prevent any future studies from making the same mistakes, versions of the transfer-line sampling systems attempted will be described here in detail, even though no version was successful at the intended task.

These versions of transfer-line sampling systems were based upon short descriptions of a past, successful sampling system in a pyrolysis laboratory at the University of Massachusetts Amherst. However, that previous transfer-line sampling system could not be replicated exactly for two reasons. First, it was not described in detail and so the exact components and their configurations were not known. Second, it connected to a different make and model TGA/DSC, which had a vertical furnace tube. This vertical furnace tube allowed a sampling tube easier access to the vicinity of the pans and the richer nearby pyrolysis vapors. The current TGA/DSC (SDT Q600, TA Instruments) has a long, moving, horizontal furnace tube. For a sample tube to sample gas near the pans in the SDT Q600, the sample tube must pass through a narrow opening of the furnace tube and extend roughly 7 cm. In addition, this horizontal furnace tube moves axially in order to expose the beams and pans for loading and unloading. With the lack of description on the previous transfer line and a very different TGA/DSC, the transfer-line sampling systems attempted at NCSU could not replicate the previous transfer-line sampling system's exact form or its satisfactory performance.

The transfer-line sampling systems at NCSU went through several iterative versions, and each version can be distinguished by the way it controlled the flow of sampled gas.

- Some versions controlled the fraction of TGA/DSC purge gas that flowed through the sampling system.
- Some versions controlled the pressure within the sampling loop, which in turn would draw different flow rates of TGA/DSC purge gas through the sampling system.

Before fully describing each variation, the components they shared will be described.

The first component shared among all variations of transfer-line sampling systems was a six-port sampling valve, which was Model 6C6UWE (Valco Instruments Company, Incorporated, Houston, Texas, USA). This six-port valve had 1/16-inch fittings and 0.75 mm ports. These narrow diameters were chosen to match the transfer-line diameters and to minimize swept and dead volumes in the sampling system, which in turn would minimize axial dispersion of the transient vapor composition. It is possible that using larger ports would help reduce the pressure drop required by the system to draw adequate flow from the TGA/DSC. In addition, it is possible that minimizing swept and dead volume of the borings provides negligible help to the transfer-line sampling system due to the inherently larger swept volume of the transfer line and sampling loop. Finally, any loss in time resolution due to swept and dead volumes within the transfer-line sampling system might be very small compared to the loss in time resolution due to the inherently larger residence time of the significantly mixed TGA/DSC furnace tube.

This six-port valve was rated for “medium temperature,” which had a maximum temperature of 225°C. A medium-temperature valve was chosen instead of a “high-temperature” valve because the medium-temperature internal materials (a “Nitronic-60” body and a “Valcon-E” rotor) could resist moisture expected in pyrolysis vapors, but the high-temperature internals (a “Valcon-T” rotor) could not.

The six-port valve and the sample loop were held inside a heated valve enclosure (Model HVE3, Valco Instruments Company, Incorporated, Houston, Texas, USA). This enclosure was powered by a 110 VAC heating probe, which was manually controlled by a 120 VAC variable transformer (variac). Thermocouples were placed on the stationary cylindrical face of the six-port valve, the outside tube wall of the sampling loop, and the transfer line tubes that entered and exited the heated valve enclosure.

The vacuum pump was Model 2561B-50 (Welch-Ilmvac, Niles, IL, USA, purchased through VWR International). This pump was necessary because the TGA/DSC furnace tube operated at atmospheric pressure, and a pressure drop was necessary to force gas to flow through the sampling system's narrow tubes and the six-port valve's narrow borings. The vacuum pump had a pressure gauge on its inlet side, and the inlet pressure could be adjusted by a small valve, which allowed additional room air to mix with gas from the sampling system just upstream of the pump inlet.

The thermocouples used throughout the sampling system were self-adhesive, fine-wire, type-K thermocouples with male sub-mini connectors (Part# SA1XL-K-SRTC) made by Omega Engineering, Inc. (Stamford, CT, USA). A hand-held thermocouple reader (Part# HH11B) (Omega Engineering, Inc.) displayed the thermocouple temperatures. The thermocouples were read one at a time, which did not present a problem because the system was not subject to significant temperature transients once the heater set points were first reached.

The tubing used to carry sample to and from the six-port valve was 1/16-inch outer-diameter "rinsed-and-cleaned" 304 stainless-steel tubing (Catalog# 21506, Lot # 520186-506, Restek Corp. Bellefonte, Pennsylvania, USA). The inner diameter was 0.0762 cm (0.030 inches). This tubing was also used for the sample loop. The sample loop was 50 cm in length before winding it into a ~5-cm diameter coil, and the resulting sample-loop volume was 0.23 cm<sup>3</sup>.

The 1/16-inch OD tubing connects all ports of the six-port valve. The stream exits the six-port valve via the 1/16-inch OD stainless-steel tubing, but after roughly 20 cm, a reducing union allows this stream to flow via a larger 1/4-inch outer diameter polyethylene tube connected to the vacuum pump's inlet.

Each version of the transfer line used these components. The first version used only the valve at the vacuum-pump inlet to adjust the flow of gas through the six-port valve. The second version used a 1/4-inch tee placed where the 1/16-inch stainless-steel tubing joined the 1/4-inch polyethylene tubing. This tee allowed ambient air to enter in its branch in order to increase the pressure in the sample loop, providing a higher gas density and a larger sample quantity for injection. The third version placed a pressure gauge on the branch of the 1/4-inch tee and installed a needle valve directly downstream of it (upstream of the 1/4-inch polyethylene tubing). The needle valve allowed fine control of the sample loop's pressure, and the pressure gauge indicated the effects. This third version was operated in two ways. The first way flowed only a small fraction of TGA/DSC effluent through the sample loop, and the second way flowed all of the TGA/DSC effluent through the sample loop. Both of these ways failed to inject a vapor quantity detectable by GC-MS, even at the maximum mass-loss period and with a splitless injection. Installing a sample loop with a larger volume would be suggested if this transfer-line sampling system is needed for future TGA/DSC experiments. However, the new sample-loop volume should be orders of magnitude larger because the current sample-loop volume fails to contain detectable quantities even with a splitless injection.

#### ***2.4. Cold-Needle Sampling of TGA/DSC Effluent***

A novel sampling method with a syringe was created to substitute for transfer-line sampling systems. A syringe's metal needle was cryogenically cooled prior to sampling. The syringe then was used to withdraw vapor from the hot TGA/DSC outlet, during which time the less-volatile components condensed on the inner surfaces of the cold metal needle. After the syringe was filled with sample, it was carried by hand to the GC inlet and inserted. As the

needle temperature increased in the hot GC inlet, the condensed materials vaporized and were swept into the GC inlet by depressing the plunger. The purpose of cooling just the syringe's needle was to accumulate all of the condensable analytes entirely on the metal needle's interior surfaces. Condensation in the needle alone was essential because only the needle will be inserted into the hot GC inlet. Any condensable analytes in the syringe's plastic barrel would not be heated by the GC inlet, and therefore these analytes would not vaporize and enter the GC inlet. Because only the syringe's needle was cooled, the method was called "cold-needle sampling."

It was not possible to use a gas-tight syringe for cold-needle sampling. Compared to general-use plastic syringes, the construction of gas-tight syringes is more trusted for sampling of gaseous analytes. In addition, gas-tight syringes have a valve between the needle and syringe barrel which can close in order to prevent sample gases from diffusing out of the syringe during transport to the GC inlet. By cryogenically cooling the gas-tight syringe's needle, it too could ensure condensable analytes would not enter and condense in the barrel and fail to be injected to the GC inlet.<sup>19</sup> However, two problems precluded the use of gas-tight syringes for cold-needle sampling. First, the plunger had much more resistance to movement within the barrel, making it very difficult to hold the syringe steady during sampling and obtain a steady volumetric flowrate sample gases. Second, the gas-tight syringe was much more difficult to disassemble for routine cleaning. Gas-tight syringes, even those of high quality, could not perform as well as plastic, disposable syringes in the cold-needle sampling technique.

Cold-needle sampling was inspired by two common analytical techniques used for gas chromatography analyses. The first technique is a sample preparation and injection method called "solid-phase-microextraction" (SPME). SPME uses a special syringe fitted

---

<sup>19</sup> Heating the gas-tight syringe's barrel and plunger was not possible because it cannot withstand the temperatures needed to vaporize all of the analytes. VICI's A-2 series gas-tight syringe had a barrel made of glass, but VICI stated it could not withstand temperatures above 105°C, while temperatures of more than 250°C are necessary to reliably vaporize key analytes like 1,6-anhydro-β-D-glucopyranose.

with an adsorbent fiber to accumulate only specific volatile analytes from a sample matrix. These fibers are designed to discriminate among analytes based upon criteria like polarity and molecular weight. Upon inserting the loaded SPME syringe into the GC inlet, the adsorbent warms and the targeted analytes desorb for injection. The second inspirational technique is a GC hardware modification called “cryofocusing,” which sharpens analyte peaks in GC separations. Cryofocusing devices create a small cold spot on the GC’s analytical column just downstream of the inlet during injection. The cold temperature causes broadly injected condensable analytes to accumulate over a very short length of column. After the injection is completed, the cold spot is rapidly warmed so the GC separation may proceed, and the tightly focused analyte bands then elute as sharper peaks. Similar to cryofocusing, the cold-needle sampling method uses cryogenic temperature to focus condensable analytes onto the walls of a specific region of tubing, although it is a metal needle instead of a capillary analytical column. The syringe needle holding the condensable analytes is inserted into the hot GC inlet, and then the analytes are desorbed, similarly to how SPME syringe fibers insert then desorb their accumulated target analytes. A benefit of cold-needle sampling over SPME is its ability to inject permanent gases in addition to the condensed analytes. SPME could not be used because the analytes may not initially adsorb onto the syringe fiber when the fiber is inserted into the warm TGA/DSC furnace-tube outlet.

The cold-needle sampling’s syringe assembly was constructed from three main parts, which were the syringe body, the needle, and the needle sheath. The syringes were NORM-JECT® 5 mL Luer-Lock syringes (REF 4050-X00V0, Lot 1L07048). These syringes consisted of a plastic barrel and plunger. The plunger appeared to be made entirely of a single piece: it did not appear to have any elastomer gasket or o-ring to seal against the barrel. The needles were “BD PrecisionGlide™ Needle” 22G x 1.5 (0.7mm x 40mm) (REF 305156, Lot 2018881). The syringe body and needle were held together with a typical “Luer-Lock” design. The needle sheath was a length of 1/16-inch outer-diameter stainless-steel tube which slid over the syringe needle to make a snug fit without requiring much force (~1 N) to install or remove. (A 1/16-inch outer-diameter tube has an inner diameter of 0.0762 mm. A

22 gauge needle has an outer diameter of 0.718 mm<sup>20</sup>.) The needle sheath did not cover the entire syringe needle. Instead, the needle sheath left several millimeters of the syringe needle's tip exposed so analytes would not be lost by condensing on the needle sheath's surfaces. This needle sheath provided extra thermal mass to help the syringe needle maintain a cold temperature for longer periods of time when carried through ambient-temperature air. The needle sheath also guarded the syringe needle from condensation due to ambient humidity. In fact, the needle sheath often kept a frosted appearance until removed just prior to injection to the GC inlet.

This sampling method worked by a simple procedure. The steps of the procedure will be outlined, and then each step will be elaborated upon in the subsequent paragraphs.

- Disassemble and clean the syringe barrel, syringe plunger, needle, and the needle sheath.
- Assemble the cleaned syringe and needle sheath.
- Cool the needle (and needle sheath) in liquid nitrogen.
- Draw a sample from the TGA/DSC furnace-tube outlet.
- Carry the syringe assembly to the GC inlet.
- Remove the needle sheath from the syringe needle.
- Insert the syringe's needle to the GC inlet.
- Start the GC method.
- Depress the syringe plunger.
- Remove the syringe from the GC inlet.

The syringe was cleaned to remove any traces of the previous experiments' analytes. The cleaning was performed by removing the needle sheath and rinsing these two parts

---

<sup>20</sup> While the manufacturer of the BD PrecisionGlide™ Needle stated their syringe needles were 0.7 mm, most technical sources claim 22 gauge to be 0.718 (Hamilton Company) or 0.720 mm (Sigma Aldrich) in outer diameter.

separately. The unsheathed syringe-needle combination was rinsed by drawing clean methanol into it, then ejecting it. This rinsing was performed three times. The needle sheath was rinsed in methanol by using the cleaned syringe to sweep clean methanol through its interior and over its exterior. Any residual liquid methanol which didn't drip off the syringe parts was then blown off with a compressed-gas dusting product called "Dust Off" (Product code DPSJMB, Falcon Safety Products, Inc., Branchburg, New Jersey, USA) compressed gas<sup>21</sup>. The syringe parts were allowed to sit on a fresh "Kimwipe" paper towel (Kimberly-Clark Worldwide, Inc, Roswell, GA, USA) for several minutes to ensure methanol was no longer present. The syringe was then assembled and the needle was inserted over the needle sheath.

The needle was cooled in a small (~1 L) liquid-nitrogen dewar filled to a liquid level high enough to submerge the syringe's needle and needle sheath. The dewar sat next to the TGA/DSC on the furnace-tube's outlet side to provide the cooled syringe assembly the shortest possible path to the furnace-tube outlet. A short path through ambient air ensured the smallest possible temperature increase of the syringe needle and needle sheath.

The syringe plunger was set at the 1 mL mark, and its needle was submerged in the liquid nitrogen. The syringe needle and needle sheath were cooled for 60 seconds.<sup>22</sup> The syringe was removed from the dewar, and immediately its plunger was depressed fully to expel any liquid nitrogen from the syringe barrel and needle. While liquid nitrogen was never observed to spray out upon depressing the plunger, it was expected that some liquid nitrogen would be drawn into the syringe needle due to the 1 mL of air within the syringe contracting as it cooled.

---

<sup>21</sup> Dust Off contains difluoroethane. Detrimental contamination from this product is not suspected because Dust Off remaining in the syringe assembly is detected as a very small peak with spectra at 51 and 65 Da e<sup>-1</sup>.

<sup>22</sup> Longer periods of time in the liquid-nitrogen bath were shown to cause contraction of the plastic syringe barrel. The contraction caused excessive and unpredictable resistance to plunger movement, which made a steady drawing of reactor gases from a steady reactor position very difficult.

After depressing the plunger completely, the syringe was moved quickly to the TGA/DSC furnace-tube outlet and inserted. It was positioned to keep it coaxially aligned with the furnace tube. Care was taken not to let the syringe assembly contact the furnace tube, as doing so would likely disrupt the TGA/DSC's mass-measurement signals. After insertion of the needle, the plunger was pulled at the desired rate. The rate of drawing gas into the syringe was either 0.5 or 1.0 mL s<sup>-1</sup> depending upon the experiment set. This rate of sampling was controlled by hand. Time was tracked by counting out loud, and volume was tracked by watching the plunger face pass the syringe barrel's graduated volume marks. With practice, a steady rate of sampling was routinely possible.

After the sample was drawn into the syringe, the syringe was carried roughly two meters to the GC inlet. The needle sheath was then removed, and the needle was inserted immediately into the GC inlet. The GC method was manually started immediately after the needle was inserted through the GC inlet's septum by pressing the start key on the instrument keypad (because carefully inserting the needle required two hands). The plunger was steadily depressed for ten seconds to allow the hot GC inlet to warm the needle as gas swept the desorbing analytes into the inlet.

Compared to a transfer-line sampling system, the cold-needle sampling method has four main advantages.

- The sample's condensable species are immediately cooled to cryogenic temperatures, which are presumably far too low for continued reaction. The transfer-line sampling systems must remain warm enough to keep any analytes from condensing, which often approaches reaction temperature (~250°C). Some evidence suggested the transfer-line system shows dehydrogenated simple alcohols evaporating in the TGA/DSC, which is expected given the results of model-compound reaction studies on simple alcohols.
- The syringe only contacted vapors while it gathered a sample, but the transfer-line sampling systems were exposed to vapors for the entire duration of each experiment.

Being exposed only to the desired sample vapors ensures the sample was not contaminated with condensed analytes accumulated at earlier times of the experiment or from different, preceding experiments.

- The syringe was dismantled and rinsed with solvent very easily after each use, at which time it was inspected for residue or leaks. The transfer-line sampling systems were not easily cleaned with solvent. It was difficult to check for residue because it was made of opaque metals with very narrow openings. Being a vacuum system without a steady-state detector, it was also not easy to be inspected for leaks.
- The syringe barrel indicates clearly the exact volume sampled, which can be adjusted between 0 and 6 mL. The transfer-line system cannot adjust its injected volume without disassembling a heated valve enclosure and replacing the sample loop.

Along with the advantages of cold-needle sampling technique come its disadvantages.

- Cold-needle sampling was not as repeatable because it required several manual motions: insertion of the needle into TGA/DSC furnace outlet, steady rate of pulling the plunger to draw sample vapors, not moving the syringe while drawing sample, speed of carrying the syringe to the GC inlet and removing the metal sheath, and rate of depressing the plunger.
- It is unknown if all of the condensable species are deposited on the metal needle's interior surfaces. It is conceivable that some vapors may form an aerosol or mist when cooled in the high-velocity stream of the needle. It is also possible the rate of heat transfer from the cold needle's surface to the warm flowing vapor might not be sufficient to condense all vapors entirely. Any mist or uncondensed material will be swept into the syringe's barrel. Once inside the syringe's barrel, any condensed low-volatility analytes may not evaporate again because the barrel is not warmed by the GC inlet as the needle is. Therefore, if the low-volatility analytes are not entirely deposited on the metal needle, then their true entire sampled quantity will not be injected to the GC inlet.

## **2.5. Pyroprobe® Micropyrolyzer**

### **2.5.1. Basic Pyroprobe® instrument description**

A commercial micropyrolyzer instrument, the Pyroprobe® 5200 model (CDS Analytical, LLC, Oxford, Pennsylvania, USA), was used for pyrolyzing small solid samples and sending vapors directly to chemical analysis by GC-MS. The Pyroprobe® 5200 is a versatile instrument designed to devolatilize and pyrolyze very small (often 0.01 to 0.1 mg) samples in semi-batch operation. In essence, it is a reactor unit spliced between the GC's carrier-gas flow controller and the GC's inlet. It can achieve heating rates as high as 1000°C s<sup>-1</sup>,<sup>23</sup> making it popular among pyrolysis researchers interested in biomass fast pyrolysis.

In this work, the Pyroprobe® was necessary for determining the composition of pyrolysis vapor products evolved from specific temperature ranges for various sample materials, as such could not be done in the TGA/DSC due to its well-mixed nature. These compositions were combined with mass-loss and heat-flow data from TGA/DSC experiments which were run at nearly identical conditions. The combination of data produced net rates of formation of specific products during pyrolysis. The major components and functions of the Pyroprobe® 5200 micropyrolyzer are described briefly in this section. Understanding these particular components and functions is vital to grasping the experiments and their conclusions, including how TGA/DSC and Pyroprobe® experiments can be performed so their data are complementary.

The Pyroprobe® has an “interface” (sometimes also called the “accessory” in the software and the operation manual) which is a ~7-mm inner-diameter, externally heated, stainless-steel tube (Figure 4, Figure 5). The interface serves as a vessel for flowing purge gas, GC carrier gas, or a reactive gas over the sample. A probe assembly slides in and out of

---

<sup>23</sup> CDS Analytical states the filament is capable of this heating rate, but it is unknown how rapidly the reactant material's temperature increases when heat from the coil must be transferred through a quartz tube with a wall thickness of roughly 0.5 mm.

the interface tube to load and unload samples (Figure 6). The probe has a coiled platinum filament at its inserted end. Disposable quartz tubes are fitted snugly inside the platinum coil when the probe assembly is removed from the interface. The quartz tubes, which measure 25 mm long and 1.9 mm inner diameter,<sup>24</sup> hold the chosen sample material by positioning it between two plugs of quartz wool. Pyrolysis vapors evolved from the sample flow/diffuse out of the quartz tube and are swept out of interface by GC carrier gas. After leaving the interface, pyrolysis vapors can flow to the transfer line or a sorbent trap depending upon whether the instrument's manual, external 8-port valve is set to "GC" or "TRAP" mode, respectively. (In this study, only the GC mode was used.) After flowing through the heated transfer line, the devolatilization/pyrolysis gases are injected directly into the GC inlet by a needle at the tip of the transfer line. The needle is fixed in a position inserted through the GC-inlet septum. This transfer line is similar to a GC syringe, but it remains fixed in the inlet and flows carrier gas continuously.

---

<sup>24</sup> In a study on optimizing the Pyroprobe® 5200 by Ronsse et al. (2012), the authors claimed the quartz tubes were 25.4-mm long and 6.35-mm inner diameter. However, such a large inner diameter is impossible for two reasons. (1) CDS Analytical, LLC states the quartz tubes are 25-mm long and 1.9-mm inner diameter in their instrument manual for the Pyroprobe® 5200 with a ¼-inch probe. This inner diameter was confirmed by measuring the quartz tubes used in this study to be ~2-mm inner diameter. (2) It is uncertain how quartz tubes (from some source other than CDS Analytical, LLC) of 6.35-mm inner diameter could be loaded into a ¼-inch probe assembly because its stainless-steel tube, which holds the quartz tube within itself, is only ~5-mm inner diameter.



Figure 4. The interface is the stainless-steel tube which houses the tip of the probe assembly. This top view shows the interface as the large, horizontal tube. The interface's left side is encased in its heating element, and the right side is exposed stainless steel.



Figure 5. The interface is the stainless-steel tube which houses the tip of the probe assembly. This side view shows the empty interface as the left tube.



Figure 6. The probe assembly has a platinum coil which mechanically holds the quartz sample tubes. The end with the platinum coil and quartz sample tube probe is inserted into the interface.

The Pyroprobe® micropyrolyzer uses two separately controlled gas flows, which are the GC carrier gas and the purge gas. The GC carrier gas flows through the interface during its temperature-ramp and final-temperature phases. The GC carrier gas is fed by the GC's electronic-pressure-control (EPC) module, and it is the sum of the column flow, split flow, and septum-purge flow. The GC's carrier gas is routed to the Pyroprobe® via 1/16-inch outer-diameter tubing connected from the GC's EPC's carrier gas line, where this line would normally connect to the GC inlet weldment. The second gas flow, referred to in this work as “purge gas,”<sup>25</sup> flows through the interface during its rest- and initial-temperature phases. It is important to note that the Pyroprobe® 5200's built-in programming switches the interface from receiving purge gas to receiving GC carrier gas when the interface begins its temperature-ramp phase. This programming cannot be adjusted or overridden, and this switch from purge gas to GC carrier gas has a profound effect upon what experiments are possible in the Pyroprobe®. The topic of designing experiments around the switching of carrier- and purge-gas flows is an important topic discussed in subsection 2.5.4.

---

<sup>25</sup> The Pyroprobe® 5200 instrument manual actually calls two separate gas flows both as “carrier gas.” (This naming is likely because upon typical Pyroprobe® installation, both gas flows are ultimately from the same gas cylinder, and hence are the same gas.) One carrier-gas flow is actually controlled by the GC and is rerouted through the Pyroprobe instrument before reaching the GC inlet. The other gas flow is taken directly from the pressure regulator to the manual flow-control valve on the Pyroprobe®. This work distinguished these two separate gas flows by renaming the gas flow controlled by the GC to “GC carrier gas” and renaming the other gas flow to “purge gas.” The purge-gas stream flows through the interface during its rest- and initial-temperature phases. The carrier gas flows through the interface during temperature-ramp and final-temperature phases.

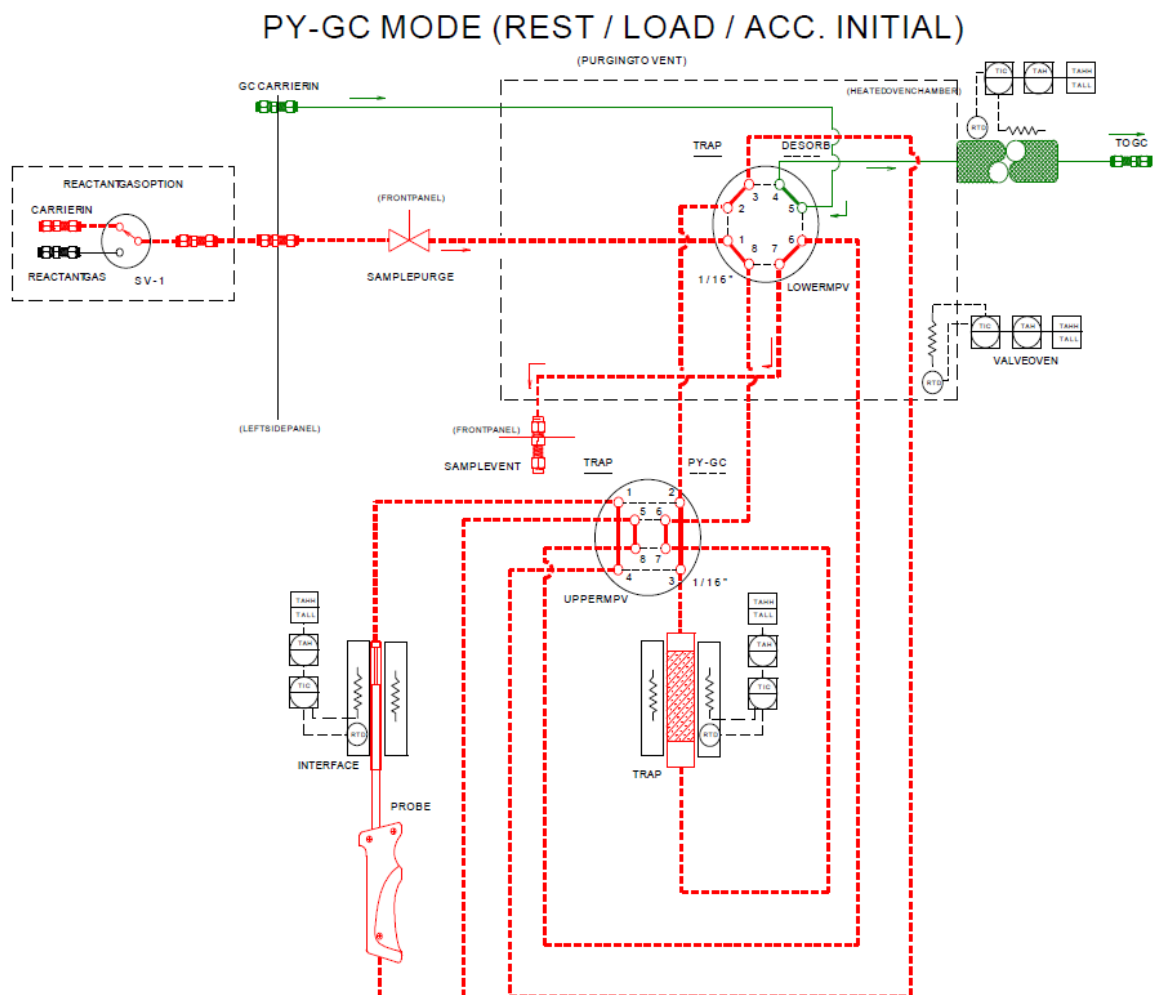


Figure 7. Schematic of the GC carrier- and purge-gas flows for the Pyroprobe® 5200 during the interface's rest and initial phases while set to Py-GC mode. (This image is from page 3.14 of CDS Analytical's manual for the Pyroprobe® instrument series. It is copied here with permission.)

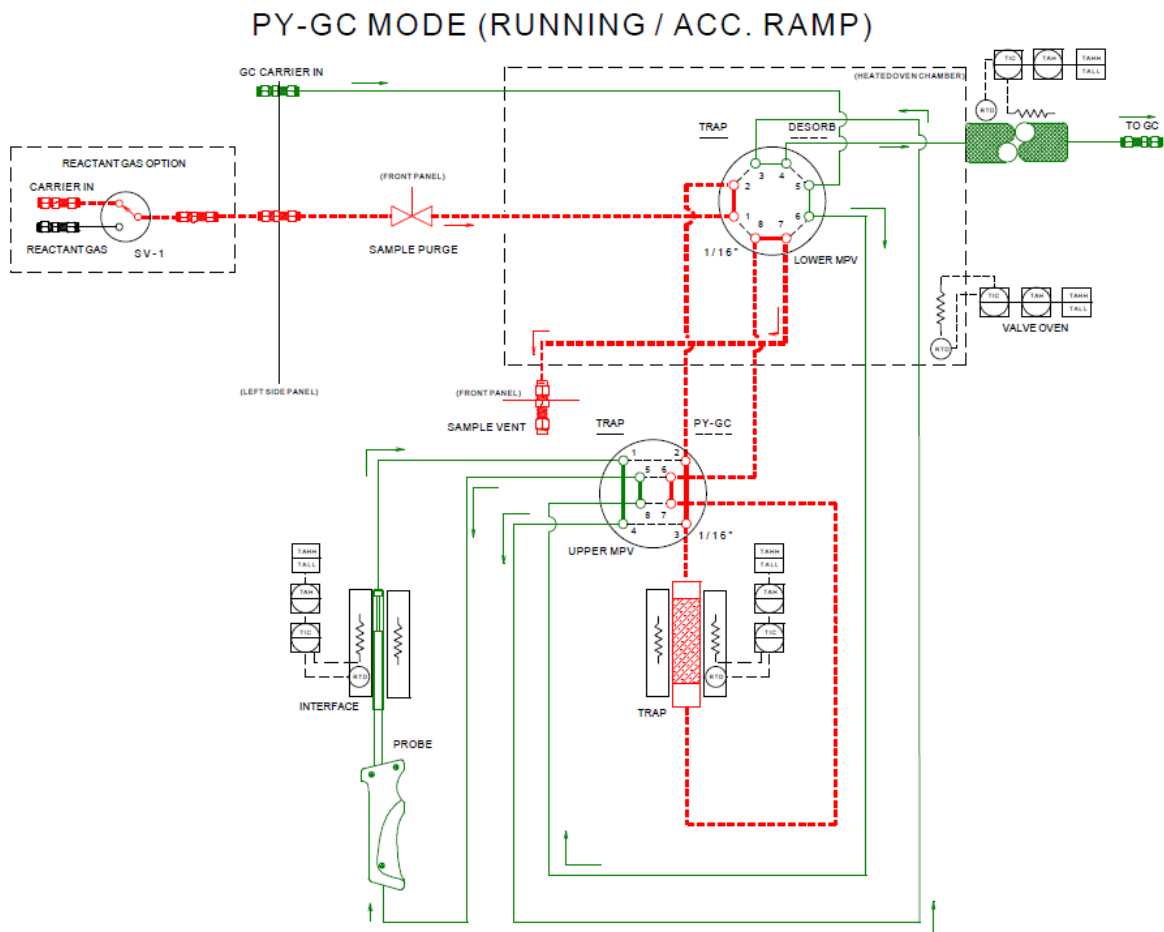


Figure 8. Schematic of the GC carrier- and purge-gas flows for the Pyroprobe® 5200 during the interface's ramp and final phases while set to Py-GC mode. (This image is from page 3.15 of CDS Analytical's manual for the Pyroprobe® instrument series. It is copied here with permission.)

The Pyroprobe® micropyrolyzer was modified to use argon for its purge gas instead of the helium that supplies the GC carrier gas. This modification was done for three reasons. First, it allowed the user to track the quantity of (Ar) purge gas residing in the reaction zone and lines at the instant the Pyroprobe®'s valves switched from flowing purge gas to flowing carrier gas over the pyrolyzing sample. Second, the modification allowed the tracking of time when chromatographically unretained purge gas would reach the mass-selective detector. (Helium purge gas is not detected by the MSD because the MSD's lowest detected mass-to-charge ratio is 5 Da  $e^{-1}$ .) Third, the use of "high-purity" argon (99.998%) instead of GC-

grade helium (99.9995 or 99.9999%) greatly reduced operating costs of Pyroprobe® experiments. Argon will appear in the chromatogram as a large peak with most Pyroprobe® methods, but it does not prevent the identification of co-eluted gases made by the pyrolyzing sample. It is unknown if other laboratories ever modify the purge gas of the Pyroprobe® in the same or a similar manner.

The major components and functions of the Pyroprobe® have been introduced. As mentioned before in this section, they are vital to understanding the design of Pyroprobe® experiments. Particular attention should be paid to the switching of gas flows, and this switching will be discussed again when describing the development of pyrolysis methods in the following section.

### ***2.5.2. Pyrolysis-method parameters for the Pyroprobe®***

The collection of parameters used to control the time-temperature programs of the Pyroprobe® 5200's heated zones, called "pyrolysis methods," varied by the experimental objective. There are five separate heated zones in the Pyroprobe® 5200, and the two heated zones useful to vary during most sets of experiments are the filament and the interface. Both the filament and the interface allow the user to determine their initial temperature and duration, temperature-ramp rate, and final temperature and duration. Due to the built-in programming of the instrument, the time-temperature programs of the filament and interface are not fully independent. Specifically, the filament's time-temperature program begins only at the instant when the interface finishes its temperature-ramp phase and begins its final-temperature phase. The programming controlling the start of the filament powering cannot be adjusted by the user.

The filament is always unpowered while a pyrolysis method is not running. Unlike the filament, the interface remains powered to a rest temperature when a pyrolysis method is not running. The rest temperature phase was selected to be 120°C, a temperature which does not allow reaction for freshly loaded carbohydrate materials. Typically, the interface's initial

temperature was specified such that it could dry samples, and the final temperature was specified to ensure evolved products do not condense.

Pyrolysis methods employed for almost all of this work did not power the filament for reaction, and instead they relied solely on the interface to heat the sample material pyrolysis temperatures. Using the interface alone is possible because it can reach 350°C, which is a temperature higher than where almost all mass loss occurs in TGA/DSC experiments.<sup>26</sup>

Two other heated zones, of the five total heated zones, are the transfer line and the valve oven. These zones were kept at 300°C for all experiments used for conclusions in this dissertation. This temperature was selected because it was above the temperature corresponding to 1,6-anhydro- $\beta$ -D-glucopyranose (levoglucosan) eluting from the chromatograph, and it was assumed to prevent the possibility of levoglucosan condensing. Early experiments where the transfer line and valve oven were kept at 250°C showed evidence of levoglucosan condensing, because this compound remained entirely undetected until the valve-oven and transfer-line temperatures were increased to 275°C.

The last of the Pyroprobe®'s five heated zones is the absorbent-trap heater. If the Pyroprobe®'s external, manual 8-port valve is set to "TRAP" mode, then the pyrolysis products are swept to an absorbent trap where they accumulate. After the pyrolysis reactions finish, the absorbent trap's temperature is increased in order to desorb the products so they all are swept to the GC inlet. This work did not use the trap feature in any experiment, and so this heated zone was unpowered, and the external, manual 8-port valve was kept on "GC" mode instead of "TRAP" mode.

---

<sup>26</sup> 350°C is far below the 400-600°C often seen in experiments with industrial fast pyrolysis in mind. However, 300-350°C is the region showing the maximum mass loss in TGA/DSC experiments of most carbohydrate materials. Since this research project had a goal of matching mass-loss data to product speciation, 350°C was sufficient for the given objectives.

### 2.5.3. *Experimental shortcomings of the Pyroprobe®*

There are several limitations on possible pyrolysis experiments due to compromises made during the design and construction of the Pyroprobe®.

- The inability to sweep only products formed at higher temperature to the GC;
- The inability to alter the reactor flowrate without affecting the comparability of GC analyses;
- The inability to greatly adjust sample quantities without affecting the comparability of GC analyses.

Modifications might eliminate these limitations, but some of these modifications, namely the programming of instrument communications, would be very complicated and likely quite costly.

The first limitation worth mentioning is the inability to create a pyrolysis method which sweeps to GC the vapors formed only at higher temperatures (i.e., vent the reaction products formed during lower temperatures). As previously noted, the interface switches from receiving purge gas to receiving GC carrier gas only when the interface finishes its initial-temperature phase and begins its temperature-ramp phase. In addition, the interface switches back from receiving GC carrier gas to receiving purge gas only when the final-temperature duration finishes. This gas-flow switching is due to how the Pyroprobe® 5200's internal 8-port valve is permanently programmed, and hence the gas-flow switching cannot be adjusted by the user to take place at different instants during the pyrolysis method. Also, recall how when the interface receives purge gas, all of the sample vapors are swept to the vent, but when the interface receives GC carrier gas, all of the sample vapors are swept to the GC. The permanent timing of gas-flow switching precludes the creation of pyrolysis methods that sweep only higher-temperature reaction products to the GC-MS for analyses. Such methods of segregating products formed at different temperatures would be particularly useful for investigating temperature-dependence of reactions because this segregation helps simplify the GC separation of the very complex mixtures. Unfortunately, the Pyroprobe®

does not provide a way to segregate products formed during different temperature ranges of a controlled ramp (or different time ranges of a temperature duration).

The second limitation is the inability to adjust reactor flowrate and GC carrier gas independently. This limitation is due to how the Pyroprobe® was designed so its interface is swept by GC carrier gas during pyrolysis reactions. A GC's carrier gas flowrate is specified to enable an effective GC separation<sup>27</sup> and is not specified for other purposes like a reactor's performance. Gas flowrate through a reactor affects important properties like vapor residence time and velocity-dependent behavior like heat and mass transfer. Using the same gas flow for the GC separation and the Pyroprobe® interface compromises the ability to test the effect of reactor flowrate because doing so inherently affects the separation quality and peak areas of the resulting set of chromatogram.<sup>28</sup>

Using the same GC method for each Pyroprobe® presents yet another experimental limitation. It is desirable to alter sample quantity as a way to test size-dependent behavior like heat and mass transfer within the assembled particles of starting reactant. However, changing sample size greatly alters the quantity of vapor products swept to the GC for an identical pyrolysis method. Using one GC method limits sample quantity to sizes which produce separated and acceptably sharp chromatographic peaks within the dynamic range of the instrument.<sup>29</sup> Smaller quantities of starting reactant will form some key analytes below detection limits while larger quantities of starting reactant will cause column overloading with other key analytes. If the same GC method must be used to compare peak sizes

---

<sup>27</sup> For an effective GC separation, the column, split, and septum-purge flow rates are each set to make the most important analytes elute as sharp peaks with signal heights within the dynamic range of the mass-selective detector. Specifying these three flow rates thus specifies the total GC carrier gas flowrate for a GC method.

<sup>28</sup> The same GC method must be used for each experiment in order for peak areas to be compared quantitatively.

<sup>29</sup> Changing the split ratio to account for different injection quantities alters the inlet's "discrimination" between different analytes. Just like in the case of changing other GC parameters, an entirely new set of analyte standards would be required for quantitative results after changing the split ratio.

effectively for a set of Pyroprobe® experiments, then sample quantity cannot be altered greatly to observe transport effects conclusively.

It is highly desirable to modify the Pyroprobe® so that the GC carrier gas is not used as the sweep gas during reaction. Instead, the purge gas could always sweep through the interface and then to a six-port valve and a sample loop. This six-port valve would inject the pyrolysis vapors to GC. Performing such a major modification to the Pyroprobe® would eliminate some compromises between GC-separation effectiveness and reaction-control flexibility. In such a case of having independent GC-carrier gas flow and reactor sweep gas flow, the flowrate-dependent effects could be observed with consistent and effective GC separations.<sup>30</sup> Using the GC carrier gas as a reactor sweep gas, in any instrument, is an issue addressed in the recommendations. It is highly recommended to avoid such a design compromise with all future reactors meant to investigate chemical reactions and their rates.

Frustratingly, having such a desirable modification and being able to observe flowrate effects would only allow semi-quantitative understanding of those potential flowrate effects. The lack of strong quantitative results is due to how the gas flowrate actually passing through the quartz tube is impossible to measure and difficult to estimate accurately. Recall that the probe's tip creates an open annular region around the quartz tube. The gas flow sent through the interface is divided between the quartz tube and the annular region, but determining what fraction goes through the quartz tube is left to a rough estimate.

Rough estimates for the fraction of carrier-gas flowing through the quartz tube were made in an effort to create bounds on residence-time ranges. The maximum flow fraction through the quartz tube was estimated as 0.176, which is the ratio of open cross-sectional areas for the quartz tube and sum of the quartz tube and annulus. Such a fraction likely was

---

<sup>30</sup> Testing large differences in sample quantity may still require changing the GC method, as the split ratio would need to be adjusted so key analytes are above detection limits yet not overloading the analytical column. A device which alters the injected volume, such as a set of different-volume sample loops, might allow the same GC method to reliably analyze Pyroprobe® experiments with large differences in sample quantity.

the upper bound of gas flow through the quartz tube, as the quartz tube had an increased resistance to fluid flow due to loaded quartz wool and reactant material. The residence times of the quartz tube and annulus are plotted as functions of the fraction of carrier gas passing through the quartz tube in Figure 9 and Figure 10. For all possible experimental temperatures, the quartz tube shows a very sharp decrease in residence time when its fraction of flow varies between 0 and 0.02. In this region, the residence time is much too slow and risks obfuscating the reaction products with gas-solid reactions and continued vapor-phase decomposition of initial products. However, the residence time in the quartz tube is below 0.83 s when the flow fraction through the quartz tube is 0.04 or greater at a temperature of 200°C. This residence-time value is important because it removes products from the quartz tube at a similar rate to the 50°C min<sup>-1</sup> (0.83°C s<sup>-1</sup>) temperature ramp rate used for experiments. Furthermore, from flow fractions of 0.04 to 0.20, the residence time only changes by much smaller fractions as flow fraction changes.

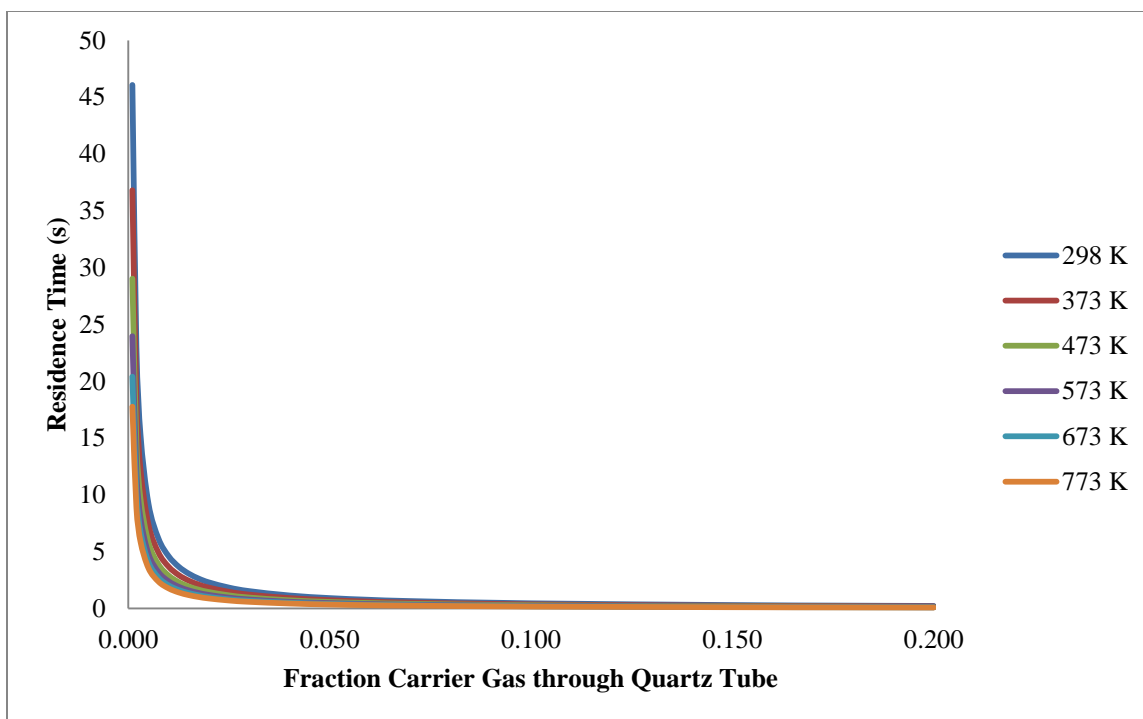


Figure 9. Residence times of the quartz tube as a function of fraction of carrier gas blowing through each zone. A flow fraction of 0.176 is the upper bound of possible fractions, as it represents zero flow restriction caused by quartz wool and sample material.

Meanwhile, the annulus residence times remain below 0.4 s, and these residence times are faster than the interface's temperature ramp rate used in comparing model compounds ( $0.83^{\circ}\text{C s}^{-1}$ ). In the case of reaction vapors diffusing in the radial direction at the outlets of the quartz tube, the annulus should quickly sweep them to the transfer line. Therefore, the annulus presents no obfuscation of the temperature dependency of reaction products with the experiments used.

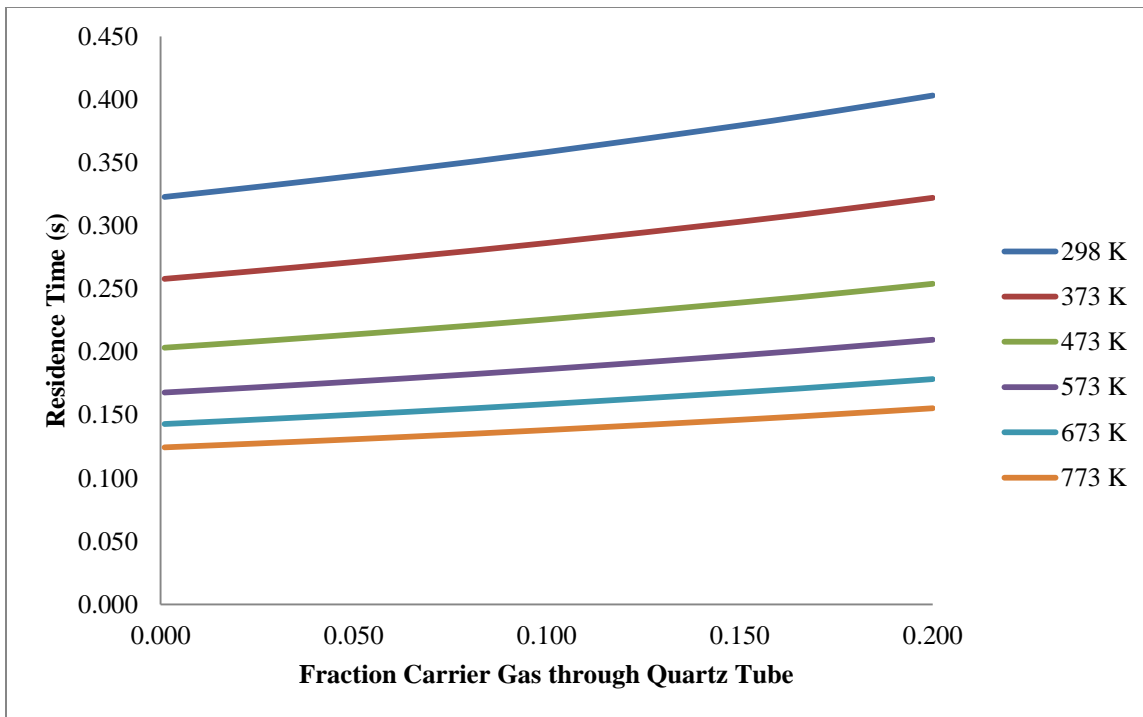


Figure 10. Residence times of the annular region as a function of fraction of carrier gas blowing through each zone.

In conclusion, some highly desirable Pyroprobe® experiments could not be performed due to limitations in the Pyroprobe® 5200's fundamental design. These highly desirable experimental capabilities are

- Sampling vapors formed only from higher reaction temperatures or longer duration periods
- Altering reactor flowrate without significantly altering the GC method
- Altering sample quantity without significantly altering the GC method
- Alter (or even estimate accurately) the vapor residence time accurately given the design of the probe tip

These experimental methods are not possible because of two main reasons.

- The user cannot adjust the time when gases are sent to GC for analyses independently of the interface heating method
- The Pyroprobe® uses the GC carrier gas to sweep the inlet during reaction.<sup>31</sup>

Modifications to solve these shortcomings would be very serious due to the missing hardware, closed control code, and difficulty in updating the necessary electronic communications between the Pyroprobe®, the PC, and the GC-MS for custom operation.

#### ***2.5.4. Cumulative-sampling technique to match TGA/DSC temperature intervals***

The Pyroprobe® experiments should pyrolyze the samples in as close a manner as possible to the TGA/DSC experiments so the Pyroprobe® experiments could serve as an artificial way to sample vapor composition of the TGA/DSC experiments. By matching the temperature-ramp rates used by both pieces of equipment, the Pyroprobe® experiments were assumed to produce identical compositions to those in the TGA/DSC experiments. Assuming identical compositions allowed the weight-loss and heat-flow data to be matched with GC-MS analyses of vapor products, and this combination allowed the net formation of specific product species to be calculated.

Creating experiments which allow such matching of TGA/DSC data and Pyroprobe® data required a method of experiments which could sample specific temperature regions of the Pyroprobe® interface's temperature-ramp phase. The Pyroprobe® has no way of doing so, and so the "cumulative-sampling technique" was developed for Pyroprobe® experiments. This cumulative-sampling technique used a series of very similar Pyroprobe® experiments for each reactant material of interest. The same initial Pyroprobe® temperature, the same temperature-ramp rate, and the same gas-chromatographic, mass-spectrometric, and data-processing methods were used for each experiment in the series. However, different

---

<sup>31</sup> Recall that this work alone distinguishes GC carrier gas from purge gas within the Pyroprobe® 5200. CDS Analytical's equipment manual calls both of the separate gas streams "carrier gas." This work not only distinguishes carrier gas and purge gas, but it also uses argon, instead of helium, for the purge gas.

experiments within a given series pyrolyzed the reactant samples to different final temperatures. Therefore, each chromatogram within the series of pyrolysis experiments showed the product vapors formed between an identical initial temperature and different final temperatures. Differences between the chromatograms' products species and quantities were due to the product vapors formed during the "difference" in the experiments' temperature ranges. This cumulative sampling technique is named after how each chromatogram shows the cumulative amount of pyrolysis vapors, and differences between a series of cumulative chromatograms show what vapors are formed during a temperature interval of interest. The cumulative-sampling technique is necessary because the Pyroprobe® is incapable of sampling only specific temperature intervals of a temperature-ramp's phase,<sup>32</sup> and this technique is what ultimately enabled the artificial chemical analyses of specific temperature ranges within TGA/DSC experiments.

#### ***2.5.5. Matching total-mass differences between TGA/DSC and Pyroprobe® experiments***

It was desirable to compare the total change in sample mass between TGA/DSC and Pyroprobe® experiments. Finding a similar mass loss would ensure reaction conversions (and hence, rates) are in fact similar between the two pieces of equipment when both specified the same reaction conditions.<sup>33</sup> In the TGA/DSC, the sample mass is continuously monitored and recorded, so the mass is known at any instant, including the final temperature. In the Pyroprobe®, only the cumulative change in sample mass can be measured, which is measured by weighing the sample tube before the experiment and after the experiment. At first consideration, it sounds sufficient to use the difference in sample-tube mass. However, there is likely a parasitic loss of volatiles when removing the hot sample tube from the interface after the final temperature was reached. The sample tube must be removed immediately to cool the tube and minimize the amount of sample pyrolyzing when the

---

<sup>32</sup> The Pyroprobe®'s nonadjustable programming sends all vapors formed after the interface's initial-temperature phase, including all of the temperature-ramp phase and final-temperature phase, to GC-MS analysis. These phases cannot be subdivided into sampled and nonsampled regions.

<sup>33</sup> Here "conditions" refers to the initial temperature, final temperature, and temperature ramp rate. Flow rates, and hence fluid velocities, could not be made identical.

interface cools from its final temperature to its rest temperature – a time over which hot vapors will be sent to GC inlet. There are no visible vapors seen above the hot sample tubes upon their removal, so there is likely not a massive quantity of pyrolyzing vapors lost to the surrounding airspace and so not sent to GC inlet.

The pyrolysis methods, which used a constant temperature ramp rate and have their total change in mass matched to mass-loss in TGA/DSC experiments, proved to be problematic. At the end of the final-temperature phase, the Pyroprobe® always does two things. First, its internal 8-port valve switches the GC carrier gas to bypass the interface and reintroduces purge gas to sweep any vapors to the vent. Second, the interface begins cooling rapidly back to its rest temperature. These two nonadjustable actions cause two corresponding consequences. First, because of the purge gas switching, any vapor products formed after the interface's final-temperature phase will be swept out the vent and will not be swept to the GC inlet for analysis. Second, because of the interface's rapid cooling, any product vapors formed very near the end (or after) the final-temperature phase might condense on the inner surfaces of the interface. The latter happened to a severe extent in the case of 1,6-anhydro- $\beta$ -D-glucopyranose (levoglucosan), which deposited and continually contaminated many early experiments where the presence or absence of levoglucosan was absolutely critical.<sup>34</sup>

To minimize any continued pyrolysis while the interface cools from its final temperature back to its rest temperature, the probe was removed immediately upon the internal 8-port valve switching back to the "REST/INITIAL" position. (Waiting for the valve to return to its REST/INITIAL position ensured GC carrier gas was not interrupted by air, which could damage the GC's analytical columns and the MS ion source.)

---

<sup>34</sup> These critical experiments were repeated, so the results of this work are not hindered by detectable experiment-to-experiment contamination.

### **2.5.6. Loading Pyroprobe® sample tubes**

All Pyroprobe® experiments used to make quantitative comparisons among different model compounds employed the same process to load starting reactant into the quartz tubes. This loading procedure worked by making a “tube assembly,” which was a quartz tube holding unmodified solid sample reactant between two plugs of quartz wool held in place by friction. The procedure of making these tube assemblies was to insert the first quartz-wool plug, insert the reactant sample, and then insert second quartz-wool plug. This procedure is very common for the Pyroprobe®, but it is described in fine detail here because loading procedure can affect profoundly any conversions, yields, or selectivities based upon the measured masses of starting reactant or residual solid product.

Cleanliness was vital to the process of loading tube assemblies. Clean nitrile gloves are always used for this entire process. Care was taken to ensure finger oils were not deposited upon any parts of the quartz tube, quartz wool, or sample. This avoidance of finger oils included not allowing the gloves to touch surfaces previously touched by ungloved hands, as deposited finger oils (or other contaminants) may be picked up by the gloves. Metal instruments like tweezers and scoopulas were cleaned before use to remove finger oil, dust, or traces of other starting reactants. These strict “cleanliness rules” ensured the purity of starting reactants remained as received from the vendors, and pyrolysis experiments were not the result of inadvertent contamination within the laboratory.

The most difficult part of loading the tube assemblies was creating and inserting the quartz-wool plugs. The quartz wool comes as a random, loose clump in a paper envelope from CDS Analytical, Inc. It is similar in appearance to a stretched ball of cotton. A small piece of quartz wool was pulled from the main clump of quartz wool by gently pulling off a ~0.5-cm piece with tweezers. This removed piece of quartz wool was stretched and elongated due to the pulling process, and it has many fibers/strands extending from where it was once attached to the main clump.

To form the removed piece of quartz wool into a quartz-wool plug, it was folded lengthwise two to three times with the tweezers and a gloved finger and thumb. Once the piece was roughly 1 cm in length, one side of the quartz-wool piece was gently rolled back and forth between the thumb and finger. This rolling action was done to “sharpen” one end of the quartz wool piece so it may be partially inserted to the quartz tube’s 1.9-mm open end. Since the piece of quartz wool could not fit entirely into the quartz tube, a “ram-rod tool” was used to push the quartz-wool piece entirely into the quartz tube. To get the quartz-wool piece entirely in the quartz tube requires several gentle pushes and repositioning of the ram tool. (This step also took finesse and practice.) Once entirely inside the quartz tube, the ram tool “compresses” the quartz-wool plug against a (gloved) finger covering the quartz tube’s far end. The quartz-wool plug is reduced to roughly 0.5 to 1.0 cm in length, but the fibers are only made dense enough to ensure particles cannot be blown out of the quartz tube during experiments. The quartz-wool plug is meant to add as little resistance as possible to gas flow within the quartz tube.<sup>35</sup>

With the first quartz-wool plug in position, the starting reactant was loaded into the quartz tube next. Starting reactant was added by dropping it into the quartz tube’s end from a folded piece of weighing paper. A piece of weighing paper was folded in half and then unfolded so a crease was left down the center of the weighing paper. The desired quantity of sample reactant was placed on the crease of the weighing paper. The weighing paper was folded again along its crease in order to leave the starting reactant inside. In one hand the quartz tube (with a single quartz-wool plug inserted) was held with tweezers so the quartz tube was vertical with the plug at its bottom side. The folded weighing paper was held by the edge made from two joined sides in the other hand. The bottom folded corner of the weighing paper was brought to and rested on the top of the quartz tube’s opening. The folded weighing paper was turned from horizontal to almost vertical while tapping it lightly against

---

<sup>35</sup> Recall that the vapor residence times within the quartz tube are shorter if the quartz tube has less resistance to gas flow.

the quartz tube. This tilting and tapping allowed most of the starting reactant to fall out of the weighing paper and into the quartz tube's opening. It was very rare for this process to transfer all of the starting reactant into the tube, especially with finer powders like cellulose.

Controlling the quantity of starting reactant added to the quartz tubes is particularly difficult. It is difficult because of several reasons.

- Particle size and apparent density changes drastically between starting reactants (e.g., glucose has much larger, denser granules than cellulose, and therefore several glucose granules can add the same mass as a clump of cellulose powder.)
- Static electricity caused fine powders like cellulose and cellobiose to cling to the weighing paper and the walls (internal and external) of the quartz tube.
- Pouring sample from weighing paper into the quartz tube's end was difficult because the weighing paper must be lightly tapped to cause the powders to move. This tapping motion caused some of the powders to miss the quartz tube's opening and fall outside of the quartz tube. This problem complicates "pre-weighing" the sample quantity on the weigh paper to ensure adding the proper quantity of sample to the quartz tube.

A second quartz-wool plug was added to the tube to hold the starting reactant in place. This second quartz-wool plug is made in the exact same fashion as the first quartz-wool plug. Care was taken when compressing the second to not push any of the first quartz-wool plug out of the tube, as doing losing any quartz-wool or starting material would make the previous mass measurements inaccurate.

This tube-loading process was repeated as closely as possible for each quartz tube to limit its variations from affecting vital comparisons between the desired experimental factors like starting material and temperature program. However, variation among loaded quartz tubes was inevitable in certain aspects. Holding powdered starting material between two quartz-wool plugs caused inherent variation in the starting materials' exact radial and axial position. The radial position always varied from being suspended at the tube's axis to resting

against the tube's inner wall ( $0 \text{ mm} \leq r \leq 1 \text{ mm}$ ). The axial position usually varied by up to 8 mm from the tube's center ( $z = \pm 8 \text{ mm}$ ) due to how the powder materials could somewhat intersperse with the loose quartz wool. Heat transfer to the starting material was expected to differ significantly with these variations in position due to the poor thermal conductivity of gas and quartz wool. Use of the filament for fast heating rates is expected to exacerbate these differences in heat transfer rates. Difference in heat transfer along the axial dimension was certainly observed during early experiments which used the filament for rapid heating.<sup>36</sup>

Care was taken to handle and transport the loaded quartz tubes in a very gentle manner so any loss of the quartz wool and solids was kept to a minimum. However, some quartz wool would inherently be lost during experimentation. Such loss of quartz wool was first reported by Ronsse et al., and it was confirmed by a series of experiments in this work [22].

It was attempted to load starting materials into the quartz-tubes by dissolving the solids, then allowing capillary action to "pull" a droplet of solution throughout a single quartz-wool plug placed in the middle of the quartz-tube. The liquid solvent would be left to evaporate, leaving a more uniformly dispersed starting material. Such a "liquid-loading" procedure would also reduce the time needed to make sample tubes because it would eliminate a stage of adding and weighing a quartz-wool plug. While monosaccharides would dissolve in water and methanol, cellulose would not.<sup>37</sup>

It was also attempted to load the non-soluble cellulose by a liquid suspension in water, but this suspension method also failed. The suspension's "concentration," (i.e., the

---

<sup>36</sup> Brown residue seen on the inside surfaces of used quartz tubes suggested tars formed during pyrolysis condensed on the quartz tube's walls outside of the filament region when Pyroprobe® methods incorporate the filament for heating. The cooler temperatures toward the quartz tube's ends suggest any starting material migrated towards the ends would not be subject to the same temperature as sample material near the center of the tube's axial length.

<sup>37</sup> Methanol and propan-1,2,3-triol were tested as solvents because, like cellulose, they had alcohol functional groups.

quantity of cellulose “held” within a droplet) was exceedingly difficult to control. In addition, depositing a droplet of suspension through the narrow (1.9-mm ID) quartz tubes and to the center of the tube was not repeatable.

Even though monosaccharides could be dissolved and distributed throughout a plug of quartz wool, the inability to load cellulose as a solution or suspension meant that all materials had to be loaded in their powder form for a proper reaction comparison.

## ***2.6. Pulse-Injected Deactivated Stainless-Steel Reactor***

The pulse-injected deactivated-stainless-steel reactor (PIDSSR) is a simple flow reactor which was built to pyrolyze volatile model compounds. Volatile compounds evaporate and escape the heated zones of the TGA/DSC and Pyroprobe® instruments. These compounds partially (or entirely) escape shortly after loading into the instrument, and sometimes they partially (or entirely) escape as the main heated zone approaches the desired reaction temperature. As a result, experiments with the TGA/DSC and the Pyroprobe® can fail to produce any reaction products. If reaction products are formed, it is difficult to estimate how much starting reactant remained in the heated zone upon reaching a desired set-point temperature. By design, the PIDSSR evaporates these compounds in its inlet and flows the vapors through a reaction zone already set to the desired reaction temperature.

There are four key benefits of the PIDSSR when compared to other pyrolysis flow reactors.

- It avoids the accumulation of carbonaceous deposits because it only reacts a single pulse of compound for each experiment.
- It precludes the need for a long transfer line because it is assembled directly upstream of the GC inlet.
- It precludes the need for a six-port sampling valve and associated components because it only reacts a single pulse of compound in a steady stream of carrier gas.
- It uses the gas chromatograph’s built-in flow controls to adjust residence time.

Drawbacks to the PIDSSR are inherent to some of its beneficial simplicity.

- The untestable assumption that volatile compounds turn entirely to gas in the inlet and do not enter the reactor tube as an aerosol.
- A flow characterized by low Reynolds numbers and Péclet numbers, which prevents the use of plug-flow reactor models.
- An axial temperature gradient measured only at three positions (5, 25, and 45 cm from the reactor tube entrance).
- A potential for user error during injections.
- Difficulty accurately measuring the injected quantities of viscous compounds like diols and triols due to stubborn bubbles in the syringe's needle and barrel before and after injection.
- The use of GC carrier gas as the reactor sweep gas, which sacrifices adjusting reactor flowrate for chromatographic repeatability.<sup>38</sup>

These drawbacks make the PIDSSR a poor tool for measuring reaction kinetics based upon precise product yields and time-temperature history. Then again, the flow characteristics and residence time of the reactor is more easily estimated than those for the TGA/DSC and Pyroprobe® instruments because it has a very simple geometry and is entirely gas phase in its reaction zone. While failing to be an accurate and precise chemical-kinetics tool, the PIDSSR is an inexpensive, simple, and robust qualitative tool.

### ***2.6.1. PIDSSR construction***

The construction of the PIDSSR was a combination of simple components: it was an inlet assembly, a reactor tube, and a short transfer line to the GC inlet. The reactor inlet

---

<sup>38</sup> As for the Pyroprobe®, the sweep-gas flowrate of the PIDSSR also could not be varied without affecting the quality and comparability of subsequent GC analyses. Such a design compromise is appealing for equipment-cost reasons, but it is highly recommended to avoid such a design for future reactors meant to investigate chemical reactions and their rates. This issue is addressed in the recommendations section of this work.

assembly was a 3/8-inch-to-1/4-inch stainless-steel Swagelok® reducer fitting. Inside the tube fitting was a GC septum held in place by a steel washer on the septum's external side. This washer was held in place by a short length of tube swaged into the fitting. The inlet assembly connected to one of two straight runs of a 1/4-inch stainless-steel Swagelok® tee. On the branch of the tee is a 1/4-inch outer diameter stainless-steel tube which delivers helium carrier gas to the reactor from the GC flow controller. On the 1/4-inch tee's remaining straight run, opposite of the reactor inlet, is the reactor tube. Figure 11 shows an exploded view of the inlet assembly.

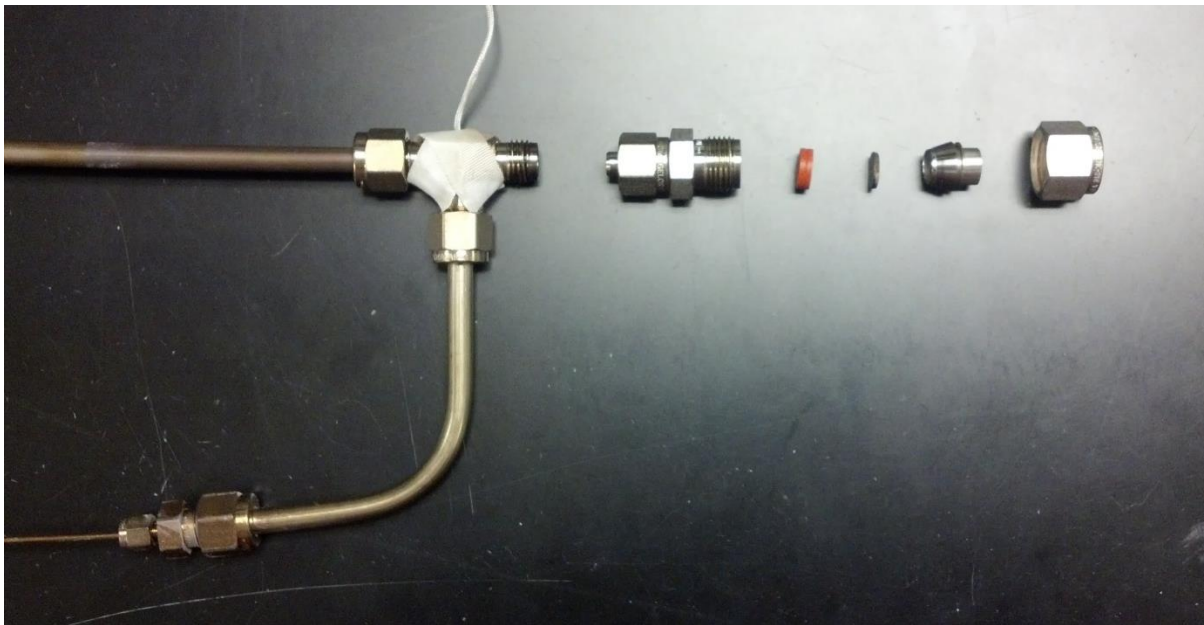
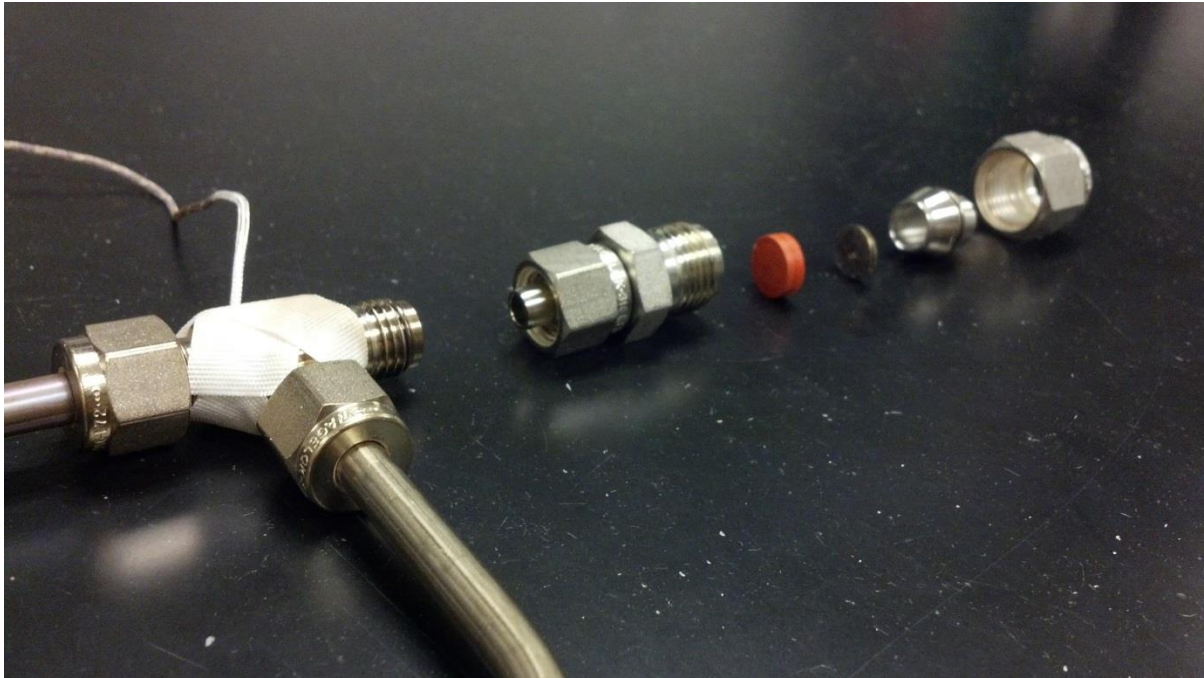


Figure 11. The exploded view of the PIDSSR inlet shows how the orange GC septum is secured in the 1/4-inch-to-3/8-inch union. The short length of ferruled tubing (second from right) presses the septum into the 3/8-inch cavity. A washer (third from right) was carefully filed down to fit into the 3/8-inch cavity and evenly apply pressure to the septum.

The PIDSSR's reactor tube is a 50-cm length of 1/4-inch outer diameter 304 stainless-steel tube. This tube has a proprietary coating called "Silcosteel®-Hydroguard"<sup>39</sup> (Catalog # 22492, Lot # 505760-492, Restek Corporation, Bellefonte, Pennsylvania, USA). The Silcosteel®-Hydroguard was described by SilcoTek® technical support as two separate coatings. The first coating is a ~1/4 micron "amorphous-silicon" layer applied to the 304 stainless-steel surface, and the second coating is a "silyl-group" layer applied after the amorphous-silicon layer. (It was not disclosed by Restek Corp. whether the silyl groups are attached to the amorphous silicon layer by silyl-ether bonds or silicon-silicon bonds. It is possible the silyl groups are attached via silyl-ether bonds, due to elemental silicon being unstable in air during transport from SilcoTek® to Restek Corp.). This Silcosteel®-Hydroguard coating was designed to prevent transfer lines and vessels from altering the composition of samples containing polar analytes. Because the Silcosteel®-Hydroguard coating can withstand temperatures up to 400°C, it was selected for use in the PIDSSR.

The PIDSSR's 1/16-inch outer-diameter transfer line was rinsed-and-cleaned 304 stainless-steel tubing with no surface coatings. (Catalog # 21506, Lot # 520186-506. Restek Corp.) This was the same tubing used in the construction of the transfer-line sampling system.

The PIDSSR is heated by two electric heating elements. A small heating tape warms the carrier gas feed before it reaches the branch of the 1/4-inch tee. A rope heater extends from the 1/4-inch tee, along the reactor tube, and along transfer line until reaching the GC inlet. The rope heater lays directly against the steel tubes in an axial fashion. Three passes of the rope heater extend along the reactor tube, and two passes extend along the transfer line. Thermocouples were placed at the 1/4-inch tee, along the reactor tube at 5, 25, and 45 cm

---

<sup>39</sup> While the final coated tube was purchased from Restek Corp, the first Silcosteel® coating was actually applied to a 304 stainless-steel tube by SilcoTek®, which is a Restek Corp spinoff company. SilcoTek® sells this Silcosteel®-coated tube to Restek Corp., but SilcoTek® actually refers to Silcosteel® as SilcoNert® 1000. The SilcoNert 1000® does not include the "Hydroguard" layer, which is applied by Restek Corp.

from the entrance of the reactor tube, and on the transfer line. Thermocouples were placed directly against the tube but adjacent to the rope heaters, and care was taken to make sure the thermocouples were not between the rope heaters and the tube. This placement was done to ensure the thermocouples measured the tube's temperature and not the heating rope's temperature.

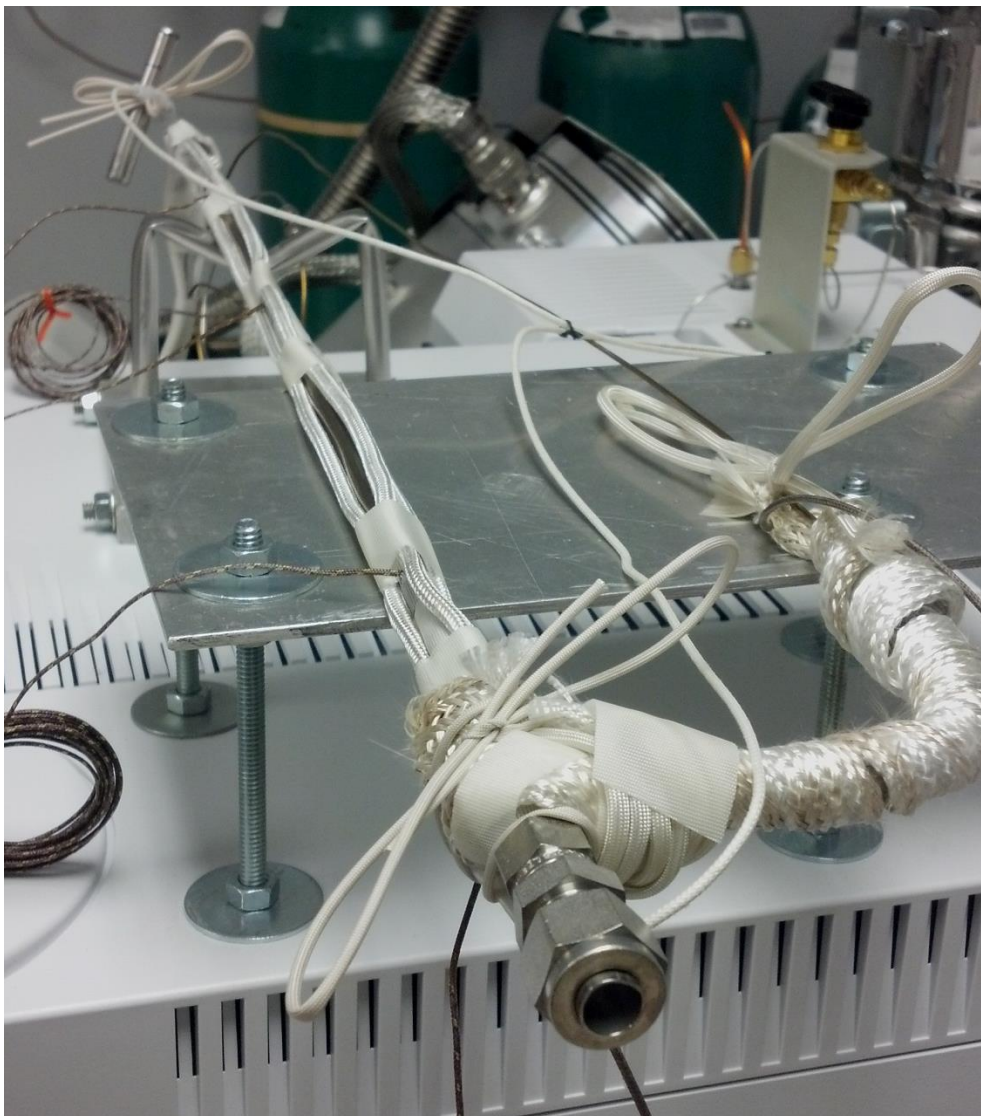


Figure 12. The partially assembled PIDSSR shows its components most easily. Here it has heating elements fixed in place, but it is yet to be wrapped with insulation. In this image, the carrier gas flow enters the inlet from the right. The sample is injected to the inlet through the open tube, where the septum is accessed. The reactor tube is shown on the far side of the 1/4-inch tee (not visible due to heating elements).

Fiberglass insulation webbing was wrapped around the heating elements. The 1-inch wide webbing was applied in a helical fashion, where each rotation overlapped the previous

rotation by 1/2 inch. Two of these helical layers, proceeding in opposite directions, were placed over the reactor tube. One helical layer was placed over the carrier gas feed line, inlet, and transfer line. The fiberglass insulation was subsequently encased by aluminum foil to prevent the fibers from shedding onto equipment surfaces and users.

### **2.6.2. *Operating the PIDSSR***

Operating the PIDSSR was very simple. The variacs were adjusted manually to achieve the desired reactor temperature. After obtaining the desired temperature, an injection was made and the GC-MS method was started immediately.

Test compounds were injected into the PIDSSR manually by a GC syringe (Model 1701, Hamilton Company, Reno, NV, USA). Very few injections to the PIDSSR were made by the typical use of syringes, where the plunger is depressed to force liquid in the syringe barrel out of the needle. Instead, injections were made by allowing some fraction of liquid in the metal needle's dead volume to evaporate as the needle sat in the PIDSSR's warm inlet. To measure the quantity injected by evaporation, the volume of liquid held within the needle was checked before and after the injection to determine the difference in liquid volume. The volume was checked by holding the syringe vertically with the needle upwards and the plunger fully depressed. Liquid was drawn into the syringe barrel, and the graduated marks on the glass barrel were used to determine the volume of liquid held within the syringe's needle. The total dead volume within the metal needle was 0.75 to 0.80  $\mu\text{L}$ , and so the liquid was usually checked by drawing the plunger down to the 1.0  $\mu\text{L}$  mark on the syringe's barrel.

The quantity of injected starting reactant was difficult to control. The temperature of the PIDSSR's inlet and the duration of time for which the syringe's needle resided in the inlet had pronounced effects upon the volume injected. Often several PIDSSR experiments were conducted to inject the desired volume of liquid successfully, but these several additional experiments test the compound several times at several quantities and bring additional confirmation of results. Using the GC syringe in this manner led to the realization that the

real injected volumes of volatile materials are often not what was indicated by the graduation marks on the syringe barrel.

### ***2.7. Comprehensive Two-Dimensional Gas Chromatograph Time-of-Flight Mass Spectrometer***

The GC-MS used in this study was a comprehensive, two-dimensional gas chromatograph time-of-flight mass spectrometer (GCxGC-TOFMS). This GCxGC-TOFMS instrument was a Pegasus 4D model from LECO Corporation (Saint Joseph, Michigan, USA). LECO Corp. built the TOFMS, but they did not build the GC (Agilent Technologies model 7890A, Santa Clara, California, USA). LECO fitted a thermal modulator and a secondary oven to the 7890A GC to enable a GCxGC capability. The entire instrument was operated by LECO Corp.'s ChromaTOF® software.

Two-dimensional gas chromatography refers to the use of two different chromatographic phases used during one separation method. Two-dimensional methods are used when some analytes of interest co-elute and prevent accurate identification or quantification. For some two-dimensional methods just a portion of the analytes is sent to a second column by a mechanical valve; e.g., a “Deans switch.” For other two-dimensional methods the entire injected sample passes through to columns in series, and this general method gathers the added distinction of “comprehensive, two-dimensional gas chromatography,” which gets the special abbreviation “GCxGC.”

Some polar compounds can front and tail during GCxGC methods due to the thermal modulator. They may not fully desorb from the cool zones in the thermal modulator. A prime example is water, but other compounds like diols, triols, and phenol also tail during GCxGC methods designed for apolar hydrocarbons.

It is important to note that after using the PIDSSR, it was realized that many previous injections (on various projects) to the GC inlet were underestimated. Past GC injections used only the difference in plunger position from one graduation mark to the zero graduation

mark, and these injections did not consider the additional volume held within the metal needle. Because many of these injections used a volatile solvent and a hot GC inlet, it is likely that some material from the syringe's needle entered the GC inlet in addition to what was contained in the syringe barrel.

## ***2.8. Pulse-Injected Quartz Reactor***

A second type of pulse-injected reactor was used twice to test pyrolysis reactions of volatile alcohols. Quartz tube was used because it could determine if deactivated stainless steel caused any catalytic effects. To distinguish this new quartz reactor from the PIDSSR described previously, it was named the pulse-injected quartz reactor (PIQR) for this work.<sup>40</sup>

The PIQR has several advantages over the PIDSSR for obtaining elementary chemistry of alcohol pyrolysis. First, as already mentioned, the reactor tube is made of quartz. Unlike the proprietary Silcosteel®-Hydroguard deactivation coating, quartz is a well characterized material many researchers consider as inert. Due to these inert characteristics, quartz is used frequently in reactor studies, making the chemistry conclusions of the PIQR experiments more easily accepted by fellow researchers. In addition, the quartz allows experimenting with temperatures above 400°C, which was the maximum temperature of the Silcosteel®-Hydroguard coating. Second, reactant injection is performed by a sample loop and an automated six-port valve. Using these valves instead of a manual syringe likely makes the injections more repeatable. Third, the reactant was evaporated in a bubbler upstream of the sample loop, and thus the reactant was injected to the reactor entirely as a vapor. Injecting only vapor in the PIQR eliminates concerns of potential droplet behavior had with the PIDSSR. Fourth, the use of the QMS allowed continuous analysis of the reaction peak.<sup>41</sup>

---

<sup>40</sup> This PIQR is owned by and resides in the laboratory of Professor Fanxing Li. Often they call it simply as the “pulse reactor,” because they have no need to distinguish it from the PIDSSR of the Westmoreland laboratory.

<sup>41</sup> The GC-MS used with the PIDSSR could not characterize the peak as a function of time because it inherently integrated the peak's species into tight bands at the entrance of the analytical column.

Continuous analysis provided information about the pulse's shapes, and doing so allowed the inspection of the injection's quality.

There were some disadvantages of the PIQR compared to the PIDSSR. First, its tubing and six-port valve could not be heated, and thus could not sustain high vapor pressures of liquid reactants. This temperature limitation precluded experiments with reactants which were not very volatile at room condition. Second, the lack of any chromatographic separation made it difficult or impossible to deconvolute ions made by two different chemical species. The "mixing" of all of the spectra meant that experiments were limited to reactants which pyrolyzed to products all with fairly different ion spectra.

### ***2.8.1. PIQR construction***

While the purpose of the PIQR was to react volatile compounds in the same manner as the PIDSSR, the PIQR was constructed in a very different manner. The PIQR is a U-shaped quartz tube sitting vertically in a cylindrical furnace. This reactor is fed with helium purge gas, and reactant vapor is introduced through a sampling loop connected by a six-port valve. A bubbler sent the vapor mixture to the sample loop by vaporizing the liquid reactant with flowing argon. A quadrupole mass spectrometer (QMS) continuously monitored the reactor's effluent. Compared to the PIDSSR, the PIQR brought the key advantages of a quartz reaction vessel and continuous measurement of the product pulse.

The reactor tube was made by Prism Research Glass (Raleigh, NC, USA). The U-shape was made by bending a 1/4-inch OD quartz tube (Figure 13). The internal diameter was measured at the ends to be 3.6 and 4.0 mm, and the mean of 3.8 mm was used for cross-sectional area and volume purposes. The outer diameter was measured to be 6.2 mm. The length of the entire U shape is 22.5 cm, and the length of the straight parallel tubes is 21.0 cm. The center-to-center distance of the parallel tube runs is 2.8 cm. A solid rod connected the parallel tube runs 5 cm from the open ends of the tubes for structural support. The total internal volume of the U-shape was 5.76 cm<sup>3</sup>. The U-shape did not fit entirely in the furnace

cavity, and 8 cm of the straight-tube portion sat outside of the furnace cavity and was held by a ring-stand clamp (Figure 14). The volume of tube residing inside the furnace was  $3.95 \text{ cm}^3$ .

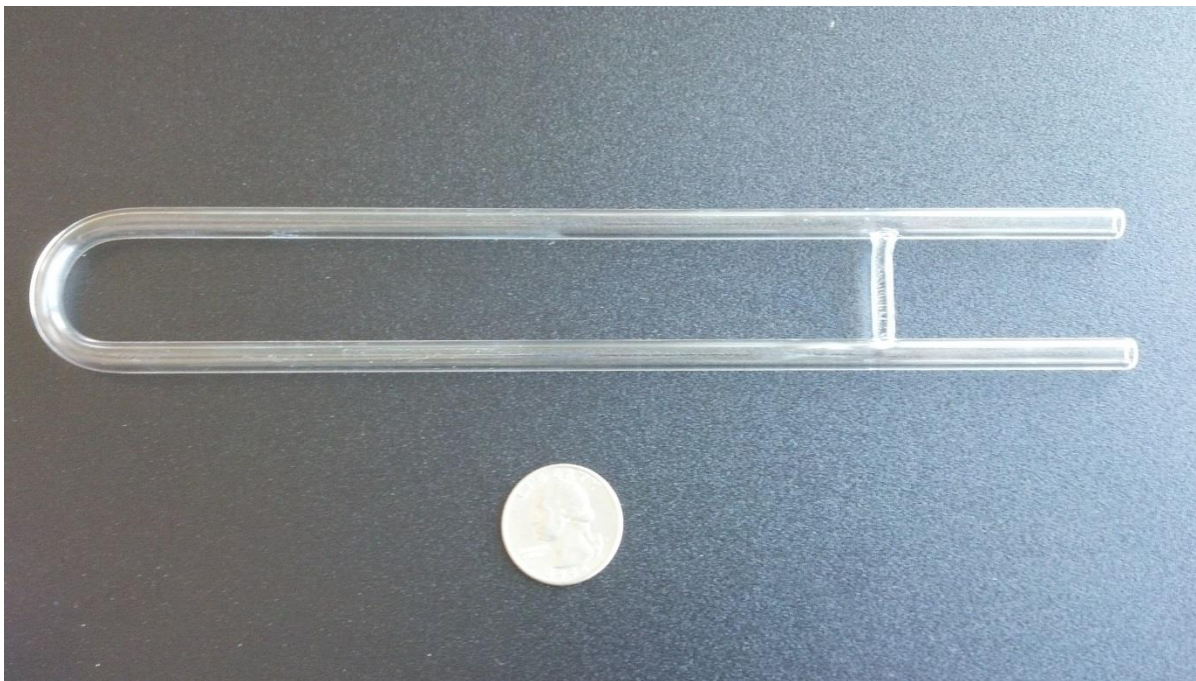


Figure 13. The U-shaped quartz tube with a US 25-cent coin for size reference.

The furnace configuration was of a vertical, regular cylindrical cavity with a depth of 16.8 cm. It was marked with “Serial # 21-104083,” but it was of unknown manufacturer. It had a maximum temperature of  $1150^\circ\text{C}$ . The thermocouple’s tip was at a depth of 9.5 cm (from cavity opening). As mentioned, the U-shape did not fit entirely inside the furnace cavity. Because temperature was not measured along points of the quartz U-tube, the extent of temperature gradients along the tube axes was unknown. It was possible that the portion of the U-tube’s volume within the furnace cavity ( $3.95 \text{ cm}^3$ ) was close to the furnace’s thermocouple temperature due to the heavy insulation surrounding the cavity and the poor

conductivity of quartz. However, the U-tube's volume outside of the furnace likely had large temperature gradients along the tube axes since this portion of the U-tube was also exposed to the direct cooling of ambient air.



Figure 14. Approximately 8 cm of the U-tube extended out of the furnace cavity. Part of the 8 cm was covered by the white insulation used to cover the furnace cavity.

Reactant vapors were mixed with flowing argon in an upstream “bubbler.” This bubbler was a vessel designed to force a steady flow of argon to form bubbles which rose through the liquid-phase reactant. The bubbles were to facilitate the liquid’s evaporation so the gas may approach saturation. The methanol experiments used a stainless-steel vessel as bubbler, which was connected to the argon feed by a threaded, bore-through NPT-to-Swagelok tube fitting. The propan-1-ol experiments used a 500-mL glass Erlenmeyer flask as a bubbler vessel. The flask was connected to the argon feed by a rubber stopper with a hole bored through it. In each case the metal tube went below the surface of the liquid to cause bubbles. The vapor phase above the liquid was assumed to be fully saturated, although this vapor saturation was not tested.



Figure 15. The stainless-steel bubbler was used during the methanol experiments. A similar bubbler using an Erlenmeyer flask was used for propan-1-ol experiments.

The helium carrier gas flow and the reactant-mixed argon pulses were delivered to the U-tube by 1/8-inch “PTFE” tubing. These 1/8-inch tubes were connected to the quartz U-tube by a reducing 1/4-inch-Ultra-Torr-to-1/8-inch-Swagelok tube fitting. The same type of fitting and 1/8-inch PTFE tubing carried the reactor effluent to a 1/8-inch Swagelok tee. At this tee, the reactor effluent was split to a waste vent and the QMS inlet capillary.

When possible, reactor equipment was cleaned before use. The bubbler and the new quartz tube were flushed with methanol three times before performing experiments. The rest of the equipment was used as-is because opening it to allow any solvent flushing would be very time-consuming on equipment with limited availability.<sup>42</sup>

### 2.8.2. *Quadrupole mass spectrometer*

The quadrupole mass spectrometer (QMS) was an MKS Instruments Cirrus 2 Model. The QMS was fed a fraction of the reactor effluent through a 1/8-inch tee split downstream of the reactor. Between the split and the QMS was a capillary tube that was heated to prevent condensation from accumulating and interrupting the chemical analyses.

The QMS did not collect data for all ions when set to a rate of data collection able to accurately monitor the reaction pulse as a function of time. It could only record spectral data for 15 ion species, which were selected before the start of an analysis. The data from the QMS was exported as text files, which were then analyzed in Microsoft Excel to compare quantities of chemical species.

A great benefit of the QMS used by the PIQR over the TOFMS used by the PIDSSR was the ability to detect ions between 1 and 4 Da  $e^{-1}$ . Ions of 2, 3, and 4 Da  $e^{-1}$  are vital for detecting H<sub>2</sub>, HD, and D<sub>2</sub>, respectively. Such ions were vital for the confirmation of alcohol dehydrogenation suggested by the PIDSSR.

---

<sup>42</sup> The equipment in Professor Li’s laboratory, especially the PIQR and the QMS, was shared by several students. Time was of essence in this shared environment. The experiments in this work had to be done overnight due to full daytime schedules for the QMS.

### **2.8.3. Evaluation of the reactant pulse and the reaction products**

There were two ways to operate the 6-port valve to send pulses to the reactor. The first way was to change the 6-port valve's position once and leave it that way for the remainder of the reaction experiment. This first way, called a "long injection," would require the helium reactor-sweep gas to pass through the sample loop for the remainder of the experiment. The second way to operate the 6-port valve was to switch the position for a very short time, roughly 0.1 seconds, then return the valve to its initial position. This second way, called a "short injection," would only pass the helium through the sample loop for a short time, again, roughly 0.1 seconds. Both long and short injections were used initially, and it was discovered that these two types of injections sent very different quantities of material to the reactor. Long injections produced sharp argon peaks and heavily-tailing methanol peaks. Short injections produced sharp peaks for both argon and methanol. Observing different injection quantities between long and short injections was not anticipated by the laboratory's PIQR's regular operators.

Data was exported as text files to Microsoft Excel where they were analyzed for peak shapes. The individual ions' peak areas were integrated manually using the trapezoidal rule. Peak areas were adjusted for background signal by subtracting an integrated baseline area for the corresponding ion. This baseline area was obtained by gathering an average signal height for each ion. The average signal height was obtained by integrating the ion signal with time outside of the peak, then dividing this integral area by the time duration used for integration.

## **2.9. Balances**

The balance used in this work was XS205 DualRange model (Mettler-Toledo, Columbus, OH, USA).<sup>43</sup> This balance was selected for two reasons. First, it had sensitivity to 0.01 mg, which was the highest sensitivity of all balances with the Department of Chemical

---

<sup>43</sup> This balance was housed in the laboratory of Professor Peter Fedkiw.

and Biomolecular Engineering as well as the Department of Materials Science and Engineering. Second, it was close to an oven for drying samples.

To use this balance, the loaded quartz tubes had to be transported from Engineering Building 1 to the Varsity Research Building, during which time they would absorb moisture in the often humid North Carolina weather. However, the Pyroprobe methods were designed to dry samples at 120°C before starting the pyrolysis reactions to ensure a similar moisture content during experiment. (The TGA/DSC samples did not require drying because each thermogram inherently shows when it is dried to a constant mass.)

### **2.10. *Gaussian 09***

The computational-quantum-chemistry (CQC) simulations were performed with the Gaussian-09 software package. Structures were drawn in GaussView, and then CBS-QB3 calculations were submitted for these structures in Gaussian. Output files for transition states were checked to have one negative frequency corresponding to the atoms involved in the reactions bond fragmentation and/or formation.

## CHAPTER 3. USE OF MCREYNOLDS CONSTANTS FOR ORTHOGONAL GCxGC COLUMN CONFIGURATIONS

### *3.1. Abstract*

McReynolds constants can be valuable aids to determining the chemical-interaction types available to stationary phases. Using McReynolds constants and additional heuristics helps ensure orthogonality. Several GCxGC stationary-phase pairs were tested for separating hydropyrolysis oils, carbohydrate-pyrolysis vapors, and alcohol-pyrolysis vapors in order to improve stationary-phase selection during GCxGC method development. McReynolds constants serve as excellent descriptions for the chemical interactions of available GC stationary phases, and they help guide the selection of stationary-phase pairs in GCxGC. Stationary-phase pairs likely capable of orthogonal GCxGC separations can be proposed by combining stationary phases that each isolate a specific, predominant chemical interaction observed in the key analyte groups.

Orthogonality is not achieved solely by using stationary phases with different McReynolds constants corresponding to functional groups of the highest interest. Three other important heuristics are necessary in addition to using stationary phases of different chemical-interaction types.

- Use a primary column similar in polarity to the bulk of the analytes to prevent primary column overloading.
- Use weaker stationary-phase/analyte interactions in the secondary column to help rapid analyte desorption within the thermal modulator.
- Use the lowest-polarity stationary phase possible (that also prevents column overloading) in order to minimize analysis time.

This GCxGC stationary-phase analysis was not a primary objective of this dissertation, but because the use of McReynolds constants appears to be nowhere else in the GCxGC literature, it is shared here to aid future method development.

### ***3.2. Introduction: The Benefit of GCxGC***

Improving biomass fast-pyrolysis, catalytic-fast pyrolysis, and hydrolysis processes requires better understanding of their fundamental reaction networks [4] [23], [24], [25], [26], [1], [27], [28]. Studying the reaction networks requires separation and identification of many similar species observed in pyrolysis vapors, which is difficult when employing conventional gas chromatography (GC) because many compounds co-elute [4], [29]. In comprehensive, two-dimensional gas chromatography (GCxGC), a secondary column is used to separate compounds which co-eluted from the primary column. A thermal modulator, an integral part of GCxGC, also adds a sharpening effect to analyte peaks [30], [31], [32]. The greatly reduced co-elution and sharpened peaks makes GCxGC well suited to separating complex mixtures encountered in various pyrolysis processes. The importance of GCxGC for pyrolysis applications was directly tested by Fullana et al. [29] and Marsman et al. [32]. These authors observed a marked increase in analytes identified when comparing GCxGC to GC separations of complex pyrolysis mixtures.

A very important decision for a chromatographer designing a GCxGC separation is the selection of stationary phases for the primary and secondary columns. Many so-called “column configurations” have been tested and discussed in the GCxGC literature. However, strong comparisons between reported column configurations are difficult to make because other GCxGC-method parameters, as well as the analyte mixtures themselves, are often not identical. If unable to find a successful column configuration in the scientific literature for a very similar analyte mixture, the chromatographer might follow common recommendations to try an “apolar-polar” configuration. This configuration is often recommended in order to obtain “orthogonal” separations, where there is no obvious correlation between primary and secondary retention times and the entire area of the GCxGC chromatogram is available to

analyte peaks [30]. Dalluge et al. [33] claimed that orthogonality is achieved with an apolar-polar column configuration. Their claim was based upon the argument that analytes are separated by their “volatility” in the primary column, and any co-eluting analytes from the primary column are separated by polar analyte/stationary-phase interactions in the nearly isothermal secondary column. Adding to this hypothesized understanding of GCxGC separation, Phillips and Xu [34] and Venkatramani et al. [35] both suggested the separation with an apolar-polar column configuration was orthogonal because any volatility-based selectivity shared by both stationary phases can be effectively eliminated by using the appropriate temperature ramps for the primary and secondary columns. This thought appears valid and useful, and it helped generate a common suggestion of using an apolar-polar column configuration for orthogonal GCxGC separations.

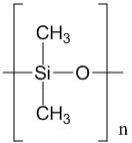
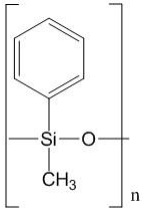
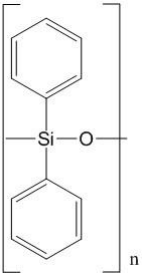
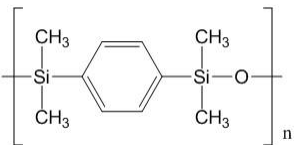
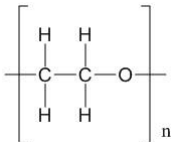
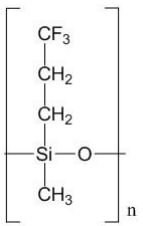
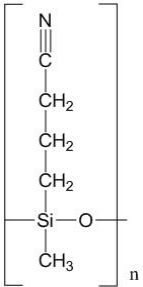
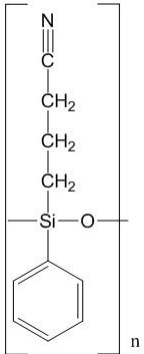
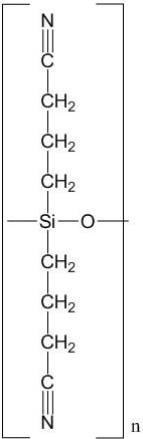
### ***3.3. Characterizing Stationary Phases***

#### ***3.3.1. Describing specific interaction types***

While effective with some analyte mixtures like hydrocarbon mixtures, the apolar-polar suggestion is oversimplified because it relies upon categorizing a set of profoundly different stationary-phase materials into the broad categories of “apolar,” “polar,” and occasionally “midpolar.” Most apolar stationary phases use a high proportion of polydimethylsiloxane due to its high maximum operating temperature (350-400°C maximum) and short retention times. Pure polydimethylsiloxane (PDMS) is considered apolar for GC stationary phases, and its polarity is increased by copolymerizing dimethylsiloxane (DMS) to contain other, more polar, monomer units. Other units commonly found copolymerized into PDMS are 1,4-bis(dimethylsiloxy)phenylene (BDMSP), phenylmethylsiloxane (PMS), diphenylsiloxane (DPS), cyanopropylmethylsiloxane (CPMS), and cyanopropylphenylsiloxane (CPPS). Increased polarity is also commonly achieved by entirely substituting PDMS with different polymers like polytrifluoropropylmethylsiloxane (PTFPMS) and polyethylene glycol (PEG). These repeating polymer units are displayed in Table 1 to highlight their chemical structures. The fact that several different chemical

moieties can be employed for increasing polarity in GC stationary phases suggests more than simple “apolar,” “midpolar,” and “polar” categories are needed for adequate distinction of chemical interactions. Orthogonal GCxGC separations could be designed more effectively with more detailed categories of stationary phase materials and their chemical interactions with analytes.

Table 1. The chemical structures of repeating units for common GC stationary phases. (The monomer units typically copolymerized purposefully do not contain the “poly” prefix, as doing so implies they are a homopolymer. While all of the repeating units carry the subscript “n” for degree of polymerization, it is not implied that n is equal for all of these different polymeric materials.)

<p style="text-align: center;">Dimethylsiloxane (DMS)</p> 	<p style="text-align: center;">Phenylmethylsiloxane (PMS)</p> 	<p style="text-align: center;">Diphenylsiloxane (DPS)</p> 
<p style="text-align: center;">1,4-Bis(dimethylsiloxy) phenylene (BDMSP)</p> 	<p style="text-align: center;">Poly(ethylene glycol) (PEG)</p> 	<p style="text-align: center;">Poly(trifluoropropylmethyl siloxane) (PTFPMS)</p> 
<p style="text-align: center;">Cyanopropylmethylsiloxane (CPMS)</p> 	<p style="text-align: center;">Cyanopropylphenylsiloxane (CPPS)</p> 	<p style="text-align: center;">Bis(cyanopropylsiloxane) (BCPS)</p> 

There are better ways to categorize the polarity of a molecule based upon chemical-interaction phenomena. Distinguishable types of intermolecular attractions are shown in Table 2, and although the categories chosen by each author may differ in name and number, the authors describe the same underlying chemical-interaction phenomena [36, pp. 80-83], [37, pp. 11-14]. Through this brief look at intermolecular chemical interactions, perhaps a more fundamentally sound way to identify orthogonal stationary phases for GCxGC can be hypothesized: Orthogonality in GCxGC is obtained by selecting two stationary phases which will each take best advantage of a different and predominant type of chemical interaction available among the most important analytes of the analyte mixture. In other words, stationary phases providing different chemical interactions tailored to the mixture will have the most appropriate selectivities for producing orthogonal GCxGC separations.

Table 2. Types of intermolecular interactions described by Rotzsche, Barry and Grob, and Kaliszan are matched by the molecular cause of attraction.

Author	Barry and Grob [38]	Rotzsche [36]	Kaliszan [37]
Force/Interaction type	“Keeson orientation forces” (p. 33)	“Orientation forces,” including “hydrogen-bridge bonds” (p. 81)	“Ion-dipole interactions” (p. 12)
			“Dipole-dipole interactions” (p. 13)
			“Hydrogen-bonding interactions” (p. 14)
		“Donor-acceptor interactions” (p. 83)	“Electron pair donor-electron pair acceptor interactions” (p. 14)
	“Debye induction forces” (p. 33)	“Induction forces” (p. 83)	“Dipole-induced dipole interactions” (p. 13)
	“London dispersion forces” (p. 33)	“London-type dispersion forces” (p. 80)	“Instantaneous dipole-induced dipole interactions” (pp. 13-14)

### 3.3.2. *McReynolds constants describe retention with groups of specific interactions*

The chemical interactions of a stationary-phase material, as well as their direct effect on retention times, are well characterized by retention indices. A once-popular system of

retention indices is McReynolds constants  $\Delta I_i$ . These experimentally determined values compare the Kováts index  $I_i^{phase}$  of a test analyte on a particular stationary phase to that test analyte's Kováts index  $I_i^{squalane}$  on a (common reference) squalane stationary phase:<sup>44</sup>

$$\Delta I_{test\ compound\ i} = I_{test\ compound\ i}^{phase} - I_{test\ compound\ i}^{squalane} \quad (3.1)$$

The McReynolds test analytes are shown in Table 2, and these compounds were chosen to target specific groups of chemical interactions. Individual chemical interactions cannot be truly isolated because real test molecules cannot display only one type of chemical interaction. However, the test analytes each contain a functionality that contributes a significant additional interaction. For example, butan-1-ol (Y) shows how replacing a hydrogen atom with a hydroxyl group increases the retention of a four-carbon chain to almost that of a six-carbon chain (590). Pentan-2-one (Z) shows how replacing two hydrogen atoms with a carbonyl oxygen increases the retention of a five-carbon chain to more than that of a six-carbon chain (627). While the London dispersion forces present in alkanes cause attraction, the added functional groups contribute a disproportionate increase in attraction due to their chemical-interaction types. These test analytes help elucidate how functional groups and their chemical-interaction types affect retention on various stationary-phase materials.

The McReynolds constants for common GC stationary-phase materials are shown in Table 3. McReynolds constants are more effective than inspecting the chemical structure of a stationary-phase material than using the structure to predict the most prevalent chemical interactions, their strengths, and their separation capability.

---

<sup>44</sup> The Kováts index is a parameter which relates an analyte's retention time to the retention times of n-alkanes on the same GC system. The use of Kováts indices allows a stronger comparison of retention behavior than simple retention times. The reason is because retention time of a particular analyte varies with differences between GC systems like column dimensions. However, the Kováts index changes very little with differences in GC systems of the same stationary phase.

Table 3. McReynolds test analytes and their associated selectivities. (Recreated from Table 9, page 92 of [36] and Table 2.9, page 40 of Barry and Grob [38])

Stationary-Phase Variable	Test Analyte	Retention Index on Squalane	Test Analyte's Measured Chemical Interaction [38, p. 40]	Analytes Expected to Display Similar Interaction [36, p. 92]
X	Benzene	653	$\pi$ -Electron-donating density	Aromatics and alkenes
Y	Butan-1-ol	590	Proton-donating and -accepting	Alcohols, acids, protic amines, and nitriles
Z	Pentan-2-one	627	Proton-accepting	Carbonyls, ethers, esters, and epoxides
U	1-Nitropropane	652	Dipole interaction	Nitro and nitrile organics
S	Pyridine	699	Proton-accepting (stronger due to nitrogen basicity)	Nitrogen heterocycles
H	2-Methylpentan-2-ol	690	Proton-donating and -accepting, specific to alkyl branching	Branched-chain alcohols
I	1-Iodobutane	818	Dipole interaction	Halogenated organics
K	2-Octyne	841	$\pi$ -Electron-donating density	Alkynes
L	1,4-Dioxane	654	Proton-accepting	Ethers and polyols
M	Cis-hydrindane	1006	Dispersion interaction	Polycyclic compounds, steroids

Table 4. McReynolds constants measured for commercially available stationary-phase materials.

Stationary-Phase Material	Example [Data Source]	Test Analyte	Benzene	Butan-1-ol	Pentan-2-one	1-Nitropropane	Pyridine	2-Methylpentan-2-ol	1-Iodobutane	2-Octyne	1,4-Dioxane	Cis-hydrindane
		Letter	X	Y	Z	U	S	H	I	K	L	M
Squalane	N/L [36, p. 92]	<i>I</i>	653	590	627	652	699	690	818	841	654	1006
		$\Delta I$	0	0	0	0	0	0	0	0	0	0
PDMS, 100%	OV-1 [36, p. 209]	<i>I</i>	669	645	671	717	741	722	822	864	700	1004
		$\Delta I$	16	55	44	65	42	32	4	23	46	-2
p(DPS-co-DMS)5/95	SE-54 [36, p. 221]	<i>I</i>	686	662	693	750	766	736	-	877	-	1074
		$\Delta I$	33	72	66	98	67	46	-	36	-	68
p(DPS-co-DMS) 5.5/94.5 (gum)	OV-73 [36, p. 220]	<i>I</i>	693	676	703	766	784	747	-	880	-	-
		$\Delta I$	40	86	76	114	85	57	-	39	-	-
p(DPS-co-DMS) 33/67	OV-61 [36, p. 220]	<i>I</i>	754	733	769	865	873	789	-	-	-	-
		$\Delta I$	101	143	142	213	174	99	-	-	-	-
p(DPS-co-DMS) 50/50	OV-17 [38, p. 42]	<i>I</i>	772	748	789	895	901	-	-	-	-	-
		$\Delta I$	119	158	162	243	202	-	-	-	-	-

Table 4, Continued.

Stationary -Phase Material	Example [Data Source]	Test Analyte	Benzene	Butan- 1-ol	Pentan-2- one	1-Nitro- propane	Pyridine	2-Methyl- pentan-2-ol	1-Iodo- butane	2- Octyne	1,4- Dioxane	Cis- hydrindane
		Letter	X	Y	Z	U	S	H	I	K	L	M
p(PMS- co-DPS) 70/30	OV-22 [36, p. 220]	<i>I</i>	813	778	818	935	952	823	-	973	882	-
		<i>ΔI</i>	160	188	191	283	253	133	-	132	228	-
p(PMS- co-DPS) 50/50	OV-25 [36, p. 220]	<i>I</i>	831	794	835	957	979	834	-	988	905	-
		<i>ΔI</i>	178	204	208	305	280	144	-	147	251	-
p(PMS- co-DMS) 20/80	OV-3 [36, p. 220]	<i>I</i>	697	676	708	776	787	745	-	887	738	-
		<i>ΔI</i>	44	86	81	124	88	55	-	46	84	-
p(PMS- co-DMS) 40/60	OV-73 [36, p. 220]	<i>I</i>	722	703	738	823	827	767	-	907	774	-
		<i>ΔI</i>	69	113	111	171	128	77	-	66	120	-
PPMS, 100	OV-17 [36, p. 220]	<i>I</i>	772	748	789	895	901	802	-	946	838	-
		<i>ΔI</i>	119	158	162	243	202	112	-	105	184	-
	DC710 [36, p. 221]	<i>I</i>	760	739	780	880	889	860	-	939	828	-
		<i>ΔI</i>	107	149	153	228	190	170	-	98	174	-

Table 4, Continued.

Stationary -Phase Material	Example [Data Source]	Test Analyte	Benzene	Butan- 1-ol	Pentan-2- one	1-Nitro- propane	Pyridine	2-Methyl- pentan-2-ol	1-Iodo- butane	2- Octyne	1,4- Dioxane	Cis- hydrindane
		Letter	X	Y	Z	U	S	H	I	K	L	M
PTFPMS, 100%	OV-210 [36, p. 228]	<i>I</i>	799	828	985	1120	1009	896	957	897	937	1066
		$\Delta I$	146	238	358	468	310	206	139	56	283	60
	OV-202 [36, p. 228]	<i>I</i>	799	828	985	1120	1009	896	-	897	-	-
		$\Delta I$	146	238	358	468	310	206	-	56	-	-
	FS-1265 [36, p. 228]	<i>I</i>	797	823	982	1115	1004	893	-	894	-	-
		$\Delta I$	144	233	355	463	305	203	-	53	-	-
p(TFPMS -co-DMS) 31/69	FS-328 [36, p. 228]	<i>I</i>	708	706	796	867	836	-	-	-	784	-
		$\Delta I$	55	116	169	215	137	-	-	-	130	-

Table 4, Continued.

Stationary -Phase Material	Example [Data Source]	Test Analyte	Benzene	Butan -1-ol	Pentan-2- one	1-Nitro- propane	Pyridine	2-Methyl- pentan-2-ol	1-Iodo- butane	2- Octyne	1,4- Dioxane	Cis- hydrindane
		Letter	X	Y	Z	U	S	H	I	K	L	M
PCPPS, 100%	SP-2300 [36, p. 234]	<i>I</i>	972	1085	1073	1289	1229	1069	-	-	-	-
		$\Delta I$	319	495	446	637	530	379	-	-	-	-
p(CPP-co- DMS-co- MVS) 14/85/1	OV-1701 [38, p. 43]	<i>I</i>	720	760	780	880	870	-	-	-	-	-
		$\Delta I$	67	170	153	228	171	-	-	-	-	-
p(CPMS- co-DMS) 10/90	OV-105 [36, p. 234]	<i>I</i>	689	698	720	791	785	764	-	-	-	-
		$\Delta I$	36	108	93	139	86	74	-	-	-	-
p(CPP- co-BCP) 20/80	SP-2330 [36, p. 234]	<i>I</i>	1143	1315	1257	1565	1477	1256	-	-	-	-
		$\Delta I$	490	725	630	913	778	566	-	-	-	-
PBCPS, 100%	SP-2340 [36, p. 234]	<i>I</i>	1173	1347	1286	1594	1499	1274	-	-	-	-
		$\Delta I$	520	757	659	942	800	584	-	-	-	-

Table 4, Continued.

Stationary -Phase Material	Example [Data Source]	Test Analyte	Benzene	Butan- 1-ol	Pentan-2- one	1-Nitro- propane	Pyridine	2-Methyl- pentan-2-ol	1-Iodo- butane	2- Octyne	1,4- Dioxane	Cis- hydrindane
		Letter	X	Y	Z	U	S	H	I	K	L	M
PEG, 100%	Carbowa x 600 [36, p. 252]	<i>I</i>	1003	1221	1055	1284	1304	1162	1126	1081	1157	1168
		$\Delta I$	350	631	428	632	605	472	308	240	503	162
	Carbowa x 1000 [36, p. 252]	<i>I</i>	1000	1197	1045	1278	1288	1139	1124	1081	1147	1167
		$\Delta I$	347	607	418	626	589	449	306	240	493	161
	Carbowa x 4000 [36, p. 252]	<i>I</i>	978	1141	1002	1234	1219	989	1103	1065	1097	1154
		$\Delta I$	325	551	375	582	520	299	285	224	443	148
	Carbowa x 6000 [36, p. 252]	<i>I</i>	975	1130	996	1229	1211	1080	1100	1063	1091	1153
		$\Delta I$	322	540	369	577	512	390	282	222	437	147
	Carbowa x 20000 [36, p. 252]	<i>I</i>	975	1126	995	1224	1209	1077	1100	1062	1088	1154
		$\Delta I$	322	536	368	572	510	387	282	221	434	148

### ***3.3.3. Using McReynolds constants to select stationary-phase pairs in GCxGC***

McReynolds constants are an excellent source of compiled retention and selectivity data. It apparently is novel to use them to select stationary-phase pairs for GCxGC separations.

### ***3.4. Methods of Comparing GCxGC Column Configurations***

Column configurations were tested in a Pegasus 4D GCxGC-TOFMS (LECO Corp.). The GCxGC portion of the instrument is a standard GC (7890A, Agilent Technologies) fitted with a thermal modulator and a secondary oven. The entire instrument was controlled through Windows software (ChromaTOF, LECO Corp.). This same software also performed the locating of peaks and identification of compounds by automatically comparing mass spectra to library entries.

The GCxGC portion of this instrument has some limitations to the experimental parameters due to its design. The secondary oven's temperature is controlled in a manner which requires it to be at least 3°C hotter than the primary GC oven. The thermal modulator's hot temperature is controlled in a manner which requires it to be at least 5°C hotter than the secondary oven. The fact that these zones must be hotter than the primary oven precludes using secondary columns with low maximum temperatures. The fact that these zones need to be hotter also means that the analytes will have relatively shorter retention times in their second dimension for column configurations which use stronger chemical interactions in the primary column.

The GCxGC methods were optimized for each column configuration to produce the sharpest peaks possible for each combination of analyte mixture and column configuration. These adjustments made it impossible to compare the stationary-phase pairs with identical experimental procedures. However, different strengths of chemical interactions are present between the same analytes and different stationary phases. These different chemic

al-interaction strengths inherently require different GCxGC method parameters like oven temperatures and thermal-modulator temperatures and pulse times.

The TOFMS methods were almost identical for all of the separations. Slight changes in detector voltage and acquisition rate were made throughout the experiments, but such adjustments were only performed to enhance the spectral matching. These adjustments did not affect the separation of the GCxGC system.

Major compromises were made while experimenting with stationary-phase pairs because improving GCxGC science was not a primary objective of this work. The primary goal was to determine pyrolysis chemistry of cellulose, and GCxGC separations were just a tool to better characterize the reaction products. More effective column configurations than those often recommended by manufacturers were needed for the identification of reaction products, so improved understanding of stationary-phase selection was sought. Because some important observations and analyses were performed and appear to be nowhere else in the GCxGC literature, they are shared here.

### **3.5. Results**

#### **3.5.1. *p(DPS-co-DMS)5/95-p(DPS-co-DMS)50/50 showed the expected orthogonality***

The p(DPS-co-DMS)5/95-p(DPS-co-DMS)50/50 stationary-phase pair grouped alkanes into an analyte-homologue group (Figure 16) separated from the remaining analyte types. However, the ketones, alkylbenzenes, alkoxybenzenes, alkylphenols, and alkylPAHs were not arranged in clearly separated homologue groups. The lack of grouping (as well as clearly separated groups) is illustrated in Figure 16 through Figure 21. Note that the steady horizontal streak near the bottom (~ 0.75 s secondary retention time) is an undesorbed quantity of acetone, the solvent used to dilute the hydrolysis oil sample.

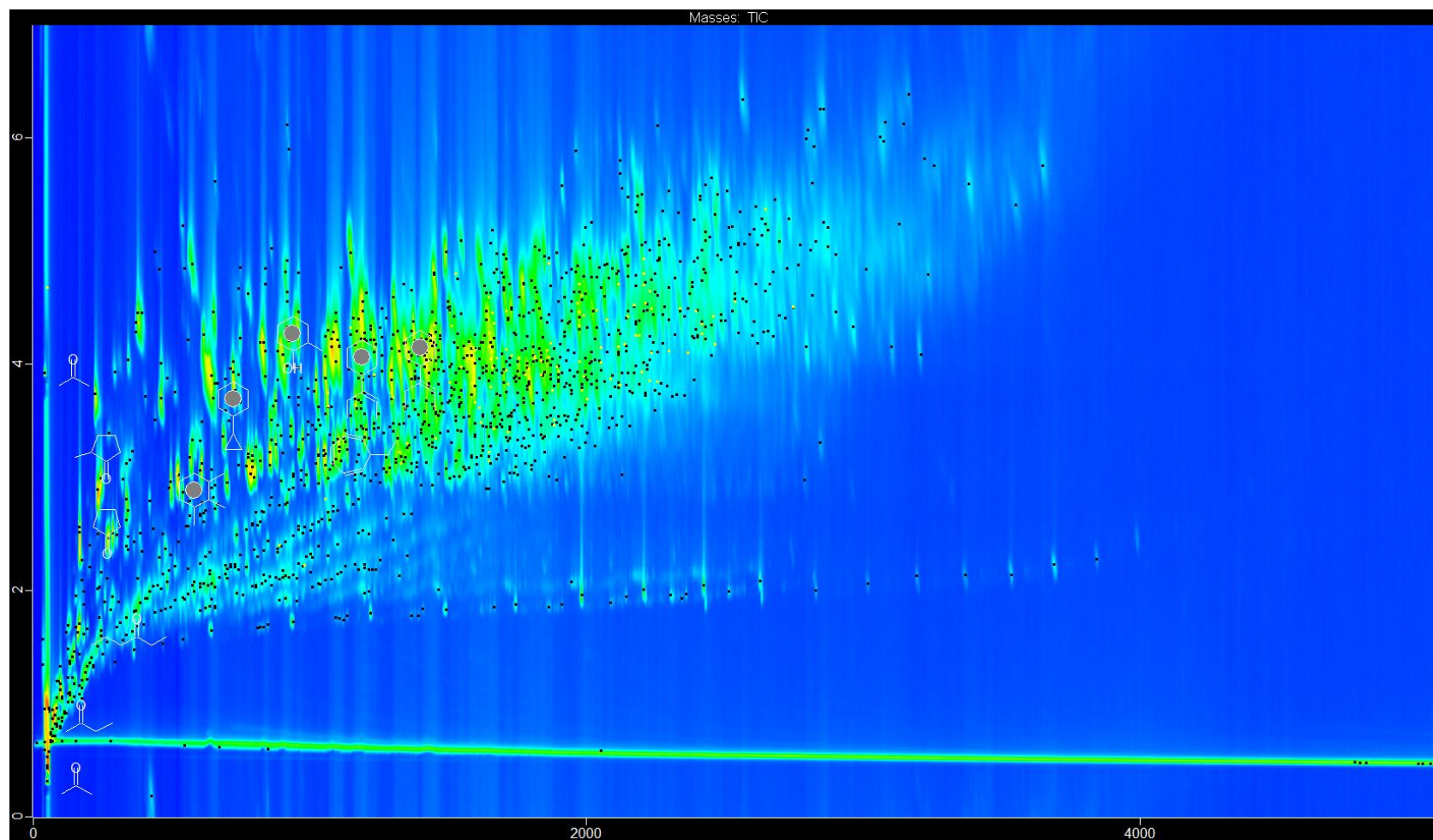


Figure 16. The p(DPS-co-DMS)5/95-p(DPS-DMS)50/50 stationary-phase pair only separated alkanes into a distinguished analyte-homologue group, seen as the peaks at lower secondary retention times than the bulk of the peaks.

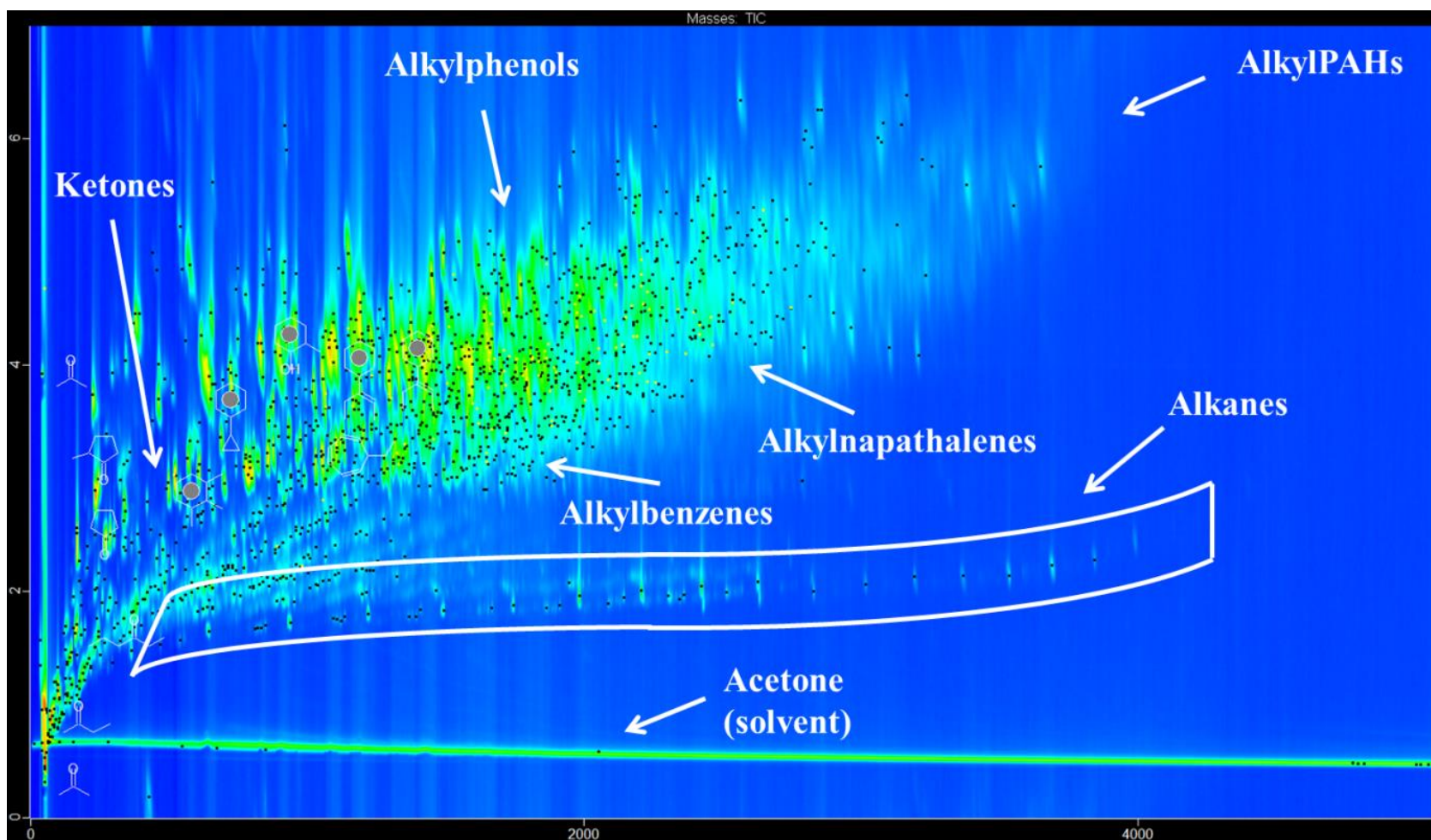


Figure 17. Annotated chromatogram highlighting general regions of analyte homologues. Only the alkanes are grouped and well separated by p(DPS-co-DMS)5/95-p(DPS-DMS)50/50.

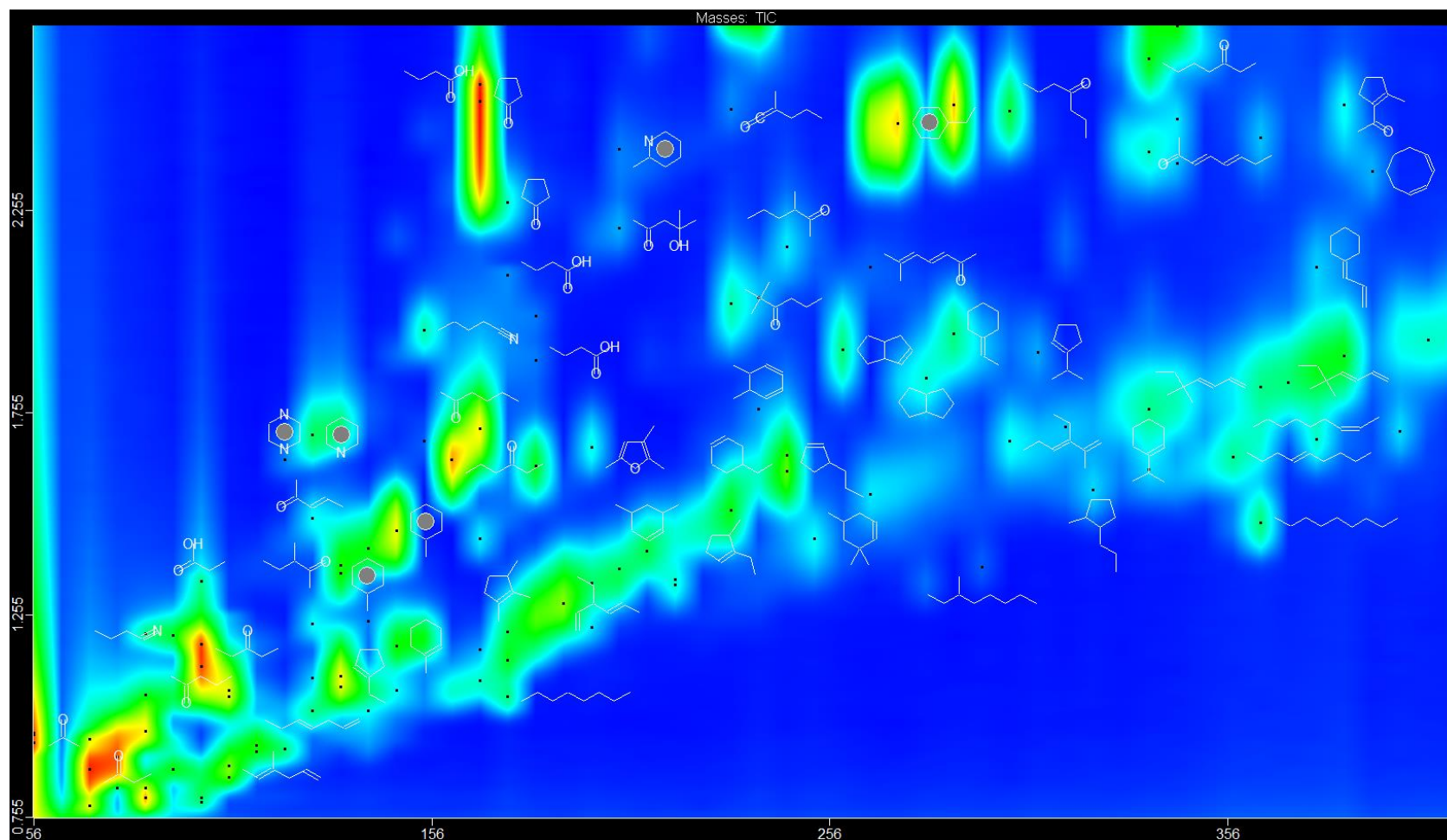


Figure 18. A closer view of the earlier primary-retention-time segment shows how the alkane analyte-homologue group separates from the remaining alkylbenzenes and ketone group.

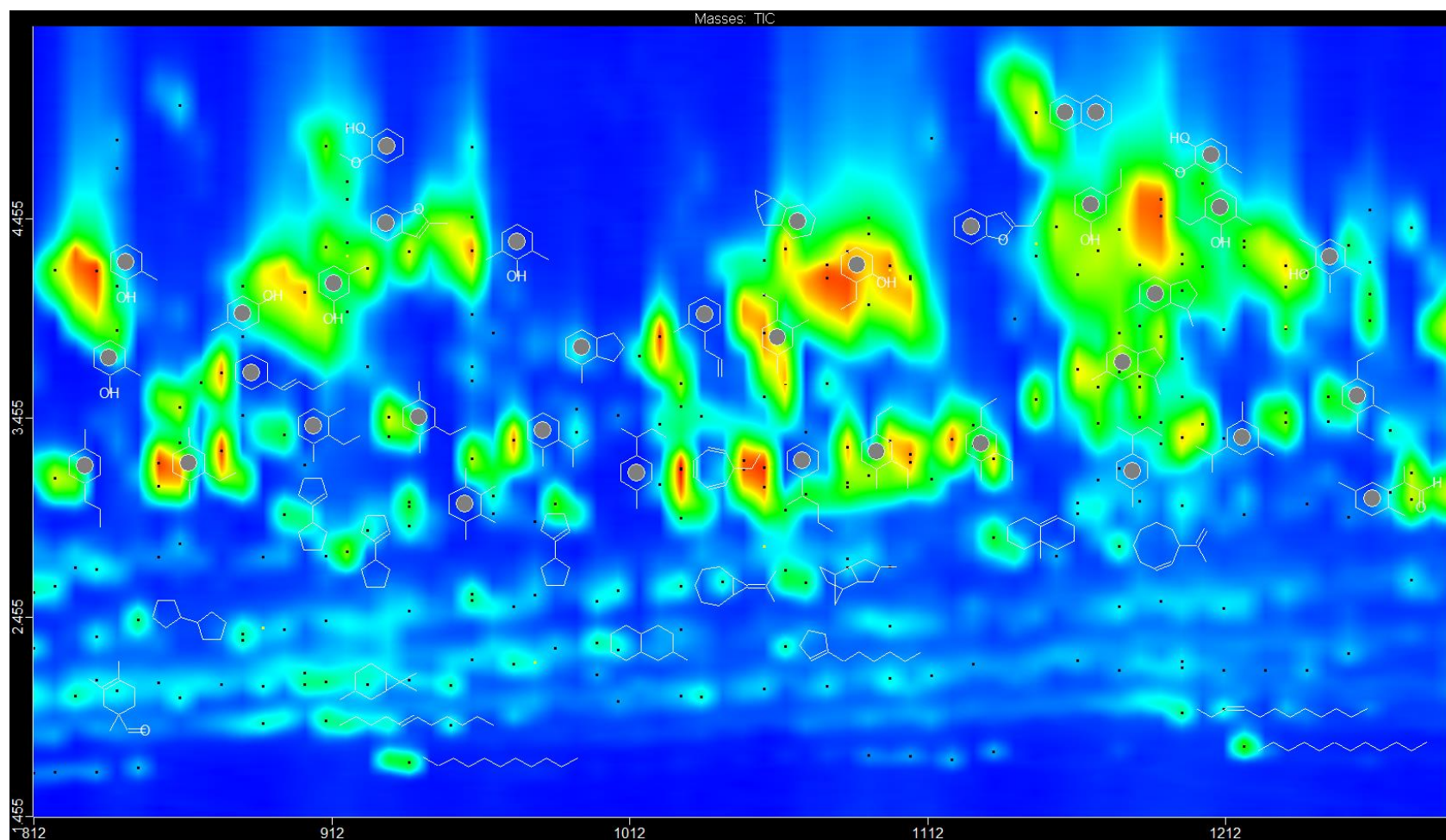


Figure 19. A closer view of the mid primary-retention-time segment shows the alkane peaks well separated from the remaining analytes. There is some slight separation of alkylbenzenes and alkylphenols.

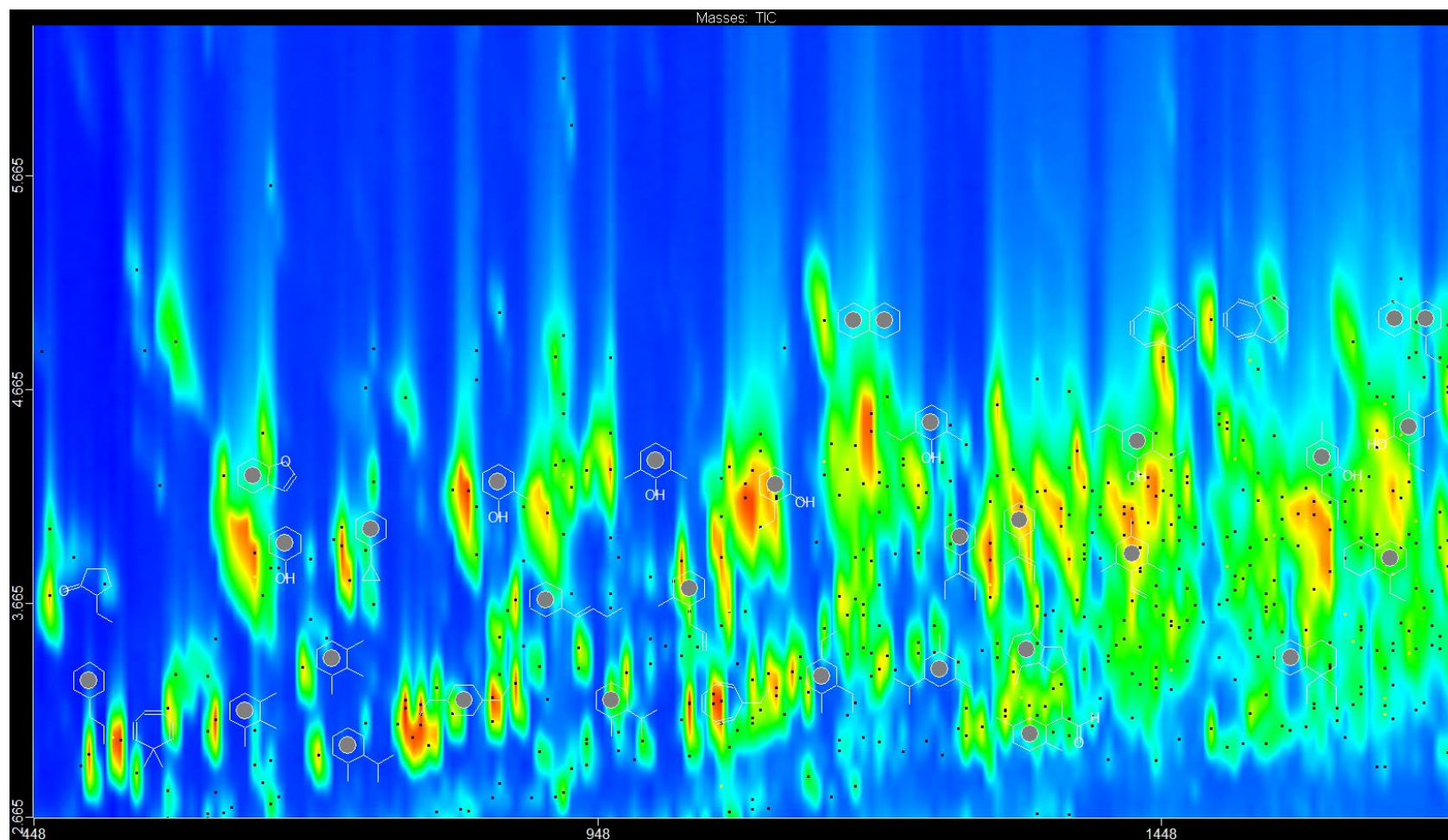


Figure 20. A closer view of the higher secondary retention-time segment shows some slight grouping of the alkylnaphthalenes, alkylnaphthalenes, and alkylphenols, but no large separation between groups.

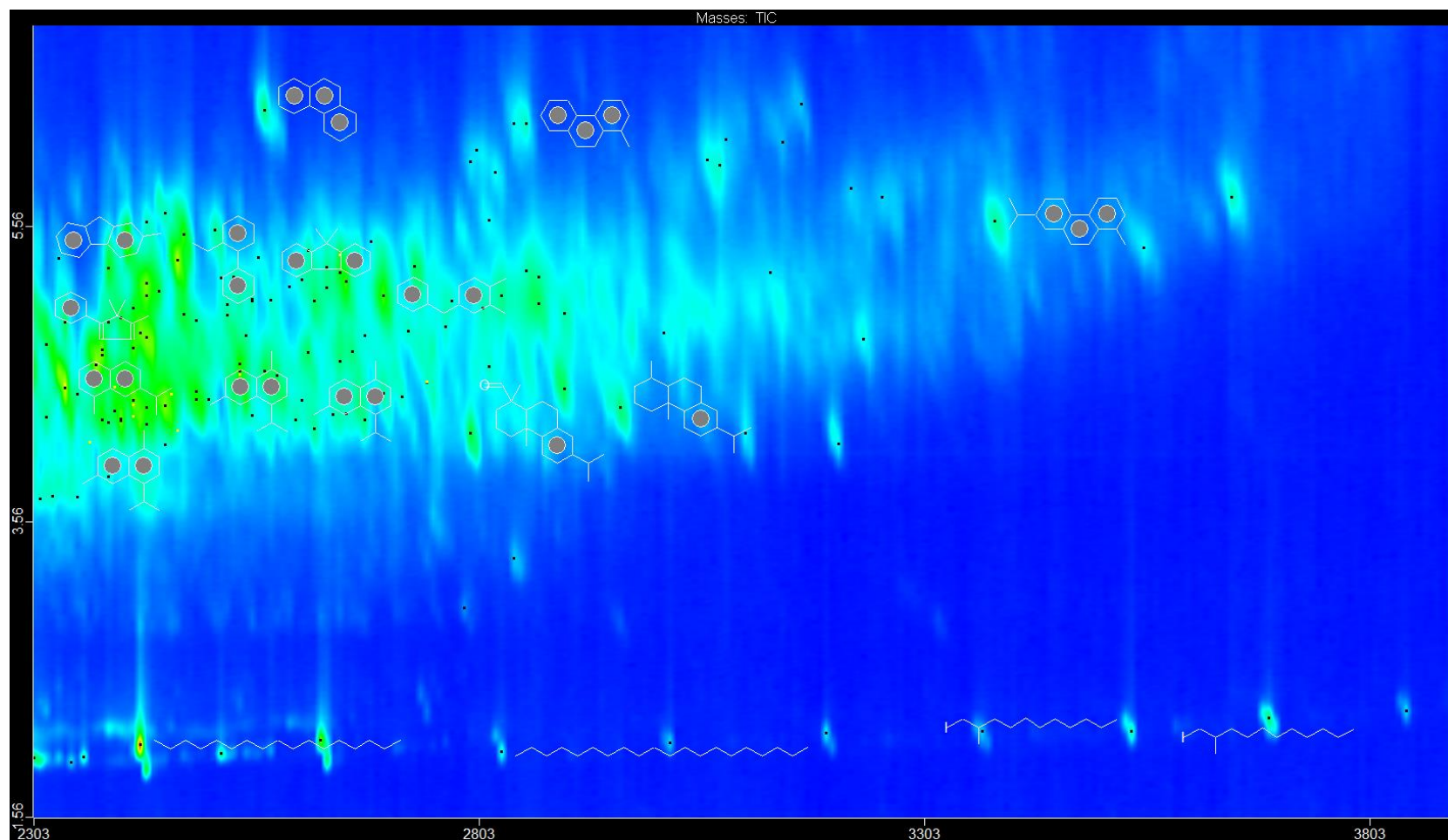


Figure 21. A closer view of the later primary retention-time segment shows the alkylnaphthalenes and alkylPAHs, but no clear grouping or separation between groups.

### ***3.5.2. PTFPMS-p(BDMSP-co-DMS)5/95 stationary-phase pairs show orthogonality and analyte grouping***

The PTFPMS-p(BDMSP-co-DMS)5/95 stationary-phase pair separated hydrolysis mixtures very well. It grouped the analytes into well distinguished sections on the 2D chromatogram (Figure 23). The secondary retention time clearly shows a demarcation among the alkanes, alkylbenzenes, alkylphenols, and ketones. There was overlap between analyte groups in two instances. First, analytes eluting before 200 s (of primary retention time) have not yet dispersed into vertically separated groups, as the relatively warmer secondary oven has weak selectivity for early primary-eluting analytes. Second, the alkylnaphthalenes begin to elute in the same region as the alkoxybenzenes.



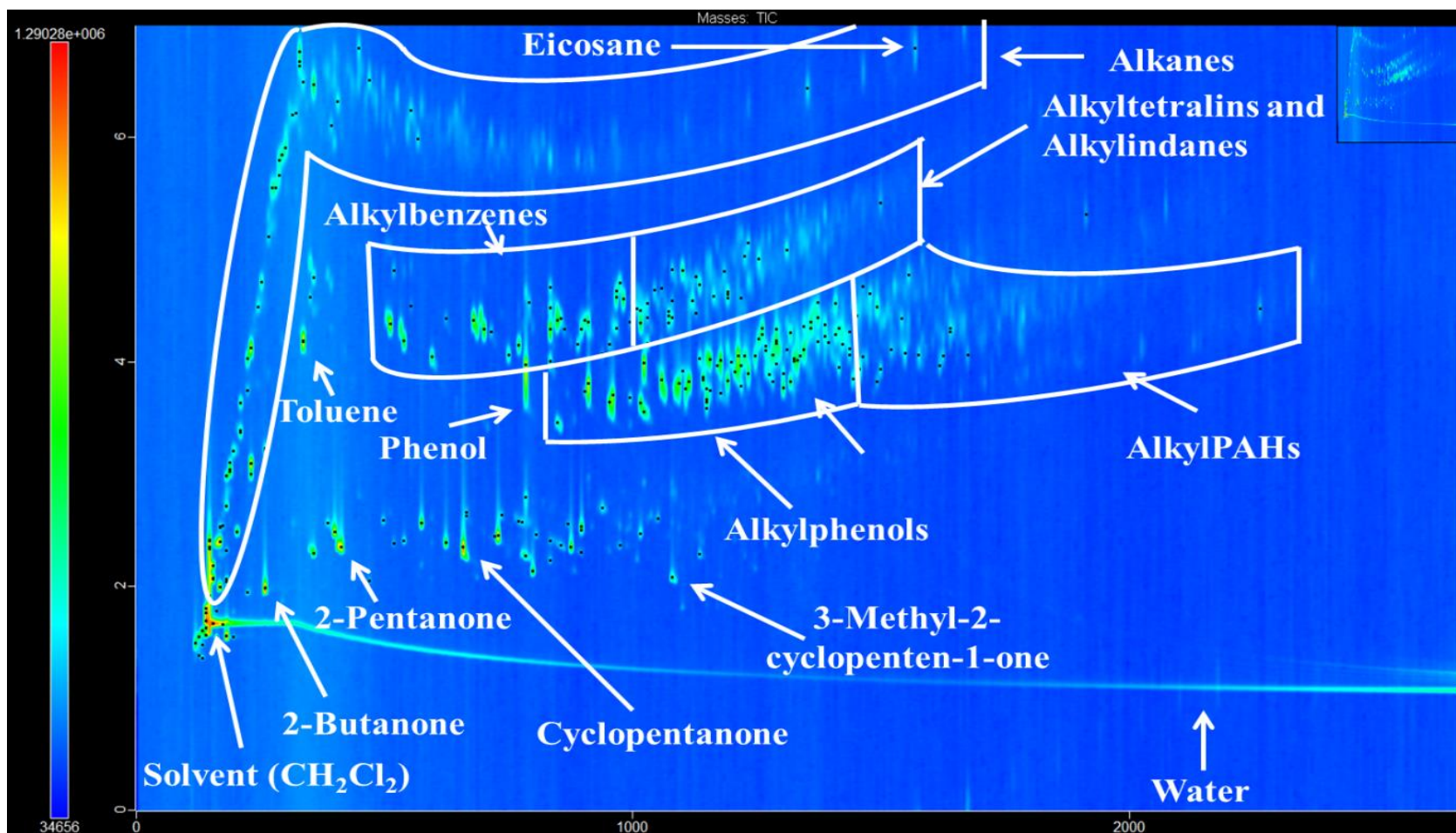


Figure 23. Annotated version of the separation showing the grouping and separation by the PTFPMS-P(5%BDMS/95%DMS).

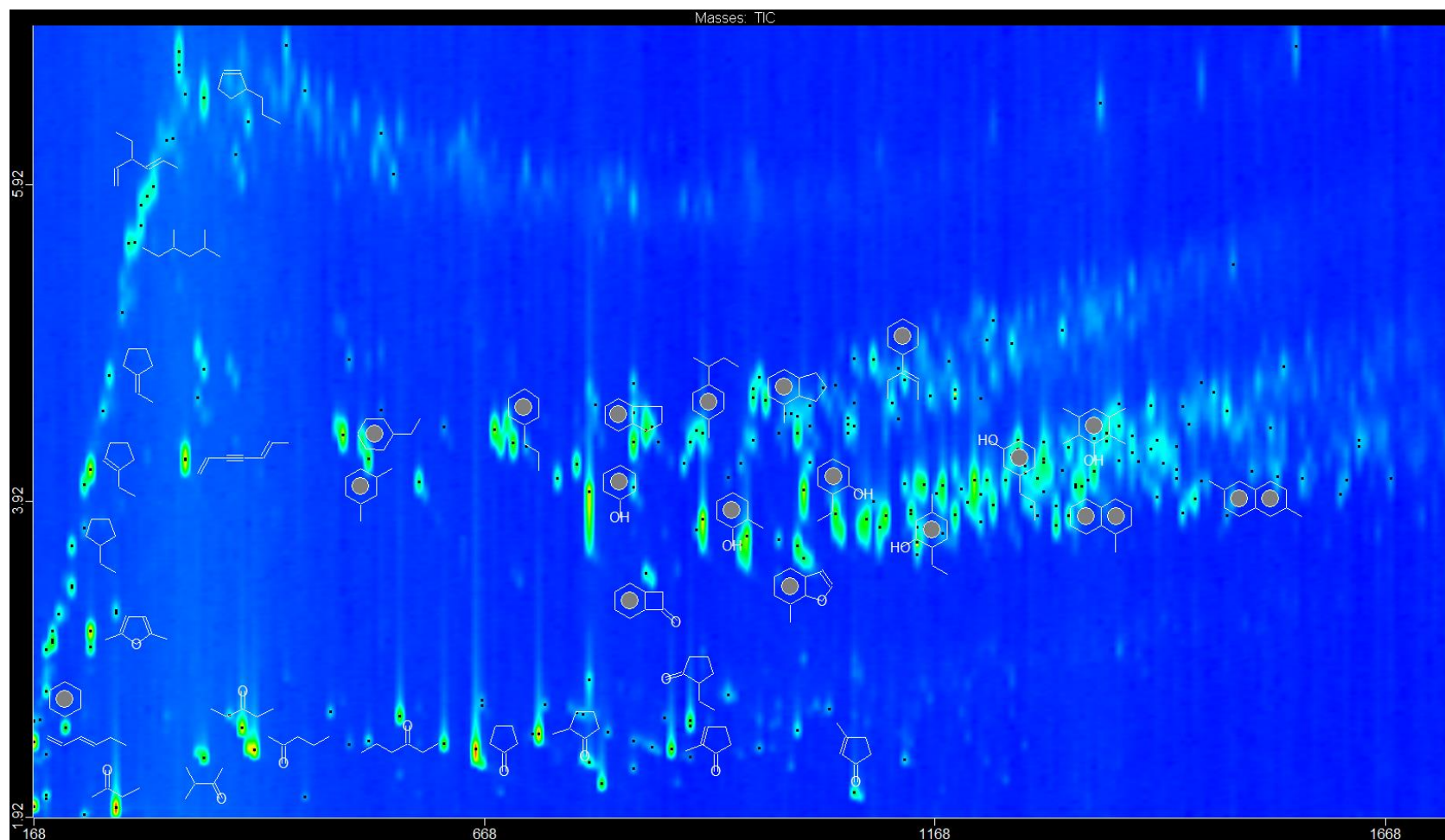


Figure 24. The chemical structures help display the analyte-homologue groups annotated in Figure 23.

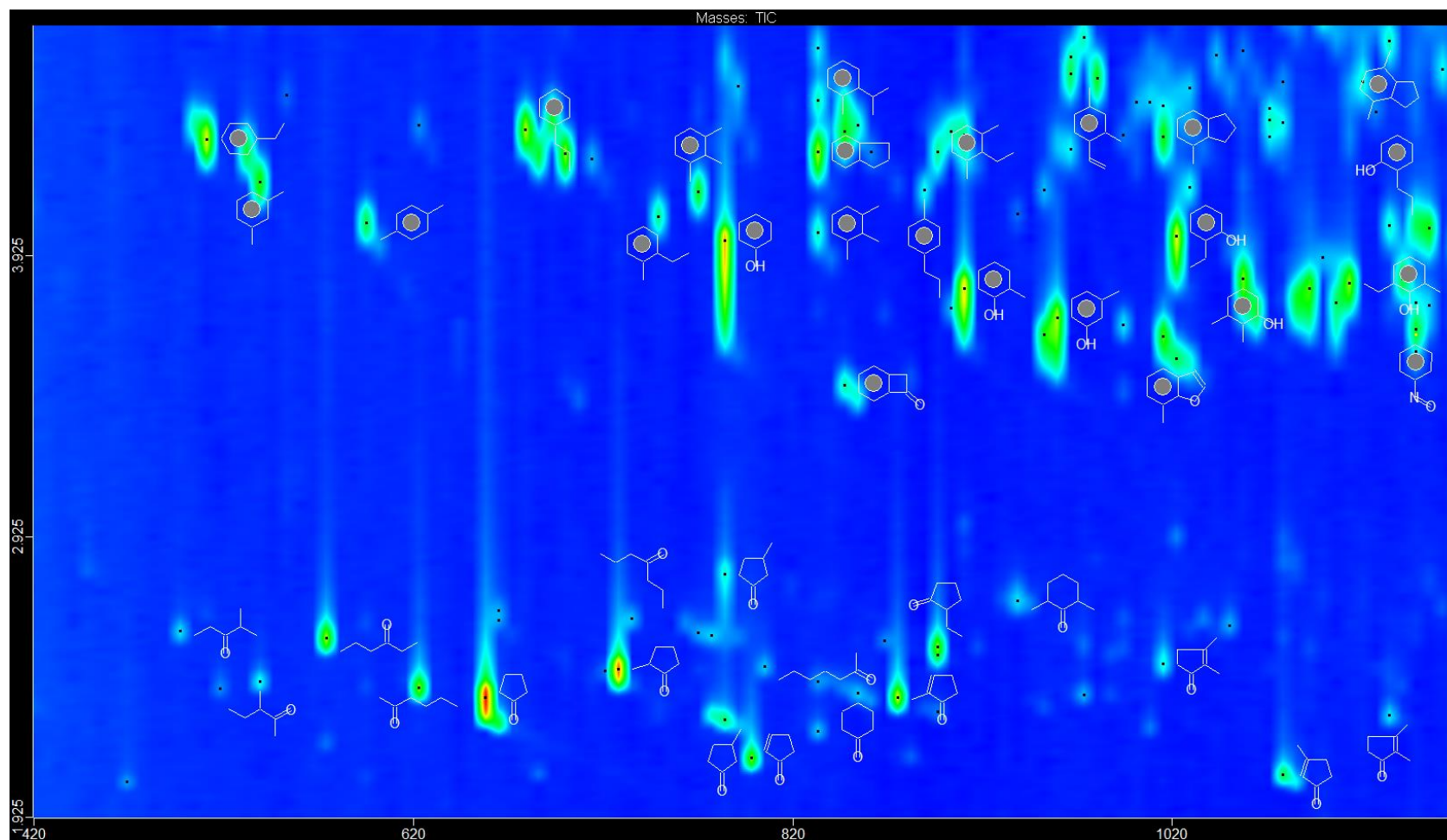


Figure 25. The ketones were not only grouped into a specific region, but their region was well separated in retention time from the other analyte-homologue groups.

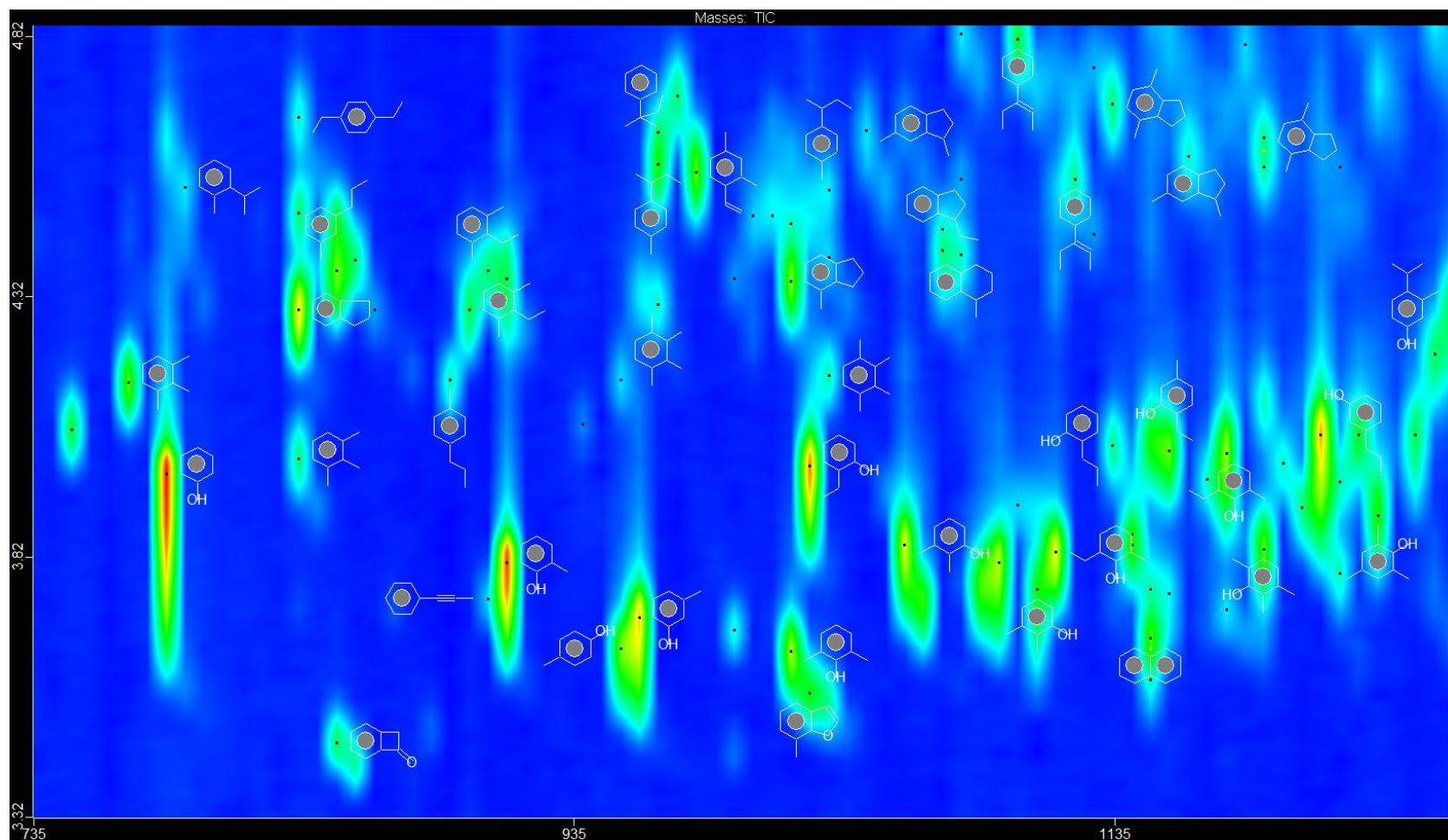


Figure 26. The alkylbenzenes and alkylphenols were grouped into regions, and these regions were well separated in retention time.

### ***3.5.3. PTFPMS-PEG stationary-phase pairs show orthogonality but no grouping***

The PTFPMS-PEG stationary-phase pair produced separations as orthogonal as PTFPMS-BDMSP for hydrolysis vapors or alcohols vapors. However, it did not produce analyte-homologue groups with the carbohydrate pyrolysis vapors.

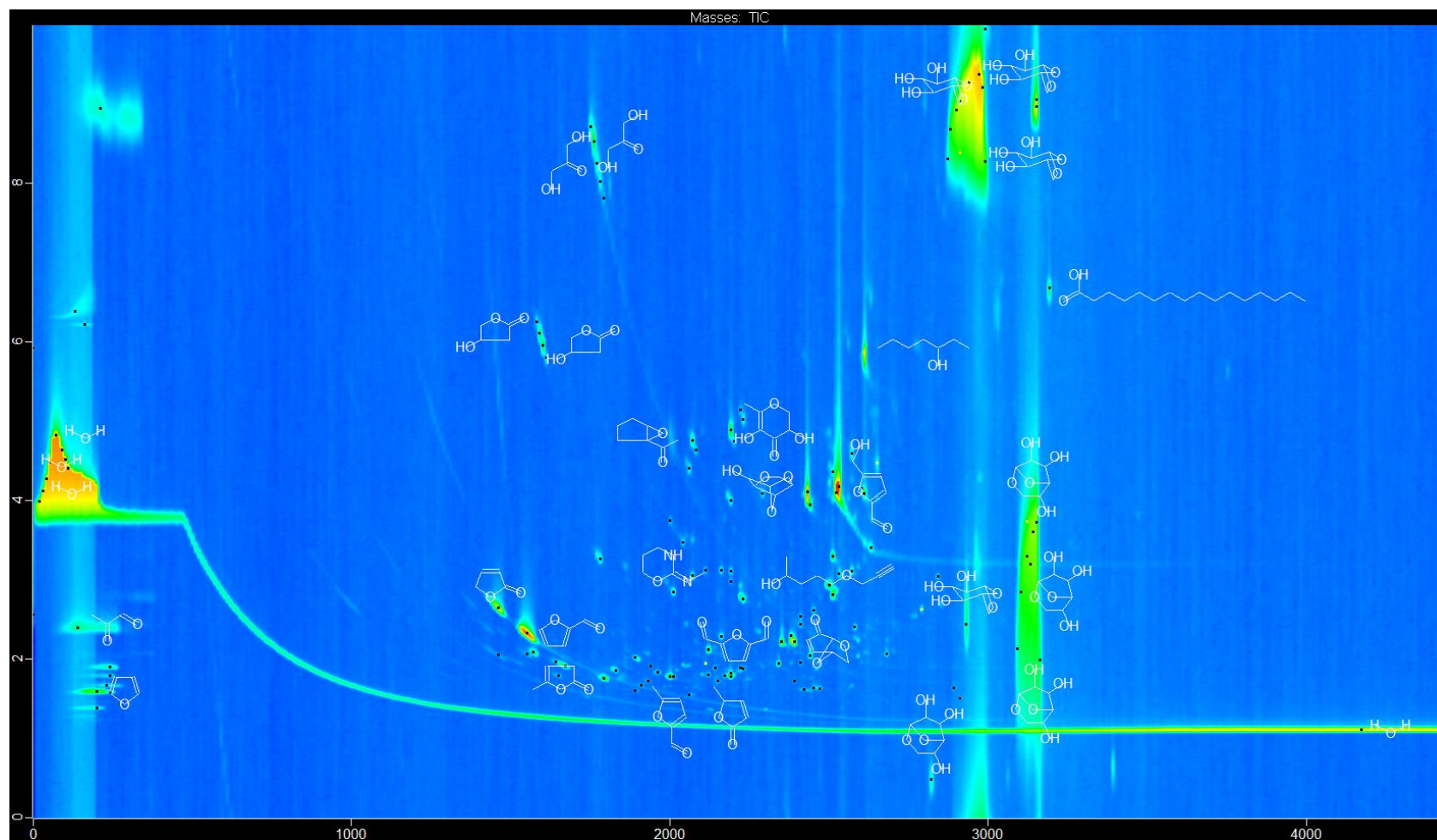


Figure 27. The PTFPMS-PEG stationary-phase pair spread the oxygenated organics into peaks with no correlation of retention time.



#### ***3.5.4. p(BCPS-co-CPPS)90/10-PEG stationary-phase pair showed analyte correlation***

The p(BCPS-co-CPPS)90/10-PEG stationary-phase pair produced separations with a strong retention-time correlation. This correlation was observed even for the mixture of analytes containing many different polar moieties. It was anticipated that having such a wide range of oxygen-containing functional groups (alcohol, carbonyl, ether, ester, carbonate, and amide) in the test mixture would produce a full range of varying retention behavior between the primary and secondary phases. However, this p(BCPS-co-CPPS)90/10-PEG stationary-phase pair offers no specific selectivities for any of the highly polar functional groups.

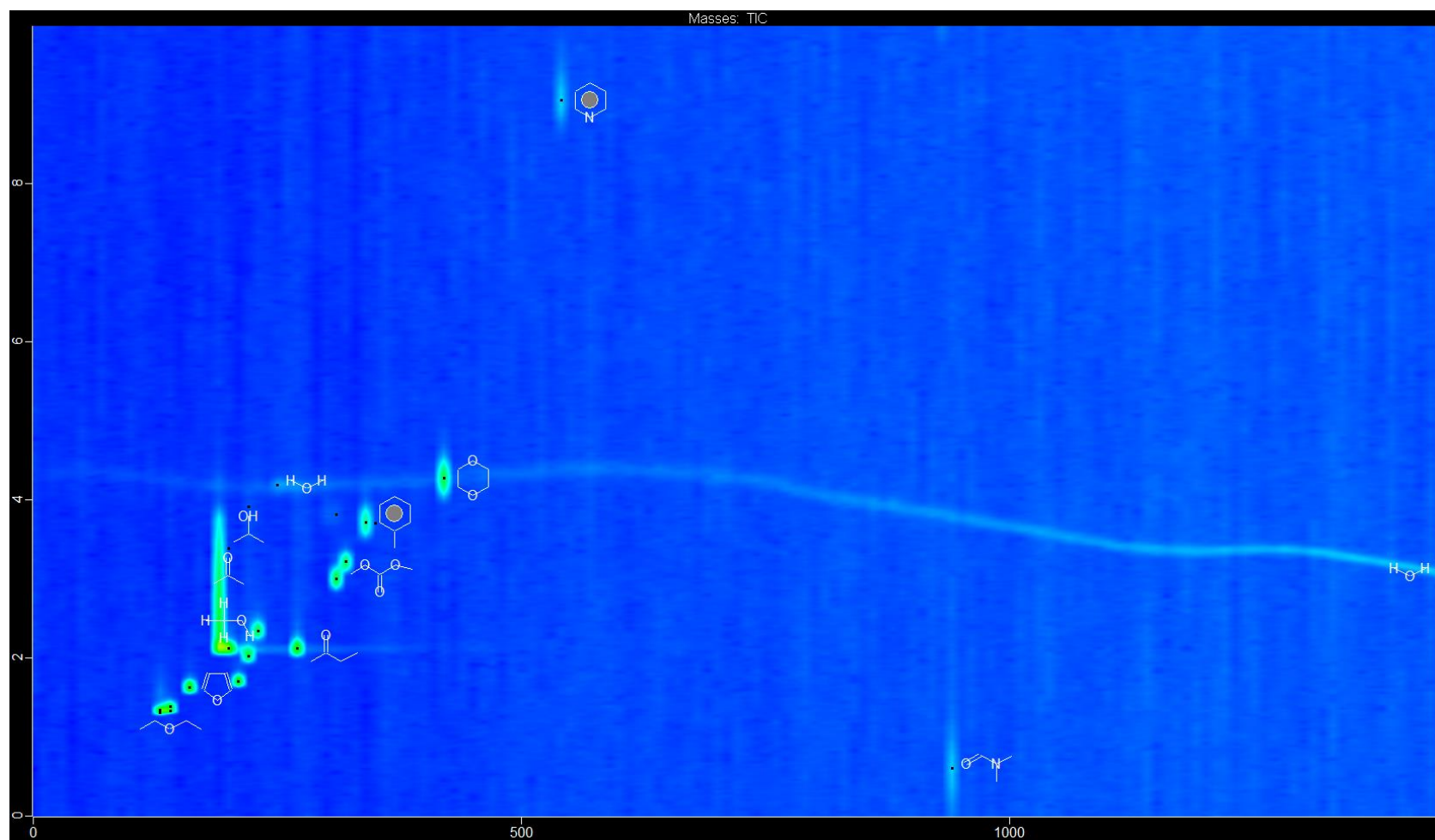


Figure 29. The full chromatogram view shows a strong retention-time correlation. Dimethylformamide is observed to “wrap around” due to the strong affinity in the second dimension.



### ***3.6. Discussion***

#### ***3.6.1. Analysis of stationary-phase pairs by analysis of McReynolds constants***

Researchers have used different stationary-phase pairs for very different analyte mixtures and obtained varying degrees of success. Table 5 displays several recent GCxGC separations relevant to the separation of pyrolysis and hydrolysis oils.

The success of a stationary-phase pair is due to many important qualities, such as peak shape, group-type separations, and the fraction of the two-dimensional chromatogram space occupied by analytes. Therefore, several important points will be discussed about these stationary-phase pairs and corresponding analyte mixtures.

Table 5. A collection of GCxGC analyses showing the importance of stationary-phase pairs.

Source	Target Analytes	Primary Column		Secondary Column	
		Stationary-Phase Material	Important McReynolds Constants*	Stationary-Phase Material	Important McReynolds Constants*
Marsman et al. [32]	Bio-oils and HDO bio-oils	PDMS (SolGel)	X = 16 Y = 55 Z = 44 U = 65 S = 42	p(DMS-co- CPPS)14/86 (Rtx-1701)**	X = 67 Y = 170 Z = 153 U = 228 S = 171
Marsman et al. [39]	Bio-oils and HDO bio-oils	p(DPS-co-DMS)5/95 (VF-5MS)	X = 33 Y = 72 Z = 66 U = 98 S = 67	p(DPS-co-DMS)50/50 (VF-17MS)	X = 119 Y = 158 Z = 162 U = 243 S = 202
This study	Bio-oils and Hydropyrolysis oils	p(DPS-co-DMS)5/95 (Rtx-5)	X = 33 Y = 72 Z = 66 U = 98 S = 67	p(DPS-co-DMS)50/50 (Rxi-17)	X = 119 Y = 158 Z = 162 U = 243 S = 202
	Bio-oils and Hydropyrolysis oils	PTFPMS (Rtx-200)	X = 146 Y = 238 Z = 358 U = 468 S = 310	p(BDMSP-co-DMS)5/95 (Rxi-5SilMS)	X = 33 Y = 72 Z = 66 U = 98 S = 67

Table 5, Continued.

Source	Target Analytes	Primary Column		Secondary Column	
		Stationary-Phase Material	Important McReynolds Constants*	Stationary-Phase Material	Important McReynolds Constants*
This study	Alcohols and carbonyls and heteroatom text mixture	PTFPMS (Rtx-200)	X = 146 Y = 238 Z = 358 U = 468 S = 310	PEG (StabilWax®-DA)	X = 322 Y = 536 Z = 368 U = 572 S = 510
		p(BCPS-co-CPP)90/10 (Rtx-2330)	X = 490 Y = 725 Z = 630 U = 913 S = 778	PEG (StabilWax®-DA)	X = 322 Y = 536 Z = 368 U = 572 S = 510
LECO Corp., Application Note [40]	Light crude oil components	p(BDMSP-co-DMS)5/95 (Rxi-5SiIMS)	X = 33 Y = 72 Z = 66 U = 98 S = 67	p(BDMSP-co-DMS)50/50 (Rxi-17SiIMS)	X = 119 Y = 158 Z = 162 U = 243 S = 202
Restek Corp., Application Note [41]	Riser pipe crude oil	p(BDMSP-co-DMS)50/50 (Rxi-17SiIMS)	X = 119 Y = 158 Z = 162 U = 243 S = 202	PDMS (Rxi-1MS)	X = 16 Y = 55 Z = 44 U = 65 S = 42

Table 5, Continued.

Source	Target Analytes	Primary Column		Secondary Column	
		Stationary-Phase Material	Important McReynolds Constants*	Stationary-Phase Material	Important McReynolds Constants*
Omais et al. [42]	Coal liquefaction middle distillate	PDMS (MTX-1)	X = 16 Y = 55 Z = 44 U = 65 S = 42	PTFPMS (Rtx-200)	X = 146 Y = 238 Z = 358 U = 468 S = 310
		PEG (SolgelWax)	X = 322 Y = 536 Z = 368 U = 572 S = 510	PTFPMS (Rtx-200)	X = 146 Y = 238 Z = 358 U = 468 S = 310
Omais et al. [43]	Coal liquefaction middle distillate	PDMS ("PONA")	X = 16 Y = 55 Z = 44 U = 65 S = 42	p(DPS-co-DMS)50/50 (BPX-50)	X = 119 Y = 158 Z = 162 U = 243 S = 202
		p(DPS-co-DMS)50/50 (DB-17)	X = 119 Y = 158 Z = 162 U = 243 S = 202	PDMS (DB-1)	X = 16 Y = 55 Z = 44 U = 65 S = 42

Table 5, Continued.

Source	Target Analytes	Primary Column		Secondary Column	
		Stationary-Phase Material	Important McReynolds Constants*	Stationary-Phase Material	Important McReynolds Constants*
Omais et al. [43]	Coal liquefaction middle distillate	PEG	X = 322 Y = 536 Z = 368 U = 572 S = 510	PDMS (DB-1)	X = 16 Y = 55 Z = 44 U = 65 S = 42
		PEG	X = 322 Y = 536 Z = 368 U = 572 S = 510	PTFPMS (Rtx-200)	X = 146 Y = 238 Z = 358 U = 468 S = 310
Ryan et al. [44]	Roasted coffee-bean volatiles	PEG (SolGel-WAX)	X = 322 Y = 536 Z = 368 U = 572 S = 510	p(BDMSP-co-DMS)5/95 (BPX-5)	X = 33 Y = 72 Z = 66 U = 98 S = 67
		p(BDMSP-co-DMS)5/95 (BPX-5)	X = 33 Y = 72 Z = 66 U = 98 S = 67	PEG (BP-20)	X = 322 Y = 536 Z = 368 U = 572 S = 510

Table 5, Continued.

Source	Target Analytes	Primary Column		Secondary Column	
		Stationary-Phase Material	Important McReynolds Constants*	Stationary-Phase Material	Important McReynolds Constants*
Johanningsmeier and McFeeters [45]	Spoilage metabolites of fermented cucumbers	PEG (SolGel-Wax™)	X = 322 Y = 536 Z = 368 U = 572 S = 510	p(CPP-co-DMS)14/86 (Rtx-1701)	X = 67 Y = 170 Z = 153 U = 228 S = 171

\* Values of McReynolds constants are available for many stationary phases. Many of these stationary phases have sets of McReynolds constants tabulated for several identical stationary phases offered by different manufacturers. Slight differences are often found between the different manufacturers' offerings of the same stationary phase. The values listed here were taken from one stationary phase, even if duplicates were available. If several identical blends from different manufacturers were available, then care was taken to ensure the selected example had McReynolds constants very representative of the collection.

- PDMS: McReynolds constants listed for "OV-1" [36, p. 209].
- p(DPS-co-DMS)5/95: McReynolds constants listed for "SE-54" [36, p. 221].
- p(DPS-co-DMS)50/50: McReynolds constants listed for "OV-17" [38, p. 42].
- p(BDMSP-co-DMS)5/95: McReynolds constants listed for "SE-54" [36, p. 221].\*\*\*
- p(BDMSP-co-DMS)50/50: McReynolds constants listed for "OV-17" [38, p. 42].\*\*\*\*
- PTFPMS: McReynolds constants listed for "OV-210" [36, p. 228].
- p(CPP-co-DMS)14/86: McReynolds constants listed for "OV-1701" [38, p. 43].\*\*\*\*\*
- PEG: McReynolds constants listed for "Carbowax 20000" [36, p. 252].

\*\* Stated by authors as "OV-1710 from Restek," and it is our assumption the authors meant Rtx-1701, as there is no OV-1710 or Rtx-1710 stationary phase.

\*\*\* Due to lack of data listed for p(BDMSP-co-DMS)5/95, McReynolds constants were approximated with data listed for p(DPS-co-DMS)5/95. (p(BDMSP-co-DMS)5/95 is designed to have the same selectivity as p(DPS-co-DMS)5/95, but provide a higher maximum temperature.)

\*\*\*\* Due to lack of data listed for p(BDMSP-co-DMS)50/50, McReynolds constants were approximated with data listed for p(DPS-co-DMS)50/50. (p(BDMSP-co-DMS)50/50 is designed to have the same selectivity as p(DPS-co-DMS)50/50, but provide a higher maximum temperature.)

\*\*\*\*\* Due to lack of data listed for true p(CPP-co-DMS)14/86, McReynolds constants were approximated with data listed for OV-1701 (which is 14% CPP, 85% DMS, and 1% methylvinylsiloxane).

The GCxGC separations listed in Table 5 collectively display several important points.

- Orthogonality does not depend upon an apolar primary stationary phase.
- Stationary phases of different corresponding McReynolds constants (or stationary phases composed of different chemical moieties) do not necessarily produce orthogonal separations.
- McReynolds constants alone do not provide sufficient data to obtain good separation of analyte-homologue groups.
- Grouping of analyte homologues and separation of these groups is vital to efficient and effective comparison and contrast of GCxGC separations.

These main points will be articulated first, then the vital individual points of each study will be discussed in further detail.

The first point is that orthogonal separations do not depend upon apolar primary stationary phases paired with polar secondary stationary phases. Very effective separations, which produced sharp peaks covering large fractions of the GCxGC space, were achieved with polar primary columns in many cases. Examples were two of four stationary-phase pairs tested in this work, three of four stationary-phase pairs tested by Omais et al. [43], one (of two) stationary-phase pairs tested by Omais et al. [42], the application note of Restek Corporation [41], one of two stationary-phase pairs tested by Ryan et al. [44], and the stationary-phase pair tested by Johanningsmeier and McFeeters [45].

The next point is that designing stationary-phase pairs by selecting stationary phases with different values of corresponding McReynolds constants does not ensure non-correlated retention times. This hypothetical design heuristic was shown to be incorrect by the p(BCPS-co-CPP)90/10-PEG pair tested in this work. With large differences between corresponding McReynolds constants, this pair produced strongly correlated retention times with test mixtures containing alcohols, aldehydes, ketones, ethers, alkanes, aromatics, and nitrogenated organics. While the chemical moieties and the retention strengths of these

phases are quite different, their relative analyte selectivity is similar. This similarity is because both phases exhibit the same predominant chemical-interaction types: electron-pair donating and proton accepting are dominant. The hypothetical, simple heuristic of selecting stationary-phase pairs to have different McReynolds constants is not sufficient for orthogonality. In the absence of McReynolds-constants data, the hypothetical, simple heuristic of selecting stationary-phase pairs to have different chemical moieties is also not sufficient for orthogonality. These first two hypothetical heuristics are unsuccessful because they are oversimplified. A sounder heuristic is to select stationary phases which have different analyte selectivities. The selectivity estimate can be based upon a more nuanced concept articulated in two ways.

- Primary and secondary stationary phases should have different “comparative chemical-interaction-type strengths.” These comparative chemical-interaction-type strengths are evaluated by comparing the fractional chemical-interaction-type strengths of two different stationary phases. The fractional chemical-interaction-type strength of a stationary phase’s chemical-interaction type is found by comparing it to another chemical-interaction type of that same stationary phase. Such fractional chemical-interaction-type strengths highlight how a particular stationary phase is selective towards particular chemical interactions and, hence, retains certain analytes preferentially.<sup>45</sup>

---

<sup>45</sup> There is a truly striking resemblance between this proposed “comparative chemical-interaction-type strength” in GCxGC selectivity and David Ricardo’s classic concept of comparative advantage in the study of international trade. (In fact, it’s where the adjective “comparative” came from in the name for our GCxGC-selectivity concept.) In the simplest case to display Ricardo’s theory, two nations can both produce two different goods with different absolute costs in terms of the required factors of production per unit good. Even though one nation might produce both goods at lower absolute costs, each nation will be comparatively better at making one good. The “comparatively better” arrives from evaluating a nation’s opportunity cost instead of that nation’s absolute cost of producing a good (i.e., how much of one potentially produced good is given up in order to produce the other good?). The key to nations successfully optimizing their wealth (via trade) is to identify what good they produce with a lower opportunity cost than the other nation. The nation produces the good in which they are comparatively better, and trades with another nation which has a comparative advantage in producing the other good. This trade maximizes both nations’ consumption of both goods. The analogy to GCxGC stationary-phase pairing works where nations are the stationary phases, goods are the chemical-interaction types, and the required factors of production are the phases’ chemical-interaction strengths. A

- Primary and secondary stationary phases should have different chemical interaction types, and, importantly, not just different strengths of the same interactions. In this light, knowing the stationary phases' McReynolds constants and chemical structures is still much more useful than relying on the oversimplified terms “apolar,” “mid-polar,” and “polar” to determine selectivity for complex mixtures of analyte homologues.

---

stationary phase has a “comparative chemical-interaction-type strength” in one of its interaction types when that interaction type’s fractional strength is higher when compared to the corresponding fractional strength of a different stationary phase. Stationary phases with comparative advantages in different interaction types can make successful GCxGC stationary-phase pairs, as long as the comparative chemical-interaction-type strengths match the interactions important to the analyte homologues of the mixture. This striking similarity between David Ricardo’s comparative advantage and selecting stationary phases based upon their comparatively stronger chemical interactions was realized when trying to articulate the comparison of multiple interaction types between multiple stationary phases. This similarity is too perfect to not mention.

Table 6. Fractional retention differences from squalane to a particular stationary-phase material.

Stationary Phase	X (Benzene)				Y (Butan-1-ol)				Z (Pentan-2-one)			
	$\Delta I_X/\Delta I_Y$	$\Delta I_X/\Delta I_Z$	$\Delta I_X/\Delta I_U$	$\Delta I_X/\Delta I_S$	$\Delta I_Y/\Delta I_X$	$\Delta I_Y/\Delta I_Z$	$\Delta I_Y/\Delta I_U$	$\Delta I_Y/\Delta I_S$	$\Delta I_Z/\Delta I_X$	$\Delta I_Z/\Delta I_Y$	$\Delta I_Z/\Delta I_U$	$\Delta I_Z/\Delta I_S$
Squalane	N/A											
PDMS	0.291	0.364	0.246	0.381	3.438	1.250	0.846	1.310	2.750	0.800	0.677	1.048
p(DPS-co-DMS)5/95	0.458	0.500	0.337	0.493	2.182	1.091	0.735	1.075	2.000	0.917	0.673	0.985
p(DPS-co-DMS)50/50	0.753	0.735	0.490	0.589	1.328	0.975	0.650	0.782	1.361	1.025	0.667	0.802
PTFPMS	0.613	0.408	0.312	0.471	1.630	0.665	0.509	0.768	2.452	1.504	0.765	1.155
p(CPP-co-DMS-co-MVS)14/85/1	0.394	0.438	0.294	0.392	2.537	1.111	0.746	0.994	2.284	0.900	0.671	0.895
p(CPP-co-BCP)20/80	0.676	0.778	0.537	0.630	1.480	1.151	0.794	0.932	1.286	0.869	0.690	0.810
PEG	0.601	0.875	0.563	0.631	1.665	1.457	0.937	1.051	1.143	0.687	0.643	0.722

Table 7. Fractional retention differences from squalane to a particular stationary-phase material, continued.

Stationary Phase	U (Nitropropane)				S (Pyridine)			
	$\Delta I_U/\Delta I_X$	$\Delta I_U/\Delta I_Y$	$\Delta I_U/\Delta I_Z$	$\Delta I_U/\Delta I_S$	$\Delta I_S/\Delta I_X$	$\Delta I_S/\Delta I_Y$	$\Delta I_S/\Delta I_Z$	$\Delta I_S/\Delta I_U$
Squalane	N/A							
p(DMS)	4.063	1.182	1.477	1.548	2.625	0.764	0.955	0.646
p(DPS-co-DMS)5/95	2.970	1.361	1.485	1.463	2.030	0.931	1.015	0.684
p(DPS-co-DMS)50/50	2.042	1.538	1.500	1.203	1.697	1.278	1.247	0.831
p(TFPMS)	3.205	1.966	1.307	1.510	2.123	1.303	0.866	0.662
p(CPP-co-DMS-co-MVS)14/85/1	3.403	1.341	1.490	1.333	2.552	1.006	1.118	0.750
p(CPP-co-BCP)20/80	1.863	1.259	1.449	1.174	1.588	1.073	1.235	0.852
PEG	1.776	1.067	1.554	1.122	1.584	0.951	1.386	0.892

An attempt was made to obtain proxies for fractional chemical-interaction-type strengths. Table 6 and Table 7 display the “fractional retention differences” of the eight basic stationary phase materials based upon the first five McReynolds constants. These fractional-retention-difference values cannot represent true fractional chemical-interaction-type strengths because McReynolds test analytes do not actually isolate individual chemical interaction types. However, these fractional retention differences still provide a quantitative understanding of the additional retention of a test analyte compared to the additional retention of another test analyte (in terms of fractional changes in Kováts Indices). For example, PTFPMS retains all compounds more strongly than PDMS, as shown by having all of its McReynolds constants greater than those of PDMS. An argument can be made that PTFPMS is relatively less selective to alcohols than PDMS by inspecting the fractional retention differences: PDMS’  $\Delta I_Y/\Delta I_X$  value is 3.44, while PTFPMS’  $\Delta I_Y/\Delta I_X$  value is only 1.63. These values explain that the added relative retention of butan-1-ol to benzene is greater when transitioning from squalane to PDMS than when transitioning from squalane to PTFPMS. Frustratingly, the fractional retention differences do not explain the correlation between the stationary-phase pair p(BCPs-co-CPP)90/10-PEG.

For the next general point, McReynolds constants also do not provide sufficient information to predict whether analyte homologues will be grouped or whether these analyte-homologue groups will overlap or be well separated. There are only ten McReynolds test analytes, and often only five are available in collections of stationary-phase data. Such a small set of test analytes is excellent for the original intended purpose of determining the effect specific functional groups have on retention. However, McReynolds constants focus only on how chemical interactions alter elution order of the five to ten test analytes relative to each other and their neighboring n-alkanes. Therefore McReynolds constants do not provide sufficient selectivity information to predict two key elements needed for most GCxGC applications, including hydropyrolysis and HDO processes:

- What stationary-phase characteristics can separate analytes within an analyte-homologue group into clearly separated peaks? For example, what stationary phase

will separate the members of alkylbenzenes (e.g., toluene, xylenes, ethylbenzene, and cumene) into clearly separated peaks?

- What stationary-phase characteristics can separate analytes of different analyte-homologue groups into clearly separated peaks? For example, what stationary phase will separate an alkylbenzene (e.g., ethylbenzene), a phenolic (e.g., phenol) an alkoxybenzene (e.g., ethoxybenzene), and an alkyl-alkoxybenzene (e.g., 2-ethoxyethylbenzene)?

These first two questions are needed to answer the following key summarizing question for GCxGC separations: Which members of the many different analyte-homologue groups will co-elute for each stationary phase? Knowledge of what analytes will co-elute is essential for selecting a primary stationary phase that will work synergistically with a secondary stationary phase. This simple, yet clever, focus upon the primary column's co-eluting analytes was pointed out by Omais et al. [42] by drastically changing the position of analyte-homologue groups by changing only the primary stationary phase. Adding the use of McReynolds constants can highlight the type and strength of chemical interactions of a stationary phase, but the small set of test compounds cannot characterize how a stationary phase will co-elute members of many different analyte-homologue groups.

Finally, it is important to stress how GCxGC separations should strive to obtain well-separated analyte-homologue groups to make for simpler comparisons of both different stationary-phase pairs and different analyte mixtures. Verbally describing the results of various GCxGC separations is very difficult due to the large number of potential differences and similarities, especially when the peaks of similar analytes appear randomly positioned in the two-dimensional space. Even displaying the chromatogram images for the reader to see the differences visually requires long, exhaustive verbal descriptions and large analyte peak tables. These tedious descriptions are made much easier if GCxGC chromatograms group the analyte homologues and separate each group by large retention-time differences. These chromatograms, if annotated with analyte homologue identifications, make comparison of

complex mixtures much more effective and time-efficient, which is the ultimate purpose of GCxGC equipment and experimentation.

Beyond the general points made apparent by the comparison of studies listed in Table 5, the findings of individual studies is very valuable. The studies by Marsman et al. [32] and Marsman et al. [39] were both directly applicable to hydrolysis oils, as their hydrodeoxygenated bio-oils were very similar in composition to the hydrolysis oils tested in this dissertation. In the first study, the authors used a PDMS-p(CPP-co-DMS)14/86 stationary-phase pair and achieved a separation with distinct groups. However, most of these groups overlapped their neighbors when all groups were present. Particularly frustrating is the overlap between alcohols, aldehydes and ketones, and alkylbenzenes, as clear visual distinction between these analyte-homologue groups on a GCxGC chromatogram allows quick evaluation of potential intermediates within the reaction networks of bio-oil hydrodeoxygenation. In a follow-up study, Marsman et al. [39] separated most of their pyrolysis oils and hydrodeoxygenated pyrolysis oils with a p(DPS-co-DMS)5/95 primary column and a p(DMS-co-DMS)50/50. Some overlap was still seen among analyte-homologue groups, particularly the alkylbenzenes and alkanes. This overlap is still very frustrating because it prevents fast and effective visual comparison of various HDO treatments.

In their second study, Marsman et al. [39] compared three other additional secondary columns of the same dimensions and different stationary phases. These other three secondary-column phases were p(DMS-co-DMS)50/50, p(CPP-co-DMS)14/86, and PTFPMS. Elution order was “essentially similar” among these three phases for an alcohol-phenol-methoxyphenol test mixture and their chromatographic resolution for hydrodeoxygenated bio-oils was “very similar.” There was a frustrating lack of description of any analyte-homologue grouping or even images of the GCxGC chromatograms among the secondary stationary-phase tests.

Another two stationary-phase pair investigations very relevant to hydrolysis oils and hydrodeoxygenated bio-oils (as well as zeolite deoxygenated bio-oils) were Omais et al. [43] and Omais et al. [42]. Their coal-liquefaction middle distillates contain many of the same analytes as the hydrolysis oils tested in this dissertation, in particular the complex set of “paraffins, naphthalenes, aromatics, oxygen-, nitrogen-, and sulfur-containing species, and phenols.” Their studies were an excellent source of data for two main reasons. First, they compared five separate stationary-phase pairs, and several important comparisons could be made between these five pairs. Two stationary-phase pairs shared the same primary stationary phase (PEG) and used different secondary stationary phases, PTFPMS and PDMS. Another two stationary-phase pairs shared the same primary stationary phase (PDMS) and used different secondary stationary phases (PTFPMS and p(DPS-co-DMS)50/50. Two stationary-phase pairs shared the same secondary column (PTFPMS) and used different primary columns (PEG and PDMS). Another two stationary-phase pairs shared the same secondary column (PDMS) and used different primary columns (p(DPS-co-DMS)50/50) and PEG). These comparisons show the effects of both the primary stationary phase’s selectivity on the secondary column’s separation potential and the secondary stationary phase’s selectivity on the primary column’s separation capability. These five pairs show the nuance of such synergy between selectivities mentioned as the third and fourth points of the preceding general points. They describe how the primary column’s selectivity has a profound effect because it determines which analytes co-elute and require separation by the secondary column. Switching the primary column (while keeping the same secondary column) can create profound differences in orthogonal separations. Omais et al. [42] were very clever to articulate the effect of the primary stationary-phase selectivity, but they did not go as far as finding ways to predict the potential synergies based upon chemical interactions as was done in our suggestion of “comparative chemical-interaction-type strengths.”

The second reason that the studies by Omais et al. [43] and Omais et al. [42] were excellent was because they could draw strong conclusions about orthogonality and analyte grouping. Such strong conclusions were possible because the peak shapes were very sharp

and the differences in retention time between homologue groups were large. Such large, clear differences were likely due to their willingness to use long analysis times ( $2^{\circ}\text{C min}^{-1}$  oven ramp) and the relatively non-polar nature of most analytes (i.e., a likely lack of the alcohols, carbonyls, and a certain lack of small saccharides and anhydrosaccharides present in bio-oils). Most importantly, three of their four stationary-phase pairs used polar primary columns, and they achieved better differences in retention time between groups and a better use of the two-dimensional GCxGC space. Such a comparison is an excellent rebuttal to the suggestion that orthogonality is achieved through apolar-polar stationary-phase pairs, as was often suggested by earlier researchers.

The application note for a GCxGC separation of a 2010 Gulf-oil-spill crude-oil sample by Restek Corporation [41] produced a chromatogram very similar to one produced by the p(DPS-co-DMS)50/50-PDMS stationary-phase pair of Omais et al. [43]. Unfortunately, Restek Corporation's chromatogram only annotated the group of alkylated polycyclic aromatic hydrocarbons (alkylPAHs), with no suggestion as to what the other analytes were. However, these GCxGC separations were very comparable for two reasons. First, this crude oil probably shared many hydrocarbon homologues with the coal-liquefaction middle distillates (alkanes, alkylbenzenes, alkyl-naphthalenes, etc.). Second, the primary p(BDMSP-co-DMS)50/50 stationary phase used by Restek Corporation is designed to give the same selectivity (with increased thermal stability) as the primary p(DPS-co-DMS)50/50 stationary phase used by Omais et al. [43]. Therefore, the results of these two slightly different chromatograms should be very comparable, and the stationary-phase pair tested by Restek Corporation can be assumed to have had many of the same analytes within the similarly positioned analyte-homologue groups. This polar-apolar pair again gave further support to how the primary column need not be apolar, even when low-polarity hydrocarbons are to be separated.

Also relevant is an application note from LECO Corporation, which highlights analyte grouping of crude oils by a p(BDMSP-co-DMS)5/95-p(BDMSP-co-DMS)50/50 stationary-phase pair [40]. Similar to the p(BDMSP-co-DMS)5/95-p(BDMSP-co-

DMS)50/50 stationary-phase pair used by Marsman et al. [39], LECO Corporation's testing of this stationary-phase pair also fails to separate the analyte-homologue groups by mostly vertically separated regions on the GCxGC space.

The stationary-phase pair investigation by Ryan et al. [44] made a comparison between a stationary-phase pair of PEG-p(DPS-co-DMS)5/95 and pair of the reverse order. The analytes separated were different from those encountered in hydrolysis oils/hydrodeoxygenated bio-oils or cellulose pyrolysis. However, most of these roasted coffee-bean volatiles were oxygenated and nitrogenated organics, which made the separation of such a mixture very applicable to carbohydrate pyrolysis. (The similarity in oxygen content was not surprising, as coffee-bean roasting is quite similar to biomass pyrolysis.) More peaks were observed in the polar-apolar configuration, possibly due to how the primary column was more compatible with the more polar analytes, and they were spread over a larger portion of the GCxGC space. There was some slight correlation between analytes by the PEG-p(DPS-co-DMS)5/95 pair, but this study provided further support that the apolar-polar heuristic does not work well for mixtures of mostly polar analytes like oxygenated and nitrogenated organics.

The volatile spoilage metabolites of fermented cucumbers separated by Johanningsmeier and McFeeters [45] were also different from either pyrolysis oils or hydrolysis oils, but similarly to Ryan et al. [44], their study was applicable due to the complexity of oxygenated and nitrogenated organics. This study found that a PEG-p(CPP-co-DMS)14/86 stationary-phase pair was very effective and showed no obvious correlation of analyte retention, and it was hence orthogonal. While the authors did not determine the ability of the stationary-phase pair to group the analytes into different regions of the chromatogram, an image of the chromatogram suggests there was not a high degree of separation between any potential groups. Also similar to Ryan et al. [44], they provided evidence of how a polar primary stationary-phase like PEG can still produce orthogonal results without relying on only "boiling-point" separation in the primary column.

### 3.6.2. *The importance of London dispersion forces for separating oxygenated analytes*

Importantly, the London dispersion forces should not be neglected when determining which chemical interactions should be employed for the separation. It is easy to focus entirely upon oxygen-containing functional groups when looking for strong chemical interactions to employ when separating hydropyrolysis oils. There are three reasons such behavior can become ingrained in a chromatographer:

- Hydropyrolysis and hydrodeoxygenation processes are focused upon removing oxygenated functional groups, so these oxygenated analyte homologues must be separated from each other and they must be separated from the hydrocarbons
- McReynolds constants are largely focused upon heteroatom-containing functional groups. Only three of ten test analytes do not contain heteroatoms, and only benzene is of the first five McReynolds constants listed most often in reference guides. Therefore, there is only implicit focus on the relative positions of n-alkanes: n-alkanes are the test analytes which provide the Kováts Index  $I$ , and  $I$  is obtained by summing the given McReynolds constant ( $\Delta I$ ) to the Kováts Index of the squalane reference stationary phase.
- The study of chemistry guides students to focus upon functional groups because common synthesis routes require their use, and common synthesis methods usually do not alter the aliphatic portions of molecules. These three reasons must not make the chromatographer forget to take advantage of important differences in the aliphatic and aromatic regions for separation purposes.

A prime example of how important London dispersion forces can be is the separation of hydropyrolysis oils by the PTFPMS-p(BDMSP-co-DMS)5/95 stationary-phase pair of this work. The phenylene and methyl groups of the p(BDMSP-co-DMS)5/95 stationary phase provided an excellent separation of alkanes, alkylbenzenes, alkoxybenzenes, and ketones in the second dimension. Such second-dimension separation was made possible only through

London dispersion forces available between the p(BDMSP-co-DMS)5/95 stationary phase and the aliphatic/aromatic regions of the analytes.

### ***3.6.3. Overloading primary columns by carbohydrate pyrolysis vapors***

Highly oxygenated analytes, like the majority of compounds formed during carbohydrate pyrolysis, can easily overload primary stationary phases which have only London-type dispersion forces. These stationary phases mainly include those with a high quantity of DMS with the balance being PMS and DPS, which represent the majority of columns used during common GC separations. (In fact, a common heuristic in method development for gas chromatography is to use the stationary phase with the least possible polarity, and so many chromatographers try these apolar and midpolar stationary phases first.) When overloaded, the analytes elute as broad, co-eluting peaks, resulting in poor analyte identification and quantification. Regardless of the ingenious argument suggesting orthogonality is achieved by analyte “volatility” in the primary column and “polar interactions” in the secondary column, stationary phases must still be selected which are compatible with the majority of analytes.

Stationary phases better suited for carbohydrate-pyrolysis vapors are those which have moieties capable of donating and accepting hydrogen bonds and electron pairs. These interactions are well suited to the oxygenated functional groups and unsaturated nature of many key reaction products. Commonly available stationary phases with moieties capable of accepting or donating hydrogen bonds and electron pairs include PEG and copolymers of CPMS or CPPS with PDMS. These stationary phases find use during the separation of carbohydrate-pyrolysis vapors but they are at times limited due to their comparatively lower maximum operating temperatures (240-280°C maximum). A slightly less common stationary phase which exhibits hydrogen-bond accepting and electron-pair donating is PTFPMS. A major benefit of PTFPMS is that its maximum temperature (340°C), while not as high as blends of PDMS with PDPS and PPMS, is much higher than both PEG and blends of PDMS with CPMS and CPPS. PTFPMS presents an excellent compromise between maximum

temperature and prevention of column overloading, and it is puzzling why PTFPMS is not encountered more often during the separation of biomass-pyrolysis products.

#### **3.6.4. PEG and separation of carbonyl and alcohol groups**

PEG did not offer an orthogonal selectivity when combined with BCPS-based primary stationary phases to separate oxygenated pyrolysis products. The ether linkages in PEG  $(-O-CH_2-CH_2-)_n$  provide a weak dipole, but they do not provide a hydroxyl group capable of forming hydrogen-bridge bonds with polar-aprotic functional groups within analytes like carbonyls. Such hydroxyl-group effects would distinguish PEG's selectivity from that of PTFPMS and BCPS and would enable a more orthogonal separation. However, the PEG tested had a very small quantity of hydroxyl groups after polymerization and offered very little ability to create hydrogen-bridge bonds with analytes containing polar-aprotic functional groups.

The incorrect assumption for PEG being capable of hydrogen-bridge bonds with polar-aprotic analytes was based on the large McReynolds constants for pentan-2-one (Z), 1-nitropropane (U), pyridine (S), and 1,4-dioxane (L). The large retention indexes for these polar-aprotic test analytes suggested PEG had a strong affinity for them compared to PTFPMS. In addition, the structure of PEG mistakenly conjured up images of hydroxyl groups, as the monomer contains two hydroxyl groups. However, the PEG structure has hydroxyl groups only at its terminal ends after polymerization, and thus it has very little ability to hydrogen-bond to electronegative groups in analytes.

The ability for PEG to hydrogen bond with polar-aprotic analytes does exist to a slight extent, and it is dependent upon the degree of polymerization (DOP).<sup>46</sup> The DOP affects PEG's selectivity because it changes the ratio of ether groups to hydroxyl groups present in a polymer chain. PEG polymer chains have hydroxyl groups present at their two

---

<sup>46</sup> Manufacturers often use the polymer chain's molecular weight as a proxy for its degree of polymerization. This dissertation uses degree of polymerization in order to avoid any potential confusion with the molecular weight of a single repeating unit or the molecular weight of an analyte.

terminal end units, but all of the internal repeating units contain only ether groups. Having a higher DOP increases this ratio of ether groups to hydroxyl groups.

Ether and hydroxyl groups do not offer the same chemical interactions to analytes even though both ether groups and hydroxyl groups contain electronegative oxygen atoms and thus contribute to increasing polarity relative to hydrocarbons. Ether groups cannot form hydrogen-bridge bonds without a protic analyte like those containing N-H, O-H, and F-H groups. On the other hand, hydroxyl groups can form hydrogen bonds with neighboring N-H, O-H, F-H, and C=O groups. Therefore, at low DOP, PEG has a strong attraction for both polar-aprotic analytes (e.g., carbonyls) and polar-protic analytes (e.g., alcohols and primary and secondary amines). As DOP increases, the selectivity of PEG changes to favor polar-protic analytes (e.g., alcohols and primary and secondary amines) [36, p. 249].

This PEG column used in this dissertation was Restek Corp.'s Stabilwax®DA column, and these columns are not in a region of DOP where selectivity changes significantly, as shown by Figure 31. These Stabilwax® stationary phases are made with "Carbowax 20M" [46]. This numerical code of 20M refers to a molecular weight of 20,000 Da (which corresponds to a DOP of roughly 450 for PEG). At this molecular weight, the changes in McReynolds constants appears to change very little when extrapolating the trends observed in a series of increasing molecular weight.

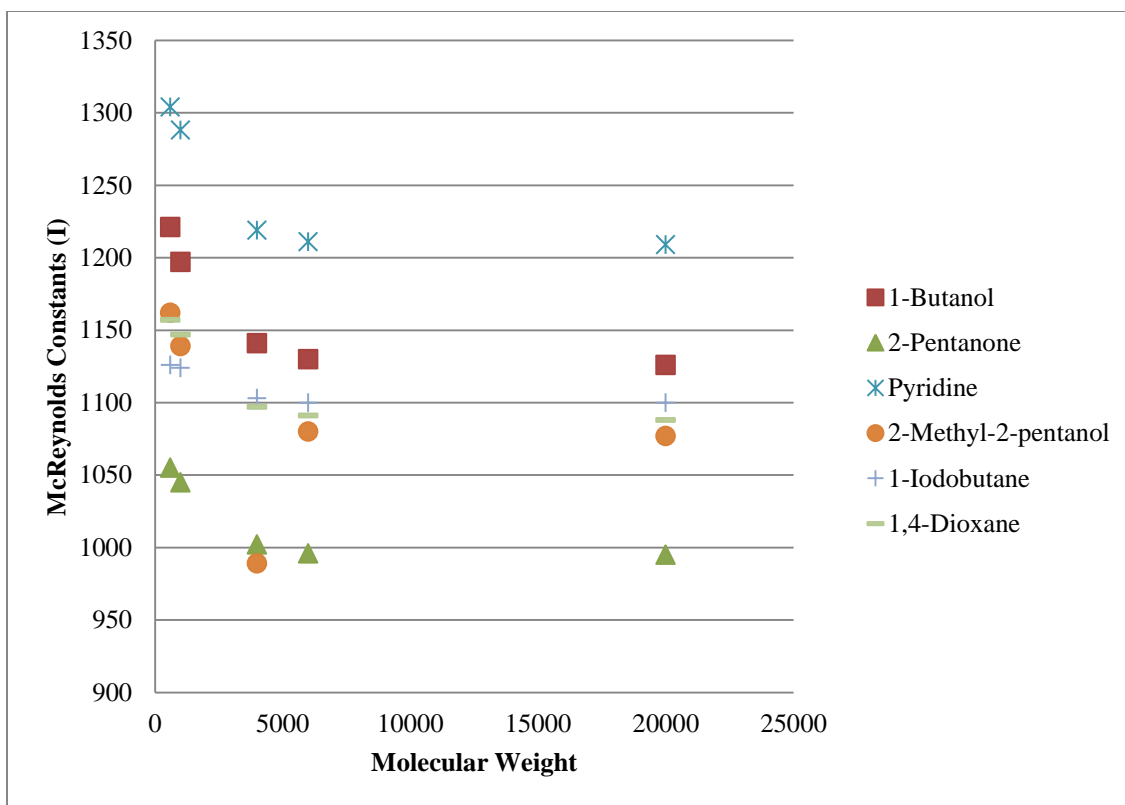


Figure 31. The retention of analytes subject to hydrogen-bridge bonds decreases as PEG's molecular weight (or DOP) increases. This decrease in retention is likely due to the decreasing presence of terminal chain units which possess hydroxyl groups.

### 3.6.5. TFPMS and separation by differences in oxygen-atom content

PTFPMS presents a good resistance to column overloading as well as a more favorable maximum temperature among polar stationary phases. After careful analysis of retention times, it was found that PTFPMS also provides an excellent advantage of providing large differences in retention time between similar compounds which differ in the number of oxygenated functional groups. This behavior was first observed by the large differences in retention time found between furan, furfural, and 5-hydroxymethylfurfural. These compounds are key analytes during pyrolysis of carbohydrates like cellulose and glucose, and they are often found in large quantities. The large differences in retention times help

ensure co-elution is easily avoided for these compounds, so peaks are easily distinguished in cases approaching column overloading.

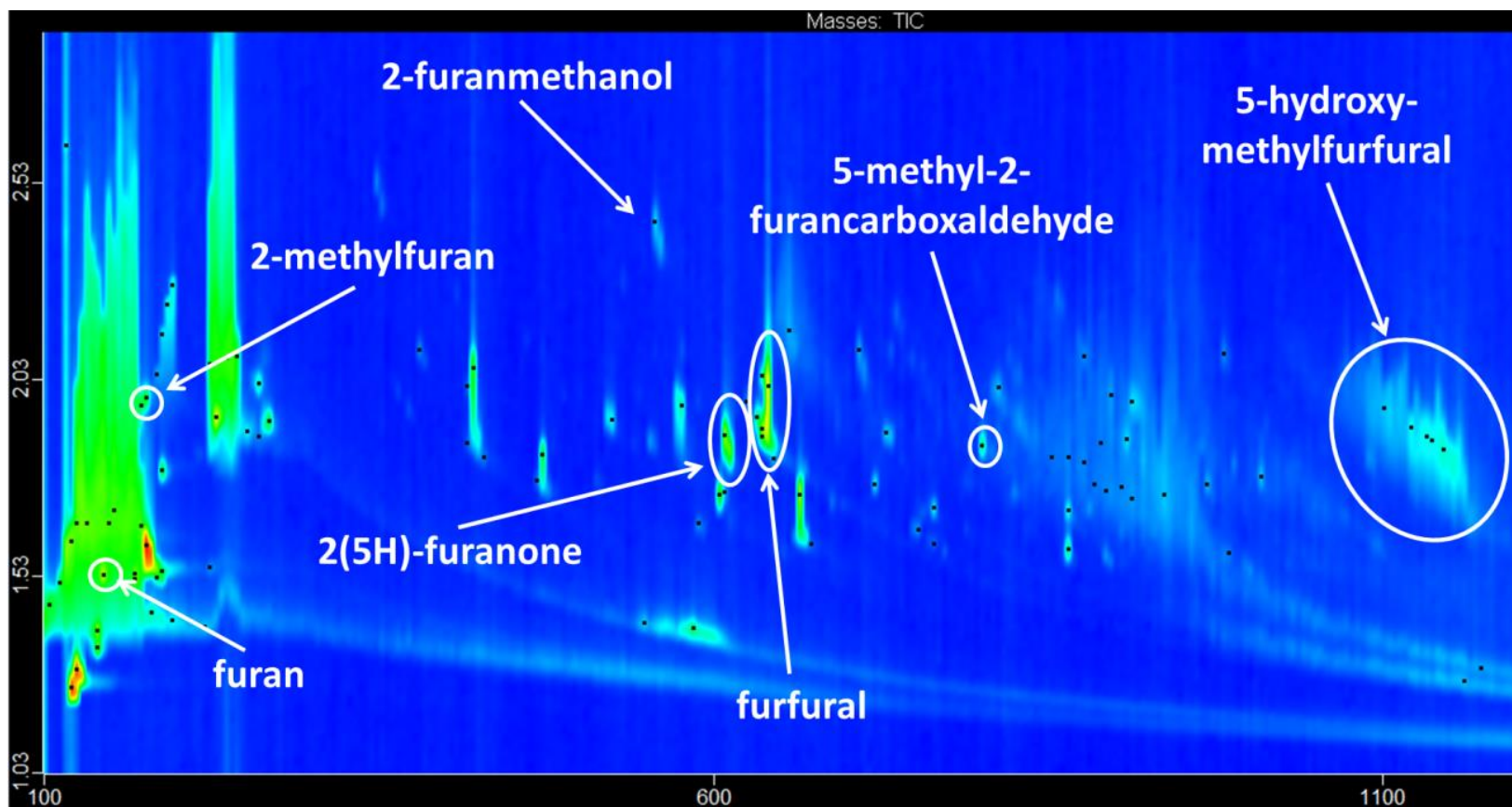


Figure 32. The large differences in primary retention time of furan-like molecules.

### ***3.6.6. Secondary-oven limitation on stationary-phase pairs in the Pegasus 4D***

With the Pegasus 4D, there is a limitation with column configurations using polar-apolar column configurations. This limitation is how apolar secondary columns, relying on relatively weaker chemical interaction with analytes, cannot be fully temperature-optimized for their maximum separation ability. Such a limitation is not imposed on all GCxGC systems, but instead it arises from compromises made during the design and construction of the Pegasus 4D.

As previously explained, there are benefits to polar-apolar column configurations when separating polar analyte mixtures like carbohydrate-pyrolysis vapors. A polar primary column prevents analyte overloading and, in the case of TFPMS, can separate similar key species by large differences in retention time as a function of their oxygen content. However, to create an orthogonal GCxGC separation, the secondary column must use a phase which relies on different interactions like London-type dispersion forces.

The full effectiveness of polar-apolar column configurations is not possible in the Pegasus 4D, however. The Pegasus 4D can only control its secondary-oven temperature by keeping it at least 5°C hotter than the primary oven. This design constraint is due to how (1) the secondary oven resides within the primary oven and (2) the secondary oven has its own heat source but no cooling source. Because of the secondary oven's temperature constraint, the secondary column's stationary phase will always be at least 5°C hotter than the primary column's stationary phase throughout a GCxGC separation method.

The inability to optimize a polar-apolar column configuration fully in the Pegasus 4D arises from the combination of a secondary oven constrained to a higher temperature and the secondary column relying on a weaker set of chemical interactions to perform its separation. The secondary column is essentially forced to operate at a temperature above that of its optimal separation performance. Being above the optimal temperature, shorter differences in retention time will be observed for the analytes. This reduction in separation will be exacerbated by the fact that secondary columns are already compromised due to their

necessarily rapid separation nature: They are much shorter in length than primary columns (~ 1 to 2 m compared to 30-m primary columns) and their carrier gas is at a velocity much higher than that which optimizes the height equivalent of a theoretical plate.<sup>47</sup>

This equipment limitation means a column configuration with weaker chemical interactions between the analytes and the secondary column's stationary phase will be artificially limited in its ability to separate analytes. This limitation of the Pegasus 4D's secondary oven is very frustrating when dealing with mixtures of polar analytes, as it impairs the inherent benefits of polar-apolar column configurations. Arguably, the simplest way to fix this problem is to construct a secondary oven outside the primary oven. Separating the secondary oven will allow it to operate at temperatures both above and below the primary-oven temperature. Original GCxGC systems used such a construction, but they are much larger in size and would likely be more expensive to produce.

In short, requiring the secondary oven to be hotter than the primary oven limits the secondary column's effectiveness in polar-apolar column configurations. With a secondary oven controlled independently from the primary oven, GCxGC chromatograms can achieve better separations in secondary retention time with highly polar analyte mixtures.

### ***3.6.7. Secondary column and thermal modulation***

The secondary column carries analytes through the thermal modulator. The ability for rapid and complete absorption and desorption of analytes in the segment of column inside the thermal modulator is vital for sharp peaks in both the primary and secondary retention-time dimensions. Given the short (4 to 10 second) time durations allowed for total analyte desorption, the strength of chemical interaction between analytes and the secondary column's stationary phase is an important parameter. This parameter has not been well discussed in the literature describing GCxGC separations.

---

<sup>47</sup> GC columns are physically quite different from distillation columns, but their classical analysis takes advantage of analogies to distillation. GC columns are treated as having a height equivalent of a theoretical plate (HETP), and HETP is a function of carrier gas velocity.

Understanding thermal modulation is important to improving peak shape of GCxGC separations. The next three paragraphs briefly explain why a thermal modulator is necessary and how it works. With an understanding of the process, the desirable properties of the column passing through the thermal modulator can be discussed.

The thermal modulator is an integral component for GCxGC separations. Its task is to “focus” analytes co-eluting from the primary GC separation into tight bands, then “re-inject” these analyte bands into the secondary GC separation. Without the thermal modulator, broad, co-eluting analyte bands would enter the secondary GC separation and fail to separate effectively. Lacking a thermal modulator would be similar to using very long-duration injections in a rapid, high-temperature GC separation, where the broad injections would cause little or no analyte separation because tight bands never formed.

The thermal modulator works by using alternating jets of hot and cold gas against short lengths (~ 0.5 cm) of the secondary column’s exterior wall to cause focused and rapid heating and cooling over this short segment of column. The location of these jets is roughly 10 cm downstream of the exit of the primary column and roughly 5 cm upstream of the secondary oven. First, the cold jet blows and causes rapid absorption of analytes in the short region of column, effectively focusing the analytes into a tight band. Immediately after the “cold pulse” ends, the hot jet blows over this same location to cause rapid desorption of the previously absorbed analytes, effectively “re-injecting” the tight band of analytes to the secondary GC separation. The durations of the cold pulse and the hot pulse together make one modulation period. The user defines the durations of hot and cold pulses while creating the GCxGC method parameters.

The thermal modulator used in the Pegasus 4D is a two-stage thermal modulator, which means there are two separate locations for pairs of cold and hot jets along the secondary column. These two jet locations are roughly 3 cm apart along the secondary column. The modulation cycles for these two locations are out of phase. This non-zero phase angle is required to ensure re-injections of tight bands are made to the secondary GC

separation without break-through of unfocused analytes from the ongoing elution of analytes from the primary GC separation. With only one pair of cold and hot jets, there would be break-through of unfocused analytes passing through the thermal modulator during the hot pulse. Such break-through would broaden the analyte bands entering the secondary GC separation and result in broader spectral peaks. Having two stages, or two separate pairs of cold and hot jets, ensures the focusing and re-injection of analytes is done with tight analyte bands.

The ability to rapidly desorb analytes from the hot/cold jet regions of the thermal modulator ensures narrow analyte bands enter the length of column within the secondary oven.<sup>48</sup> Without narrow analyte bands entering the secondary GC separation, the observed peaks will be broad.

Obtaining narrow peaks in the first retention-time dimension relies on two things. First, narrow analyte bands must exit the primary GC separation. Without a good-quality primary GC separation, the GCxGC separation will never produce sharp peaks. Second, the analyte bands absorbed during the cold pulses must be entirely (and rapidly) desorbed by the hot pulse. If these analyte bands are only partially desorbed, then some of the analyte will remain in the thermal modulator region until the next hot pulse. This behavior of “left-over” analyte can broaden tight analyte bands made by the primary column. This broadening is easily observed with very polar analytes like phenol, 2-hydroxyethanal, 2,3-dihydroxypropanal, 1,3-dihydroxypropanone, and water. Broadening of very polar analytes is determined by comparing the GCxGC separation to a GC separation, as the GC separation keeps the thermal modulator hot, preventing any absorption.<sup>49</sup>

---

<sup>48</sup> ~10 cm of the secondary column lies within the thermal modulator, and ~30 cm of the secondary column lies in the transfer line to the TOFMS. The remaining length of secondary column lies coiled within the secondary oven.

<sup>49</sup> By “turning off” the thermal modulator ( i.e., eliminating gas jets and setting it to a constant temperature) and slightly increasing the secondary oven’s temperature, the short secondary column has a negligible effect on the primary column’s separation. With this adjustment to the GCxGC method parameters, a GCxGC system operates as a GC system.

Using a fused-silica column with no stationary phase within the thermal modulator could improve the desorption performance. The lack of a stationary phase could hasten the desorption process in two ways. First, it eliminates the chemical interactions which attract the analytes and depress the analytes' vapor pressure by liquid-solution behavior. Second, a lack of stationary phase would allow faster heat transfer by (1) eliminating the thermal resistance of the stationary phase and (2) allowing a higher hot-jet temperature due to no concerns over column bleed.<sup>50</sup>

Integrated guard columns present a potential way to place a stationary-phase-free column within the thermal modulator yet not require additional column unions. Guard columns are short (several meters long) columns placed upstream of the analytical column, and they are meant to capture any non-volatile contaminants upstream of the analytical column in order to preserve the effectiveness of the stationary phase.

Using a stand-alone guard column would require an additional column union in the GCxGC system, which is problematic in two ways. First, there is not sufficient room to insert a column union reliably inside ~10-cm-diameter, cylindrical secondary oven. Second, if it were possible to install a column union within the secondary oven, doing so adds a difficult-to-maintain connection through which air can leak due to being on the vacuum-side of the capillary system.

Some analytical columns have guard columns integrated, so additional (and potentially problematic) column unions are not necessary. Such an integrated guard-analytical column could be used for the secondary column. It would be installed so the guard region passes through the thermal modulator and the analytical region resides in the secondary oven. The only problem with this proposal is that integrated guard columns are only found with inner diameters down to 0.25 mm, while the typical secondary columns are

---

<sup>50</sup> "Column bleed" is the thermal breakdown of stationary-phase material into volatile components. These volatile components mix with injected analytes and are also observed in the detector.

0.15 mm in inner diameter. It is not certain how the change in inner diameter would affect the secondary GC's rapid-operation.

In conclusion, thermal-modulator performance is important for both enhancing secondary-GC peak shape and preserving primary-GC peak shape. Sharp analyte peaks depend upon rapid and complete desorption of focused analyte bands. Reducing the polarity of the secondary column's stationary phase may sharpen peaks by increasing desorption rates. It is desirable to eliminate the stationary phase altogether in the secondary column in attempt to further increase desorption rates.

### ***3.6.8. Obtaining orthogonality is important to simpler comparisons of analyte mixtures***

There is an important difference between preventing co-elution and obtaining very orthogonal separations in GCxGC: Preventing co-elution does not necessarily imply using all of the available two-dimensional space on a GCxGC chromatogram. This distinction is very important and the need for excellent orthogonality is based upon the desired purpose of the GCxGC chromatogram. If a computer algorithm is simply going to match detected mass spectra to libraries for identification and quantification in an automated report, then orthogonality is not required (although it will likely only help this desired outcome). Such a case makes sense if very similar complex analyte mixtures will be routinely analyzed, and a GCxGC separation must focus upon certain key analytes which are well separated. On the other hand, if many different complex analyte mixtures must be analyzed and compared, then orthogonality is vital to visual inspections of the resulting series of chromatograms. Comparing tables of identified analytes and their quantities is much too difficult when comparing hundreds of different analytes within several key analyte homologues. Such a case makes sense for determining the effect of pyrolysis, hydrolysis, and hydrodeoxygenation/deoxygenation processes on bio-oils, as these samples vary in their abundance (or even presence) of entire homologues like alcohols, aldehydes and ketones, alkylbenzenes, alkoxybenzenes, alkylnaphthalenes, and alkanes. Without excellent orthogonality, the visual indications are much too subtle (or impossible) to see and these

samples cannot be analyzed quickly for their intended purpose of general process performance.

If given the choice, a chromatographer would always choose a perfectly orthogonal separation if the perfectly orthogonal separation also prevents co-elution of vital analytes. However, developing such a demanding separation, even with advanced GCxGC systems, is very difficult, and often compromises must be made between preventing co-elution between the most vital analytes and ensuring a wide range of homologues are arranged in a perfectly orthogonal manner.

### ***3.7. Conclusion***

Developing GCxGC separations was seen as a “means to an end” to support the primary research objective of determining pyrolysis reaction chemistry, and compromises were made in this investigation. The necessary GCxGC separations were very demanding, as they must separate a range of analyte homologues which varied greatly in vapor pressure, degree of unsaturation, and the number and type of oxygen-containing functional groups. The need for the GCxGC chromatogram to group analyte homologues into distinct regions quickly became apparent, as comparing and contrasting GCxGC chromatograms is difficult without clear visual differences between regions. The novel stationary-phase pair PTFPMS-p(BDMSP-co-DMS)5/95 proved successful, and the novel stationary-phase pair p(BCPS-co-CPP)90/10-PEG proved unsuccessful. The need for a steady supply of an identical complex mixture is also vital, as comparing and contrasting GCxGC chromatograms is made even more difficult when both the stationary-phase pairs and the analyte homologues change.

After finding no detailed system to predict the separation capabilities of stationary-phase pairs for various mixtures, it was attempted to develop such a system. “Comparative chemical-interaction-type strengths” were suggested as a way to identify stationary-phase pairs which provide more effective GCxGC separations. McReynolds-constants data were used to evaluate the fractional retention differences, but these did not provide a clear explanation of why some stationary-phase pairs were orthogonal and some were not. A

justification for why some stationary-phase pairs are orthogonal, at a level deeper than qualitative understanding of chemical-interaction types, is still desired.

## CHAPTER 4. DEHYDRATIONS AND DEHYDROGENATIONS OF ALCOHOLS

### *4.1. Abstract*

Alcohols were pyrolyzed in the gas phase within a range of 200-400°C. These alcohols served as model compounds for the alcohol functional groups found throughout cellulose. These model compounds were grouped into two sets, a set of nine monols and a set of three diols and one triol. Primary and secondary monols primarily dehydrogenated. The tertiary monol dehydrated. The diols and triol underwent a combination of dehydrogenation, dehydration, and fragmentation of carbon-carbon bonds. Reactions fragmenting carbon-carbon bonds followed both the cyclic Grob fragmentation and a possible new, unknown fragmentation pattern.

Concerted elementary dehydrogenation and dehydration reactions were evaluated with computational-quantum-chemistry (CQC) simulations. The evaluations found potential transition-state structures indicated by one negative rovibrational frequency. The relative likelihood of mechanisms was proposed based upon comparing their enthalpies of activation. For dehydrogenation, the meta-oxygen, six-center bimolecular mechanism is predicted to be drastically more favorable than the para-oxygen, six-center bimolecular mechanism due to a difference of roughly 50 kcal mol<sup>-1</sup> for each of the four separately evaluated monols. This meta-oxygen, six-center bimolecular dehydrogenation mechanism is potentially more favorable than the four-center, unimolecular dehydrogenation mechanism due to a difference of roughly 30 kcal mol<sup>-1</sup> for each of the four separately evaluated monols. For dehydration, the meta-oxygen, six-center bimolecular mechanism is potentially more favorable than the four-center, unimolecular mechanism due to a difference of roughly 13 kcal mol<sup>-1</sup> for each of the three separately evaluated monols. Comparison of reaction mechanisms by enthalpy of activation alone is not sufficient for accurate prediction of reaction flux, especially when comparing unimolecular to bimolecular reactions. Nevertheless, the results of the CQC simulations provide a valuable basis for predicting Arrhenius parameters, which are capable of comparing likelihood of reaction flux among all hypothesized reaction mechanisms. These

elementary reactions appear promising in understanding the detailed reactions of cellulose pyrolysis, as well as pyrolysis of other materials with a prevalence of alcohol groups like polysaccharides, oligosaccharides, and monosaccharides.

#### ***4.2. Introduction***

The omnipresence of water in pyrolysis products suggests that the formation of any organic products is inherently linked to dehydration activity. Fast pyrolysis of biomass, cellulose [47], and hemicellulose [48] form a significant fraction of water along with the volatile organic products of interest. Slow pyrolysis forms a significant fraction of water along with the organic gases like CO and CO<sub>2</sub> and organic char products.

The formation of the organic products and water may occur concomitantly in the same elementary reaction, or the organic products and water may be formed separately in a series of elementary reactions. In either case, the elementary chemistry of dehydration is important to the understanding how organic products form during pyrolysis.

Several elementary dehydration reactions have already been suggested to explain the pyrolysis of carbohydrate materials in biomass. Seshadri and Westmoreland [3] suggested that a vital pathway for levoglucosan formation proceeds by dehydration. Nimlos et al. [1] suggested that various dehydrations may occur involving the multiple adjacent hydroxyl groups present throughout cellulose and hemicellulose. One of their simulated reactions, a 1,3-dehydration, was supported by the experimental observations of Paine et al. [23]. This “cyclic Grob fragmentation,” as it was called, is very important to biomass pyrolysis because it showed how a single elementary reaction can form both water and fragments of monosaccharide rings

This work aims to elucidate elementary dehydration reactions by using simpler model compounds than cellulose, D-glucose, or propan-1,2,3-triol. These compounds provide many possible ways one can hypothesize elementary dehydrations. Upon using even smaller

compounds, it is shown that pyrolysis of small alcohols allows dehydrogenation to occur in addition to dehydration.

#### ***4.2.1. Model compounds effectively test hypothesized reactions***

Model compounds simplify the chemical structure of the ultimate compound or compound mixture of interest. They can provide several types of simplifications:

- Reduce a complex mixture of many different molecules into a simpler mixture with fewer different molecules. (For example, the complex mixture of gasoline with many compounds could be represented by a simpler surrogate composed of n-heptane and 2,2,4-trimethylpentane, cyclohexane, benzene, and ethanol.)
- Reduce a single molecule with many functional groups to a molecule with fewer functional groups. (For example, propan-1,2,3-triol can be simplified by using propan-1-ol and propan-2-ol.)
- Reduce a single, large molecule into a smaller or simpler molecule. (For example, octan-1-ol can be simplified by using methanol.)

When evaluating chemical reactions, each method helps isolate of chemical-reaction propensities. Additionally, careful selection of model compounds may also help by modifying thermophysical or transport properties. These simplifications are needed for a variety of purposes.

- In the case of simpler mixtures, the complexity of chemical-reaction networks can be greatly reduced to isolate or enhance the detection of specific chemical reactions.
- In the case of reducing the number of functional groups in a single molecule, the fewer functional groups will also greatly reduce the complexity of chemical-reaction networks to isolate or enhance the detection of specific chemical reactions.
- In the case of decreasing the size of a molecule, the decreased molecular weight can increase the vapor pressure enough to ensure a vapor-phase reaction medium at less severe conditions.

Chemical reactions can be determined by creating a set of model compounds that have specific differences among their chemical structures. Comparison of the reaction products formed from these different model compounds allows the detailed testing of hypothesized reactions. For example, one can test the validity of a hypothesized reaction that requires a 1,2,3-triol system by comparing the pyrolysis products of propan-1,2,3-triol to the reaction products of propan-1,2-diol and propan-1,3-diol. If analogous products are formed from both propan-1,2,3-triol and propan-1,2-diol, then the hypothesized reaction requiring a 1,2,3-triol system is likely incorrect. Additionally, if analogous products are formed by propan-1,3-diol as well as 1,2,3-triol and 1,2-diol systems, then a 1,2-diol system is also not likely necessary to achieve the reaction. Hypothesis testing is made much simpler by testing a large set of model compounds with single structural differences between members, as opposed to testing a small set of complicated model compounds with many structural differences between members.

#### ***4.2.2. Alcohols form model compound sets for cellulose's reaction-pattern hypotheses***

Because cellulose contains many hydroxyl functional groups, it is natural to use alcohols to construct a model-compound set. Figure 33 displays cellulose's molecular structure in order to highlight the prevalence and exact location of hydroxyl groups. The D-glucose monomer takes four forms when polymerized into cellulose, and each form will have a slightly different arrangement of hydroxyl groups. The central repeating unit greatly outnumbers the end units,<sup>51</sup> but the end units are still inspected in order to locate all useful model compounds should cellulose pyrolysis involve any unzipping reactions initiated by end units. Table 8 lists the specific locations of the hydroxyl groups in each of the four D-glucose forms in cellulose. Table 8 then goes on to list the locations of "alcohol systems," which can be employed as model-compound sets. Three important observations summarize the breakdown of alcohol groups and their locations within cellulose.

---

<sup>51</sup> Typical celluloses often have a degree of polymerization of 2000, so the n repeating  $\beta$ -D-anhydroglucopyranose units outnumber either terminal end unit by three orders of magnitude.

- On the repeating  $\beta$ -D-anhydroglucopyranose units are three monols, one 1,2-diol, and no triols. Of the monols, one is a primary alcohol.
- On the non-reducing end of cellulose, the  $\beta$ -D-glucopyranose unit has four monols, two 1,2-diols, two 1,3-diols, and one 1,2,3-triol.
- On the reducing end of cellulose,  $\beta$ -D-glucopyranose can take two forms, as shown in Figure 33.
  - On the glucopyranose form are four monols, two 1,2-diols, and a 1,2,3-triol.
  - On the acyclic form are four monols and two 1,2-diols.

A drastic difference in reaction rates between either 1,3-diols or 1,2,3-triols and monols could allow for reactions on the end units to become important to the overall product composition.

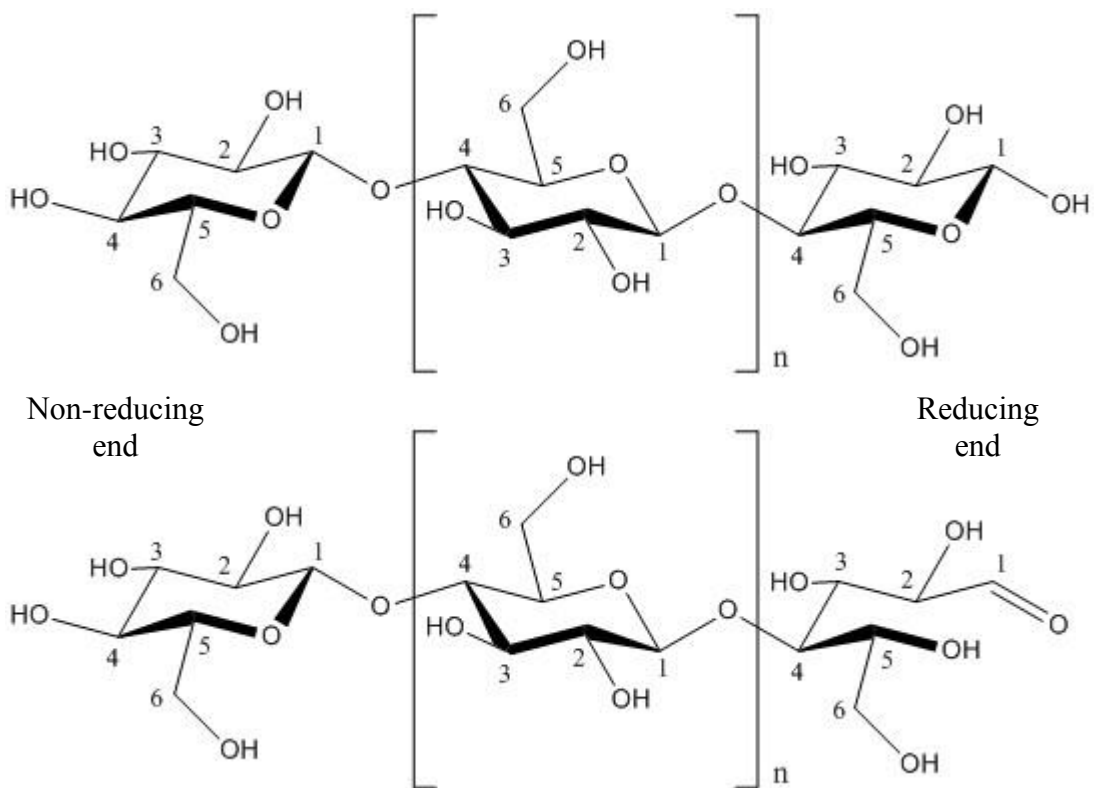


Figure 33. Hydroxyl groups are predominant in cellulose. The numbering scheme of D-glucose is kept for each unit to describe the location of functional groups specifically. (Hydrogen atoms bonded to carbon are not shown for simplicity.)

Table 8. The presence of alcohol functional groups in cellulose lend themselves to representation by monol, diol, and triol systems. (The oxygen atoms are numbered according to the carbon number to which they are bonded.)

Alcohol functionality	Cellulose Component			
	Non-reducing-end unit	$\beta$ -D-anhydroglucopyranose repeating units	Reducing-end unit	
			Glucopyranose from	Acyclic Form
Hydroxyl group	<ul style="list-style-type: none"> <li>• C2(O2-H)</li> <li>• C3(O3-H)</li> <li>• C4(O4-H)</li> <li>• C6(O6-H)</li> </ul>	<ul style="list-style-type: none"> <li>• C2(O2-H)</li> <li>• C3(O3-H)</li> <li>• C6(O6-H)</li> </ul>	<ul style="list-style-type: none"> <li>• C1(O1-H)</li> <li>• C2(O2-H)</li> <li>• C3(O3-H)</li> <li>• C6(O6-H)</li> </ul>	<ul style="list-style-type: none"> <li>• C2(O2-H)</li> <li>• C3(O3-H)</li> <li>• C5(O5-H)</li> <li>• C6(O6-H)</li> </ul>
Primary alcohol	<ul style="list-style-type: none"> <li>• C6(O6-H)</li> </ul>	<ul style="list-style-type: none"> <li>• C6(O6-H)</li> </ul>	<ul style="list-style-type: none"> <li>• C6(O6-H)</li> </ul>	<ul style="list-style-type: none"> <li>• C6(O6-H)</li> </ul>
Secondary alcohol	<ul style="list-style-type: none"> <li>• C2(O2-H)</li> <li>• C3(O3-H)</li> </ul>	<ul style="list-style-type: none"> <li>• C2(O2-H)</li> <li>• C3(O3-H)</li> </ul>	<ul style="list-style-type: none"> <li>• C1(O1-H)</li> <li>• C2(O2-H)</li> <li>• C3(O3-H)</li> </ul>	<ul style="list-style-type: none"> <li>• C2(O2-H)</li> <li>• C3(O3-H)</li> <li>• C5(O5-H)</li> </ul>
1,2-Diol system	<ul style="list-style-type: none"> <li>• C2(O2-H)C3(O3-H)</li> <li>• C3(O3-H)C4(O4-H)</li> </ul>	<ul style="list-style-type: none"> <li>• C2(O2-H)C3(O3-H)</li> </ul>	<ul style="list-style-type: none"> <li>• C1(O1-H)C2(O2-H)</li> <li>• C2(O2-H)C3(O3-H)</li> </ul>	<ul style="list-style-type: none"> <li>• C2(O2-H)C3(O3-H)</li> <li>• C5(O5-H)C6(O6-H)</li> </ul>
1,3-Diol system	<ul style="list-style-type: none"> <li>• C2(O2-H)C3C4(O4-H)</li> <li>• C4(O4-H)C5C6(O6-H)</li> </ul>	(None)	<ul style="list-style-type: none"> <li>• C1(O1-H)C2C3(O3-H)</li> </ul>	<ul style="list-style-type: none"> <li>• C3(O3-H)C4C5(O5-H)</li> </ul>
1,2,3-Triol system	<ul style="list-style-type: none"> <li>• C2(O2-H)C3(O3-H)C4(O4-H)</li> </ul>	(None)	<ul style="list-style-type: none"> <li>• C1(O1-H)C2(O2-H)C3(O3-H)</li> </ul>	(None)

Figure 34 shows how these primary and secondary monols, diols, and triols may be “extracted” from the cellulose structure to generate model compounds. These alcohols might share the same pyrolytic elementary reactions as the local region of cellulose from which they are extracted. These alcohols are much simpler to experiment with because their volatility allows their pyrolysis reactions to be entirely gas-phase. Gas-phase reactions can be analyzed more easily than typical solid-phase reactions for several reasons:

- Complicated condensed-phase phenomena are eliminated, such as:
  - Surface reactions like vapor-char interactions and
  - Solvent effects like ion solvation and stabilization of reaction intermediates.
- The gas phase is closer to the conditions of common CQC simulations used to predict transition-state properties like enthalpy of activation.

Elimination of condensed-phase chemistry might eliminate some key phenomena inherent to biomass pyrolysis, but eliminating these complicating phenomena is necessary to obtain a more elementary level of understanding.<sup>52</sup>

---

<sup>52</sup> Most experimental reactions capable of determining elementary pyrolysis chemistry must eliminate some complicating phenomena which are inherently important in real biomass pyrolysis. For example, cellulose is often purified of mineral matter to understand its elementary pyrolysis chemistry, yet real biomass pyrolysis processes will likely never demineralize their feeds and will always need to account for mineral matter catalyzing reactions [21].

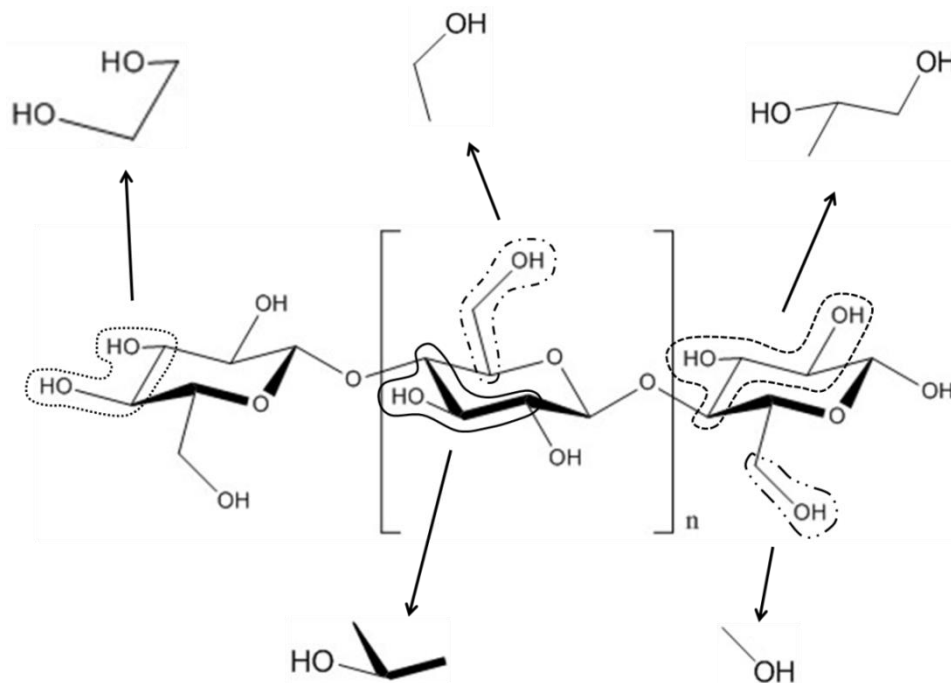


Figure 34. Examples of extracting alcohol model compounds from the cellulose chain.

### 4.3. Methods and Procedures

#### 4.3.1. Selection of alcohols for members of model-compound sets

The alcohols were divided first into two main sets based upon having one or more than one hydroxyl groups, providing the two main model-compound sets of “monols” and “diols and triol,” respectively. Further subdivisions of these main model-compound sets can be made based upon the nature of the carbon atoms in both type and configuration. Important comparisons can be made between members of the same subset and set, as well as between members of different subsets and sets.

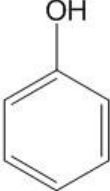
Monols are the model-compound set with the most members because many monols are easily available for purchase at a high purity. The monols tested were methanol, ethanol,

propan-1-ol, 2,2-dimethylpropan-1-ol, 5-hydroxymethylfurfural, propan-2-ol, butan-2-ol, 2-methylpropan-2-ol, and phenol. This monol set is displayed in

Table 9, where the chemical structures are aligned vertically to highlight their similarities and differences.

Table 9. The monols group can be divided into subgroups describing the substitution of the  $\alpha$  carbon.

Primary Monol	Methanol	
	Ethanol	
	Propan-1-ol	
	2,2-Dimethylpropan-1-ol	
	5-Hydroxymethylfuran	
Secondary Monol	Propan-2-ol	
	Butan-2-ol	
Tertiary Monol	2-Methylpropan-2-ol	

Aromatic Monol	Phenol	
----------------	--------	---

Several subsets of the monol set were created by classifying the carbon substitution of the  $\alpha$  carbon.<sup>53</sup> The first five monols (methanol, ethanol, propan-1-ol, 2,2-dimethylpropan-1-ol, and 5-hydroxymethylfurfural) form a subset of primary monols. The members of this subset differ only by the size and shape of their alkyl chains. The differences in alkyl chains are highlighted in

Table 9 by how their alkyl chains extend away from the hydroxyl group's  $\alpha$  carbon, which is held in the same horizontal position. The sixth and seventh monols (propan-2-ol and butan-2-ol) form a subset of secondary monols. Two alkyl chains still are bonded to its  $\alpha$  carbon, which remains in the same horizontal position relative to the first five monols to show structural differences easily. The eighth monol (2-methylpropan-2-ol) is a tertiary monol, showing a three alkyl groups bonded to its  $\alpha$  carbon. The ninth monol, phenol, could be considered a secondary monol due to the  $\alpha$  carbon being bonded to only two other carbon atoms. However, the  $\alpha$  carbon is a part of an phenyl ring. The phenyl ring's aromaticity potentially makes phenol's alcohol group subject to additional reaction possibilities compared to the secondary alcohols with saturated  $\alpha$  carbons, causing it to be its own monol subset.

Three diols and a triol formed the diol-and-triol model-compound set. Figure 35 arranges the diols and triol along with some of the monols in a way which highlights their

---

<sup>53</sup> The  $\alpha$  carbon is the carbon atom directly bonded to the hydroxyl group's oxygen atom. Proceeding away from the  $\alpha$  carbon are first the  $\beta$  carbon and then the  $\gamma$  carbon.

structural similarities and differences. The lines connect structures which differ only by substituting a hydrogen atom with a methyl, methylene, or hydroxyl group.

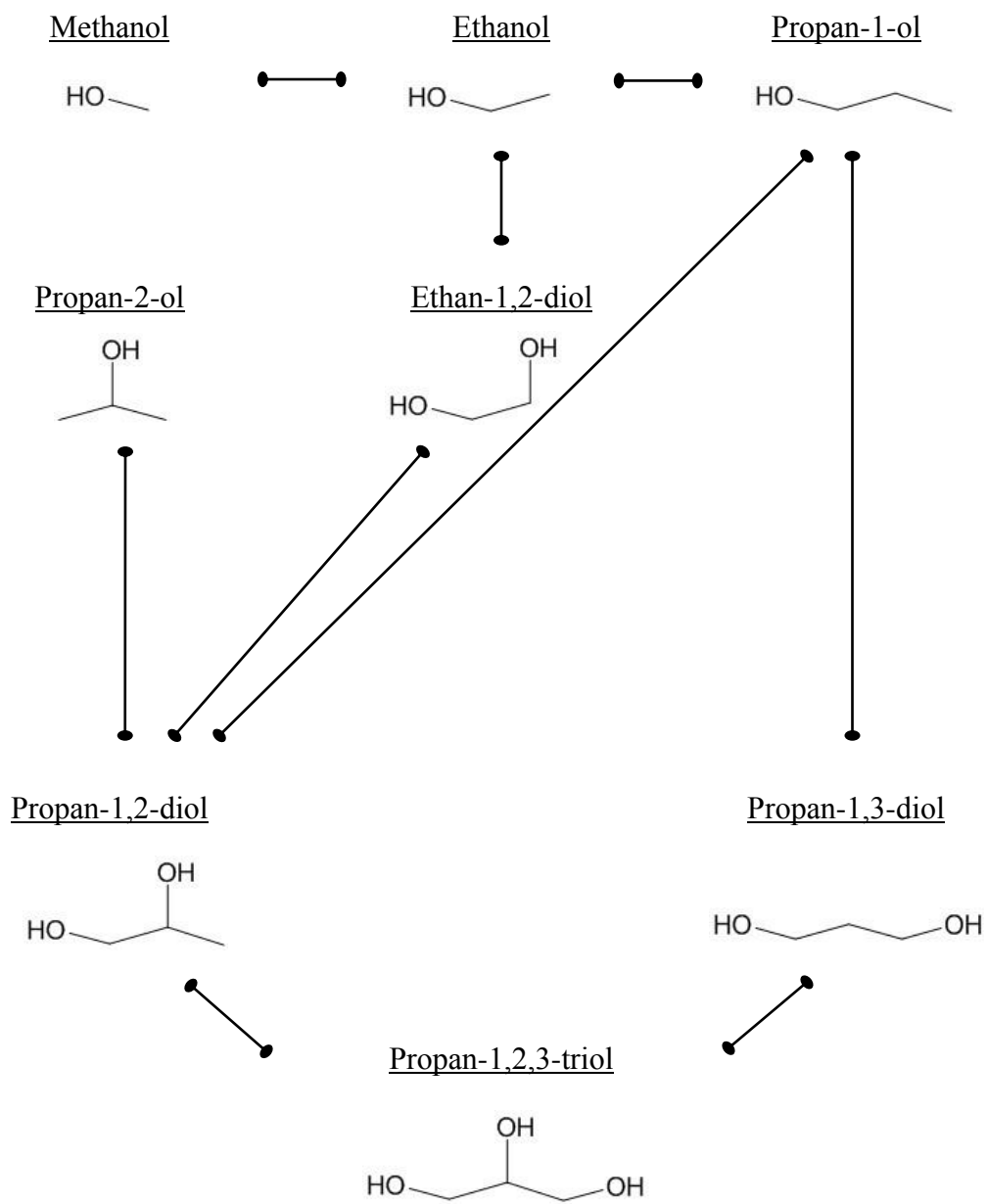


Figure 35. Comparison of the diols and triol to some of the monols. Lines indicate the simplest possible structural change between stable molecules.

The model-compound set containing diols and a triol was much smaller than the monol set. Three practical reasons limited the members of the diol and triol sets.

- A much more limited commercial availability of variations in alkyl groups when requiring a 1,2-diol, 1,3-diol, or 1,2,3-triol system;
- A rapidly increasing viscosity with increasing molecular weight; and
- A rapidly decreasing vapor pressure with increasing molecular weight.

Viscosity of the reactants was important to PIDSSR experiments (described in Section 4.3.3) because a syringe injected these liquid reactants to its inlet, and knowing the quantity of liquid injected required that the syringe contain a column of liquid with no bubbles or breaks. The more viscous diols and triol often produced bubbles, which separated the column of liquid into several segments within the syringe's needle and barrel. The volumes of these segments could not be accurately determined against the syringe barrel's graduation marks. In addition, it was seen that some of the more viscous liquids would not entirely draw out of the needle and into the syringe barrel, as a small portion would remain at the edge of the needle.

The vapor pressure was also important because the PIDSSR's residence times might be significantly altered if entrained liquid droplets are delivered to the reactor tube instead of vapors. In addition, the droplets may promote condensed-phase reactions instead of gas-phase reactions, especially if the droplets contact walls and create traces of coke as the droplet pyrolyzes. As for the PIQR (described in Section 4.3.3), high volatility was essential in order to deliver sufficient reactant to the reactor tube because the bubbler assembly, sample valve, and tubing were/contained plastic materials and thus could not be heated. Without heating the reactant feed, materials without a high volatility will only deliver a reactant pulse with a low vapor concentration of reactant. The less volatile materials like diols and triol were not attempted in the PIQR because of their very low volatilities.

- 2-Methylpropan-2-ol presented a problem of freezing near room temperature (melting point ~ 25°C), but it never had issues solidifying in vessels other than its original

container from the vendor. It was assumed that handling the syringe and vials by hand kept them warm enough to prevent any freezing.

- Phenol and 2,2-dimethylpropan-1-ol were also solid at room temperature, but they would not melt at temperatures which could allow easy handling of vials and syringes. Instead, they were dissolved in toluene to allow injection.

#### **4.3.2. *Materials***

All chemicals were used as received without any added purification, stabilization, or degassing. Table 10 lists the exact chemicals used with their vendors/manufacturers. Product numbers and lot numbers are included should inquiries need be made about the presence of potential impurities of stabilizers not explicitly stated in product literature.

Table 10. List of reagents used in the study of alcohol model compounds, ordered alphabetically.

Reactant	Manufacturer	Purity	Product Code	Lot Number
Butan-2-one ("2-Butanone")	Sigma-Aldrich	≥99.7%	34861-100ML	SHBC8895V
2,2-Dimethylpropan-1-ol	Sigma-Aldrich	99%	N7206-10G	MKBL5441V
Ethanal	Sigma-Aldrich	≥99.5%	402788	SHBC0936V
Ethanol	Acros Organics	99% (<0.005% water at packaging)	397690025	1286417
Ethan-1,2-diol ("Ethylene Glycol")	Fluka/Sigma-Aldrich	"≥99.5 (GC)"	03750-250ML	BCBJ7957V
Helium	Airgas	99.9995% (certified 0.34 ppm O <sub>2</sub> )	325541	38224-88
5-Hydroxymethylfurfural	SAFC/Sigma-Aldrich	">99%"	W501808-1G-K	MKBJ8116V
Methanol	Sigma-Aldrich	≥99.9% "CHROMASOLV"	34860-4L-R	SHBC0287V
2-Methylpropan-2-ol ("tert-Butyl Alcohol")	Acros Organics	99.5%	107710025	1212421
Phenol	Sigma-Aldrich	≥99%	328111-100G	SHBC6998V
Propanal ("Propionaldehyde")	SAFC/Sigma-Aldrich	≥97%	W292303-1KG-K	MKBN6298V
Propan-1-ol	Sigma-Aldrich	99.7%, anhydrous	279544-100ML	SHBC3061V
Propan-2-ol	Fisher BioReagents®	99.9%	BP2632-4	102116
Propan-2-ol D8	Sigma-Aldrich	99.5 atom %	175897-5G	CC0668V
Propan-1,2-diol ("Propylene Glycol")	SAFC/Sigma-Aldrich	≥99.5%	W294004-1KG-K	MKBK1806V
Propan-1,3-diol	Aldrich/Sigma-Aldrich	98%	P50404-100G	STBC7959V
Propan-1,2,3-triol ("Glycerol")	BDH/VWR	Assay 99.7%	BDH1172-1LP	080910D
Toluene	Sigma-Aldrich	99.5+%, A.C.S.	443395-1L	02744EB

#### 4.3.3. Pyrolysis reactors and chemical analyses

The monols, diols, and triol were all pyrolyzed in the pulse-injected deactivated-stainless-steel reactor (PIDSSR). The PIDSSR was fully described in Section 2.6. In short, it is a gas-phase reactor spliced between the GC's carrier-gas flow controller and the GC's

inlet. A GC syringe was used to inject 0.1 to 1.0  $\mu\text{L}$  of liquid reactant, which vaporized in the PIDSSR inlet. The vapor was entrained in the helium carrier-gas flow to pass through the PIDSSR's 50-cm reactor tube. The reactor tube was able to obtain a wall temperature of 400°C at its center thermocouple (25-cm position). After exiting the reactor, the reactor's entire effluent was sent directly to the GC inlet for analysis by GCxGC-TOFMS. The PIDSSR was developed to pyrolyze volatile compounds, as volatile compounds would evaporate and exit the TGA/DSC and the Pyroprobe® without reaction.

The GCxGC-TOFMS was operated in either its GC or GCxGC mode. The reason for using both modes was to ensure highly polar analytes like propan-1,2-diol, propan-1,3-diol, and propan-1,2,3-triol were observed as peaks because thermal modulation in GCxGC often caused their peaks to be so broad that they fell below detection limits. (The importance of rapid desorption during thermal modulation for successful analyte peaks was discussed in Section 3.6.7.)

The reactants were analyzed for purity by direct injection to the GC inlet to ensure any impurities were not mistaken for reaction products. The GC inlet's temperature was adjusted to find a temperature high enough to ensure vapors did not condense but low enough to prevent the thermal reactions designed to take place in the PIDSSR's reactor tube.

The GC syringe (Hamilton Part Number 80000, Model 1701N, 10  $\mu\text{L}$ , 26s gauge, 2 inch needle, point style 2) was prepared for the next alcohol to be tested by filling and purging it with the next alcohol ten times. Purging was performed by drawing 10  $\mu\text{L}$  of fresh liquid into the syringe and ejecting it. During the first of the ten fill-and-purge cycles, the new alcohol was given one minute to remain in the syringe barrel and thoroughly dissolve the previous alcohol.

Two monols, methanol and propan-1-ol, were also pyrolyzed in the pulse-injected quartz reactor (PIQR). The PIQR was fully described Section 2.8 as a gas-phase reactor using helium as a purge gas. The helium purge gas first flowed through a six-port valve before reaching the reactor inlet. A steady stream of reactant vapor in argon flowed through this six-

port valve as well as a sample loop connected to the six-port valve. Upon switching the six-port valve's position, the argon and reactant vapor within the sample loop was sent as a pulse to the reactor, being "pushed" by the helium flow now forced through the sample loop. After passing through the reactor tube, a stream split sent a portion of the reactor effluent to a quadrupole mass spectrometer (QMS). There are two benefits of the PIQR-QMS system compared to the PIDSSR-GCxGC-TOFMS system.

- The PIQR's reactor tube was quartz, which has surface effects much better understood by kinetics researchers than the proprietary deactivation coating ("Silcosteel®Hydroguard") on the PIDSSR's reactor tube.
- The QMS was capable of detecting ion spectra with a mass-to-charge ratio as small as  $1 \text{ Da e}^{-1}$ , which allows it to detect  $\text{H}_2$  spectra directly (at  $2 \text{ Da e}^{-1}$ ). The GCxGC-TOFMS could only detect ion spectra with a mass-to-charge ratio as small as  $5 \text{ Da e}^{-1}$ , likely to avoid interference from helium carrier gas at  $4 \text{ Da e}^{-1}$ .

The PIQR-QMS system also has two disadvantages compared to the PIDSSR-GCxGC-TOFMS system.

- The reactant was injected by vaporizing it in flowing argon. The bubbler, the tubing, sample loop, and six-port valve could not be heated effectively, so the quantities which could be injected depended entirely upon the volatility of the reactant. Methanol's volatility was sufficient for easy spectral detection for expected pyrolysis products. On the other hand, spectra of expected pyrolysis products from propan-1-ol became more difficult to observe, likely due to its lower vapor pressure producing a smaller injected quantity. Pyrolyzing the diols or triol was not attempted in the PIQR-QMS due to their substantially lower vapor pressures.
- There is no chromatographic separation upstream of the QMS, so all product spectra are observed in the same pulse time span. Any spectra shared between expected analytes make spectra interpretation more complicated.

- The QMS (associated with the PIQR) operates with an ionization energy of 40 eV, instead of the 70 eV commonly used for GC-MS and GCxGC-TOFMS. Identifying the compounds responsible for mixed (non-chromatographically separated) spectra became difficult because it was uncertain how similar they should be to the 70-eV spectra within the NIST MS 2.0 Database and the spectra obtained by the GCxGC-TOFMS.

#### ***4.3.4. Computational-quantum-chemistry simulations***

The computational-quantum-chemistry (CQC) simulations were performed with Gaussian 09 software. The CBS-QB3 method was employed to find transition-state structures and energies.

### ***4.4. Results***

#### ***4.4.1. Most monols dehydrogenated in the PIDSSR-GCxGC-TOFMS***

The major and minor products obtained from pyrolysis of monols are displayed in Table 11. All but one of the saturated primary and secondary monols dehydrogenated to form a carbonyl group in place of the alcohol group: Primary alcohols formed an aldehyde and secondary alcohols formed a ketone without any change to the alkyl chains. These carbonyl compounds were the major products obtained for primary and secondary monols, and other products like alkenes created much smaller chromatographic peaks. The single exception to this trend for primary and secondary monols was 2,2-dimethylpropan-1-ol, which both dehydrogenated and dehydrated. Even with its furan ring and carbonyl functionalities, 5-hydroxymethyl furfural underwent dehydrogenation of its alcohol group to form 2,5-furandicarboxaldehyde, but some of the 5-hydroxymethylfurfural also deformedylated to furfural and methanal.

Monols other than the primary and secondary alcohols performed differently. The saturated tertiary monol, 2-methylpropan-2-ol, only dehydrated. Phenol (dissolved in toluene), the aromatic alcohol, did not form any reaction products.

Table 11. Reaction products observed from pyrolyzing monols in the PIDSSR at 400°C.

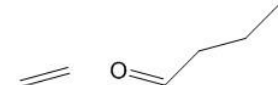
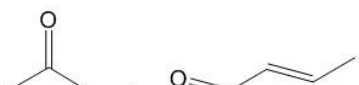
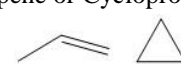
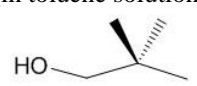
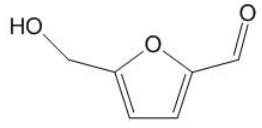
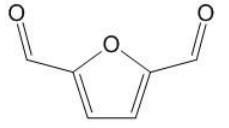
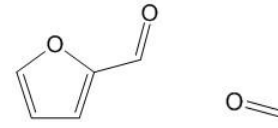
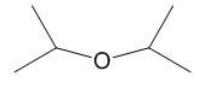
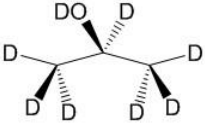
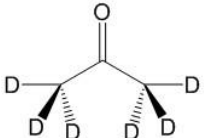
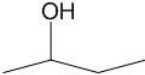
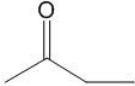
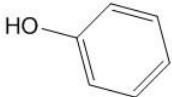
Reactant	Major Product(s)	Minor Product(s)
Methanol 	Methanal 	CO, CO <sub>2</sub> $C\equiv O$ $O=C=O$
Ethanol 	Ethanal 	Ethene, Butanal,  Butanone, But-2-enal 
Propan-1-ol 	Propanal 	Ethanal,  Propene or Cyclopropane* 
2,2-Dimethylpropan-1-ol (in toluene solution) 	2,2-Dimethylpropanal, 2-Methylpropene 	Isobutane 
5-Hydroxymethylfurfural 	2,5-Furandicarboxaldehyde 	Furfural, Methanal,  Furan 
Propan-2-ol 	Propanone 	Diisopropyl Ether,  Propene or Cyclopropane* 

Table 11, Continued.

Reactant	Major Product(s)	Minor Product(s)
Propan-2-ol D8 	Propanone D6 	(None)
Butan-2-ol 	Butanone 	But-2-ene 
2-Methylpropan-2-ol 	2-Methylpropene 	(None)
Phenol (in toluene solution) 	(None)	(None)

#### 4.4.2. The butan-2-ol impurity became an useful model compound

Butan-2-ol was pyrolyzed in the presence of 2-methylpropan-2-ol, where using a non-reactive GC-inlet temperature of 150°C it was incidentally an impurity. This butan-2-ol impurity became a very useful model compound itself. A GC-inlet temperature of 200°C produced four peaks: Two major peaks for 2-methylpropan-2-ol and 2-methylpropene and two minor peaks for butan-2-ol and butanone. At 400°C in the PIDSSR, the same products formed: 2-methylpropan-2-ol and its dehydration product 2-methylpropene, as well as butan-2-ol and its dehydrogenation product butanone (Figure 36). Also seen in the chromatogram is a trace of but-2-ene (likely a dehydration product form butan-2-ol), but combination products suggesting interactions between butan-2-ol and 2-methylpropan-2-ol are absent. From these direct GC analyses and the PIDSSR experiment, three important conclusions are drawn.

- Butan-2-ol and butanone were not products of 2-methylpropan-2-ol pyrolysis.
- Butan-2-ol pyrolyzed to form butanone.

- There was likely no reaction between butan-2-ol and 2-methylpropan-2-ol, as there were no products different from those that would be made by pyrolyzing pure butan-2-ol or pure 2-methylpropan-2-ol.

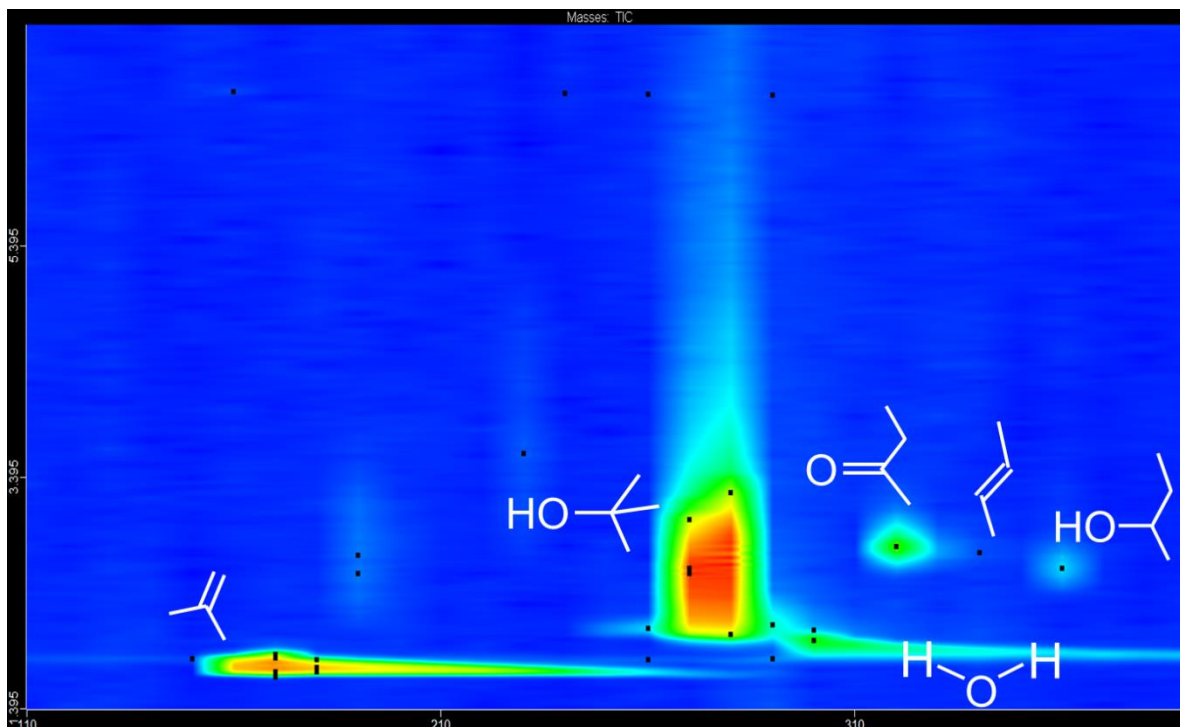


Figure 36. 2-Methylpropan-2-ol contained butan-2-ol as an impurity. Its pyrolysis in the 400°C PIDSSR-GCxGC-TOFMS revealed how the butan-2-ol impurity mainly dehydrogenated to butanol but also dehydrated to but-2-ene.

#### 4.4.3. Hydrogen was observed as a monol pyrolysis product with the PIQR-QMS

Hydrogen (H<sub>2</sub>) was not detected in the PIDSSR-GCxGC-TOFMS experiments because the TOFMS could not detect ion spectra below 5 Da e<sup>-1</sup>. However, most monol experiments only produced analyte peaks for themselves and their respective carbonyl compound. The lack of any new hydrogen-containing reaction product leads to the deduction

that the two hydrogen atoms removed from each dehydrogenated alcohol likely formed H<sub>2</sub>, based upon conservation of hydrogen atoms.

With the PIQR-QMS system, H<sub>2</sub> was detected directly from methanol and propan-1-ol pyrolyses because of the 2 Da e<sup>-1</sup> peaks observed in the collection of product spectra.

Methanol was used for the limited PIQR experiments due to its being most volatile among monols and due to its anticipated pyrolysis products having distinguishable ion spectra. Figures 37 through 40 show the spectra for the expected products. Only H<sub>2</sub> can form the 2 Da e<sup>-1</sup> ion, making H<sub>2</sub> easy to distinguish. Methanal (formaldehyde) and methanol were distinguished by the fact that methanal's abundance of 30 Da e<sup>-1</sup> ion is much larger than that of methanol's. Because ethene was not an expected product of methanol pyrolysis, the 28 Da e<sup>-1</sup> ion was unlikely to appear from any other reaction product.

Air leaks causing 28 and 32 Da e<sup>-1</sup> ion peaks were shown to be absent by the help of Figure 41, as these peaks were shown to proceed to small values when methanal was not formed (30°C), and methanol was almost completely converted to products (800°C).

The only problem arose from the possible presence of carbon monoxide, which also has a 28 Da e<sup>-1</sup> ion. Carbon monoxide was unlikely the only product of methanol because some species had to produce 30 Da e<sup>-1</sup> ions while methanol was consumed.

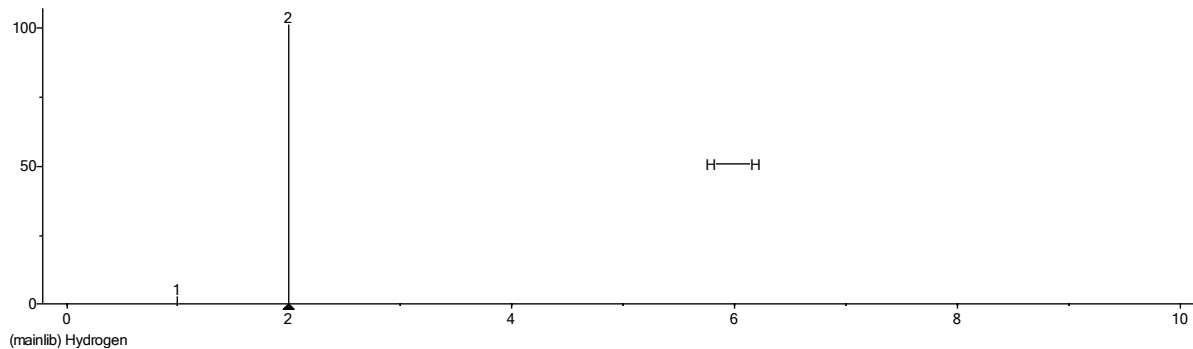


Figure 37. Spectra of H<sub>2</sub> from NIST MS 2.0 Database (70 eV ionization energy).

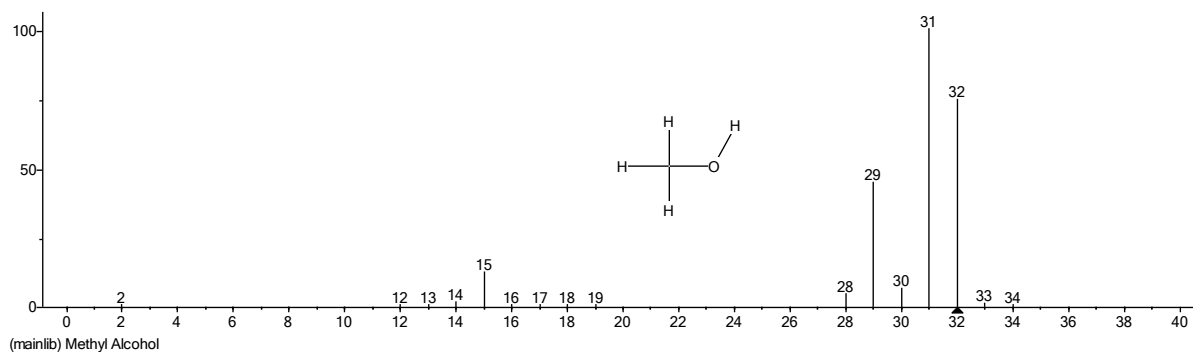


Figure 38. Spectra of methanol from NIST MS 2.0 Database (70 eV ionization energy).

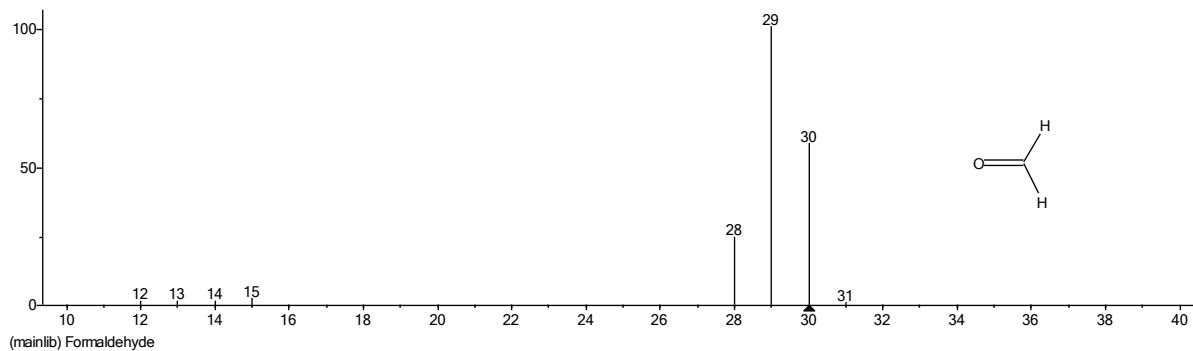


Figure 39. Spectra of methanal from NIST MS 2.0 Database (70 eV ionization energy).

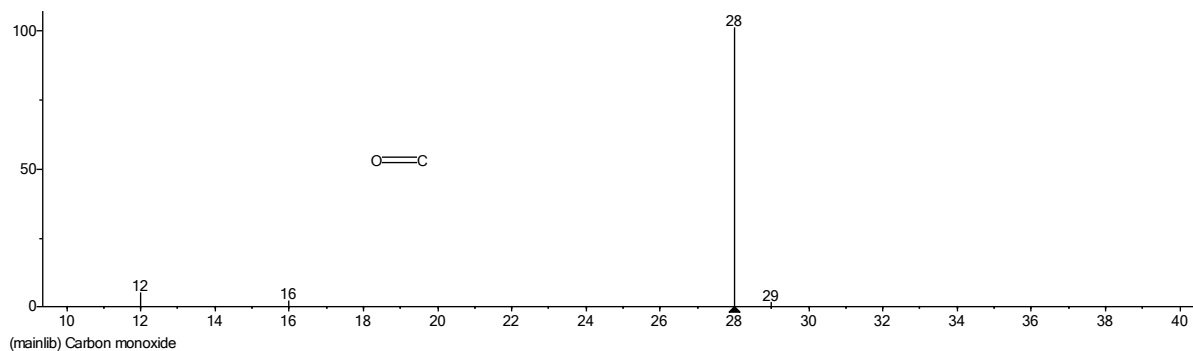


Figure 40. Spectra of carbon monoxide from NIST MS 2.0 Database (70 eV ionization energy).

Figures 41 and 42 show the integrated peaks for important spectral signals for methanol pyrolysis in the PIQR. These spectral signal areas were obtained by integrating ion signals across only the pulse's time duration. The resulting peak areas were corrected by subtracting the signal's baseline area (estimated from pre-pulse baseline height for each signal) from the corresponding total signal area. Three identical PIQR experiments were averaged for each furnace temperature setting to obtain "mean, corrected peak areas" for each ion.

A furnace temperature of 400°C produced a small methanol conversion in the PIQR based upon the small yield of H<sub>2</sub> (seen by the small values for 2 Da e<sup>-1</sup> in Figure 42) and the small difference in methanol conversion (seen by the small difference between 30°C and 400°C for 32 Da e<sup>-1</sup> in Figure 27). At first the difference in surface effects between quartz and deactivated stainless steel was considered the reason for the need for higher temperatures to obtain conversion in the PIQR. However, two effects other than surface influences might have caused the difference in conversion:

- The PIQR's reactor-tube temperature could have been considerably different from the PIDSSR's reactor-tube temperature. The PIQR's only temperature reading was the furnace's thermocouple, which only measured the temperature of the airspace within the furnace cavity. Meanwhile the PIDSSR's reactor tube had three thermocouples positioned directly on the exterior of the reactor tube's wall. There could have been considerable differences in temperature distribution among the reactor tubes, especially due to the PIQR's thin, irregular layer of insulation over its furnace cavity and quartz's poor thermal conductivity compared to stainless steel.
- The PIQR (at 400°C) had a residence time of 2.10 s, while the PIDSSR (at 400°C) had a residence time of 5.67 s.

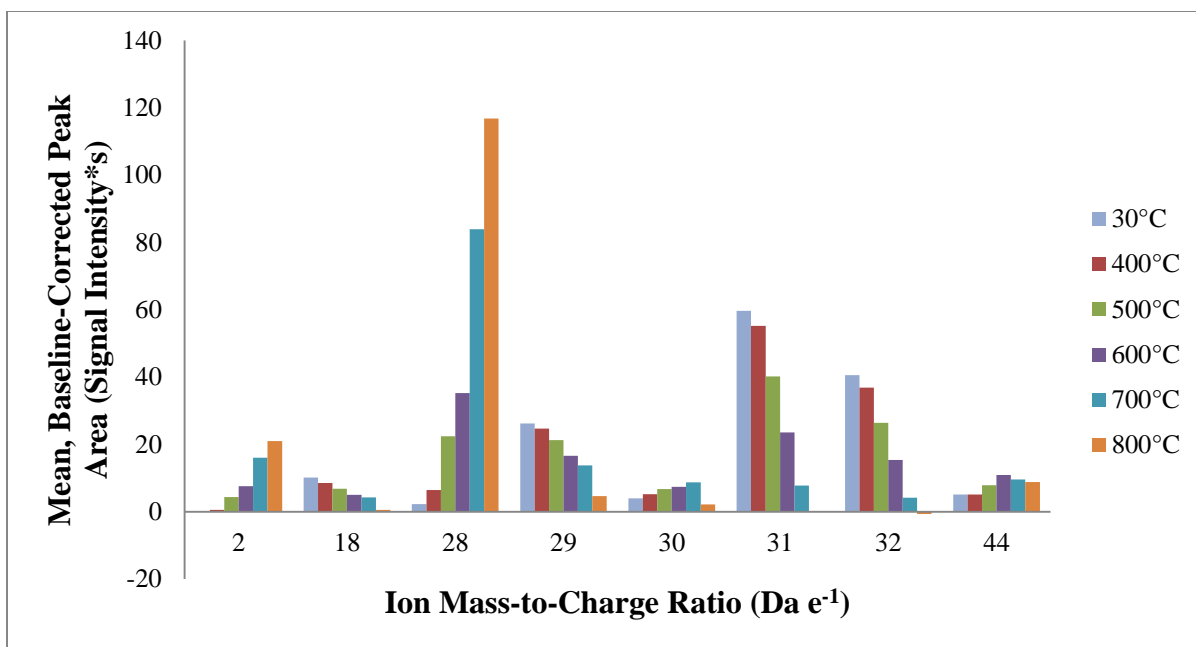


Figure 41. Mean, baseline-corrected peak areas for ion spectra observed from methanol pyrolysis in the PIQR-QMS system. Note the 2 Da e<sup>-1</sup> peaks likely represent H<sub>2</sub> dehydrogenation product. Spectra below 5 Da e<sup>-1</sup> could not be detected by the TOFMS, and therefore H<sub>2</sub> is not seen with the PIDSSR-GCxGC-TOFMS experiments.

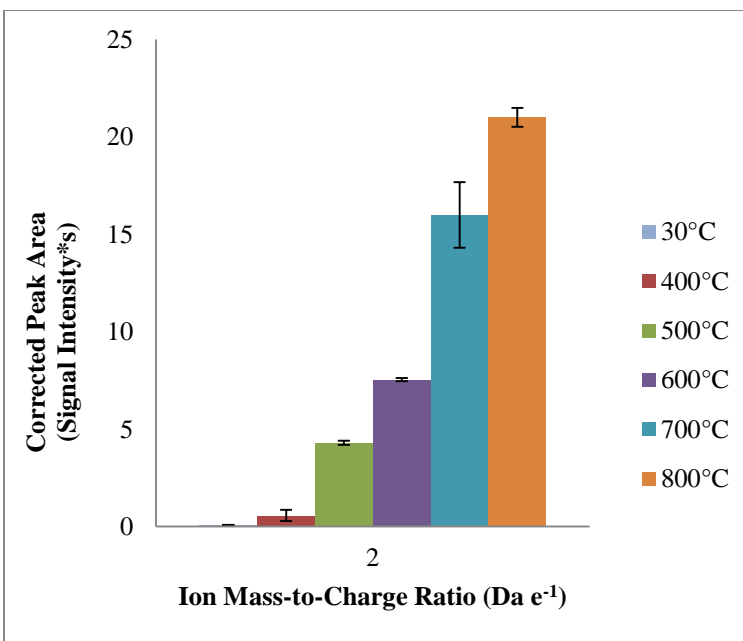
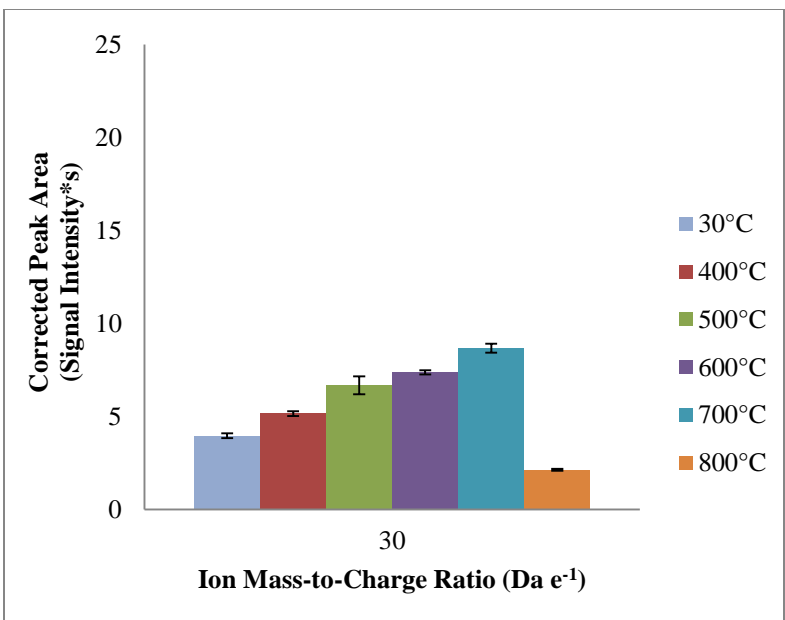


Figure 42. Peak areas of 2 and 30 Da e<sup>-1</sup> to highlight the formation of H<sub>2</sub> and methanal (with some slight addition of a 30 Da e<sup>-1</sup> methanol fragment) in the PIQR-QMS system.

Propan-1-ol was also tested in the PIQR-QMS system, but this set of experiments did not produce useful results for two reasons:

- Analysis of signal areas showed that the injected quantity of propan-1-ol varied greatly. Propan-1-ol quantity is best represented by the integrated ion signal of 31 Da  $e^{-1}$ , and four identical room-temperature injections provided a standard-deviation-to-mean ratio of 49.3% for this integrated ion signal. Argon quantity is best represented by the integrated ion signal for 40 Da  $e^{-1}$ , and the same four identical room-temperature injections provided a standard-deviation-to-mean ratio of 5.3% for this integrated ion signal. Propan-1-ol varying by much greater amounts than argon is only possible if different vapor concentrations of propan-1-ol were present in the pulse's gas feed. As a comparison, three identical room-temperature injections for methanol provided standard-deviation-to-mean ratios of 3.3% and 6.8% for integrated ion signals of 31 and 40 Da  $e^{-1}$ , respectively. These variances between argon and propan-1-ol and methanol and propan-1-ol are shown in Figures 43 and 44.
- The ion spectrum from anticipated  $H_2$  was not detected significantly above signal noise until furnace temperatures of 700°C or higher, making this observation of  $H_2$  product questionably applicable to the propan-1-ol dehydrogenation observed with the PIDSSR at 200-400°C.

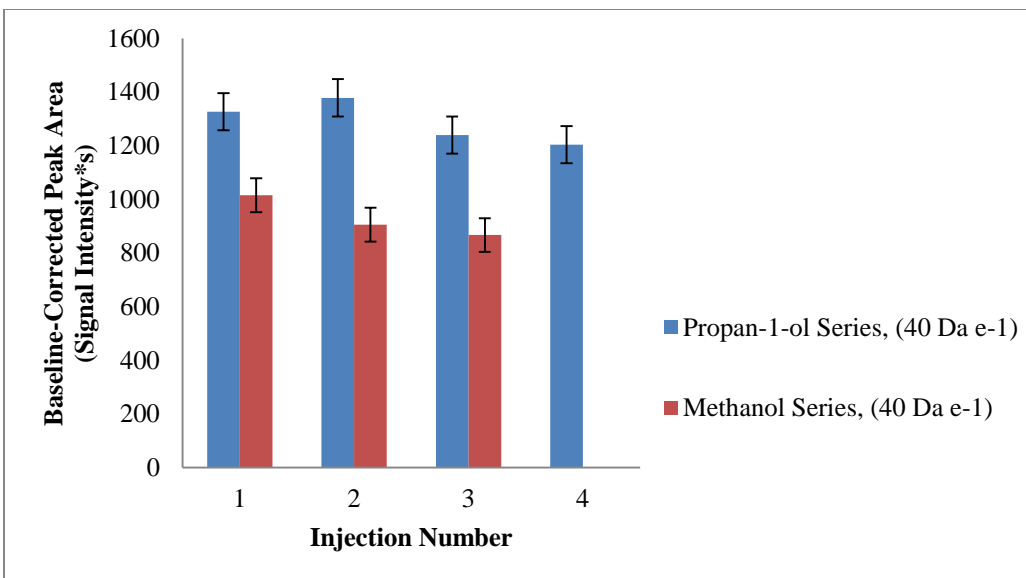


Figure 43. The injected quantity for argon was different between the propan-1-ol series and the methanol series. However, the standard deviations of argon-injected quantities were very similar in magnitude: the propan-1-ol series' argon-quantity standard deviation was 69.2 units, and the methanol series' argon-quantity standard deviation was 63.1 units.

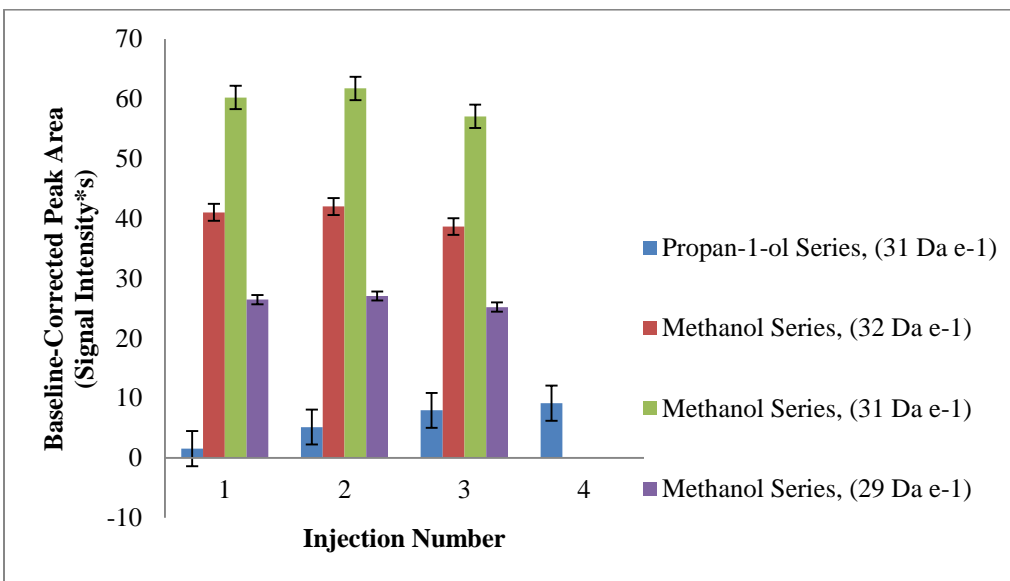


Figure 44. The injected quantity of propan-1-ol varied much more than the injected quantity of methanol. This caused poor repeatability for the propan-1-ol series of experiments in the PIQR-QMS.

The reason H<sub>2</sub> was detected easily for methanol yet was not adequately detected above the noise for propan-1-ol was due to the combination of differences in volatility and inadequate vaporization equipment.

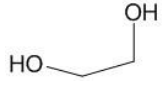
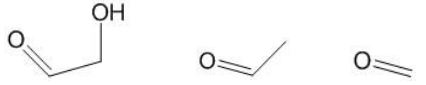
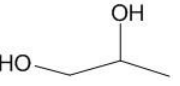
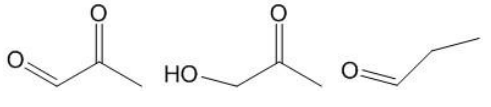
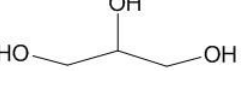
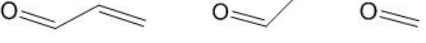
- Propan-1-ol's volatility is much lower than methanol's. (Propan-1-ol's boiling point is 97°C, and methanol's boiling point is 65°C.) The difference in volatility probably prevented propan-1-ol from rapidly reaching a near-saturation composition with the entering dry argon stream.
- The propan-1-ol series of experiments used a much larger vessel for the bubbler assembly than the methanol series of experiments. The small quantity of propan-1-ol available could not submerge the tip of the tube through which dry argon flowed to produce bubbles. To facilitate evaporation of propan-1-ol, the bubbler vessel was shaken vigorously before delivering a pulse to the reactor. Shaking was done to coat the vessel walls with liquid in order to create a larger vapor-liquid interfacial area – assumed to increase the rate of evaporation. From the results displayed in Figure 44, shaking did not provide a constant vapor composition like the smaller bubbler vessel did in the methanol series of experiments.

#### ***4.4.4. Reaction products of the diols-and-triol set***

The diols and triol set provided more complicated results for two reasons.

- The reactants and products produced much broader peaks (especially in GCxGC separations), making the identifications more difficult.
- The reactants and products produced many more products due to increased reaction possibilities.

Table 12. The reaction products observed from pyrolyzing three diols and a triol in the PIDSSR.

Reactant	Product(s)	
	Major	Trace Products
Ethan-1,2-diol 	2-Hydroxyethanal, Ethanal, Methanal 	(None)
Propan-1,2-diol 	2-Oxopropanal, 1-Hydroxypropanone, Propanal  Ethanal, Methanal 	(None)
Propan-1,3-diol 	Propanal, Prop-2-enal,  Ethanal, Methanal 	Prop-2-en-1-ol,  Propan-1-ol 
Propan-1,2,3-triol 	Prop-2-enal, Ethanal, Methanal  2-Oxopropanal, 1-Hydroxypropanone 	(None)

#### 4.5. Discussion

Pyrolyzing the alcohol model compounds formed very few products compared to the wide range of products observed when pyrolyzing polysaccharides like cellulose or even monosaccharides like D-glucose. This decrease in reaction products was the intended purpose of using simpler model compounds, as hypothesizing and testing elementary reactions became drastically easier with such simplified product profiles. In fact, many experiments only required hypothesizing and testing reactions responsible for just one or two products, being the dehydrogenation and dehydration products.

The primary and secondary monols show selectivity for dehydrogenating to their respective aldehyde or ketone at the 200-400°C conditions tested. This selectivity to dehydrogenation was surprising, as dehydration was expected based upon previous studies of alcohols [1]. [2].

#### ***4.5.1. Proposed mechanistic explanation of dehydrogenation with concerted reactions***

Concerted reactions with cyclic transition-state structures were evaluated with computational-quantum-chemistry (CQC) simulations to explain the dehydrogenation seen in the alcohol model compounds. These concerted transition-state structures were considered due to the low activation energies of concerted dehydrations found by Seshadri and Westmoreland [3] and Nimlos et al. [1].

Three types of concerted, cyclic elementary reactions were evaluated for the dehydrogenation.

- Four-centered, unimolecular dehydrogenation
- Meta-oxygen, six-centered, bimolecular dehydrogenation
- Para-oxygen, six-centered, bimolecular dehydrogenation

These three elementary reactions are shown in Figure 45 for the dehydrogenation of generic alcohols. (The R<sup>1</sup> and R<sup>2</sup> groups of these generic alcohols can represent either a hydrogen atom or an arbitrary alkyl group.)

The two bimolecular elementary reactions both involve the simultaneous transfer of three hydrogen atoms.

- Two hydrogen atoms are donated by the dehydrogenating alcohol.
  - One hydrogen atom from the hydroxyl group is donated to form the H<sub>2</sub> molecule.
  - One hydrogen atom from the alcohol's  $\alpha$ -carbon is donated to the hydroxyl group on the assisting molecule.

- One hydrogen atom is donated from the assisting hydroxyl group to form the H<sub>2</sub> molecule.

These three transfers of hydrogen atoms occur in concert, and they can be viewed as a net loss of just two hydrogen atoms to the forming H<sub>2</sub> molecule, because the assisting hydroxyl group is regenerated to its original state. Due to regenerating one of the reactants, the assisting hydroxyl group can be seen as a catalytic reaction partner. This bimolecular assistance with hydrogen-atom transfer was described by Seshadri and Westmoreland [3] for their dehydration reactions. Importantly, they found that the assisting hydroxyl group can be part of a water molecule or an alcohol molecule. The presence of many hydroxyl groups throughout cellulose makes bimolecular “hydroxyl-assisted” reactions very compelling, especially because cellulose produces additional hydroxyl-containing molecules as it pyrolyzes.

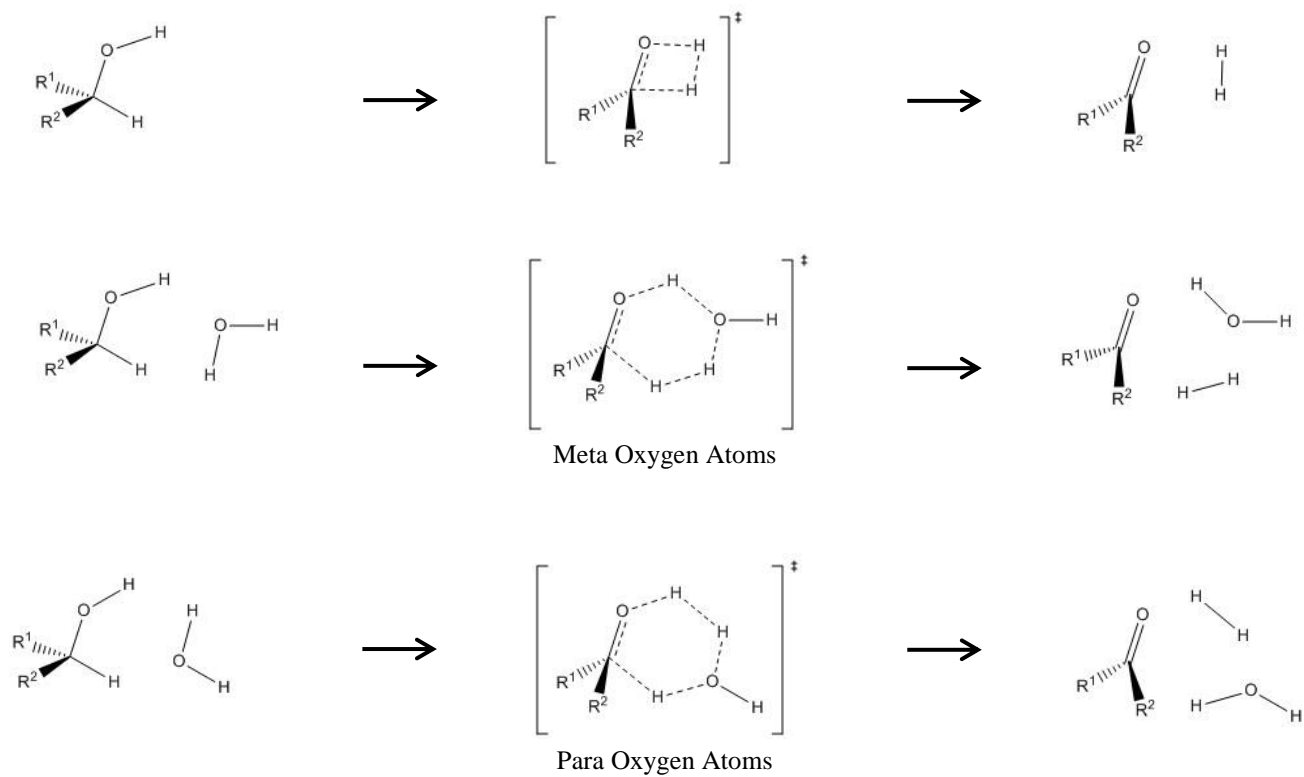


Figure 45. The three hypothesized cyclic transition-state structures for dehydrogenation applied to generic alcohols.

Computational-quantum-chemistry (CQC) simulations provided estimates for the enthalpy of formation for each of the three hypothesized transition-state types. The enthalpy of activation at 298 K was obtained by subtracting enthalpy of formation for the reactant(s)<sup>54</sup> from that of simulated transition state. The elementary dehydrogenations whose enthalpies of activation are listed in Table 13 are displayed in Figures 46 through 48,<sup>55</sup> and their chemical structures mimic the form of generic-monol dehydrogenations in Figure 45.

Table 13. The computed enthalpy of activation for hypothesized dehydrogenation transition states for monols.

Monol	Computed Enthalpy of Activation		
	Four-Center Transition-State	Six-Center Transition State	
		Meta-Oxygen	Para-Oxygen
(kcal mol <sup>-1</sup> )	(kcal mol <sup>-1</sup> )	(kcal mol <sup>-1</sup> )	
Methanol	90.7	59.1	111.4
Ethanol	85.3	55.4	109.7
Propan-1-ol	85.8	55.5	110.1
Propan-2-ol	82.3	53.5	109.9

---

<sup>54</sup> The NIST Webbook data were used for obtaining enthalpies of formation for reactant and product molecules.

<sup>55</sup> The GaussView structure images (used to visualize Gaussian structures) were not used for these figures because distinguishing their atoms is difficult, especially if viewed in black and white. ChemBioDraw was used to recreate the same structures. The ChemBioDraw structures are not to exact scale as provided by the Gaussian optimizations.

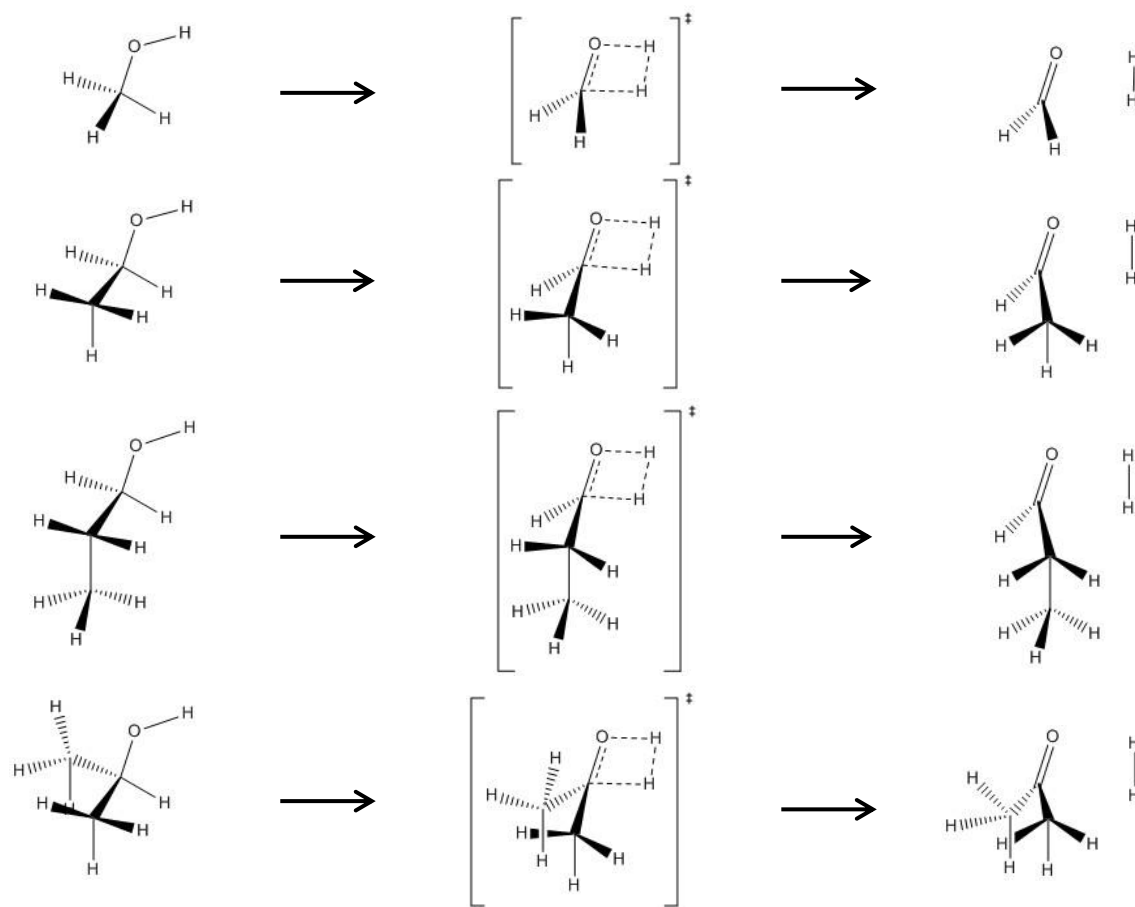


Figure 46. The hypothesized four-centered unimolecular dehydrogenation transition-state structure was evaluated for each of the four evaluated monols.

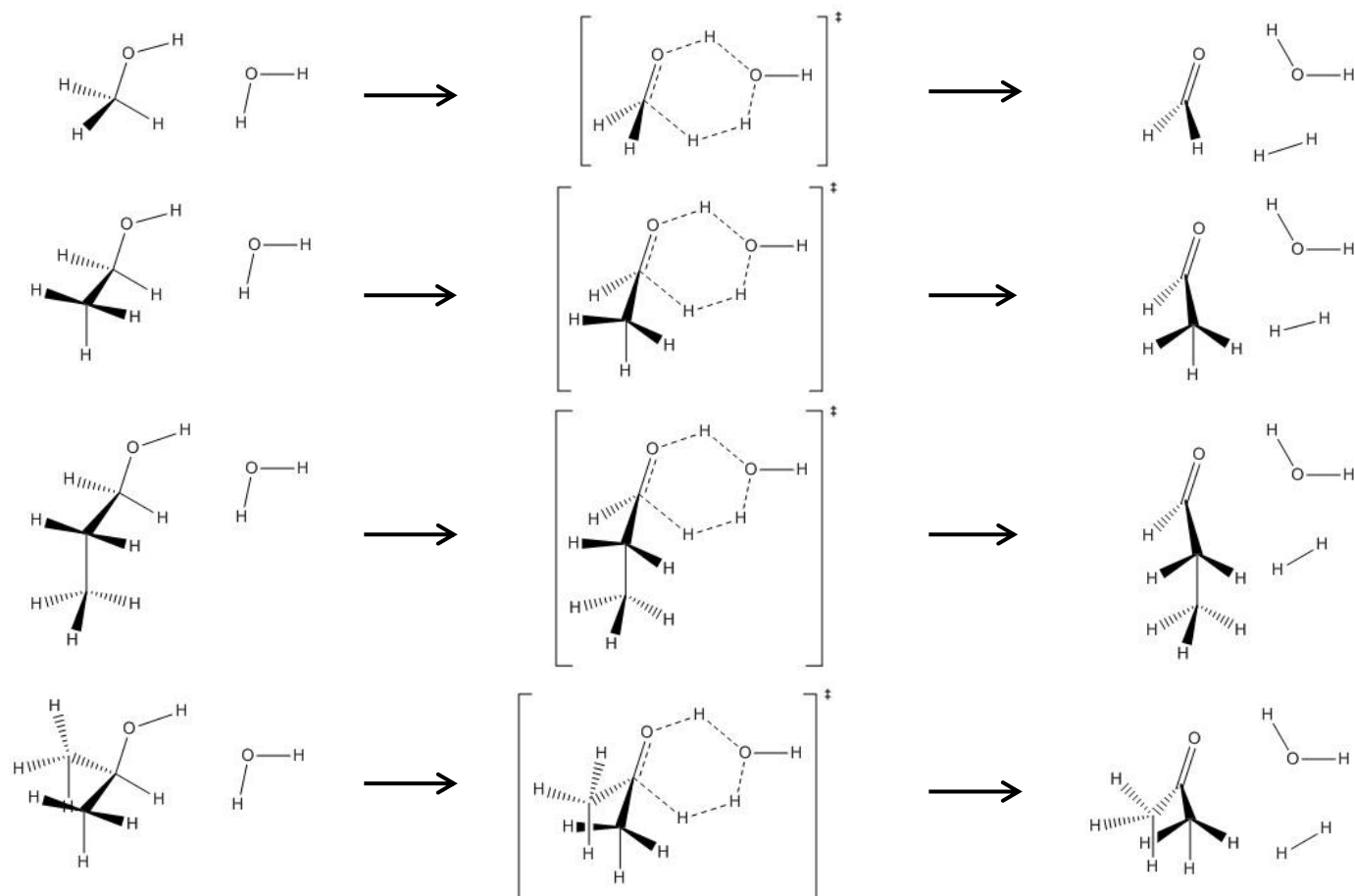


Figure 47. The hypothesized meta-oxygen, six-centered, bimolecular dehydrogenation transition-state structure was evaluated for each of the four evaluated monols.

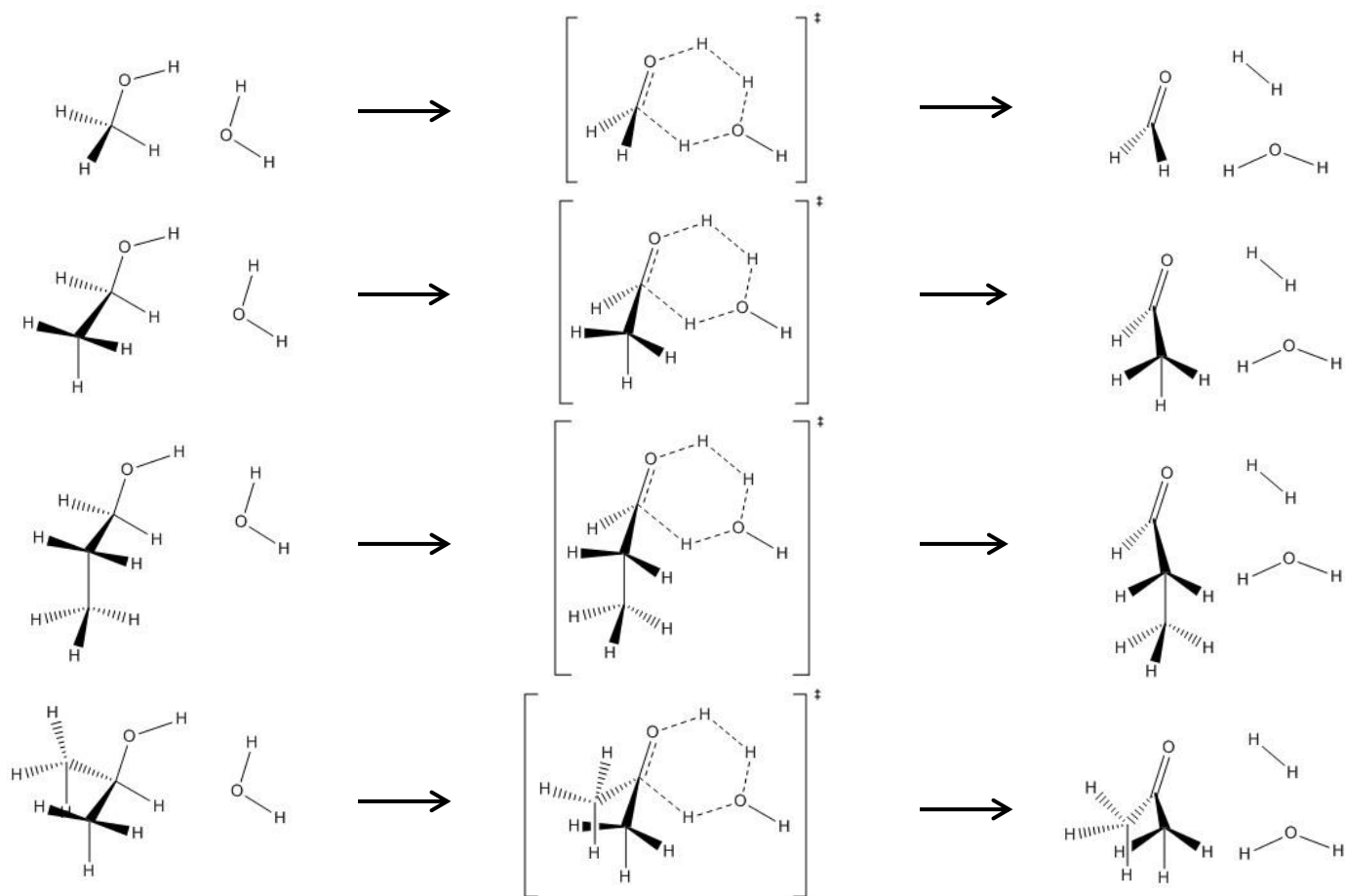


Figure 48. The hypothesized para-oxygen, six-centered, bimolecular dehydrogenation transition-state structure was evaluated for each of the four evaluated monols.

For each of the four monols, the meta-oxygen, six-center, bimolecular transition state offered the lowest enthalpy of activation of the three elementary dehydrogenations. It was lower than the four-center unimolecular dehydrogenation and the para-oxygen, six-center bimolecular dehydrogenation by roughly 30 kcal mol<sup>-1</sup> and roughly 50 kcal mol<sup>-1</sup>, respectively.

These enthalpy-of-activation estimates can help suggest that the para-oxygen, six-center, bimolecular dehydrogenation is not likely the “true” elementary reaction because it is much less energetically favorable than the meta-oxygen, six-center, bimolecular dehydrogenation. However, it is premature to suggest that the meta-oxygen, six-center bimolecular elementary reaction is the “true” elementary reaction through which alcohol dehydrogenation occurs because of two reasons.

- Enthalpy of activation alone cannot determine whether the four-center unimolecular transition state or the meta-oxygen, six-center, bimolecular transition most accurately describes the “true” reaction. The reason for this ambiguity is that successful bimolecular collision is not accounted for with enthalpy-of-activation comparisons, and such successful collision is essential for the two six-center, bimolecular reactions but not the four-center, unimolecular reaction. (Meanwhile, the difference between the two six-center transition states’ enthalpy of activation is very large. Because both of these six-center transition states are bimolecular, their likelihoods for successful collision might be very similar, making their large difference in enthalpy of activation enough to suggest the para-oxygen, six-centered, bimolecular transition state is physically not feasible.)
- More CQC simulations must be performed for other conceivable elementary dehydrogenation reactions until all possibilities are exhausted. Evaluating all of the possible dehydrations is necessary to ensure that the concerted, meta-oxygen, six-center, bimolecular transition state remains the most favorable in terms of enthalpy of activation. (Finding one local minima does not ensure the global minimum was found.) Other possible elementary reactions worth considering would be bimolecular

entities stabilized through hydrogen-bridge bonds or even radical-chain processes. The radical-chain processes are possibly very important because the four-center dehydrogenations are similar in magnitude to typical values for homolytic scission.

Transition states often cannot be identified directly during physical experiments, which is why CQC simulations can provide very valuable insight. However, data from physical experiments are still sought to support or refute elementary-reaction conclusions based solely upon CQC simulations. Certain physical-experiment data might confirm or refute the presence of intermediate species vital to a hypothesized reaction network. Such data are directly useful themselves, and it can also guide CQC simulations to focus on the most promising elementary reactions. In this vein, experiments employing *in-situ* electron paramagnetic resonance (EPR) are highly recommended to determine if any elementary reactions in gas-phase pyrolysis of alcohols involve unpaired electrons. Experimental evidence for the absence or presence of radical species is vital for determining if elementary reactions of radical-chain processes should be investigated further by CQC simulation.

#### ***4.5.2. Deuterated alcohols didn't provide conclusive evidence for the six-center, bimolecular dehydrogenations***

Isotopically labelled alcohols were co-pyrolyzed to find experimental evidence for the presence or absence of the meta-oxygen, six-center, bimolecular dehydrogenation mechanism. The experiment's results suggested that any hydrogen transfer between alcohols (e.g., during hypothesized meta- or para-oxygen, six-center bimolecular dehydrogenations) was limited to quantities not noticeable above noise in the TOFMS spectral signals. Failing to detect prominent signals for partially deuterated products is inconclusive evidence for the absence of the bimolecular dehydrogenation mechanisms, however, because the PIDSSR-GCxGC-TOFMS' spectral signals could not be analyzed to the quantitative detail of the QMS' spectral signals.

The experiment was designed to locate ion spectra for alcohols that "assisted" in the bimolecular dehydrogenation reactions; i.e., the member which would not dehydrogenate

because its hydroxyl group both donated and accepted a hydrogen atom. Two cases are possible with the co-pyrolysis of different alcohols.

- If a non-deuterated alcohol assisted the dehydrogenation of a deuterated alcohol in either of the two proposed bimolecular mechanisms, then the assisting non-deuterated alcohol would exchange a deuterium atom for its hydrogen atom on the hydroxyl group.
- If a deuterated alcohol assisted the dehydrogenation of a non-deuterated alcohol in either of the two proposed bimolecular mechanisms, then the assisting deuterated alcohol would exchange a hydrogen atom for its deuterium atom on the hydroxyl group.
- In either case, the hydrogen product would be partially deuterated.

If partially deuterated alcohols were formed due to bimolecular assistance, then their resulting spectra should contain some modified mass-to-charge ratios due to losing one Da  $e^{-1}$  or gaining one Da  $e^{-1}$ .

Different alcohols were selected for the deuterated and non-deuterated reactants so that chromatographic separation would isolate the hypothesized assisting products. Isolation was vital so that the spectral lines were kept as simple as possible for identifying the partially deuterated assistance products co-eluting with either fully deuterated or non-deuterated assistance products. Figures 49 and 50 show how both para-oxygen and meta-oxygen, six-center bimolecular dehydrogenations would yield partially deuterated alcohols as assistance products should non-deuterated propan-1-ol assist the dehydrogenation of fully deuterated propan-2-ol or vice-versa.

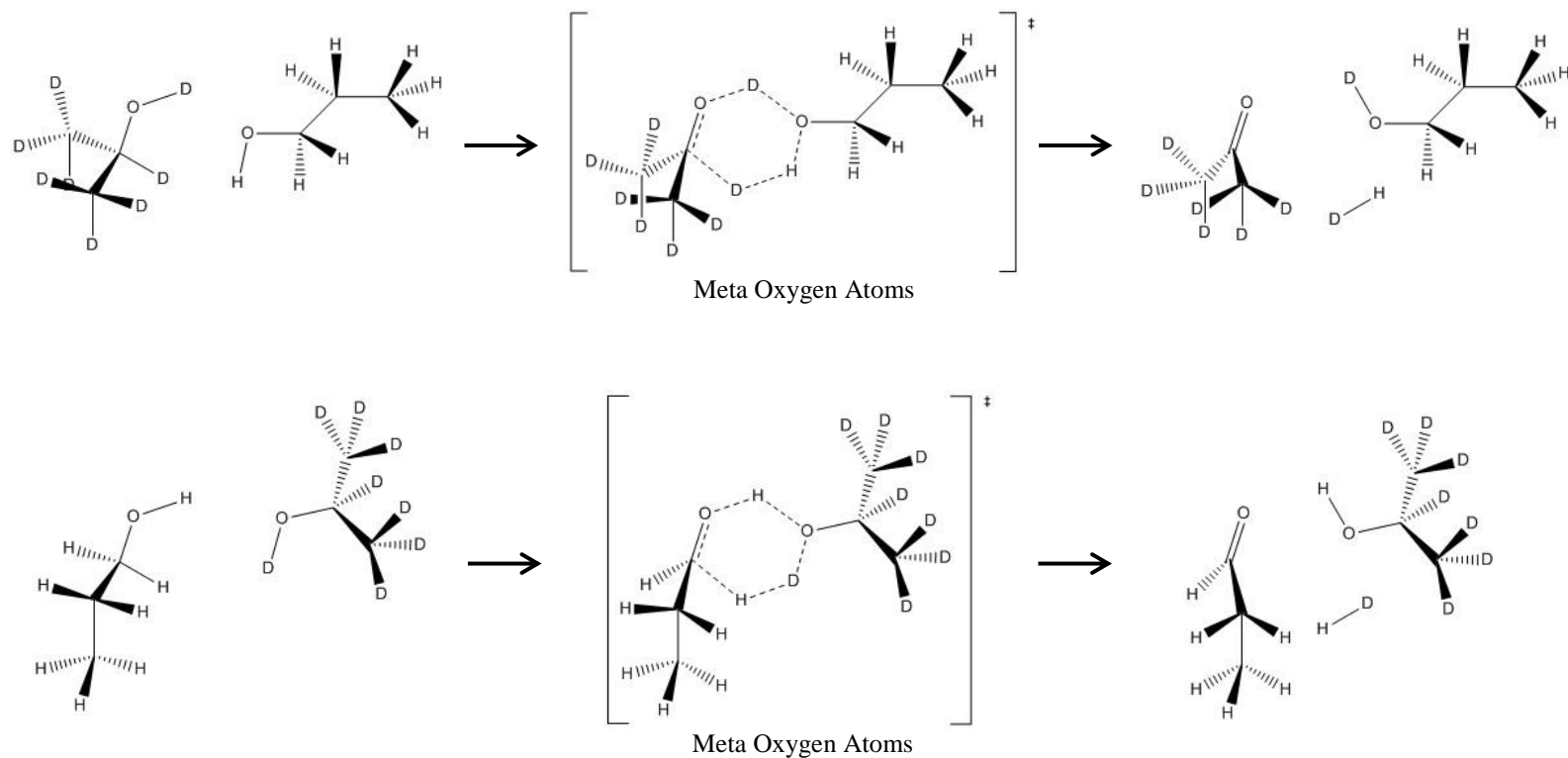


Figure 49. If monol dehydrogenation proceeded via the concerted “meta-oxygen” bimolecular transition state, then co-pyrolysis of non-deuterated propan-1-ol and fully deuterated propan-2-ol would provide a fraction of its hydrogen product as H-D and a fraction of its assisting alcohols as partially deuterated alcohols.

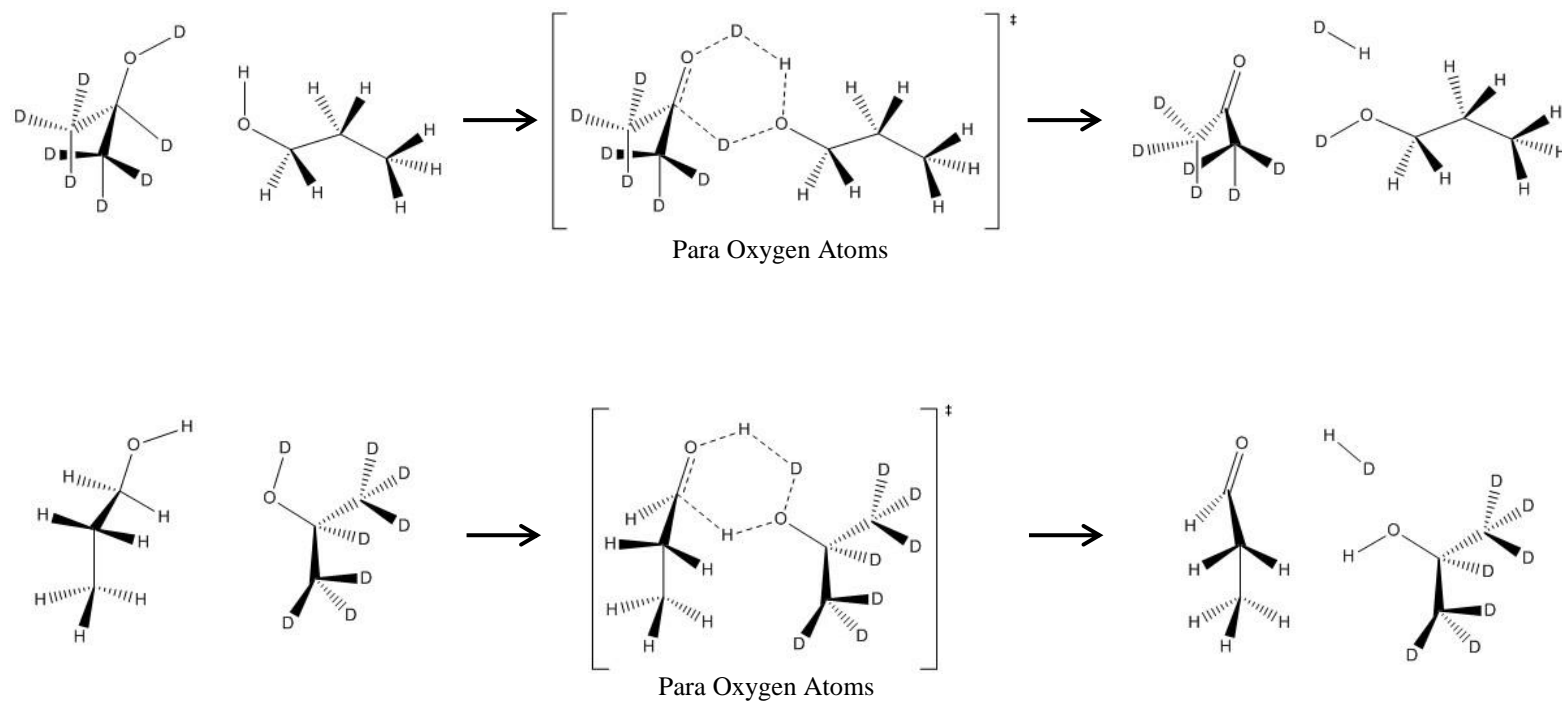


Figure 50. If monol dehydrogenation proceeded via the concerted “para-oxygen” bimolecular transition state, then co-pyrolysis of non-deuterated propan-1-ol and fully deuterated propan-2-ol would provide a fraction of its hydrogen product as H-D and a fraction of its assisting alcohols as partially deuterated alcohols.

The non-deuterated propan-1-ol was not fully dehydrogenated during the reaction experiment, so there was a chromatographic peak for “un-dehydrogenated propan-1-ol.”<sup>56</sup> The chromatographic peak for un-dehydrogenated propan-1-ol did not show any spectra with one (or more) additional mass unit compared to the spectra expected for undeuterated propan-1-ol. This failure to detect different spectra was apparent by visually inspecting the spectra of the un-dehydrogenated propan-1-ol peak.

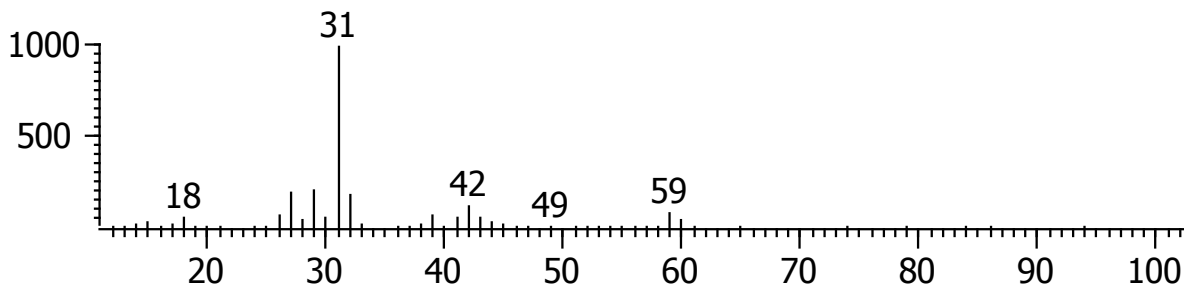
Figure 51 shows that the spectra observed by the TOFMS (“Caliper”) for propan-1-ol’s chromatographic peak contained only spectra expected for the non-deuterated propan-1-ol (“Library Hit”). Therefore, there was no obvious evidence that undeuterated propan-1-ol assisted the dehydrogenation of fully-deuterated propan-2-ol in the two proposed bimolecular reactions.

The fully deuterated propan-2-ol was completely dehydrogenated to fully-deuterated propanone, which prevented the inspection of a chromatographic peak for undehydrogenated, propan-2-ol for spectra of one fewer mass unit compared to those expected for fully-deuterated propan-2-ol. Therefore, there was no evidence that fully-deuterated propan-2-ol assisted the dehydrogenation of undeuterated propan-1-ol.

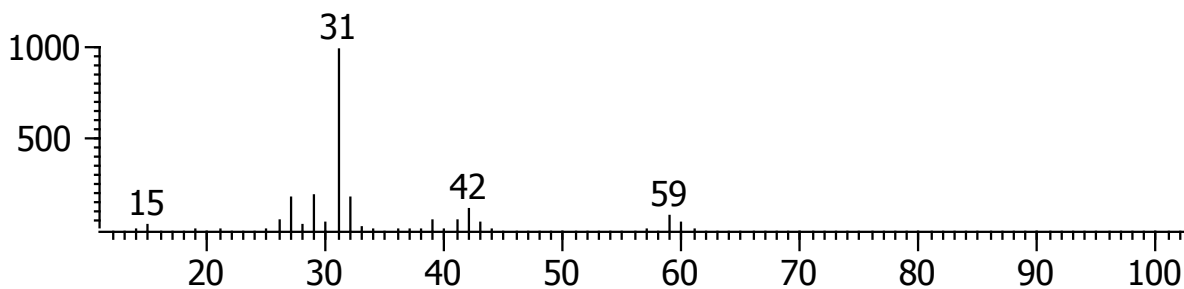
---

<sup>56</sup> “Undehydrogenated alcohols” refer to how alcohols in the reactor effluent may have taken part in a dehydrogenation reaction as the assisting molecule. To call these alcohols as simply “unconverted” would lead to confusion as to whether they were not converted to their aldehyde or ketone via dehydrogenation or whether they were not converted to a partially deuterated form via a proposed bimolecular dehydrogenation reaction.

Caliper - sample "Propan-2-ol D8 and porpan-1-ol, 400C, 13:40, 30 Aug 2013:1",



Peak True - sample "Propan-2-ol D8 and porpan-1-ol, 400C, 13:40, 30 Aug 2013



Library Hit - similarity 858, "1-Propanol"

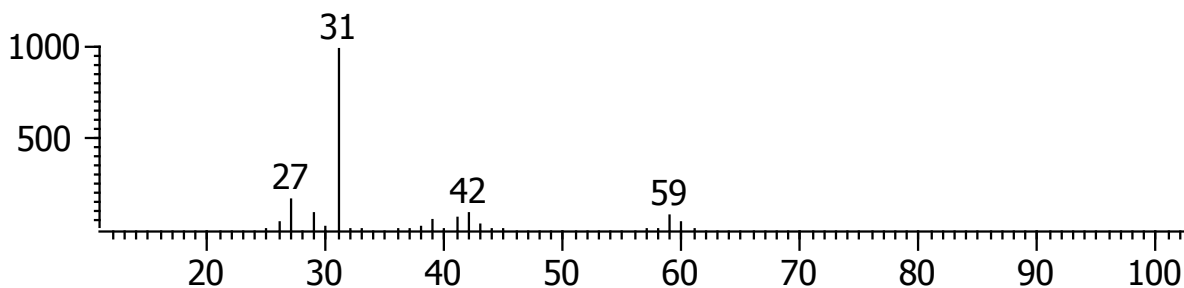


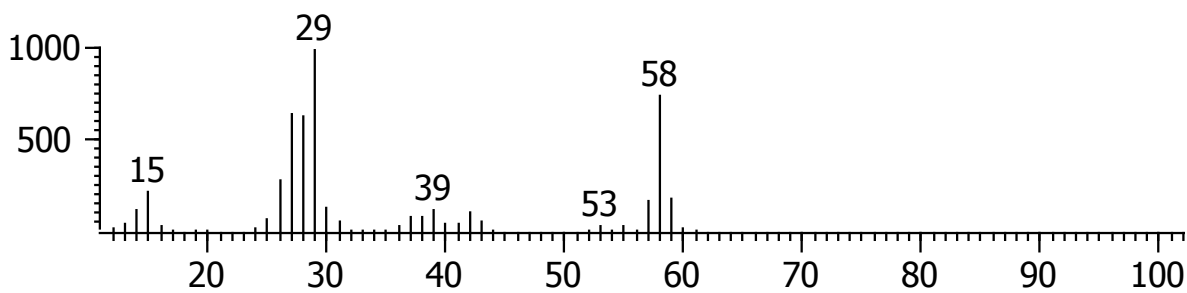
Figure 51. Using the ChromaTOF software's spectral observation ("Caliper" at top) and spectral deconvolution ("Peak True" in middle) both show no significant spectral lines with additional masses compared to the spectral-library identification of propan-1-ol ("Library Hit" at bottom).

Also important was the observation that the propanal and propanone formed via dehydrogenation did not show any partial deuteration.

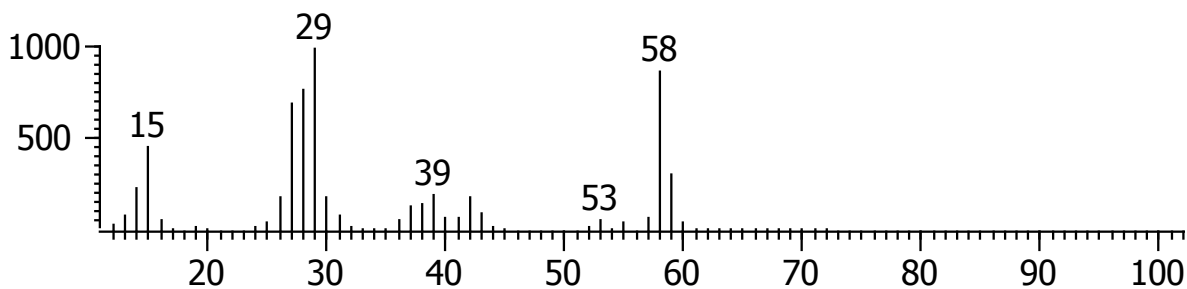
Figure 52 shows that the chromatographic peak for propanal contained no spectra for one greater mass unit, and

Figure 53 shows that the chromatographic peak for fully deuterated propanone (“Acetone D6”) contained no spectra for one fewer mass units. Even the trace products of carbon-carbon bond fragmentation, ethanal and methanal, did not show any partially deuterated spectra. Like the lack of partially-deuterated undehydrogenated alcohols, this lack of dehydrogenation and fragmentation products suggests that hydrogen atoms are not transferred between species to a significant extent.

Caliper - sample "Propan-2-ol D8 and porpan-1-ol, 400C, 13:40, 30 Aug 2013:1",



Peak True - sample "Propan-2-ol D8 and porpan-1-ol, 400C, 13:40, 30 Aug 2013



Library Hit - similarity 814, "Propanal"

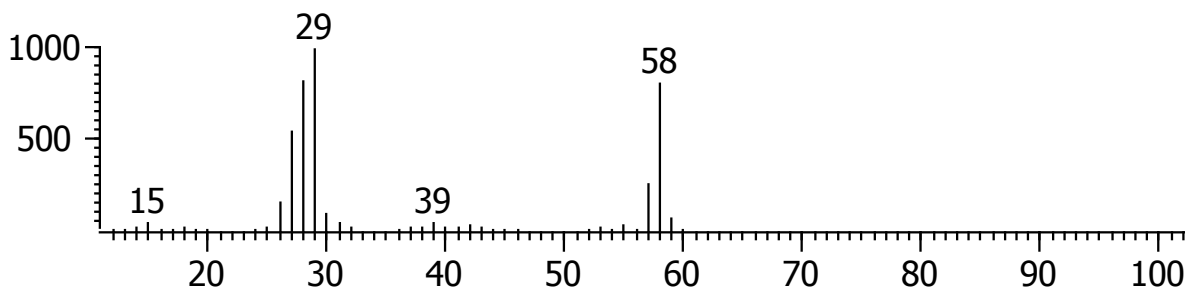
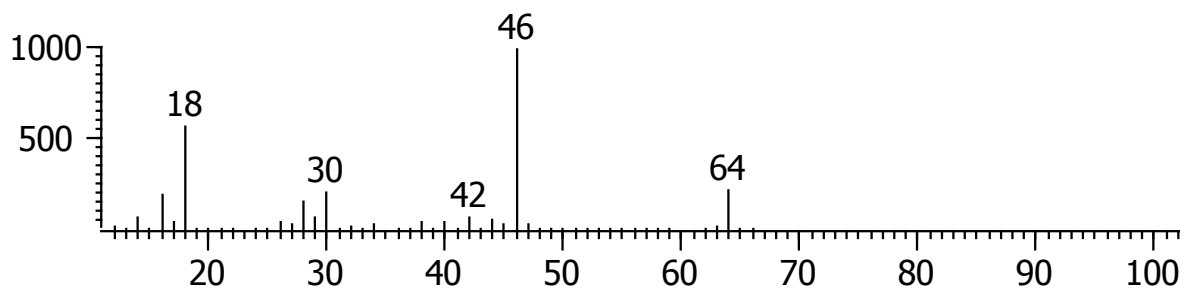
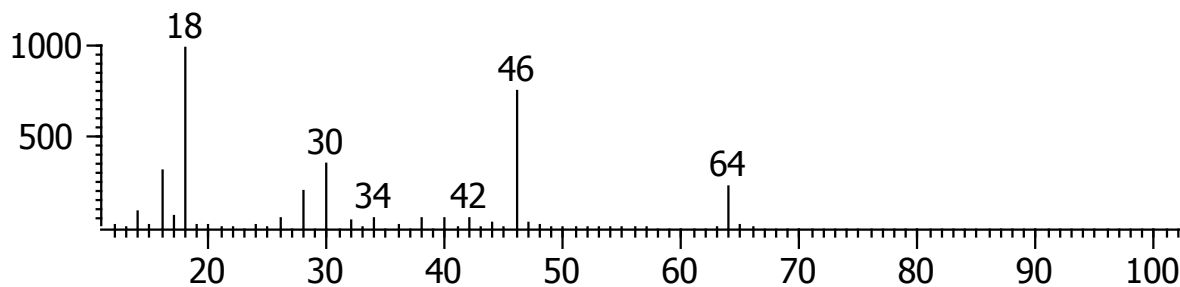


Figure 52. ChromaTOF's spectral observation ("Caliper" at top) and spectral deconvolution ("Peak True" in middle) both show no significant spectral lines with additional or fewer masses compared to the spectral-library identification of propanal ("Library Hit" at bottom).

Caliper - sample "Propan-2-ol D8 and porpan-1-ol, 400C, 13:40, 30 Aug 2013:1",



Peak True - sample "Propan-2-ol D8 and porpan-1-ol, 400C, 13:40, 30 Aug 2013



Library Hit - similarity 768, "Acetone-D6"

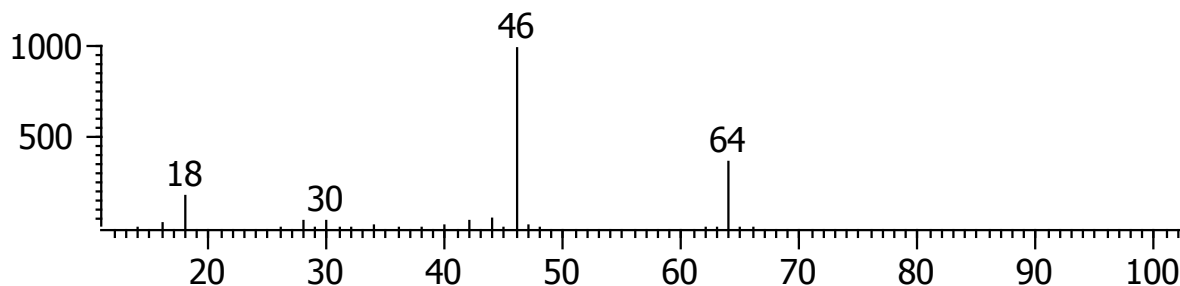
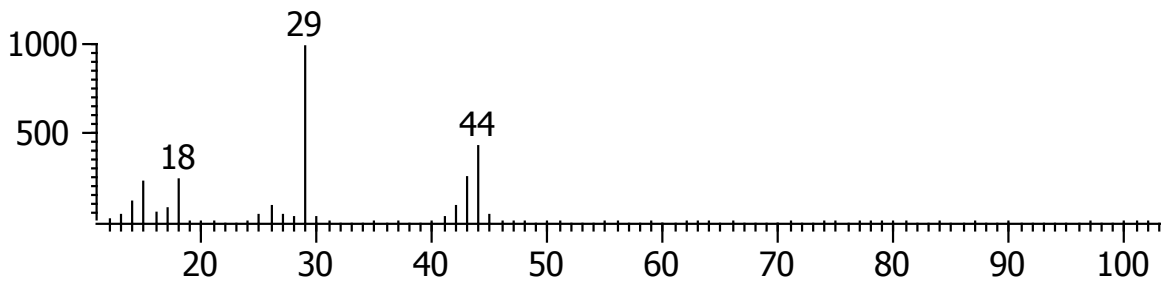
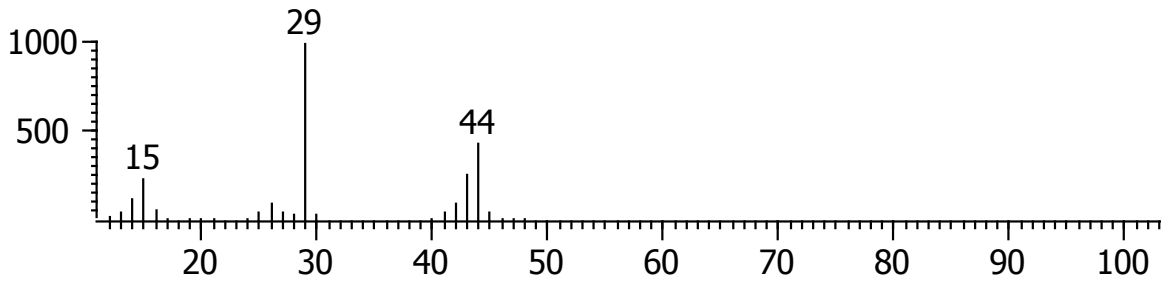


Figure 53. ChromaTOF's spectral observation ("Caliper" at top) and spectral deconvolution ("Peak True" in middle) both show no significant spectral lines with additional or fewer masses compared to the spectral-library identification of fully-deuterated propanone "Acetone-D6" ("Library Hit" at bottom).

Caliper - sample "Propan-2-ol D8 and porpan-1-ol, 400C, 13:40, 30 Aug 2013:1",



Peak True - sample "Propan-2-ol D8 and porpan-1-ol, 400C, 13:40, 30 Aug 2013:",



Library Hit - similarity 881, "Acetaldehyde"

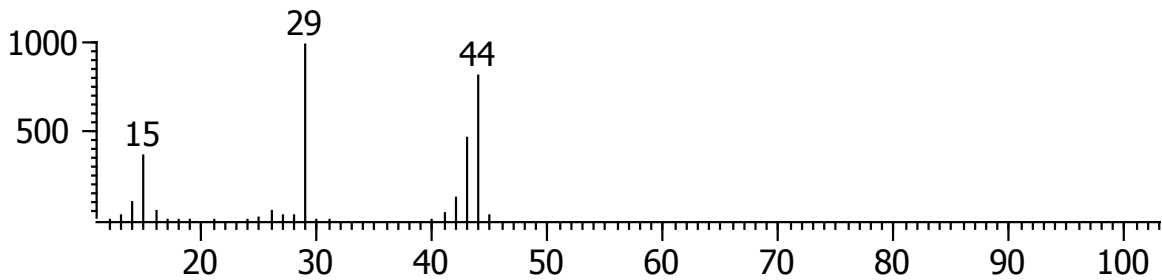
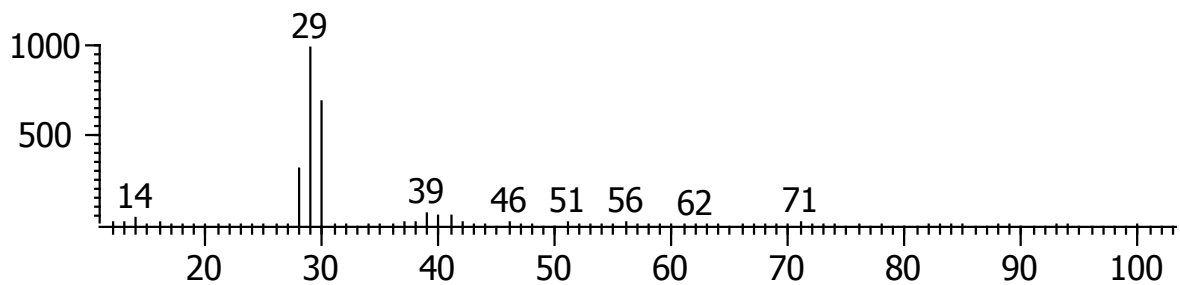
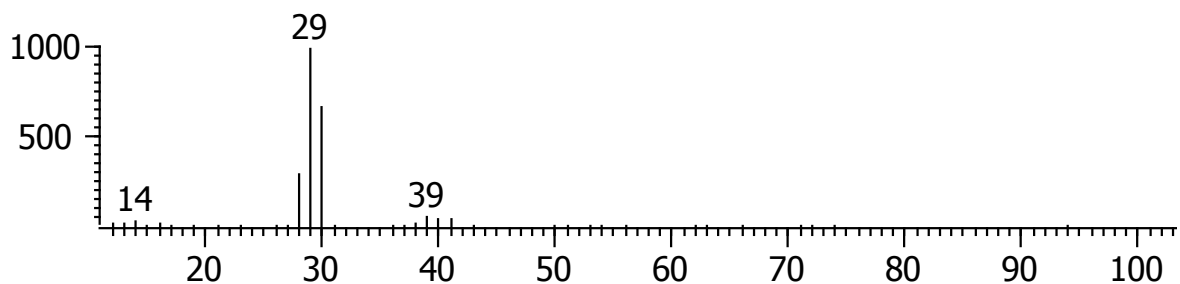


Figure 54. ChromaTOF's spectral observation ("Caliper" at top) and spectral deconvolution ("Peak True" in middle) both show no significant spectral lines with additional masses compared to the spectral-library identification of ethanal ("Library Hit" at bottom).

Caliper - sample "Propan-2-ol D8 and porpan-1-ol, 400C, 13:40, 30 Aug 2013:1",



Peak True - sample "Propan-2-ol D8 and porpan-1-ol, 400C, 13:40, 30 Aug 2013:",



Library Hit - similarity 856, "Formaldehyde"

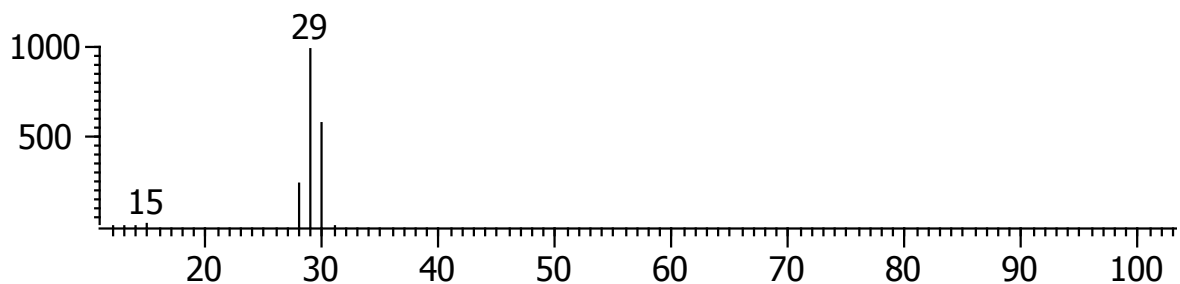


Figure 55. ChromaTOF's spectral observation ("Caliper" at top) and spectral deconvolution ("Peak True" in middle) both show no significant spectral lines with madditional masses compared to the spectral-library identification of ethanal ("Library Hit" at bottom).

For future research, the most important test with deuterated alcohols would be finding the presence or absence of 3 Da  $e^{-1}$  ion spectra representative of the D-H product formed in

the hypothesized six-center dehydrogenations. The D-H product would be vital because H<sub>2</sub> formed from either of the proposed six-center, bimolecular dehydrogenations obtains one hydrogen atom from the molecule undergoing dehydrogenation and one hydrogen atom from the assisting hydroxyl group. The TOFMS system was limited to a lower range of 5 Da e<sup>-1</sup>, however, so locating the spectra for D-H will require the PIQR-QMS system.

Finally, these results suggest that extensive hydrogen transfer among molecules via radical-chain processes is also unlikely yet inconclusive given the qualitative nature of the spectral comparisons.

#### ***4.5.3. Past evidence of hydrogen formation during cellulose pyrolysis***

Hydrogen (H<sub>2</sub>) is often not discussed as a product of biomass pyrolysis. However, some studies verify its formation at small quantities. In their study of cellulose pyrolysis, Patwardhan et al. identified ~0.1 wt% H<sub>2</sub> in their fluidized-bed experiments [49]. In their studies on cellulose and hemicellulose, Patwardhan et al. [49] and Patwardhan et al. [48] also suggested H<sub>2</sub> was partly responsible for the discrepancies in their hydrogen-balance calculations, as their gases were not completely identified during micropyrolyzer experiments.<sup>57</sup>

Hosoya et al. [50] reported H<sub>2</sub> formation from levoglucosan pyrolysis at 400°C when using lower levoglucosan loadings and longer (batch) reaction times. However, this same study also showed that some levoglucosan polymerizes into a cellulose-like material during pyrolysis. With this polymerization observation, it becomes ambiguous whether cellulose, levoglucosan, or even smaller vapor products are what immediately formed the H<sub>2</sub> product. Importantly, this finding may suggest that H<sub>2</sub> may form directly or indirectly from both

---

<sup>57</sup> Both the cellulose study and the hemicellulose study used a micropyrolyzer coupled to a GC-MSD/FID. While the range of collected mass-to-charge ratios were not specified in their methods, it was likely their MSD did not detect H<sub>2</sub> (but did detect CO and CO<sub>2</sub>) because it started collection at a mass-to-charge ratio above that of helium, 4 Da e<sup>-1</sup>.

cellulose as well as its subsequent products like levoglucosan, ring-fragmentation products, and char.

#### ***4.5.4. Why is the small quantity of hydrogen rarely mentioned in most biomass-pyrolysis studies?***

Biomass fast pyrolysis does not form significant quantities of gases like H<sub>2</sub>, CO, or CO<sub>2</sub><sup>58</sup> because it was purposefully developed to improve the yield of condensables (i.e., bio-oil) at the expense of gas and char yields. Because the permanent gases are not the most desired products, chemical analyses made during biomass-pyrolysis studies have not emphasized the exact composition of the gases. The analyses of the non-condensable gases suffer for several reasons.

- GC separations focused on resolving volatile and semi-volatile analytes do not separate most gases effectively like H<sub>2</sub>, CO, CO<sub>2</sub>, and gaseous hydrocarbons like methane or ethane, ethene, propane, and propene. The poor separation causes them to co-elute, resulting in poor identification and quantification.
- The detectors commonly used for GC separations of bio-oils are mass-selective detectors (MSDs) and flame-ionization detectors (FIDs), and both of these detectors have problems detecting hydrogen.
  - MSDs connected to GCs usually have their collected ranges of ion mass-to-charge ratios beginning above the mass-to-charge ratio of carrier gas. Because the mass-to-charge ratio of this carrier gas is invariably equal to or above that of H<sub>2</sub>, any hydrogen-ion spectra will not be collected. (In addition, some MSDs, like the TOFMS used in this work, are by design incapable of detecting mass-to-charge ratios as low as hydrogen's 2 Da e<sup>-1</sup>.)
  - FIDs cannot detect hydrogen due to their inherent method of operation.

---

<sup>58</sup> This argument excludes pyrolysis processes that approach gasification conditions like high temperature (>800°C) or partial oxidation.

- Pyrolysis researchers are much more interested in the larger, carbon-containing volatile and semi-volatile analytes due to two reasons:
  - Those researchers interested in fuel applications are focused on reaction products of larger carbon number for simpler downstream upgrading to make gasoline- and diesel-range hydrocarbon fuels.
  - Those researchers interested in improving the mechanistic understanding of cellulose decomposition are focused upon molecules bearing a closer structural resemblance to cellulose (e.g., anhydroglucopyranoses, oligosaccharides, and ring-fragmentation products) because these molecules are more likely to have resulted from fewer elementary reaction steps than gases like CO, CO<sub>2</sub>, CH<sub>4</sub>, and H<sub>2</sub>.

#### ***4.5.5. Proposed mechanistic explanation of dehydration with concerted reactions***

Concerted reactions with cyclic transition-state structures were evaluated with CQC simulations to explain the dehydration seen in the alcohol model compounds. Like the dehydrogenation transition states, these dehydration transition-state structures were assumed to be cyclic due to the low activation energies of concerted dehydrations found by Seshadri and Westmoreland [3] and Nimlos et al. [1]. Only monol simulations were considered here due to their simpler structures that avoid the many conformations possible with multiple hydroxyl groups.

Two types of concerted, cyclic elementary reactions were evaluated for the dehydrogenation.

- Four-centered, unimolecular dehydrogenation
- Meta-oxygen, six-centered, bimolecular dehydrogenation

These two elementary reactions are shown in Figure 56 for the dehydrogenation of generic alcohols. (The R<sup>1</sup> and R<sup>2</sup> groups of these generic alcohols can represent either a hydrogen atom or an arbitrary alkyl group.)

The meta-oxygen, six-centered bimolecular dehydration involves the simultaneous transfer of two hydrogen atoms.

- One hydrogen atom is donated by a carbon atom on the dehydrating alcohol to the hydroxyl group on the assisting molecule.
- One hydrogen atom is donated by the assisting molecule's hydroxyl group to the hydroxyl group leaving the dehydrating alcohol [as water].

These two transfers of hydrogen atoms occur in concert, and they can be viewed as a net loss of one hydrogen atom and one hydroxyl group from the dehydration alcohol because the assisting hydroxyl group is regenerated to its original state. Due to regenerating one of the reactants, the assisting hydroxyl group can be seen as a catalytic reaction partner. This bimolecular assistance with hydrogen-atom transfer was described by Seshadri and Westmoreland [3] for their dehydration reactions. Importantly, they found that the assisting hydroxyl group can be part of a water molecule or an alcohol molecule. The presence of many hydroxyl groups throughout cellulose makes bimolecular "hydroxyl-assisted" dehydrations very compelling, especially because cellulose produces many hydroxyl-containing molecules as it pyrolyzes.

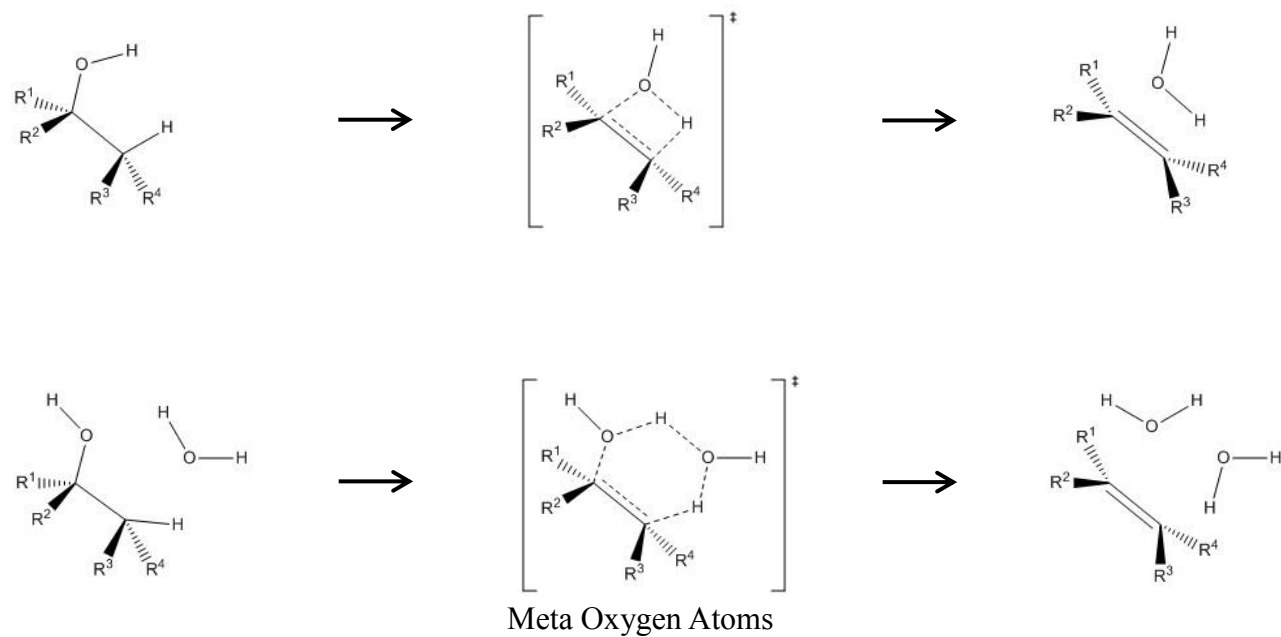


Figure 56. The two hypothesized cyclic transition-state structures for dehydration applied to generic alcohols.

Computational-quantum-chemistry (CQC) simulations provided estimates for the enthalpy of formation for each of the two hypothesized transition-state types. The enthalpy of activation at 298 K was obtained by subtracting the reactant(s)' enthalpy of formation<sup>59</sup> from simulated transition state's enthalpy of formation. The elementary dehydrations whose enthalpies of activation are listed Table 14 are displayed in Figures 57 and 58,<sup>60</sup> and their chemical structures mimic the form of generic-monol dehydrogenations in Figure 56.

Table 14. The computed enthalpy of activation for hypothesized dehydration transition states for monols.

Monol	Computed Enthalpy of Hypothesized Transition State	
	Four-Center	Six-Center
	(kcal mol <sup>-1</sup> )	(kcal mol <sup>-1</sup> )
Methanol	N/A	N/A
Ethanol	66.7	53.2
Propan-1-ol	68.1	55.0
Propan-2-ol	66.2	52.8

The meta-oxygen, six-center, bimolecular transition state offered the lower enthalpy of activation of the two elementary dehydrations tested for each of the three monols: It was lower than the four-center unimolecular dehydration and by roughly 13 kcal mol<sup>-1</sup> for these three monols.

However, it is premature to suggest that the meta-oxygen, six-center bimolecular elementary reaction is the “true” elementary reaction through which alcohol dehydrogenation occurs because of two reasons.

---

<sup>59</sup> The NIST Webbook data were used for obtaining enthalpies of formation for reactant and product molecules.

<sup>60</sup> The GaussView structure images (used to visualize Gaussian structures) were not used for these figures because distinguishing their atoms is difficult, especially if viewed in black and white. ChemBioDraw was used to recreate the same structures. The ChemBioDraw structures are not to exact scale as provided by the Gaussian optimizations

- Enthalpy of activation alone cannot determine whether the four-center unimolecular transition state or the meta-oxygen, six-center, bimolecular transition most accurately describes the “true” reaction. The reason for this ambiguity is that successful bimolecular collision is not accounted for with enthalpy-of-activation comparisons, and such successful collision is essential for the two six-center, bimolecular reactions but not the four-center, unimolecular reaction.
- More CQC simulations must be performed for other conceivable elementary dehydrogenation reactions until all possibilities are exhausted. Evaluating all of the possible dehydrations is necessary to ensure that the concerted, meta-oxygen, six-center, bimolecular transition state remains the most favorable in terms of enthalpy of activation. (Finding one local minimum does not ensure the global minimum was found.) Other possible elementary reactions worth considering would be bimolecular entities stabilized through hydrogen-bridge bonds or even radical-chain processes. The radical-chain processes are possibly important because the four-center dehydrogenations are similar in magnitude to typical values for homolytic scission.

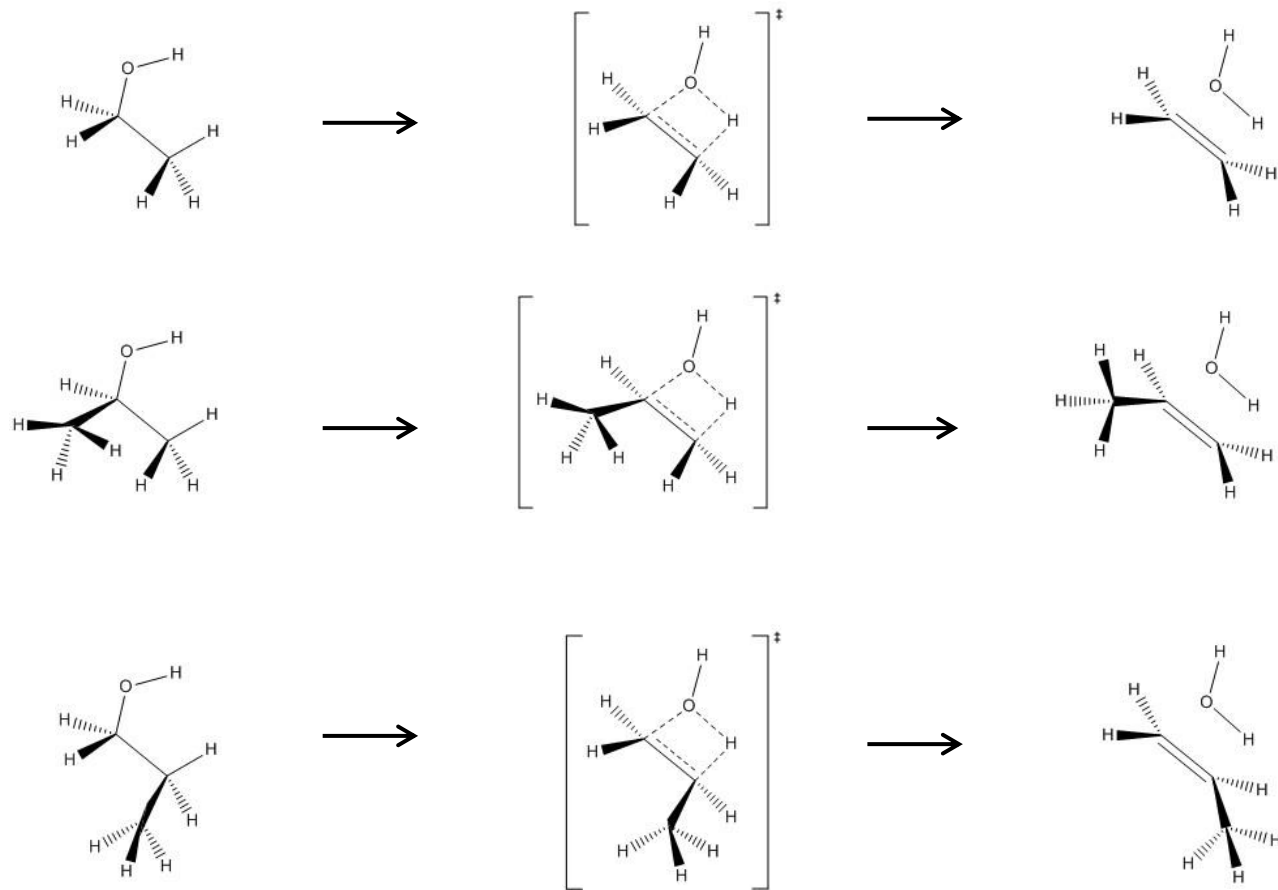


Figure 57. The hypothesized four-centered unimolecular dehydration transition-state structure was evaluated for each of the three evaluated monols.

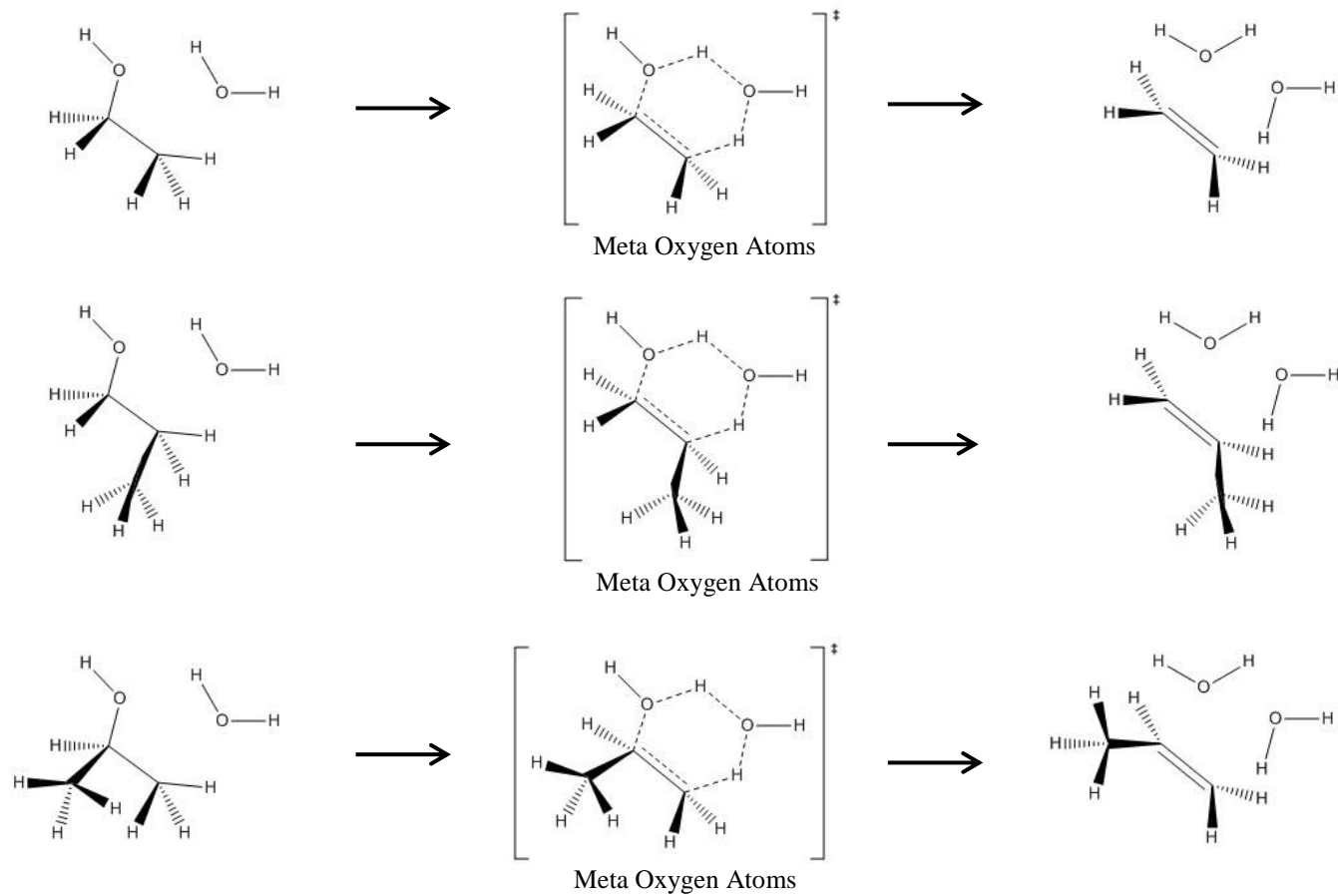


Figure 58. The hypothesized four-centered unimolecular dehydration transition-state structure was evaluated for each of the three evaluated monols.

#### 4.5.6. *Other studies focused upon dehydrations including the 1,2-elimination dehydration*

Dehydration is a vital reaction for biomass pyrolysis, yet little experimental work has been reported for alcohol pyrolysis in the conditions of biomass pyrolysis. There have been some important CQC simulations, however, and their results help us understand the possible elementary reactions observed in the PIDSSR and PIQR experiments of this work.

Moc et al. [2] performed a computational study for several elementary dehydration reactions for butan-1-ol. They found 14 conformers of butan-1-ol and tested concerted unimolecular 1,1-, 1,2-, 1,3-, and 1,4-dehydrations. The 1,2-dehydration proceeding via a concerted, four-center transition state was most favorable energetically. This concerted, four-center 1,2-dehydration had an activation enthalpy of 67.88 kcal mol<sup>-1</sup>, which is very close to the enthalpy of activation found in this work for four-center dehydrations of ethanol, propan-1-ol (68.1 kcal mol<sup>-1</sup>), and propan-2-ol (66.2 kcal mol<sup>-1</sup>) with the same CBS-QB3 method.

Nimlos et al. [51] simulated concerted eliminations to show that protonated alcohols and alcohols complexed with alkali ions have reduced activation energy compared to pure alcohols, but their estimates of pure alcohols are consistent with those provided here. Specifically, their CBS-QB3 methods yielded enthalpies of activation of at 67.4, 67.0, 65.9, and 69.6 kcal mol<sup>-1</sup> for ethanol, propan-2-ol, 2-methylpropan-2-ol, and ethan-1,2-diol, respectively.

Nimlos et al. [1] used propan-1,2,3-triol as a model compound for carbohydrates, and they computationally determined the activation energies of several 1,2-dehydrations and 1,3-dehydrations at CBS-QB3 level of theory. These authors showed that a 1,3-dehydration, which breaks one of propan-1,2,3-triol's carbon-carbon bonds to form methanal, ethenol, and water, is lower in activation energy than two possible 1,2-dehydrations by 8.0 and 5.7 kcal. mol<sup>-1</sup>.

Paine et al. [23] experimented with pyrolyses of <sup>13</sup>C<sub>1</sub>- and <sup>13</sup>C<sub>2</sub>-labelled propan-1,2,3-triol, and suggested the cyclic 1,3-dehydration (naming it the “cyclic Grob fragmentation”) to

explain the labelling patterns observed in their methanal and ethanal products. This cyclic Grob fragmentation was identical to the 1,3-dehydration found by Nimlos et al. [1].

Zhang et al. [52] used density-functional methods to search for dehydration reactions on cellulose and found most 1,2-dehydrations of hydroxyls at carbons 2 and 3 were less favorable energetically than the 1,3-dehydration of Nimlos et al. [1].

#### ***4.5.7. Comparing the products obtained by experiment to those predicted by the elementary mechanisms***

Reaction networks were proposed based upon elementary reactions suggested here and in the studies of Seshadri and Westmoreland [3], Nimlos et al. [1], and Paine et al. [23].

- Dehydration via concerted 1,2-elimination (four-centered, unimolecular mechanism or meta-oxygen, six-centered, bimolecular mechanism)
- Dehydrogenation via concerted alcohol dehydrogenation (four-centered, unimolecular mechanism or meta-oxygen, six-centered, bimolecular mechanism)
- Fragmentation dehydration via the cyclic Grob fragmentation
- Isomerization between enols and aldehyde/ketone
- Isomerization between hydroxyaldehyde and hydroxyketone

The reaction networks were constructed by exhaustively applying these three reactions wherever possible in the initial molecule and any of its subsequent products.

The importance of using drastically smaller model compounds is shown clearly by comparing the suggested reaction networks proceeding from Figures 59 to 67. One must evaluate a rapidly increasing reaction network upon increasing the complexity of an alcohol in two ways.

- Replacing a hydrogen atom on the  $\alpha$ -carbon by another alcohol group ( $-\text{C}(\text{OH})\text{H}_2$ )
- Replacing a hydrogen atom on the  $\alpha$ -carbon by a methyl group

For the set of monols, methanol (Figure 59), ethanol (Figure 60), propan-2-ol (Figure 61), and 2-methylpropan-2-ol (Figure 62) all produced the dehydrogenation and dehydration compounds expected for the GCxGC-TOFMS (Table 11). Additional products were observed in trace amounts, however.

- Methanol formed CO and CO<sub>2</sub>, but these gases were not seen reliably in the other monols.
- Ethanol formed several four-carbon products in trace quantities. The three trace products, butanal, butanone, and but-2-enal, suggest a strong likelihood of trace combination between ethanol and/or ethanol's two-carbon products. This pattern of combination was not seen in the other monols.
- Propan-2-ol formed a trace of diisopropyl ether, but this pattern of alcohol combination to ether was not seen in the other monols.

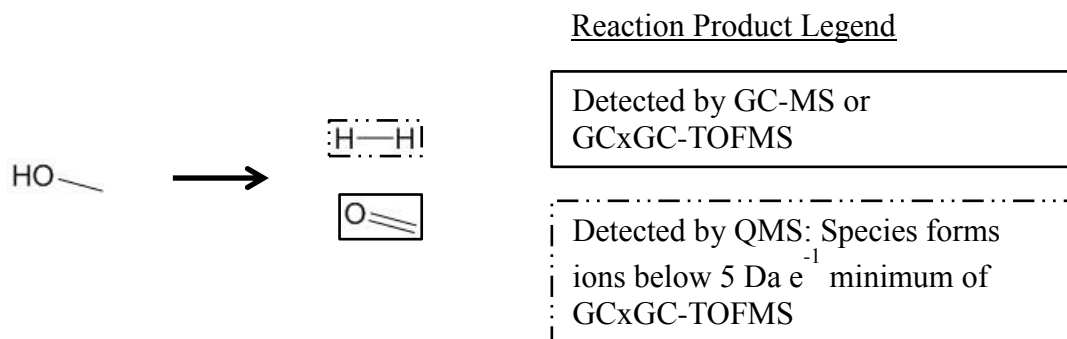


Figure 59. The reaction scheme for low-temperature pyrolysis of methanol.

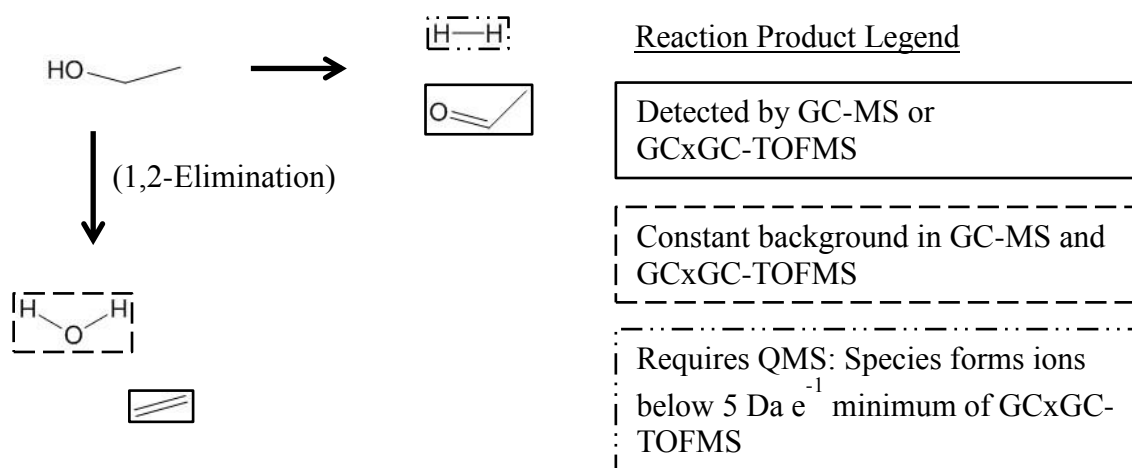


Figure 60. The reaction scheme for low-temperature pyrolysis of ethanol (left) and generic saturated primary monols (right).

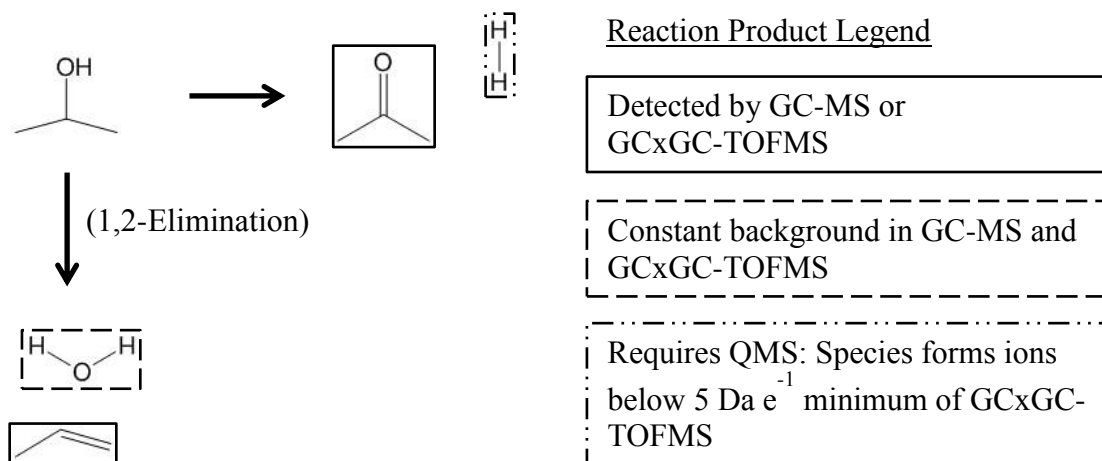


Figure 61. The reaction scheme for low-temperature pyrolysis of propan-2-ol (left) and generic saturated secondary monols (right).

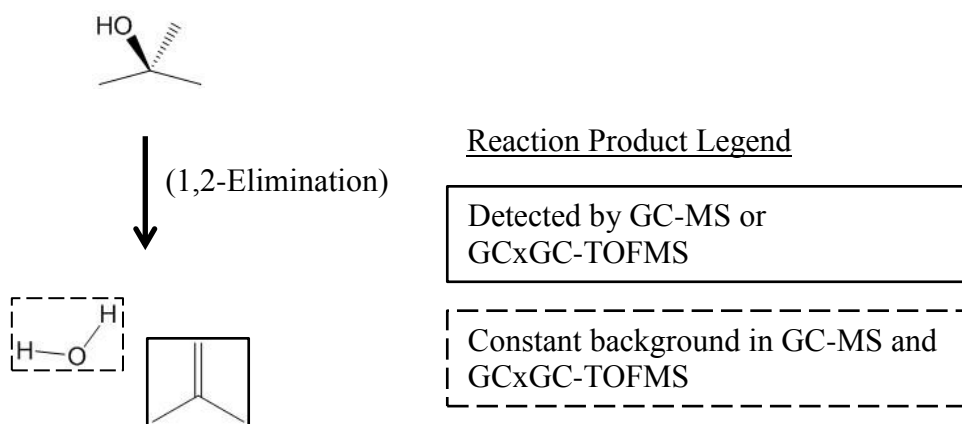


Figure 62. The reaction scheme for low-temperature pyrolysis of 2-methylpropan-2-ol (left) and generic saturated tertiary monols (right).

As for the set of diols and triol, experiments were less successful in locating all of the expected products.

Ethan-1,2-diol experiments (Figure 63) provided all of the expected products. In addition to the products expected by the proposed dehydrogenation and dehydration mechanisms, ethan-1,2-diol showed that the carbon-carbon bond can fragment to produce methanal by an undetermined route. It is different from the cyclic Grob fragmentation because the undetermined route breaks carbon-carbon bonds in 1,2-diol systems as opposed to 1,3-diol systems.

Propan-1,2-diol experiments (Figure 64) provided all but one of the predicted dehydrogenation products (2-hydroxypropanal was missing) and provided the one predicted dehydration product. Importantly, propan-1,2-diol formed methanal and ethanal, which were not predicted by any of the anticipated reaction mechanisms, and might have been formed by the same undetermined route(s) seen in ethan-1,2-diol.

Propan-1,3-diol experiments (Figure 65) provided most of the expected products, but the products obtained differed in two important ways. Propan-1,3-diol formed no ethene, which would be required for the cyclic Grob fragmentation. This lack of ethene is possibly due to failing to detect a small, broad peak, as GC capillary columns cannot focus gases. The other important difference is how some observed compounds were not predicted: ethanal, propanol, and propanal. Propanol is unable to form via unimolecular reaction because it has lost a single oxygen atom compared to propan-1,3-diol.

Propan-1,2,3-triol experiments (Figures 66 and 67) did not provide most of the anticipated products. It formed the anticipated products of the cyclic Grob fragmentation (methanal and ethanal), which were expected due to results in the literature. Propan-1,2,3-triol also formed one product of a single dehydration (1-hydroxypropanone) and one product of a double dehydration (prop-2-enal). It also formed one product of a combined single

dehydration and single dehydrogenation (2-oxopropanal). These dehydrogenation and dehydration products are very important because they highlight the importance of reactions that do not fragment carbon-carbon bonds in compounds with as many as three adjacent alcohol groups. An important discrepancy between expected and observed products is the absence of the dehydrogenation products with three oxygen atoms. This absence could suggest dehydrogenation is much less rapid than other reactions like dehydration or fragmentation.

There were unanticipated fragmentation products observed in ethan-1,2-diol and propan-1,2-diol. For ethan-1,2-diol, this product was methanal, and for propan-1,2-diol, these products were ethanal and methanal. Because the cyclic Grob fragmentation cannot apply to the 1,2-diol system present in these ethan-1,2-diol and propan-1,2-diol, another fragmentation was considered. It is necessary to determine if  $H_2$  is formed in this undetermined fragmentation route, because finding  $H_2$  allows a unimolecular reaction to form only methanal from ethan-1,2-diol and only methanal and ethanal from propan-1,2-diol. This undetermined fragmentation likely did not apply to propan-1,3-diol, because propan-1,3-diol would have formed ethanal (Figure 65).

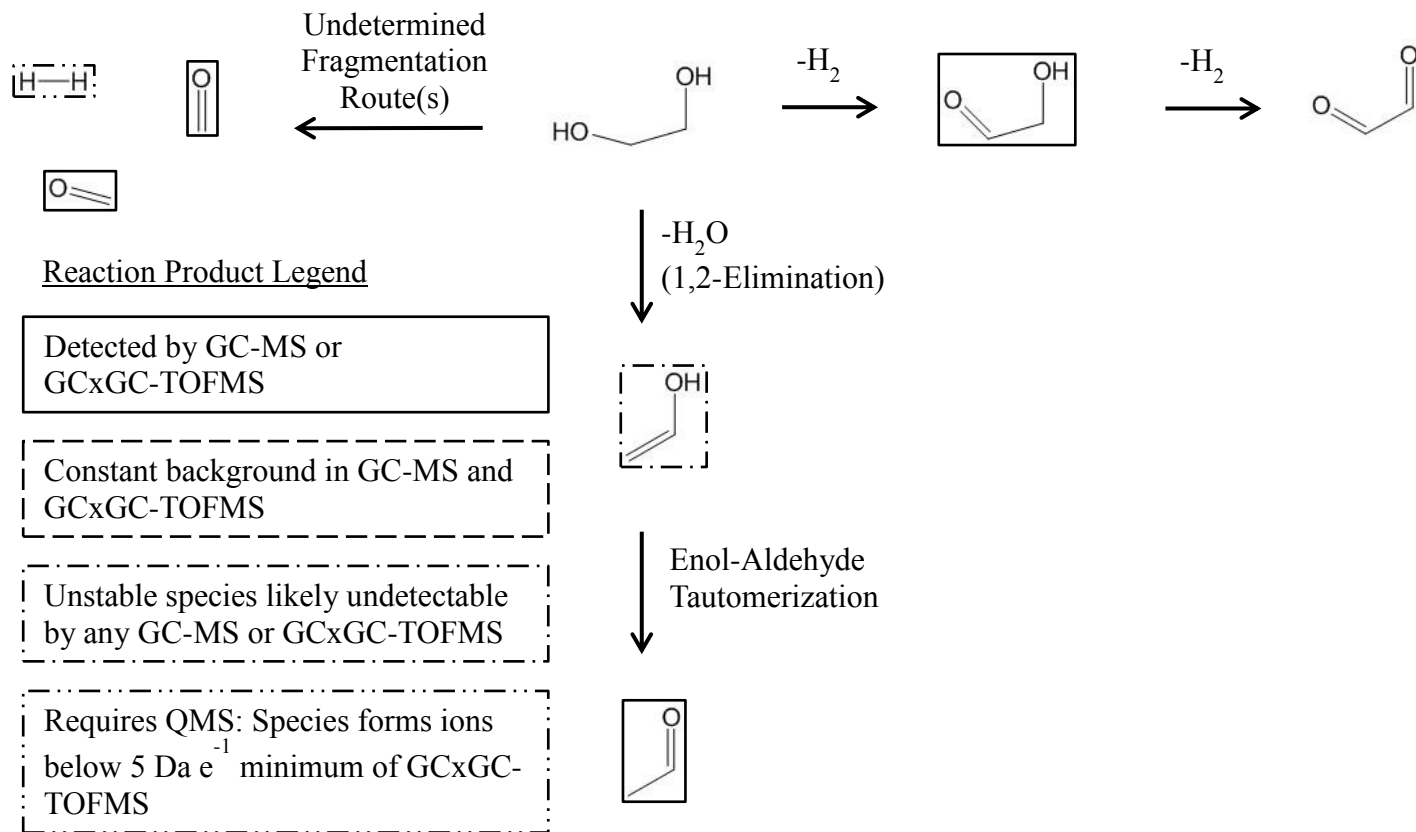


Figure 63. The reaction scheme for pyrolysis of ethan-1,2-diol when considering only the concerted alcohol dehydrogenation, concerted 1,2-elimination of water, and an undetermined fragmentation route.

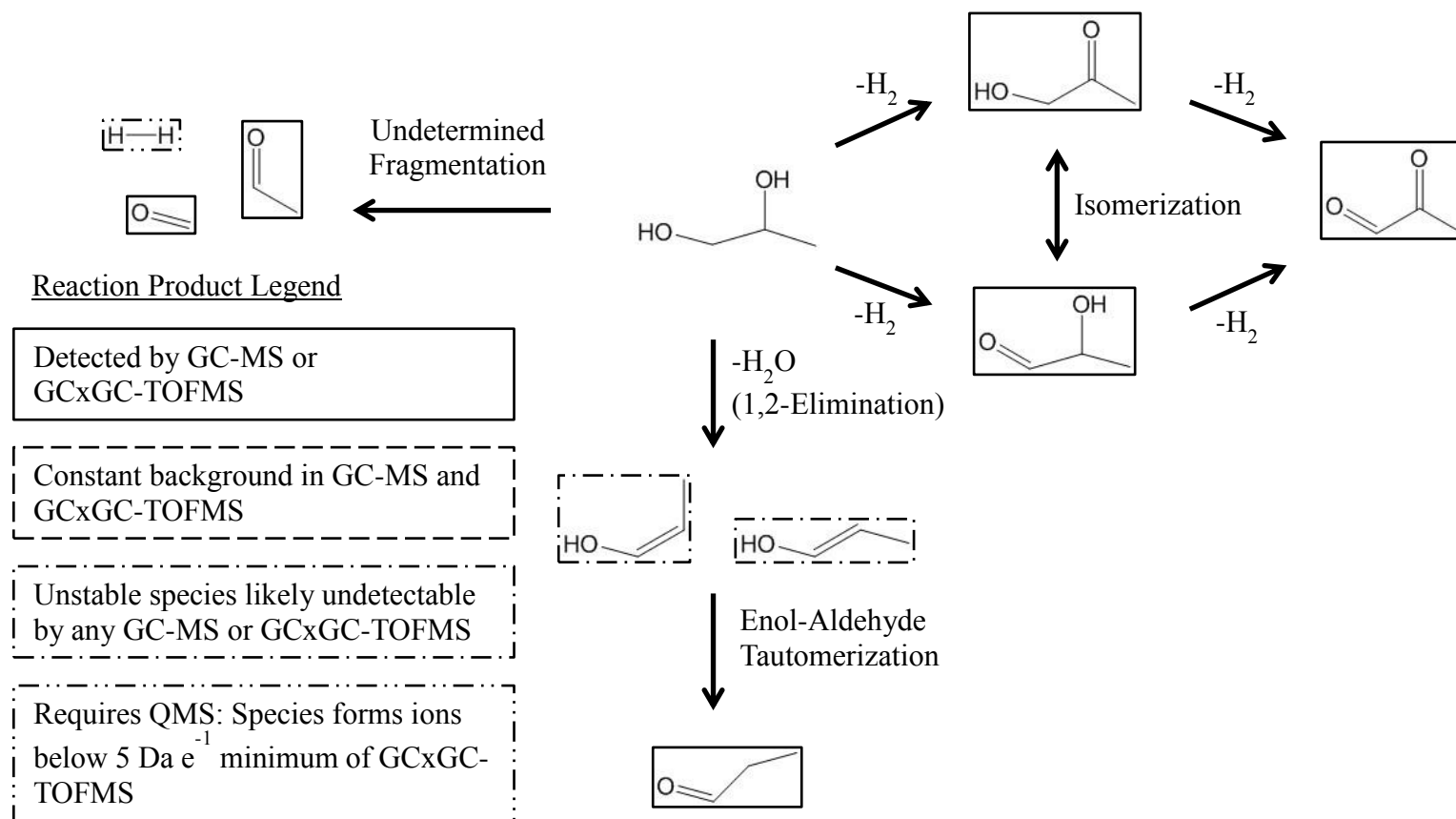


Figure 64. The reaction scheme for pyrolysis of propan-1,2-diol when considering only the concerted alcohol dehydrogenation, the concerted 1,2-elimination of water, the concerted hydroxyketone-hydroxyaldehyde isomerization, and a necessary undetermined fragmentation reaction.

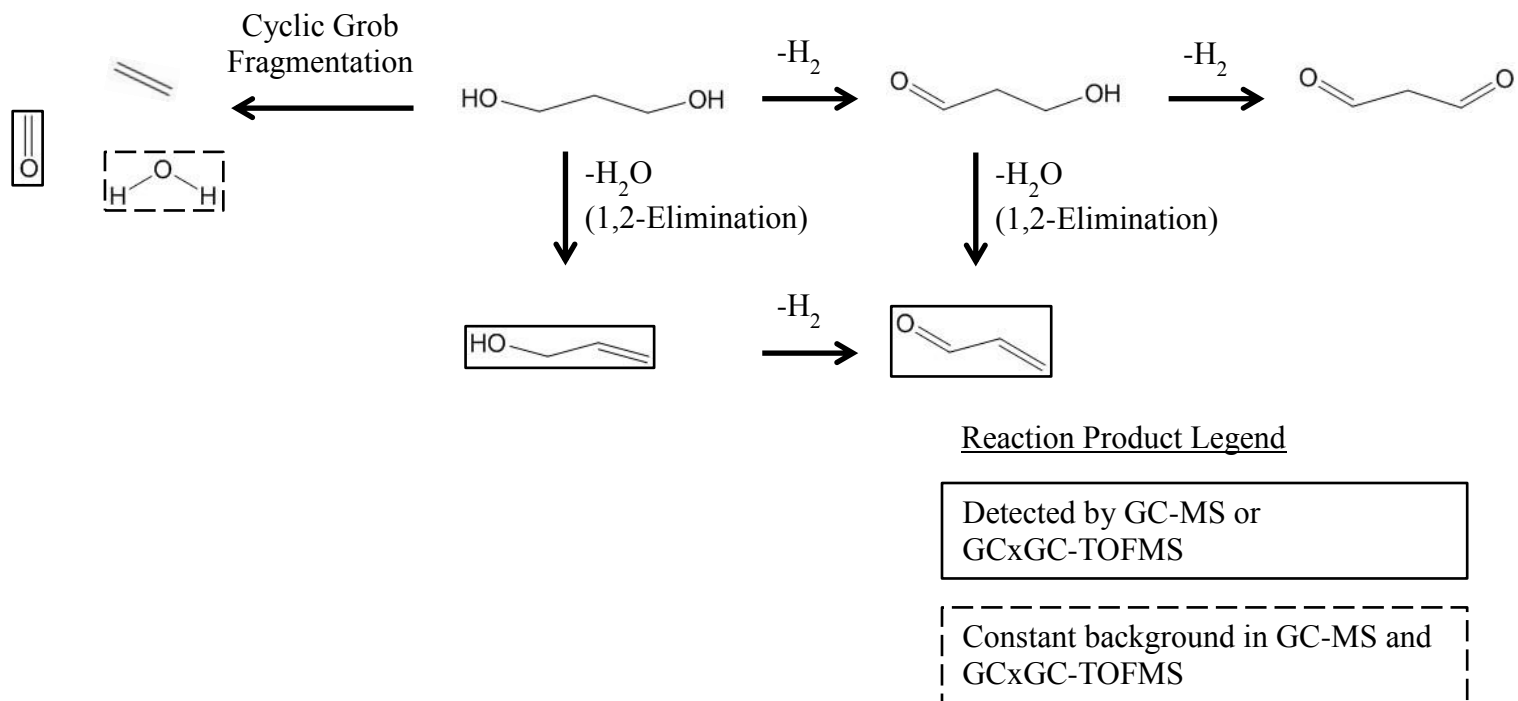


Figure 65. The reaction scheme for pyrolysis of propan-1,3-diol when considering only the cyclic Grob fragmentation, concerted alcohol dehydrogenation, and concerted 1,2-elimination of water.

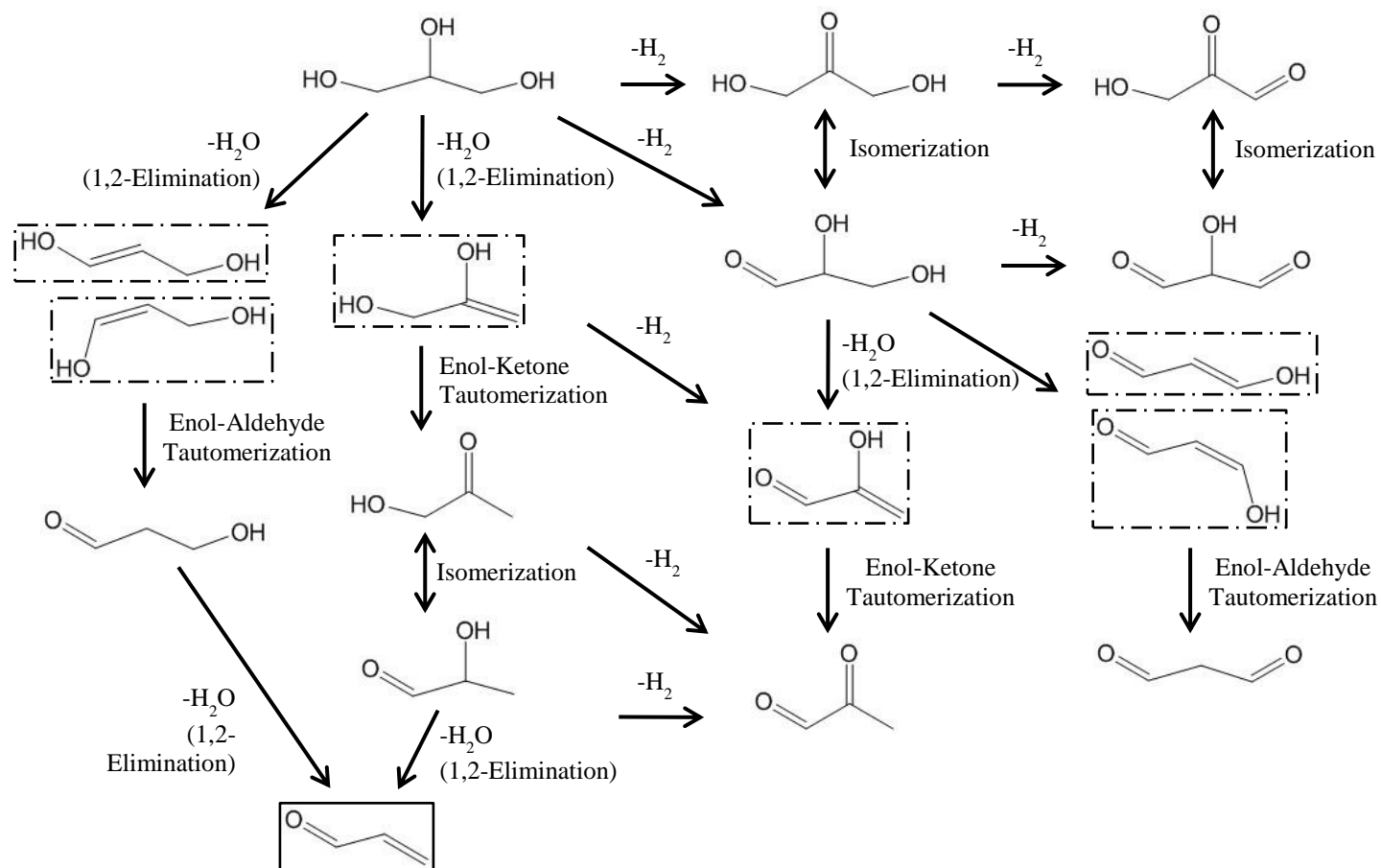


Figure 66. The reaction scheme for pyrolysis of propan-1,2,3-triol when considering only the concerted alcohol dehydrogenation, the concerted 1,2-elimination of water, and enol-aldehyde and hydroxyketone-hydroxyaldehyde isomerizations.

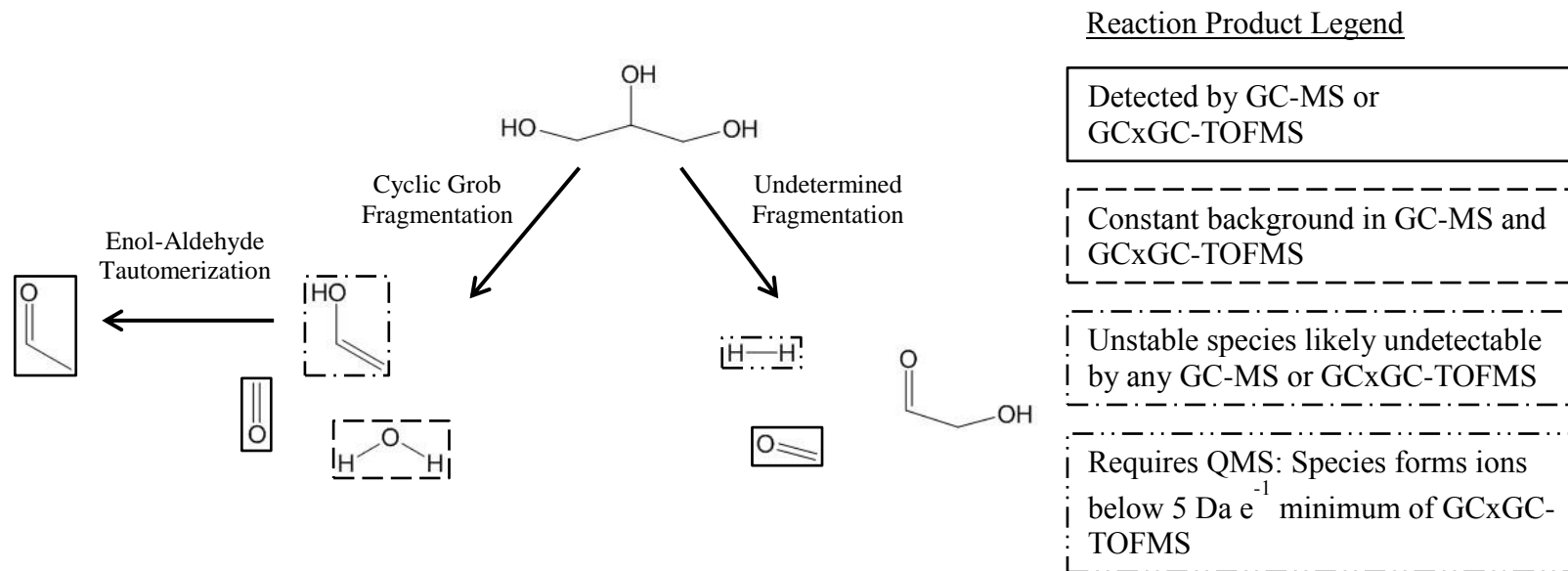


Figure 67. The reaction scheme for pyrolysis of propan-1,2,3-triol when considering only the cyclic Grob fragmentation, enol-aldehyde tautomerization, and an unidentified fragmentation.

#### 4.5.8. *Dehydrogenation inhibits some subsequent adjacent 1,2-dehydrations*

An important impact of including alcohol dehydrogenations in the reaction network of cellulose pyrolysis is the inhibition of some subsequent 1,2-dehydrations. The concerted 1,2-elimination is unable to operate on a primary alcohol group that is adjacent to a ketone because a ketone lacks a hydrogen atom by definition. Three model compounds serve as examples for this concept.

- Propan-1,2-diol contains one primary alcohol, one secondary alcohol, and one methyl group. If the secondary alcohol (carbon 2) were to dehydrogenate, then the primary alcohol (carbon 1) could not be dehydrated via a concerted 1,2-elimination. If instead propan-1,2-diol's primary alcohol (carbon 1) dehydrogenated, then the secondary alcohol could dehydrate via the 1,2-elimination because of the hydrogen atoms available on the methyl group (carbon 3).
- Propan-1,2,3-triol contains two primary alcohols, one secondary alcohol, and no methyl groups. If the secondary alcohol (carbon 2) were to dehydrogenate, then either primary alcohol (carbons 1 and 3) could not be dehydrated via a concerted 1,2-elimination.
- Ethan-1,2-diol contains no secondary alcohols. If it were to dehydrogenate, then a subsequent dehydration via concerted 1,2-elimination would form ethenone.

While the concerted 1,2-elimination is unable to cause dehydration in primary alcohols adjacent to ketones, dehydration of these primary alcohols may still occur through more complicated dehydration mechanisms which include molecular rearrangements. Perhaps the hydroxyketone can isomerize to a hydroxyaldehyde, as suggested in the pathways by Seshadri and Westmoreland [3]. After such an isomerization, the newly formed secondary alcohol could dehydrate via the 1,2-elimination because it has a neighboring carbonyl group and a neighboring methyl group (for propan-1,2-diol) or hydroxyl group (propan-1,2,3-triol).

#### 4.5.9. *Recommended future research*

To identify the elementary reactions responsible for dehydrogenation and dehydration with greater certainty, several types of experiments are considered vital.

- PIQR-QMS and PIQR-GC-MS experiments with heated sample-feed lines and product-effluent lines. The PIQR-QMS proved very useful without a GC separation because it directly analyzes the reactant-feed pulse by QMS (without the GC separation). If products can be analyzed by both the QMS and a GC-MS (in simultaneous or even alternating fashion), then the PIQR can obtain much more accurate species identifications as well as residence time estimates. This combination of data is necessary to obtaining residence-time measurements and individual product yields needed for kinetic estimates.
- Test deuterated alcohols in the PIQR-QMS/PIQR-GC-MS to establish if dehydrogenations and dehydrations are bimolecular or unimolecular in nature. A co-pyrolysis of a fully deuterated alcohol and a non-deuterated alcohol can provide strong evidence for whether dehydrogenations and dehydrations are unimolecular or bimolecular.
  - A combination of 2, 3, and 4 Da  $e^{-1}$  spectral peaks for hydrogen product (H-H, H-D, and D-D, respectively) suggests bimolecularity, and a combination of only 2 and 4 Da  $e^{-1}$  spectral peaks suggests unimolecularity.
  - A combination of 18, 19, and 20 Da  $e^{-1}$  spectral peaks for water (H-O-H, H-O-D, and D-O-D, respectively) suggests bimolecularity, and a combination of only 18 and 20 Da  $e^{-1}$  spectral peaks for water (H-O-H and D-O-D, respectively) suggests unimolecularity.
- Test alcohols with  $\pi$ -bonds joining  $\beta$  and  $\gamma$  carbons, like allyl alcohol and benzyl alcohol. These  $\pi$ -bond groups often stabilize ions and reaction intermediates via resonance stabilization, and they may alter the likelihood of dehydrogenation, dehydration, and carbon-carbon bond fragmentation. Such  $\pi$ -bond groups may be vital to understanding cellulose pyrolysis because allyl-alcohol like moieties will

likely form after suspected dehydration of the alcohols on anhydroglucopyranose units. The formation of methanal and furfural from 5-hydroxymethylfurfural was observed (Table 11), and the ability to substitute a hydrogen atom on the furan ring's carbon 5 while simultaneously eliminating methanal suggests particular reactivity for alcohols with their  $\beta$  carbons involved in  $\pi$ -bonded systems.

#### **4.6. Conclusion**

Sets of alcohol model compounds demonstrated the power of using simpler molecules for determining detailed reactions of cellulose and hemicellulose pyrolysis. As expected, their number of reaction products was greatly reduced. Having fewer reaction products made comparing products made by different model compounds much easier, resulting in formulating and testing reaction hypotheses much faster than formulating and testing reaction hypotheses based upon comparisons between more complicated primary and secondary structures of materials like cellulose, starch, and xylan.

CQC simulations were performed to evaluate concerted mechanisms for dehydrogenation and dehydration. Simulation results for dehydrogenation suggested that a meta-oxygen, six-centered, bimolecular mechanism is more favorable than a four-center, unimolecular mechanism because of a roughly 30 kcal mol<sup>-1</sup> lower enthalpy of activation. Simulation results for dehydration suggested that meta-oxygen, six-centered, bimolecular mechanism is more favorable than a four-center, unimolecular mechanism because of a roughly 13 kcal mol<sup>-1</sup> lower enthalpy of activation. Co-pyrolysis of fully deuterated and non-deuterated monols were employed to evaluate whether dehydrogenation was unimolecular or bimolecular. Initial results suggested that a bimolecular mechanism is unlikely due to the lack of partially-deuterated products. This experimental result suggested that the likelihood of bimolecular reaction may be less favorable than the simulated enthalpy of activation suggested.

The presence of dehydrogenation was unexpected for these model compounds because hydrogen is seldom reported for pyrolysis, and dehydration is the most prominent

reaction for the alcohol groups in cellulose and hemicellulose. Future work with understanding the vital dehydration mechanisms with smaller model compounds should pay careful attention to the competing effect of dehydrogenation.

## CHAPTER 5. PYROLYSIS OF D-GLUCOSE-LIKE MODEL COMPOUNDS FOR ELUCIDATING D-GLUCOSE PYROLYSIS REACTIONS

### *5.1. Abstract*

A model-compound set of materials similar in structure to D-glucose were used to better understand the detailed reaction networks for pyrolysis of D-glucose and cellulose. Thermogravimetric experiments and Pyroprobe® experiments with this model-compound set allowed isolation of anticipated reactions by specific changes to D-glucose's molecular structure. Such isolation is not possible with experiments using only D-glucose and D-glucose-based materials like D-cellobiose and cellulose.

Two stages of mass loss occurred during pyrolysis of five D-aldohexoses, two D-aldopentoses, and two deoxyhexoses, but only one stage of mass loss occurred during pyrolysis of the D-alditols. In addition, very little or no levoglucosan formed during the pyrolysis of D-alditols, D-aldopentoses, and 6-deoxy-L-galactose, while a large yield of levoglucosan formed during the pyrolysis of D-aldohexoses. The combination of these mass-loss and reaction-product results suggests that neither levoglucosan formation nor levoglucosan polymerization is primarily responsible for the common two-stage mass-loss phenomena. Additionally, levoglucosan or levoglucosan-like molecules were formed from each D-aldohexose tested in the Pyroprobe®, suggesting that the stereochemistry at carbons 2, 3, and 4 is not vital to the yield of a respective C6-O-C1 bicyclic product. Additional observations were that both 2-deoxy-D-glucose and 6-deoxy-L-galactose produced the two-stage mass-loss phenomenon and only the D-alditols left no char.

Two stages of mass loss also occurred during pyrolysis of cellobiose, dextran, starches, and xylan, but only one stage of mass loss occurred during pyrolyses of trehalose and cellulose. The combination of these two observations suggests that the fraction of reducing sugar, in addition to a 1,6-bicyclic formation, is also not solely responsible for the common two-stage mass-loss behavior. As with the monosaccharide-like model compounds,

neither levoglucosan formation nor levoglucosan polymerization is necessarily responsible for the two-stage mass-loss phenomenon in dimers, oligomers, and polymers of saccharides.

Finally, D-alditols left essentially no char, suggesting that true saccharides (i.e., a 1:2:1 ratio of carbon, hydrogen, and oxygen atoms, implying alcohol groups and either one acyclic carbonyl or a cyclic ether) are necessary for the formation of char. Importantly, this result suggests that

- Carbonyl or ether groups are necessary for char formation, and
- The presence of only alcohol groups within molecules causes fragmentations to only volatile products when the initial reactant molecule is in a range of 6 carbon atoms.

These conclusions shed light upon why pyrolysis of cellulose provides many of the same pyrolysis products as D-glucose but provides them at a different compositions compared to other D-glucose-based materials. The knowledge gained from this model-compound set provides important insight to elementary mechanisms of cellulose pyrolysis as well as general saccharide pyrolysis. These insights must be used if an elementary model is to be constructed accurately.

## ***5.2. Introduction***

### ***5.2.1. Understanding cellulose pyrolysis requires more than just cellulose experiments***

Cellulose pyrolysis has been studied extensively, and the understanding of its fundamental chemistry has progressed significantly from simple mechanisms based upon lumped species. Reaction models based upon elementary reaction networks are showing promise for predicting yields for specific products. Arguably the most important reaction(s) of the network used by these models is what cleaves the many glycosidic bonds in the cellulose chain. This reaction mechanism is likely responsible for two important observations:

- Oligomers up to five anhydroglucopyranose units in length were observed during cellulose pyrolyses by Pouwels et al. [53] and Pastorova et al. [54] when pyrolyzing cellulose rapidly on a filament in a special mass-spectrometry technique. From this observation it was suggested that the mechanism of breaking glycosidic bonds is likely the fundamental reaction responsible for the initial destruction of the long polymer chains in cellulose, even with rapid heating.
- Levoglucosan is observed in a high yield compared to all other products of cellulose pyrolysis, making the cleaving of glycosidic bonds near the initial-reactant or intermediate cellosan chains' end responsible for a large reaction flux.

These two observations thus imply that having an accurate elementary understanding of levoglucosan-forming reaction(s) is vital for assembling a predictive model for cellulose pyrolysis.

Cellulose pyrolysis has been studied for several decades, and reaction products have been well characterized [27], [28], [47], [49]. However, even with these important data, the reaction network is too complex for individual detailed reactions to be identified and measured with accuracy. This complexity of cellulose pyrolysis has led many researchers to use D-glucose as a model compound for cellulose due to its simpler structure.<sup>61</sup> However, even with well-characterized products, the reaction network of D-glucose pyrolysis has also been too complex to identify individual detailed reactions with accuracy. Two different stages of model-compound experimentation were performed in this work to gain a better understanding of cellulose pyrolysis.

- Experiment with much simpler model compounds than D-glucose, namely monols, diols, and a triol. This method and its results were described in Chapter 4, where dehydration, dehydrogenation, and carbon-carbon bond fragmentation tendencies

---

<sup>61</sup> Work by Mettler et al. suggested that D-glucose is a poor substitute for cellulose because the two materials do not produce the same products [27]. Subsequent work by Seshadri and Westmoreland implied that some of the same chemical-reaction steps occur in both glucopyranose and cellulose [3].

were identified for small alcohol molecules. Alcohol groups are omnipresent throughout cellulose, so it is assumed the same reaction mechanisms may apply to both small alcohol molecules as well as both saccharides (e.g., D-glucose) and polysaccharides (e.g., cellulose and hemicellulose).

- Experiment with a model-compound set of D-glucose and other molecules very similar in structure. Each member of the model-compound set has specific difference in its chemical structure relative to one or more other members of the set. The differences in reaction products between members of the “D-glucose-like” model-compounds set can be attributed to specific structural moieties within these more complicated structures. The detailed reactions learned from monols, diols, and triols can also be applied to this more complex set of D-glucose-like model compounds to hypothesize on an elementary level why different functional groups cause different reaction behaviors.

### ***5.2.2. Model compounds, revisited***

Section 4.2.1 explained how assembling model-compound sets provides a way to attribute specific reaction behaviors to specific portions of complex molecules. The members of these model-compound sets differ in chemical structure only slightly from one another. Any differences in observed reaction behavior (e.g., observed products, mass-loss rates, or melting temperatures) among the members can be attributed to specific structural moieties. Therefore, differences in products formed by members of the model-compound set create strong evidence to support detailed reactions, even if each model compound is composed of too many functional groups to allow isolation of elementary reactions when experimented with alone.

Noting how compound comparisons are necessary to isolate reaction behaviors for complicated molecules leads to an important conclusion: Testing compounds other than those based directly upon D-glucose or D-glucofuranose is necessary to understand cellulose pyrolysis chemistry. This approach appears novel for experiments designed to understand cellulose-pyrolysis chemistry.

### 5.2.3. *The selection of D-glucose-like model compounds*

Non-D-glucose materials were carefully chosen to differ only slightly from D-glucose so that their different products can be attributed to specific components of D-glucose's complicated structure. Several types of structural differences were evaluated for their effect on reaction behavior.

- The effect of stereochemistry was evaluated by four diastereomers of D-glucose, which were D-allose, D-altrose, D-galactose, and D-mannose (Figure 86). Two of these compounds, D-galactose and D-mannose are epimers of D-glucose, importantly exhibiting only a single stereochemical change in comparison to D-glucose.<sup>62</sup>
- The effect of replacing the carbonyl at carbon 1 with an alcohol by selecting two alditols, D-glucitol and D-mannitol (Figure 68). This structural modification prevents the molecule transforming from acyclic form into pyranose or furanose forms.
- The effect of replacing a hydroxyl group with a hydrogen atom was evaluated by selecting two deoxy-hexoses. These hydroxyl groups selected for replacement were in two vital locations.
  - 6-Deoxy-L-galactose (“L-fucose”) was selected for replacing the hydroxyl group on carbon 6 of L-galactose<sup>63</sup> with a hydrogen atom. The hydroxyl group on carbon 6 of aldohexoses is vital for the formation of levoglucosan.
  - 2-Deoxy-D-glucose was selected for replacing the hydroxyl group on carbon 2 of D-glucose with a hydrogen atom. The hydroxyl group on carbon 2 creates a key 1,2-diol system within anhydroglucopyranose units of cellulose and a key 1,2,3-triol system within glucose and glucopyranose.

---

<sup>62</sup> Epimers are diastereomers which differ by a single stereochemical center. Acyclic D-glucose is an epimer with both acyclic D-galactose and acyclic D-mannose. However, when cyclized, D-glucopyranose and D-galactopyranose (and D-glucopyranose and D-mannopyranose) can be diastereomers with differences in two stereochemical centers due to the creation of  $\alpha$  and  $\beta$  anomeric centers at carbon 1.

<sup>63</sup> The reactions of enantiomers should proceed in the same fashion (aside for making products which are also enantiomers) when not reacting with a chiral co-reactant or in a chiral environment. This concept is addressed in section 5.6.5.

- The effect of replacing carbon 6 ( $-\text{CH}_2(\text{OH})$ ) with a hydrogen atom was evaluated by selecting D-xylose. While there are four D-aldopentoses, only D-xylose matches the stereochemistry of D-glucose on carbons 2 through 4.

This set model compounds is displayed in Figure 68. This figure is not a reaction scheme; the lines connecting model compounds specifically do not have arrow symbols to help avoid this confusion. Both the Fischer projections and both of the Haworth projections are shown (where applicable) due to the ability for most of these D-glucose-like model compounds to form pyranose and furanose rings. Also note that only the  $\alpha$  anomers are shown for the cyclic structures, but a fraction of  $\beta$ -anomers are also expected with anomeric carbons.

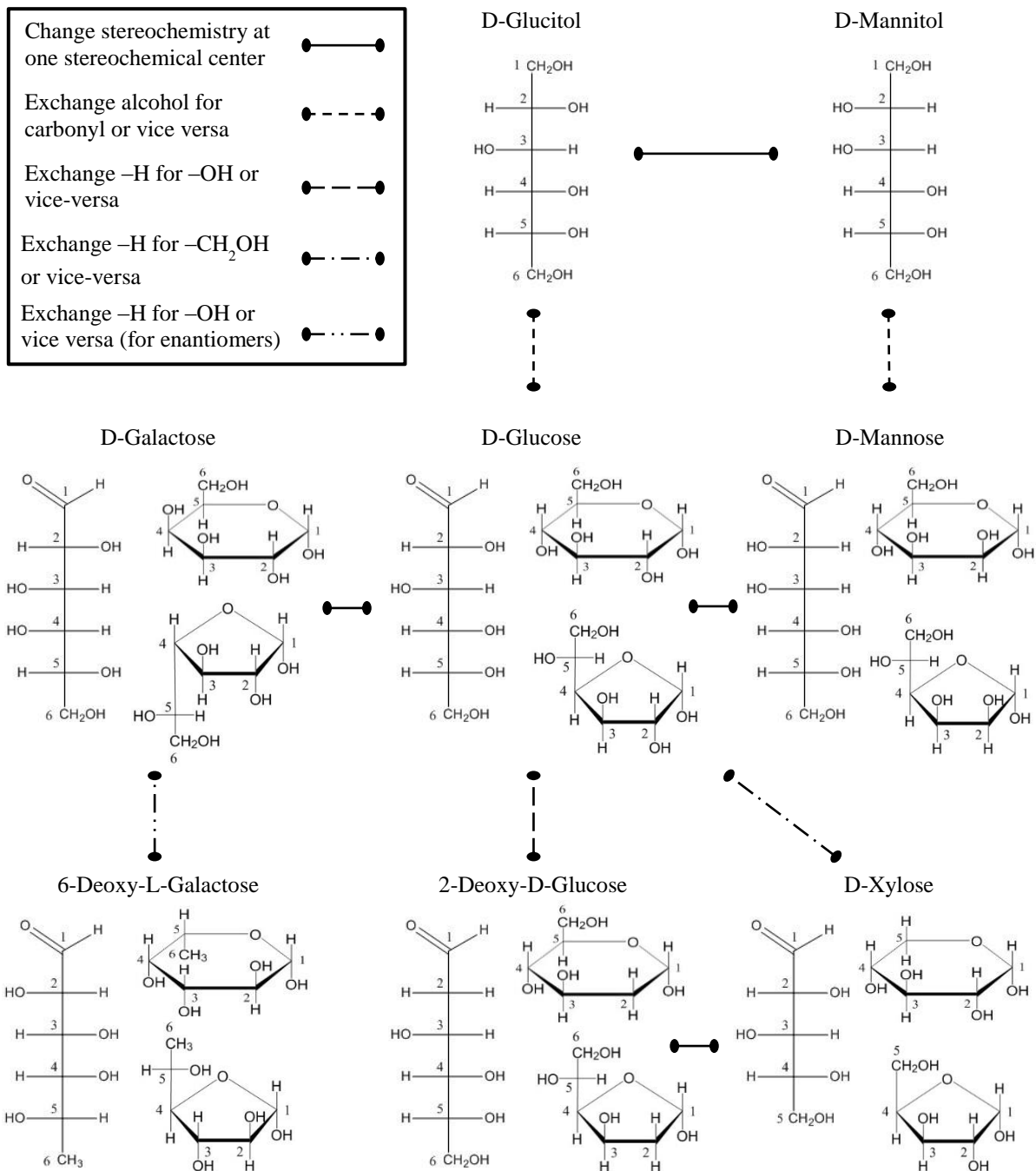


Figure 68. The D-glucose-like model compounds used to probe the chemistry of cellulose pyrolysis. Only the  $\alpha$  anomers are shown in this image. The line types connecting model compounds depict the differences between chemical structures. Aldopentose and aldohexose structures are obtained from Collins and Ferrier [55, pp. 16, 18] and Shallenberger [56, pp. 81, 103-105].

Several additional compounds were evaluated for other important comparisons.

- The effect of enantiomerism was evaluated by comparing D-arabinose and L-arabinose.
- The effect of diastereomerism which differed by two stereochemical centers was evaluated by comparing D-allose and D-altrose to D-glucose, as well as comparing D-arabinose to D-xylose.

#### ***5.2.4. The complication of isomerism with saccharides like aldohexoses and aldopentoses***

Figure 68 immediately uncovers a difficult aspect of determining the pyrolysis chemistry of saccharide materials: Their exact structures are not well known in the solid phase, melt phase, or pyrolysis conditions. Data for the solution suggests most aldohexoses and aldopentoses prefer their pyranose forms, but no data have been found for the solid phases important to pyrolysis experiments.

### ***5.3. Review of Structural Concepts in D-Aldohexoses and D-Aldopentoses***

Several important concepts in saccharide chemistry are reviewed here. These concepts and terms are quite useful in subsequent sections because they make descriptions of many complicated molecular structures both more precise and more succinct. The ability to compare and contrast molecular structures clearly allows the conclusions to be much better understood. A short review of examples is provided in this section. Further reading for more detailed descriptions is available in several recommended resources:

- Section 25.1 through 25.3 of J. M. Hornback, *Organic Chemistry, Second Edition*, 2006 [57].
- Sections 2.1 through 2.3.7 of D. E. Levy and P. Fügedi, *The Organic Chemistry of Sugars*, 2006 [58].
- Section 8.1 through 8.4 of H. R. Horton, L. A. Moran, K. G. Scrimgeour, M. D. Perry, J. D. Rawn, *Principles of Biochemistry, Fourth Edition*, 2006 [59].

There are many monosaccharides with molecular structures very close to that of D-glucose, and stereochemistry is the reason for having so many similar molecular structures. There are eight distinct acyclic D-aldohexoses because D-aldohexoses have three stereocenters (on carbons 2, 3, and 4), and three stereocenters enable eight diastereomers in total ( $2^3 = 8$ ). These eight acyclic D-aldohexoses are D-allose, D-altrose, D-galactose, D-glucose, D-gulose, D-idose, D-mannose, and D-talose. Each acyclic D-aldohexose is a diastereomer with the seven other remaining acyclic D-aldohexoses. In addition, each acyclic D-aldohexose has two epimers among the seven diastereomers.

There are four distinct acyclic D-aldopentoses because D-aldopentoses have two stereocenters (on carbons 2 and 3), and two stereocenters enable four diastereomers in total ( $2^2 = 4$ ). These four acyclic D-aldopentoses are D-arabinose, D-lyxose, D-ribose, and D-xylose. Each acyclic D-aldopentose is a diastereomer with the three other remaining acyclic D-aldopentoses. In addition, each D-aldohexose has two epimers among its other seven D-aldohexoses and each D-aldopentose has two epimers among its other three D-aldopentoses.

Aldohexoses and aldopentoses can cyclize to both furanose and pyranose structural isomers. Upon cyclization of an aldohexose or aldopentose, carbon 1 becomes a new “anomeric” stereocenter because three distinguishable ligands are now bonded to it. This new stereocenter at carbon 1 exhibits both possible diastereomers due to the non-stereospecificity of the alcohol-addition reaction responsible for cyclization. The absolute stereochemical configuration at carbon 1 in a furanose or pyranose ring is described as either  $\alpha$  or  $\beta$ . With the ability to cyclize and the anomeric carbon formed upon cyclization, there are five forms in which each aldohexose and aldopentose may exist: Acyclic,  $\alpha$ -furanose,  $\beta$ -furanose,  $\alpha$ -pyranose, and  $\beta$ -pyranose.

Examples are used to recap the important descriptive terms described briefly in this section. The terms and concepts in these examples are essential to understand the descriptions and logic used later in the chapter.

- Acyclic D-glucose and acyclic L-glucose are enantiomers. Acyclic D-galactose and acyclic L-galactose are also enantiomers.
- The acyclic forms of D-allose, D-altrose, D-galactose, D-glucose, D-gulose, D-idose, D-mannose, and D-talose are all diastereomers of one another.
- Acyclic forms of D-glucose and D-galactose are epimers. Acyclic forms of D-glucose and D-mannose are also epimers.
- $\alpha$ -D-glucopyranose and  $\beta$ -D-glucopyranose are anomers.  $\alpha$ -D-glucofuranose and  $\beta$ -D-glucfuranose are also anomers.
- $\alpha$ -D-glucopyranose and  $\alpha$ -D-galactopyranose are epimers.  $\beta$ -D-glucopyranose and  $\beta$ -D-galactopyranose are also epimers.  $\beta$ -D-glucopyranose and  $\beta$ -D-mannopyranose are also epimers.
- $\alpha$ -D-glucopyranose and  $\beta$ -D-galactopyranose are diastereomers and are not anomers or epimers.

#### ***5.4. Methods and Procedures***

##### ***5.4.1. Materials***

All chemicals were used as received without any added purification or alteration. For the preparation of Pyroprobe® sample tubes, materials were dried at 120°C for 20 minutes to obtain their “dry” mass. A measurable mass of moisture from the air was reabsorbed into these saccharide materials (as well as the quartz tube and quartz wool) within 30 seconds. To minimize the water injected to the GC-MS, a temperature of 120°C was used in the Pyroprobe® methods as the rest temperature, so the pyrolysis experiments began with the material in a dry state identical to that of the mass measurements during sample-tube preparation.

Table 15. Materials used for the D-glucopyranose-like model-compound set.

Reactant	Manufacturer	Purity	Product	Lot Number
D-Allose	Aldrich	98%	285005-100MG	09405CJ
D-Altrose	Sigma	>97.0% HPLC	63963 50 mg 2178704	1349650 14907244
D-Arabinose	Sigma	≥98%	A3131-25G	100M1365V
L-Arabinose	Sigma	99%	A3256-25G	098K0164
D-Cellobiose	Sigma	≥98%	C7252-25G	SLBB6804V
Cellulose	Aldrich	“Cotton linters, microcrystalline 20µm”	310697-50G	MKBB6521V
2-Deoxy-D-Glucose	Sigma	“Grade II”	D-8375	40H0478
6-Deoxy-L-Galactose (“L-(-)-Fucose”)	Sigma	≥99%	F2252-5G	SLBB1522V
D-Fructose	Sigma	≥99%	F0127-100G	110M0185V
D-Galactose	Acros	99+%	15061-5000	N/A
D-Glucose	Sigma	≥99.5%	G8270-100G	080M0182V
D-Glucitol “D-Sorbitol”	Aldrich	99%	240850-5G	MKBM0921
D-Mannose	Acros	99+%	150600250	N/A
D-Mannitol	Sigma-Aldrich		M9647-250G	
D-(-)-Tagatose	Sigma	99%	T2751-1G	025K1150
D-(+)-Trehalose Dihydrate	Sigma	“Reduced metal- ion content”	T9531-25G	047K7350
D-Xylose	Acros	99+%	141001000	A0264898
Xylan (from beechwood)	Sigma	N/A	X4252-100G	BCBH7762V

#### 5.4.2. Pyrolysis reactors

The majority of the results were mass-loss and heat-flow data obtained by the TGA/DSC. These data are to show the temperature dependency of two criteria used for detecting some reactions during pyrolysis: Mass-loss data show the formation of volatile products, and heat-flow data show the consumption or generation of heat. Temperature ramp rates of 50°C min<sup>-1</sup> were used for all materials. Initial sample masses of 4 to 6 mg were used. These parameters were chosen to be very similar to the “round-robin” study on cellulose thermogravimetry described by Grønli et al. [20], whose parameters were selected for high precision with intrinsic mass-loss kinetics among several laboratories.

The Pyroprobe® was also used to determine the temperature-dependency of products formed by some of the D-glucose-like model compounds. GC separations were necessary to form a sharper peak than what was possible with GCxGC separations, as discussed in Section 3.6.7.

Regardless of whether a GC or GCxGC separation was used, the analyte identifications recommended by the mass-spectral-matching algorithm should be used with caution among the larger furanose and pyranose molecules. The accuracy of these “library hits” were questionable because of their poor repeatability in identification and residence time. In addition, the similarity values were rarely above 800 for these larger analytes, and 800 is often seen as a threshold for a strong spectral match. They were also questionable due to the likelihood of mass spectra to be very similar when slight but vital structural differences are present. A particularly important example was the spectral library’s suggestions for levoglucosan when other 1,6-anhydropyranoses were expected, such as 1,6-anhydro- $\beta$ -galactopyranose from D-galactose pyrolysis or 1,6-anhydro- $\beta$ -mannopyranose from D-mannose pyrolysis.

## **5.5. Results**

### **5.5.1. Results for D-aldohexoses – effect of stereochemistry**

Five of eight possible D-aldohexoses were tested, which were D-glucose, D-galactose, D-mannose, D-allose, and D-altrose. Each of these D-aldohexoses produced thermograms with two distinct stages of mass loss, as shown in Figures 69 through 73. Comparing their curves in a succinct manner proved difficult, and currently the best method is by comparing the temperatures and reaction rates corresponding to the maximums of the two stages, as well as the minimum between stages. Tables 16 and 17 show this summarizing data, and interestingly, D-glucose produced an extreme value in each of these comparisons.

- D-Glucose has its first-stage maximum, mid-stage minimum, and second-stage maximum at the highest temperature of all of the D-aldohexoses.
- D-Glucose has the highest mass-loss rate during its first-stage maximum and mid-stage minimum.
- D-Glucose has the lowest mass-loss rate during its second-stage maximum.

These results are interesting because D-glucose is the only D-aldohexose to have all of its hydroxyl groups in an equatorial position when in the pyranose  ${}^4C_1$  conformation.

Table 16. Summary of mass-loss character for five D-aldohexoses pyrolyzed at 50°C min<sup>-1</sup>.

D-Aldohexose	Mean Residual Char at ~480°C (% Initial Mass)	Mean Melting Temperature (°C)	Mean Temperature of First-Stage Maximum (°C)	Mean Temperature of Mid-Stage Minimum (°C)	Mean Temperature of Second-Stage Maximum (°C)
D-Allose*	18.6	159.3	252.0	277.2	317.9
D-Altrose	17.3 ± 0.7	135.8 ± 0.3	258.6 ± 1.4	275.9 ± 0.1	331.6 ± 0.4
D-Galactose	19.6 ± 0.9	183.9 ± 1.0	249.6 ± 0.8	282.1 ± 0.6	332.6 ± 1.2
D-Glucose	20.2 ± 0.6	175.3 ± 0.3	264.1 ± 1.3	289.0 ± 0.3	335.4 ± 0.8
D-Mannose**	22.9 ± 2.9	153.9 ± 0.7	248.7 ± 5.6	267.9 ± 3.6	310.9 ± 7.6

\* Only one test was possible with D-allose due to its cost.

\*\* Only two tests were considered for D-mannose due to poor reproducibility of the third test.

Table 17. Summary of mass-loss rates for five D-aldohexoses pyrolyzed at 50°C min<sup>-1</sup>.

D-Aldohexose	Mean First-Stage-Maximum Reaction Rate (% min <sup>-1</sup> )	Mean Mid-Stage-Minimum Reaction Rate (% min <sup>-1</sup> )	Mean Second-Stage-Maximum Reaction Rate (% min <sup>-1</sup> )
D-Allose*	19.7	18.7	59.1
D-Altrose	18.3 ± 0.7	17.8 ± 0.8	58.0 ± 3.0
D-Galactose	20.3 ± 0.6	13.0 ± 0.4	60.8 ± 2.0
D-Glucose	23.9 ± 1.6	20.0 ± 1.2	44.3 ± 1.3
D-Mannose**	19.3 ± 0.4	17.9 ± 1.6	50.6 ± 3.1

\* Only one test was possible with D-allose due to its cost.

\*\* Only two tests were considered for D-mannose due to poor reproducibility of the third test.

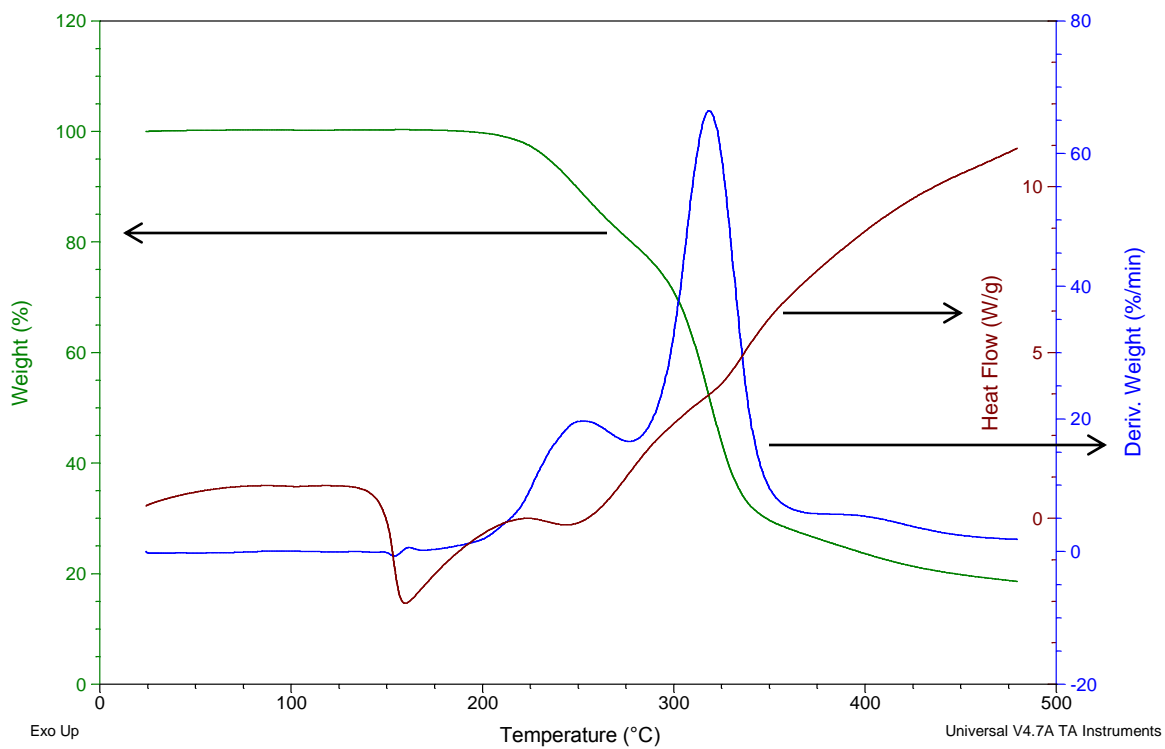


Figure 69. Pyrolysis of D-allose at 50°C min<sup>-1</sup>.

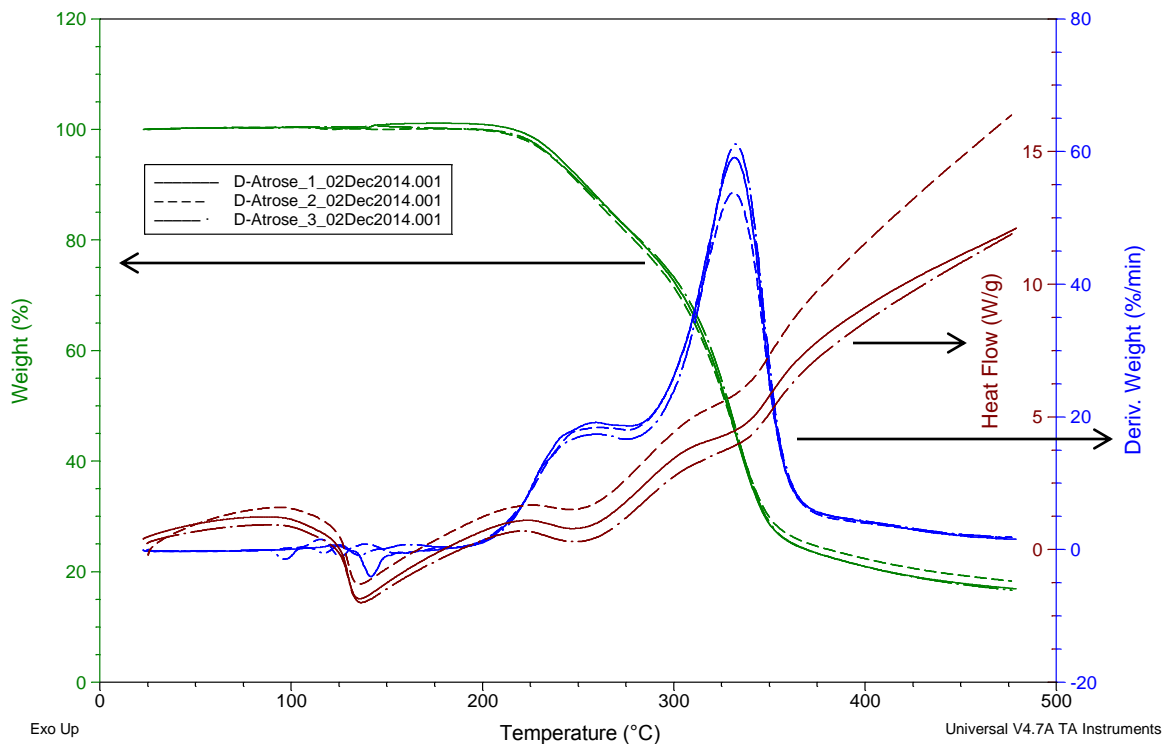


Figure 70. The comparison of three pyrolyses of D-altrose at  $50^{\circ}\text{C min}^{-1}$  shows the mass-loss behavior is very repeatable.

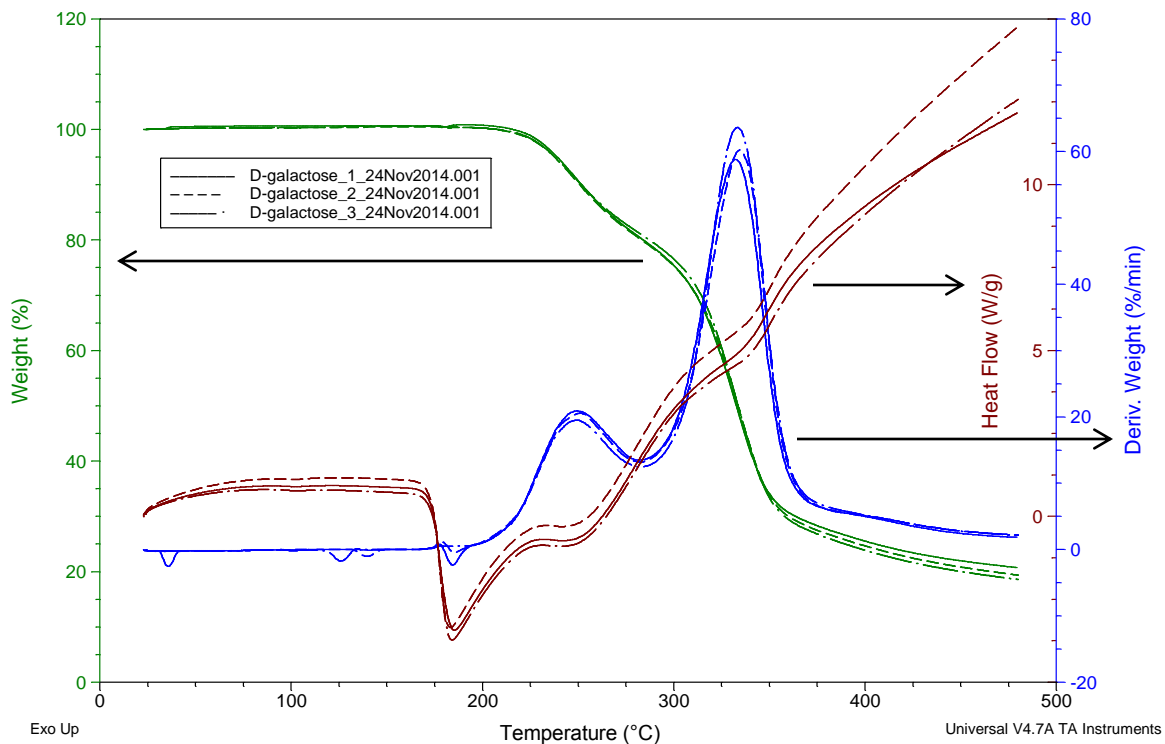


Figure 71. The comparison of three pyrolyses of D-galactose at  $50^{\circ}\text{C min}^{-1}$  shows the mass-loss behavior is very repeatable.

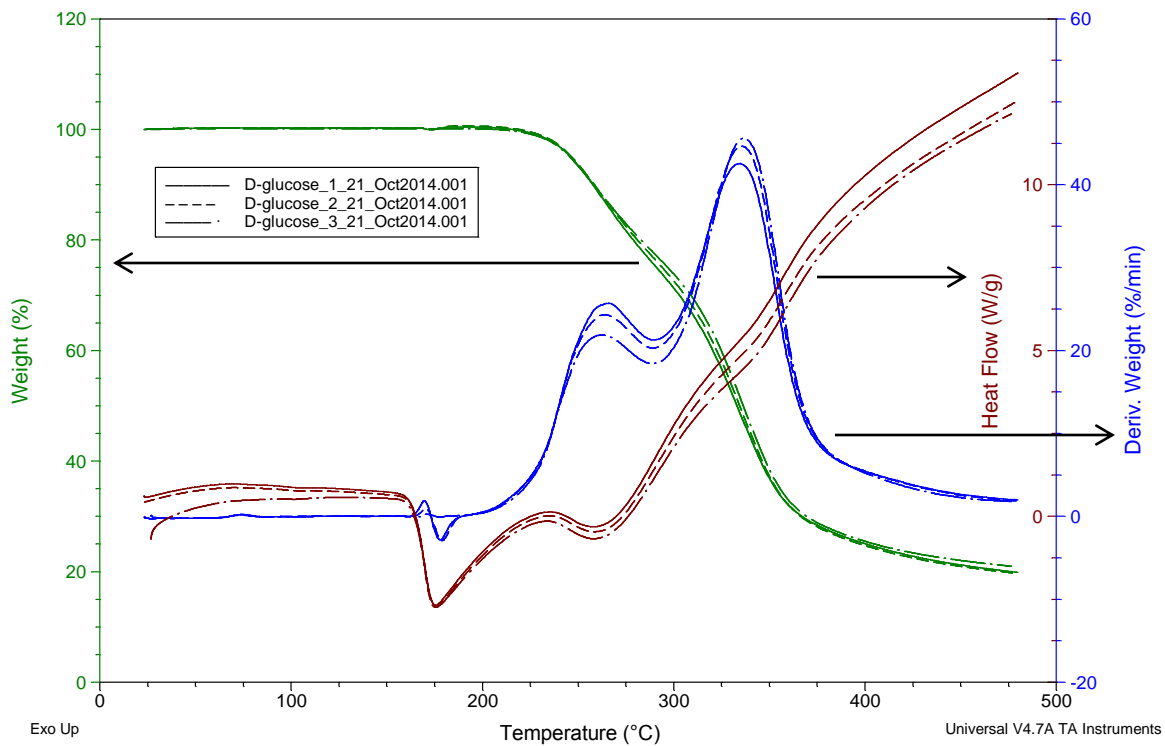


Figure 72. The comparison of three pyrolyses of D-glucose at  $50^{\circ}\text{C min}^{-1}$  shows the mass-loss behavior is very repeatable.

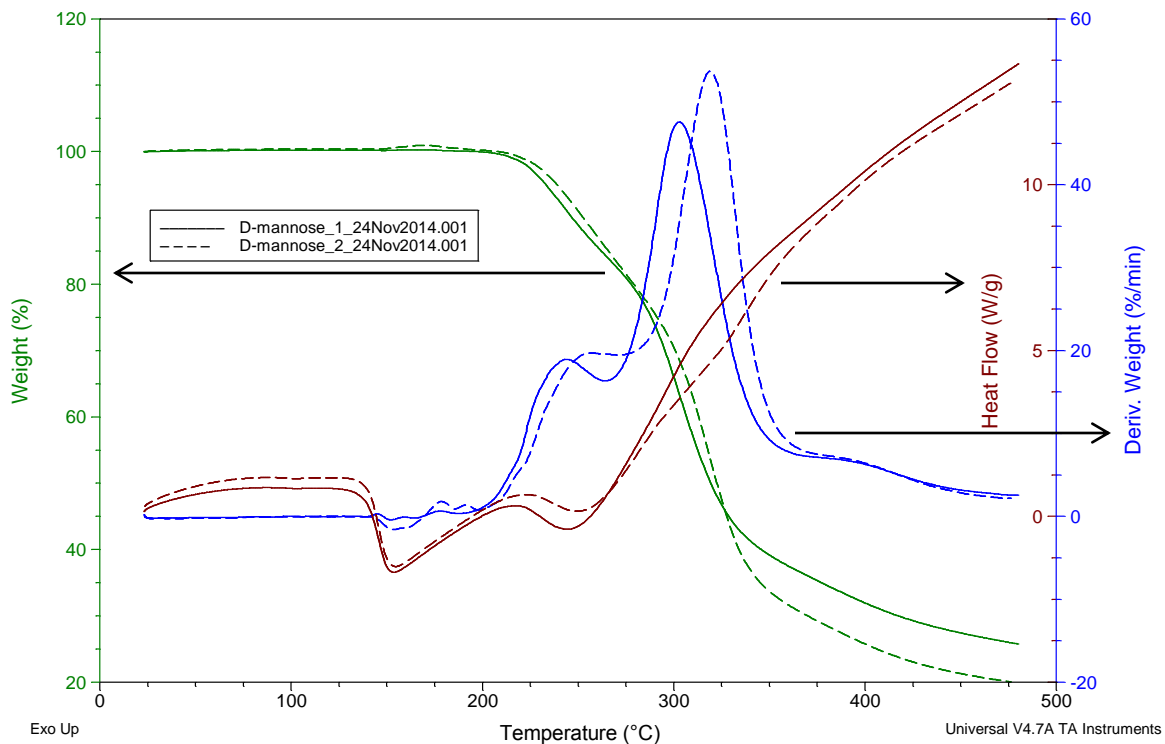


Figure 73. The comparison of two pyrolyses of D-mannose at  $50^{\circ}\text{C min}^{-1}$  shows that this D-aldohexoses is somewhat less repeatable than the others.

### 5.5.2. Results for D-alditols

D-Glucitol and D-mannitol both pyrolyzed in the TGA/DSC with a single mass-loss stage.

Table 18 summarizes their mass-loss character, and Figures 74 and 75 show their specific mass-loss behaviors. Interestingly, they differed in three ways from most other saccharide materials.

- They had a single stage of mass loss,
- They left no visible char in the sample pan,
- They had a high onset temperature of reaction and very high maximum rates of reaction.

Table 18. Summary of mass-loss and heat-flow character for D-aldohexoses pyrolyzed at  $50^{\circ}\text{C min}^{-1}$ .

D-Alditol	Residual Char at ~480°C (%)	Melting Temperature (°C)	Mean Temperature of Maximum Reaction Rate (°C)	Mean Maximum Reaction Rate (% min <sup>-1</sup> )
D-Glucitol	1.30 ± 0.6	109.1 ± 0.6	393.6 ± 0.8	108.5 ± 0.9
D-Mannitol	1.11 ± 0.8	173.7 ± 0.1	393.64 ± 1.3	111.4 ± 2.7

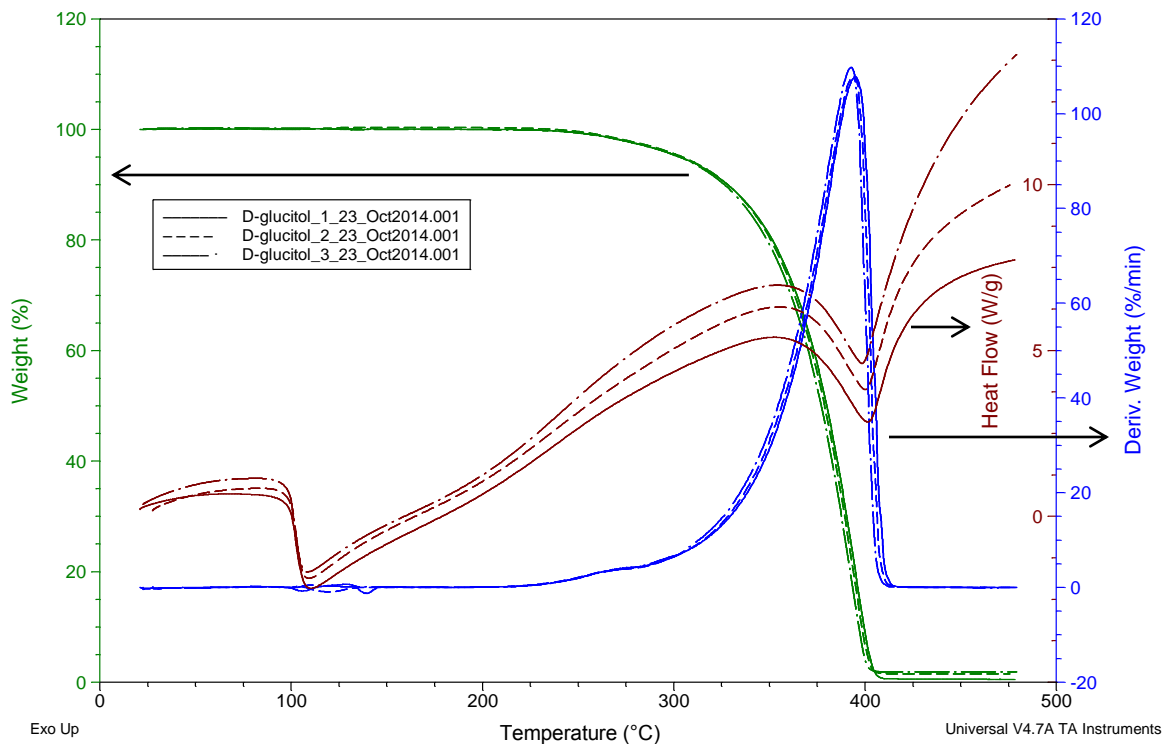


Figure 74. The comparison of three pyrolyses of D-glucitol at  $50^{\circ}\text{C min}^{-1}$  show a repeatable mass-loss and heat-flow behavior.

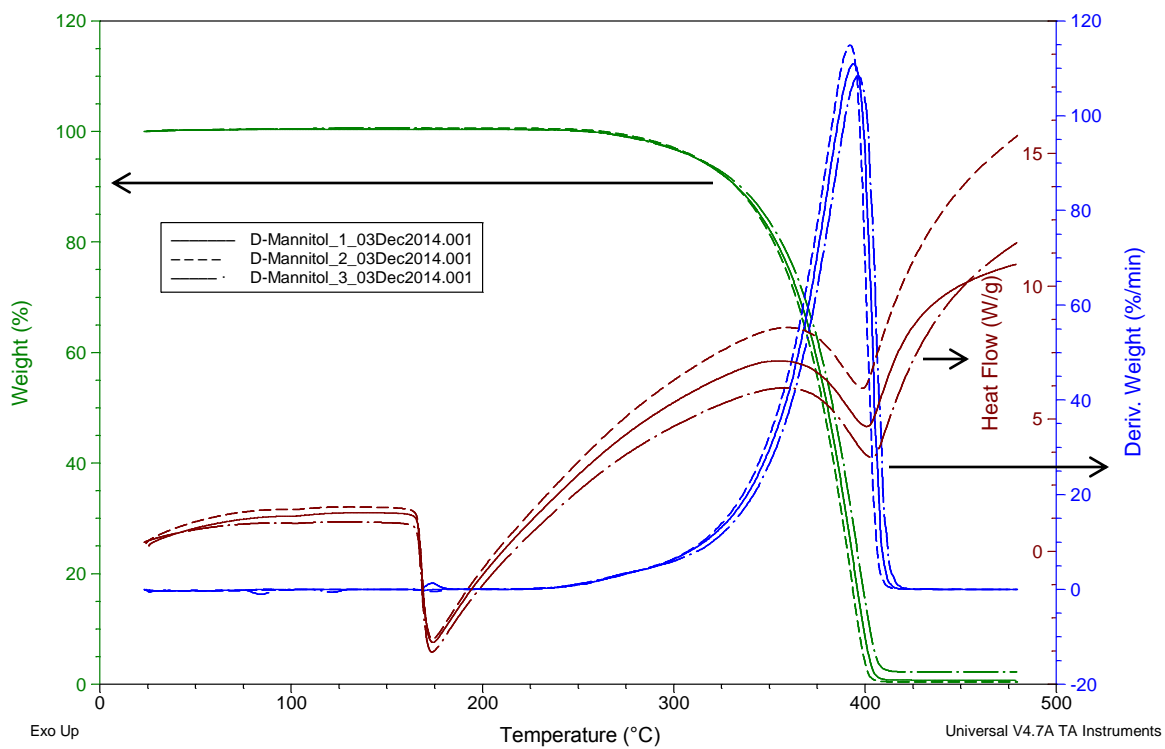


Figure 75. The comparison of three pyrolyses of D-mannitol at  $50^{\circ}\text{C min}^{-1}$  show a repeatable mass-loss and heat-flow behavior.

Interestingly, both D-glucitol and D-mannitol produced small yields for levoglucosan during Pyroprobe®/GC-MS experiments. Their similarity values for levoglucosan identifications were 769 and 775 for D-glucitol and D-mannitol, respectively. These similarity values are relatively low, but very polar, late-eluting compounds often produce poor similarity values.

### 5.5.3. Results for deoxy-D-aldohexoses

The two deoxy-D-aldohexoses, 2-deoxy-D-glucose and 6-deoxy-L-galactose (“L-fucose”) also both produced thermograms with two distinct stages of mass loss, as shown in Figures Figure 76 and Figure 77. Their mass-loss behaviors are listed in Tables 19 and 20.

Table 19. Summary of mass-loss character for deoxy-D-aldohexoses pyrolyzed at 50°C min<sup>-1</sup>.

Deoxy-D-Aldohexose	Mean Residual Char at ~480°C (% Initial Mass)	Mean Melting Temperature (°C)	Mean Temperature of First-Stage Maximum (°C)	Mean Temperature of Mid-Stage Minimum (°C)	Mean Temperature of Second-Stage Maximum (°C)
2-Deoxy-D-Glucose	6.20 ± 1.0	172.1 ± 1.1	247.1 ± 1.3	262.7 ± 0.3	306.0 ± 0.3
6-Deoxy-L-Galactose	4.82 ± 0.1	170.5 ± 0.4	261.3 ± 0.4	283.5 ± 1.8	339.5 ± 0.2

Table 20. Summary of mass-loss rates for deoxy-D-aldohexoses pyrolyzed at 50°C min<sup>-1</sup>.

Deoxy-D-Aldohexose	Mean First-Stage-Maximum Reaction Rate (% min <sup>-1</sup> )	Mean Mid-Stage-Minimum Reaction Rate (% min <sup>-1</sup> )	Mean Second-Stage-Maximum Reaction Rate (% min <sup>-1</sup> )
2-Deoxy-D-Glucose	32.9 ± 0.4	31.7 ± 0.3	59.7 ± 0.7
6-Deoxy-L-Galactose	30.0 ± 0.4	24.5 ± 0.7	61.3 ± 0.2

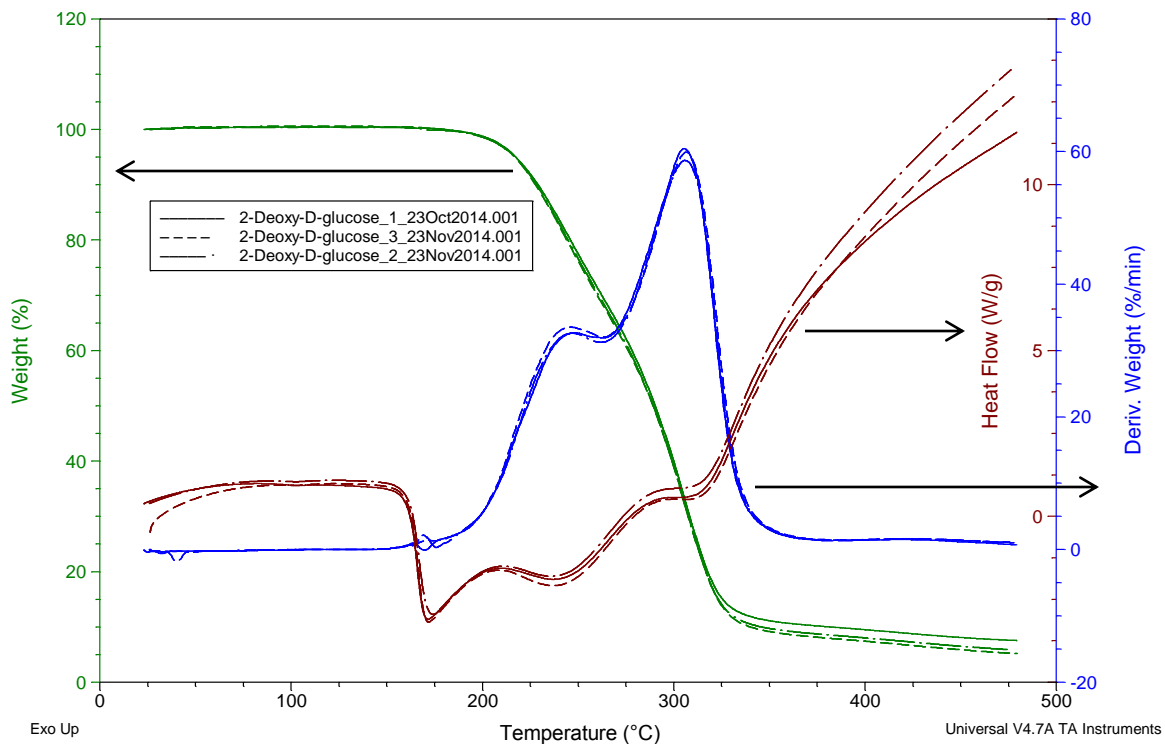


Figure 76. The comparison of three pyrolyses of 2-deoxy-D-glucose at  $50^{\circ}\text{C min}^{-1}$ .

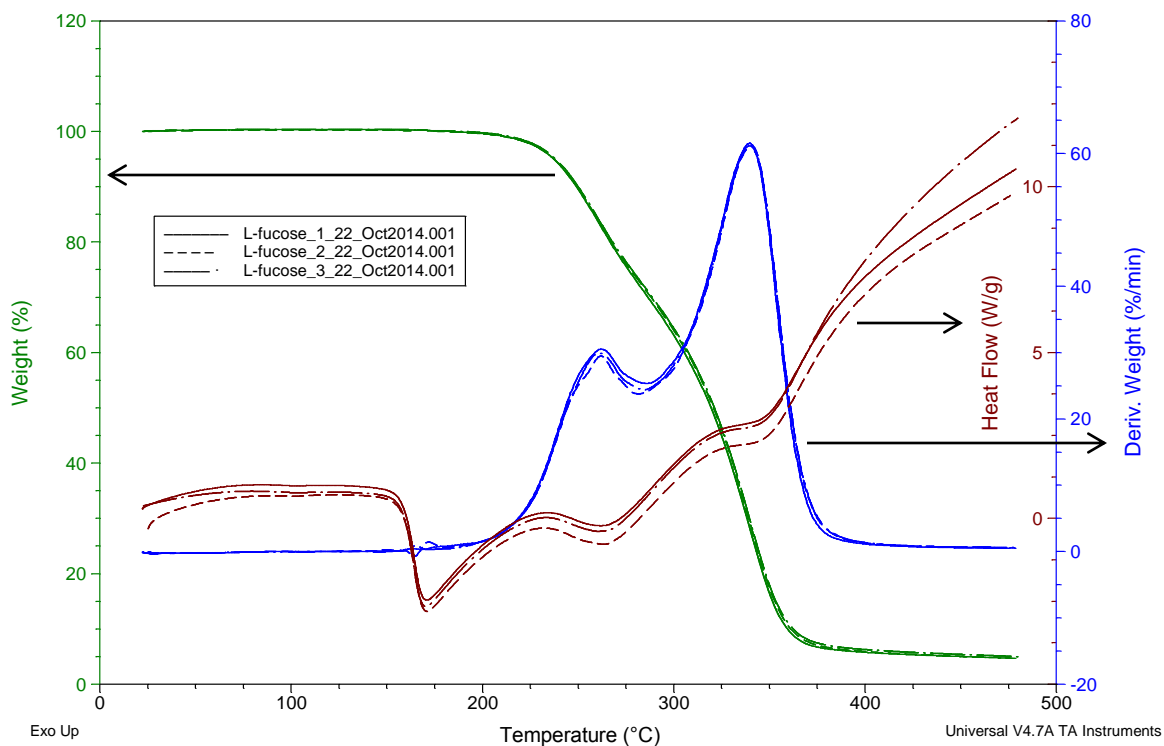


Figure 77. Three pyrolyses of three 6-deoxy-L-galactose (also known as “L-fucose”) is uniform at  $50^{\circ}\text{C min}^{-1}$ .

#### 5.5.4. Results for D-aldopentoses and L-aldopentose

Tables 21 and 22 outline the mass-loss characteristics of the two D-aldopentoses and an L-aldopentose. As seen in Figures 78 and 79, these aldopentoses also exhibit the two stages of mass loss, seen with the two well-separated peaks in their mass-vs.-temperature derivatives.

Table 21. Summary of mass-loss character for three D-aldopentoses pyrolyzed at 50°C min<sup>-1</sup>.

D-Aldopentose	Mean Residual Char at ~480°C (% Initial Mass)	Mean Melting Temperature (°C)	Mean Temperature of First-Stage Maximum (°C)	Mean Temperature of Mid-Stage Minimum (°C)	Mean Temperature of Second-Stage Maximum (°C)
D-Arabinose	21.6 ± 0.7	173.9 ± 0.5	244.9 ± 0.5	284.2 ± 2.1	333.8 ± 0.2
L-Arabinose	19.3 ± 0.5	176.7 ± 0.3	251.0 ± 0.7	286.8 ± 0.1	334.8 ± 0.8
D-Xylose	19.1 ± 0.9	171.0 ± 0.2	257.2 ± 3.8	287.4 ± 0.4	327.7 ± 1.7

Table 22. Summary of mass-loss rates for three D-aldopentoses pyrolyzed at 50°C min<sup>-1</sup>.

D-Aldopentose	Mean First-Stage-Maximum Reaction Rate (% min <sup>-1</sup> )	Mean Mid-Stage-Minimum Reaction Rate (% min <sup>-1</sup> )	Mean Second-Stage-Maximum Reaction Rate (% min <sup>-1</sup> )
D-Arabinose	22.4 ± 1.1	10.8 ± 2.8	60.1 ± 1.4
L-Arabinose	22.6 ± 0.3	14.1 ± 0.3	58.4 ± 2.5
D-Xylose	25.9 ± 2.0	20.9 ± 1.1	44.3 ± 1.7

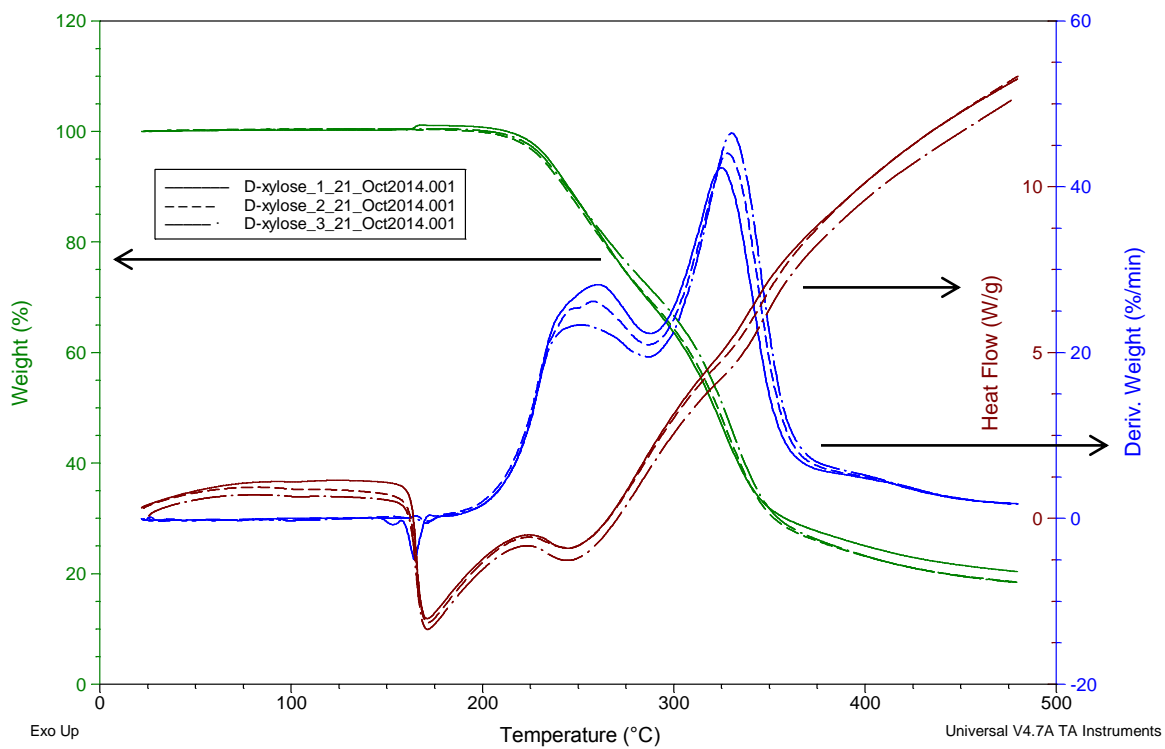


Figure 78. The comparison of three identical pyrolyses of D-xylose at  $50^{\circ}\text{C min}^{-1}$ .

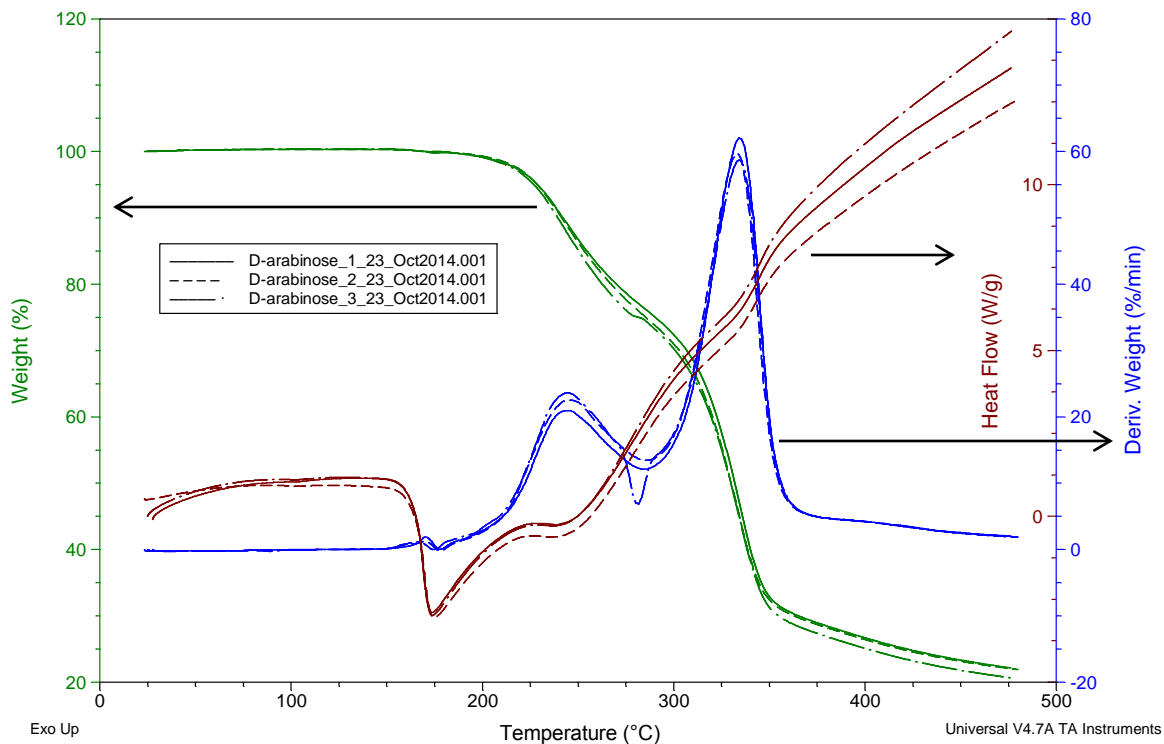


Figure 79. The comparison of three identical pyrolyses of D-arabinose at  $50^{\circ}\text{C min}^{-1}$ .

Pyroprobe®-GC-MS experiments showed that D-xylose formed very little levoglucosan (1,6-anhydro- $\beta$ -D-glucopyranose), although like D-glucitol and D-mannitol, the sample-to-library similarity number of 798 indicates uncertainty.

### 5.5.5. Results for D-ketohexoses

Tables 23 and 24 display the mass-loss behaviors of the two D-ketohexoses; D-fructose and D-tagatose. Their thermograms are displayed in Figures 80 and 81. Interestingly, neither of these D-ketoses had two well-separated stages of mass loss. D-fructose produced only a plateau in its derivative of mass-vs.-temperature function, where the D-aldohexoses and deoxysugars had produced very clear first-stage maximums. Meanwhile, D-tagatose did not even produce a clear plateau in its mass-vs.-temperature function during its first stage of mass loss. However, both D-fructose and D-tagatose obviously have some

temperature dependence of their mass-loss rates, as neither produced ideal exponential curves in their mass-vs.-temperature derivatives.

Table 23. Summary of mass-loss character for D-ketoses pyrolyzed at 50°C min<sup>-1</sup>.

D-Ketohexose	Mean Residual Char at ~480°C (% Initial Mass)	Mean Melting Temperature (°C)	Mean Temperature of First-Stage Maximum (°C)	Mean Temperature of Mid-Stage Minimum (°C)	Mean Temperature of Second-Stage Maximum (°C)
D-Fructose	21.7 ± 0.7	146.4 ± 0.8	214.5 ± 0.8	234.3 ± 3.7	296.7 ± 1.0
D-Tagatose	25.3 ± 1.5	155.1 ± 0.5	209.1*	213.8*	27.9 ± 1.0

\* D-Tagatose only had a clear first-stage maximum and mid-stage minimum for one of its three experiments.

Table 24. Summary of mass-loss rates for D-ketoses pyrolyzed at 50°C min<sup>-1</sup>.

D-Ketohexose	Mean First-Stage-Maximum Reaction Rate (% min <sup>-1</sup> )	Mean Mid-Stage-Minimum Reaction Rate (% min <sup>-1</sup> )	Mean Second-Stage-Maximum Reaction Rate (% min <sup>-1</sup> )
D-Fructose	12.1 ± 0.2	11.4 ± 0.1	52.9 ± 1.6
D-Tagatose	11.7*	11.4*	33.4 ± 0.4

\* D-Tagatose only had a clear first-stage maximum and mid-stage minimum for one of its three experiments.

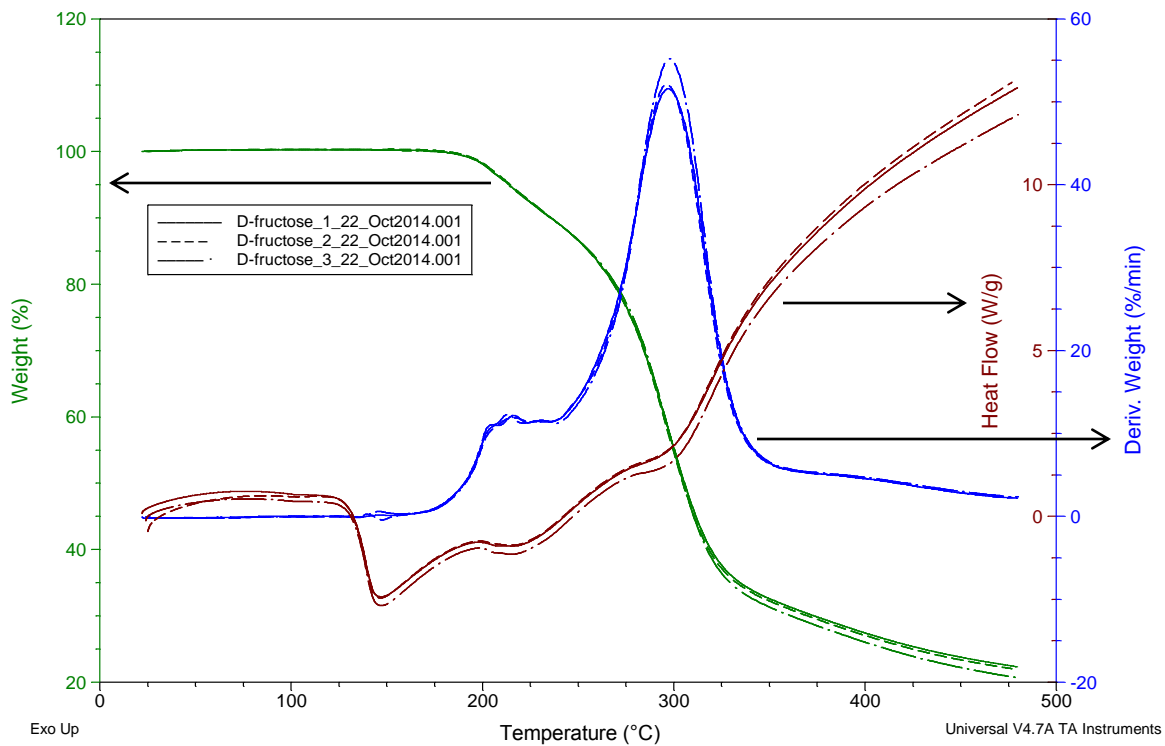


Figure 80. The comparison of three pyrolyses of D-fructose at  $50^{\circ}\text{C min}^{-1}$ .

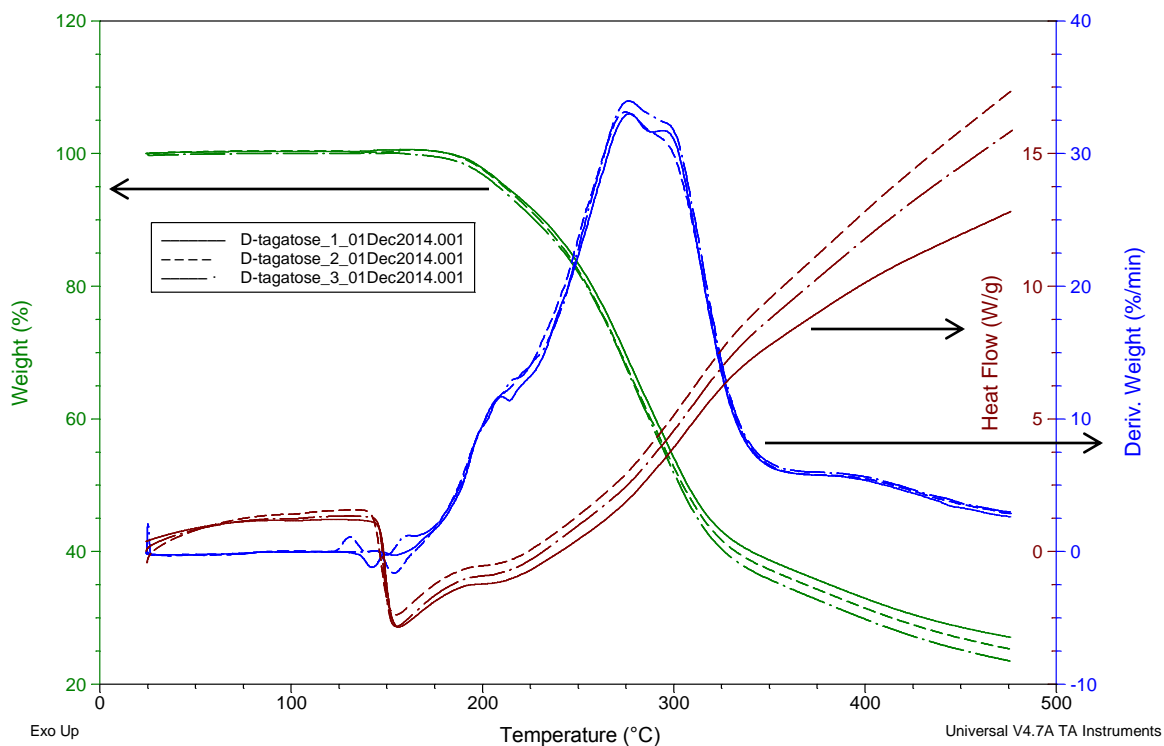


Figure 81. The comparison of three pyrolyses of D-tagatose at  $50^{\circ}\text{C min}^{-1}$ .

### 5.5.6. Results for dimers of D-glucose

D-cellobiose and D-trehalose dihydrate produced very different thermograms, as displayed in Figures 82 and 83. D-cellobiose produced two maximums in its mass-loss rate, but D-trehalose dihydrate produced only one maximum. Note that the mass-loss maximums considered here are “reactive mass losses,” which exclude the loss of the two hydrated water molecules at roughly 102 and 136°C for D-trehalose dihydrate.

Table 25. Summary of mass-loss character for D-glucose dimers pyrolyzed at 50°C min<sup>-1</sup>.

D-Glucose Dimer	Mean Residual Char at ~480°C (% Initial Mass)	Mean Melting Temperature (°C)	Mean Temperature of First-Stage Maximum (°C)	Mean Temperature of Mid-Stage Minimum (°C)	Mean Temperature of Second-Stage Maximum (°C)
D-Cellobiose	17.2 ± 0.4	259.0 ± 1.1	287.2 ± 0.5	302.5 ± 0.7	337.9 ± 0.3
D-Trehalose	12.1 ± 0.5	215.6 ± 0.5	347.7 ± 0.4	N/A	N/A

Table 26. Summary of mass-loss rates for D-glucose dimers pyrolyzed at 50°C min<sup>-1</sup>.

D-Glucose Dimer	Mean First-Stage-Maximum Reaction Rate (% min <sup>-1</sup> )	Mean Mid-Stage-Minimum Reaction Rate (% min <sup>-1</sup> )	Mean Second-Stage-Maximum Reaction Rate (% min <sup>-1</sup> )
D-Cellobiose	30.5 ± 2.2	27.7 ± 1.5	62.7 ± 3.0
D-Trehalose	76.0 ± 2.3	N/A	N/A

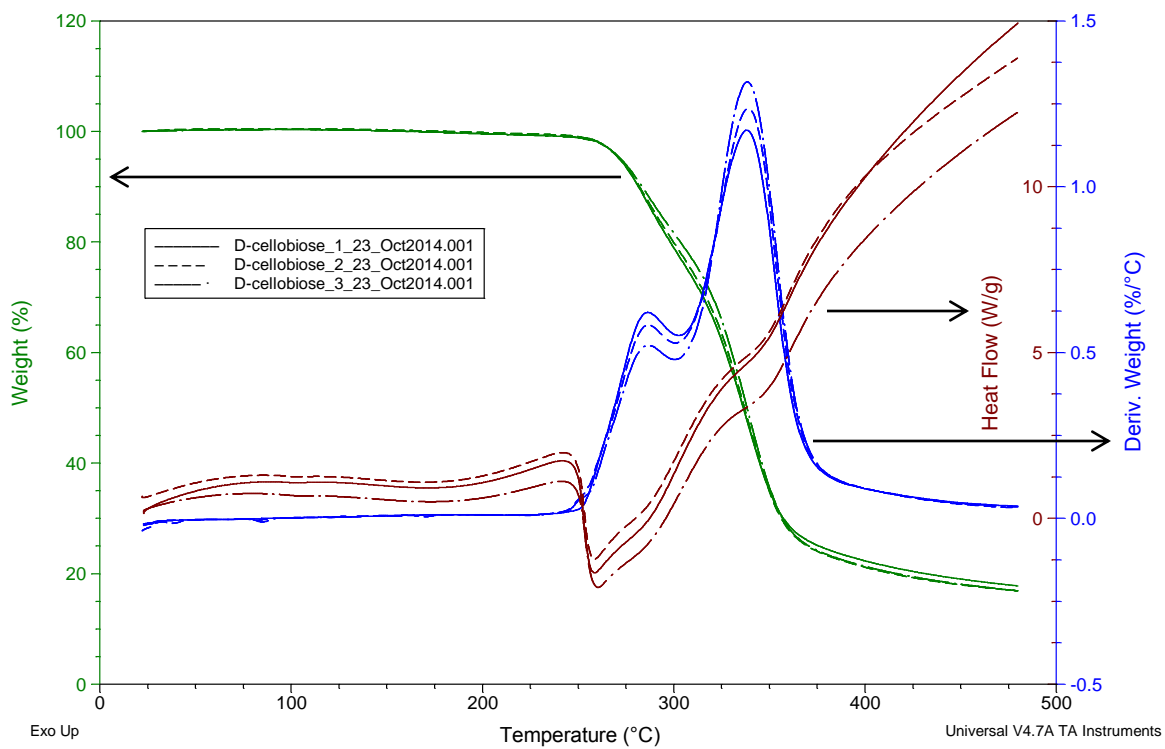


Figure 82. The comparison of three pyrolyses of D-cellobiose at  $50^{\circ}\text{C min}^{-1}$ .

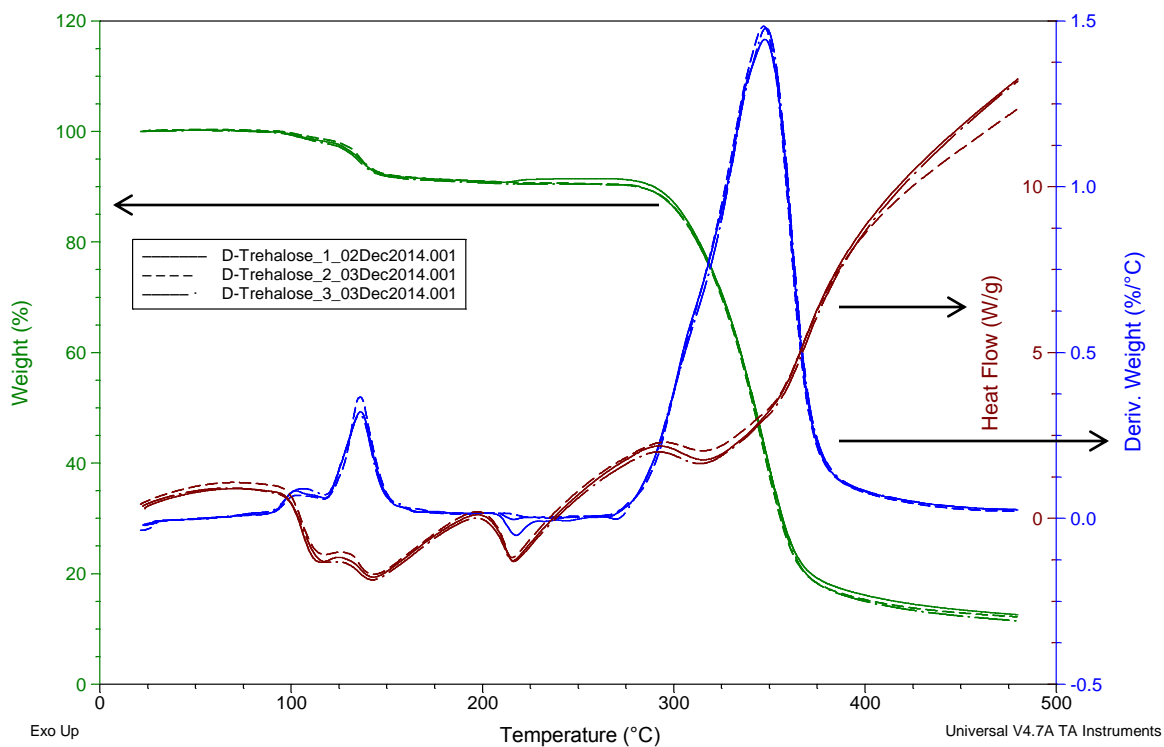


Figure 83. The comparison of three pyrolyses of D-trehalose dihydrate at  $50^{\circ}\text{C min}^{-1}$ .

### 5.5.7. Results for pyranose-based polymers

Cellulose produced only one stage of mass loss, but xylan produced two stages of mass loss, as shown in Figures 84 and 85, and Tables 27 and 28. Strikingly, cellulose required a much higher temperature than xylan to reach both its onset and its maximum mass-loss rate. Also striking is the large difference in rates of mass loss and the mass of char remaining after the experiment.

Table 27. Summary of mass-loss character for the two pyranose-based polymers cellulose and xylan.

Polymer	Mean Residual Char at ~480°C (% Initial Mass)	Mean Melting Temperature (°C)	Mean Temperature of First-Stage Maximum (°C)	Mean Temperature of Mid-Stage Minimum (°C)	Mean Temperature of Second-Stage Maximum (°C)
Cellulose	7.0 ± 1.1	N/A	363.2 ± 5.9	N/A	N/A
Xylan*	31.73	N/A	242.2	258.7	294.8

\* Only one test was possible with xylan due to its availability.

Table 28. Summary of mass-loss rates for the two pyranose-based polymers cellulose and xylan.

Polymer	Mean First-Stage-Maximum Reaction Rate (% min <sup>-1</sup> )	Mean Mid-Stage-Minimum Reaction Rate (% min <sup>-1</sup> )	Mean Second-Stage-Maximum Reaction Rate (% min <sup>-1</sup> )
Cellulose	101.9 ± 4.5	N/A	N/A
Xylan*	5.3	4.4	5.9

\* Only one test was possible with xylan due to its availability.

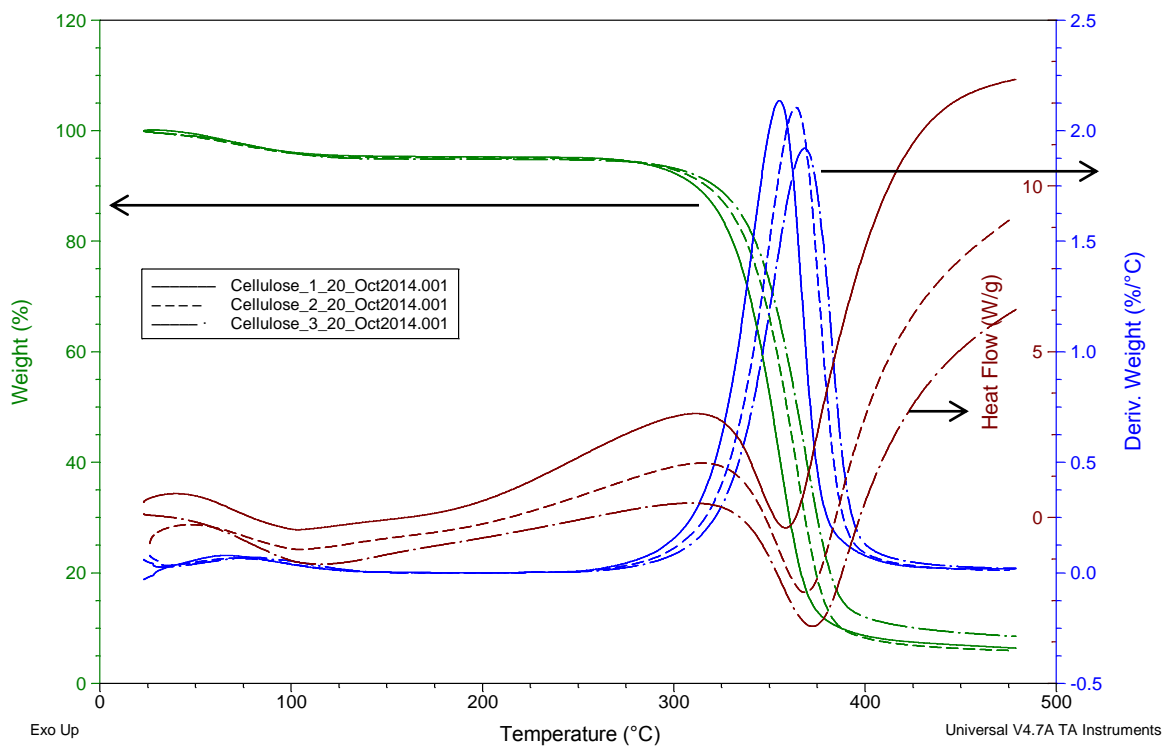


Figure 84. The comparison of three pyrolyses of cellulose at  $50^{\circ}\text{C min}^{-1}$ .

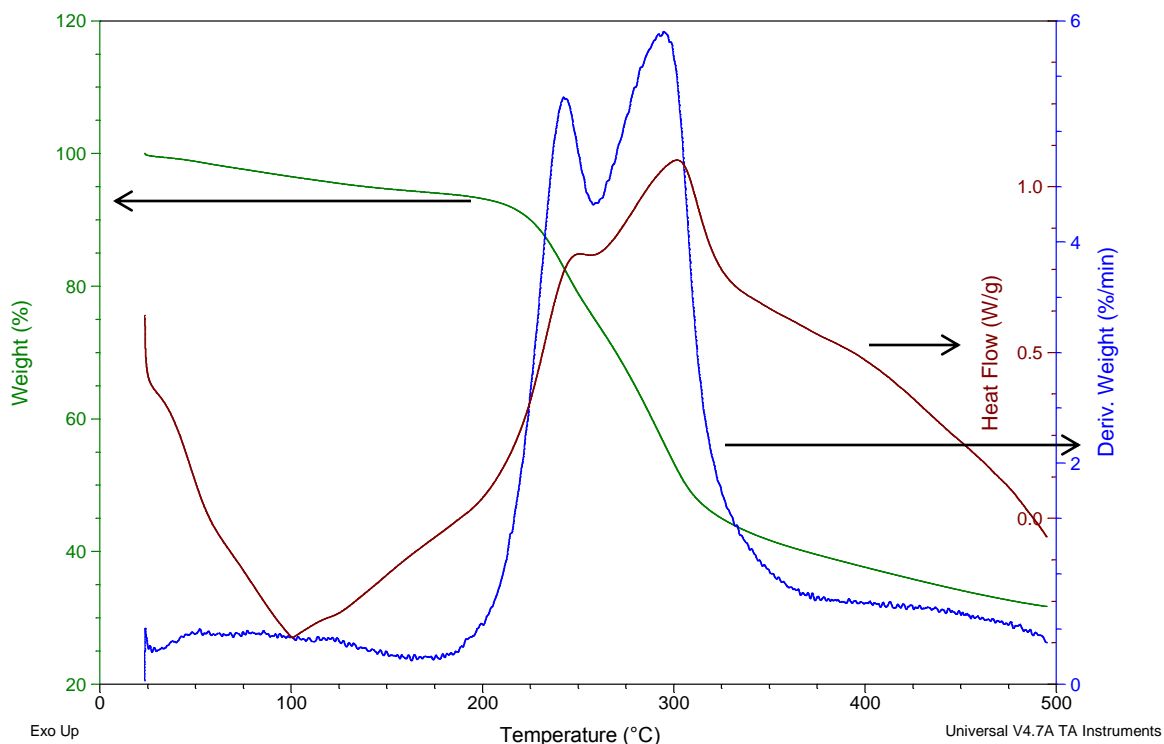


Figure 85. The pyrolysis of xylan at  $50^{\circ}\text{C min}^{-1}$ .

## 5.6. Discussion

### 5.6.1. Understanding differences between mass-loss behavior of D-glucopyranose's D-aldohexose stereoisomers

Pyrolyzing different D-aldohexoses was expected to deconvolute the expected concerted-cyclic-1,2-dehydration and the cyclic-Grob-fragmentation mechanisms from the 1,6-bicyclic forming reaction mechanism(s). This expected ability to deconvolute the reaction mechanisms is due to the D-aldohexoses having identical stereochemistry at carbon 5 and different stereochemical arrangements at carbons 2, 3, and 4. By definition, D-aldohexoses have identical stereochemistry at carbon 5, and this stereochemical arrangement is vital for placing carbon 6 in close proximity to carbon 1 for a 1,6-bicyclic-forming reactions when in pyranose form. If this 1,6-bicyclic-forming dehydration is possible among

all of the D-aldohexoses, then the effect of different stereochemical arrangements on carbons 2, 3, and 4 can be evaluated on how they affect other anticipated reactions like concerted 1,2-dehydrations and cyclic Grob fragmentations. This potential isolation is something no reactor experiments can do effectively with varying conditions (e.g., temperature, temperature ramp rate) on a single material (e.g., D-glucose or cellulose).

One way to state the stereochemical differences between the D-aldohexoses and D-aldopentoses is their different sets of dihedral angles relating adjacent pairs of hydroxyl groups and hydrogen atoms. These dihedral angles are important because 1,2-dehydrations and cyclic Grob fragmentations likely depend upon adjacent hydroxyl groups and hydrogen atoms existing in preferable geometries. The available set of dihedral angles depends upon three ways in which an aldohexose or aldopentose structure may vary.

- The specific aldohexose/aldopentose's identity (e.g., D-glucose vs. D-galactose)
- The structural isomer of the specific aldohexose/aldopentose (i.e., acyclic vs.  $\alpha$ -pyranose vs.  $\beta$ -pyranose vs.  $\alpha$ -furanose vs.  $\beta$ -furanose form)
- The conformation of the specific structural isomer of the specific aldohexose/aldopentose (e.g., chair vs. inverse chair vs. boat)

One can control the specific aldohexose/aldopentose chosen, but one cannot independently control the partitioning between structural isomers and conformations taken by the specific aldohexose or aldopentose. Attributing reactive differences among the chosen D-aldohexoses or D-aldopentoses based solely on their different stereochemistries requires knowing the structural partitioning in two vital categories.

- What fraction of each reactant molecule (e.g., D-glucose, D-galactose, etc.) is present in the acyclic,  $\alpha$ - and  $\beta$ -furanose, and  $\alpha$ - and  $\beta$ -pyranose forms?
- What fraction of each reactant molecule's structural forms (e.g.,  $\beta$ -D-glucopyranose,  $\beta$ -D-glucofuranose, etc) is present in the various possible conformations?

Without a way of measuring how an aldohexose or aldopentose partitions among five main isomers and their conformations, one must assume fraction values based upon some available data. Data was not found for saccharide materials in the conditions similar to pyrolysis: only data for these materials in solution was found. Tables 29 and 30 show how several aldohexoses and aldopentoses partition among their five possible isomers in when dissolved in a liquid phase.<sup>64</sup> Data for how the isomer partitioning changes with temperature, solvent type, or alternately substituted groups was much more scarce.

- Collins and Ferrier [55, p. 43] briefly mentioned the effect of temperature, stating that increasing temperature to 82°C increases the fraction of  $\alpha$  and  $\beta$  furanose isomers to 0.6% and 0.7%, respectively.
- Collins and Ferrier [55, p. 43] stated that replacing the hydroxyl group with a hydrogen atom at carbon 3 of glucose or carbon 2 of galactose increases the furanose isomer fraction of to 20 or 16% respectively, in D<sub>2</sub>O at equilibrium.
- Collins and Ferrier [55, p. 41] assembled the data (

---

<sup>64</sup> Note that the data in Tables 29 and 30 must contain some error because the sum of the percentage of each stereoisomer for a given compound is greater than 100% for all of the saccharides. The lack of an exact 100% total suggests all five isomers were truly measured, instead of measuring all but one isomer and assuming the unmeasured isomer is the balance to 100%.

- Table 31) for how methyl glycosides partition among furanoside and pyranoside forms. While replacing the anomeric carbon's hydroxyl group with a methoxy group is a significant change to the molecule, it offers some insight as to what aldopyranoses and aldofuranoses will do in methanol and perhaps in other protic organic solvents like larger alcohols.

Table 29. The equilibrium composition of saccharides in aqueous solution. (Recreated from Table 2.1 in Levy and Fügedi [58, p. 36]. The sum of the percentages was not present in the original Table 2.1.)

Saccharide	Pyranose Structural Isomer		Furanose Structural Isomer		Acyclic Structural Isomer (%)
	$\alpha$ -Anomer (%)	$\beta$ -Anomer (%)	$\alpha$ -Anomer (%)	$\beta$ -Anomer (%)	
Glucose	38.0	62.0	0.5	0.5	0.002
Mannose	65.6	34.5	0.6	0.3	0.005
Galactose	30.0	64.0	2.5	3.5	0.02
Rhamnose	65.5	34.5	0.6	0.3	0.005
Fructose	2.5	65.0	6.5	25.0	0.8
Xylose	36.5	63.0	0.3	0.3	0.002
Ribose	31.5	58.5	6.4	13.5	0.05

Table 30. The equilibrium composition of saccharides in aqueous solution. (Recreated from data in Table 2.4 in Collins and Ferrier [55, p. 41]. The sum of the percentages was not present in the original Table 2.4.)

Saccharide	Temperature (°C)	Pyranose Structural Isomer		Furanose Structural Isomer		Acyclic Structural Isomer (%)
		$\alpha$ -Anomer (%)	$\beta$ -Anomer (%)	$\alpha$ -Anomer (%)	$\beta$ -Anomer (%)	
Allose	31	14	77.5	3.5	5	0.01
Altrose	22	27	43	17	13	0.04
Glucose	31	38	62	-	0.14	0.02
Mannose	44	64.9	34.2	0.6	0.3	0.005
Galactose	31	30	64	2.5	3.5	0.02
Fructose	31	2.5	65	6.5	25	0.8
Tagatose	31	71	18	2.5	7.5	0.3
Arabinose	31	60	35.5	2.5	2	0.03
Xylose	31	36.5	63	< 1	< 1	0.02
Ribose	31	21.5	58.5	6.5	13.5	0.05

Table 31. Equilibrium composition of methyl glycoside mixtures in methanol at 35°C. (Recreated from data in Table 3.1 in Collins and Ferrier [55, p. 63].)

Saccharide	Pyranose Forms			Furanose Forms		
	$\alpha$ -Pyranoside (%)	$\beta$ -Pyranoside (%)	Total Pyranoside (%)	$\alpha$ -Furanoside (%)	$\beta$ -Furanoside (%)	Total Furanoside (%)
D-Ribose	12	66	78	5	17	22
D-Arabinose	24	47	71	22	7	29
D-Xylose	65	30	95	2	3	5
D-Glucose	66	32.5	98.5	0.6	0.9	1.5
D-Mannose	94	5.3	99.3	0.7	0	0.7
D-Galactose	58	20	78	6	16	22

Based upon Tables 29 and 30, a first approximation for the isomers present in the pyrolysis of D-aldohexoses would be to neglect the small contribution of furanose and very small contribution of acyclic isomers and use the pyranose forms to represent the molecules. (Tables 32 through 36 explicitly show these dihedral angles with Newman projections.) Such an approximation would be represented by the structures in Figure 86.

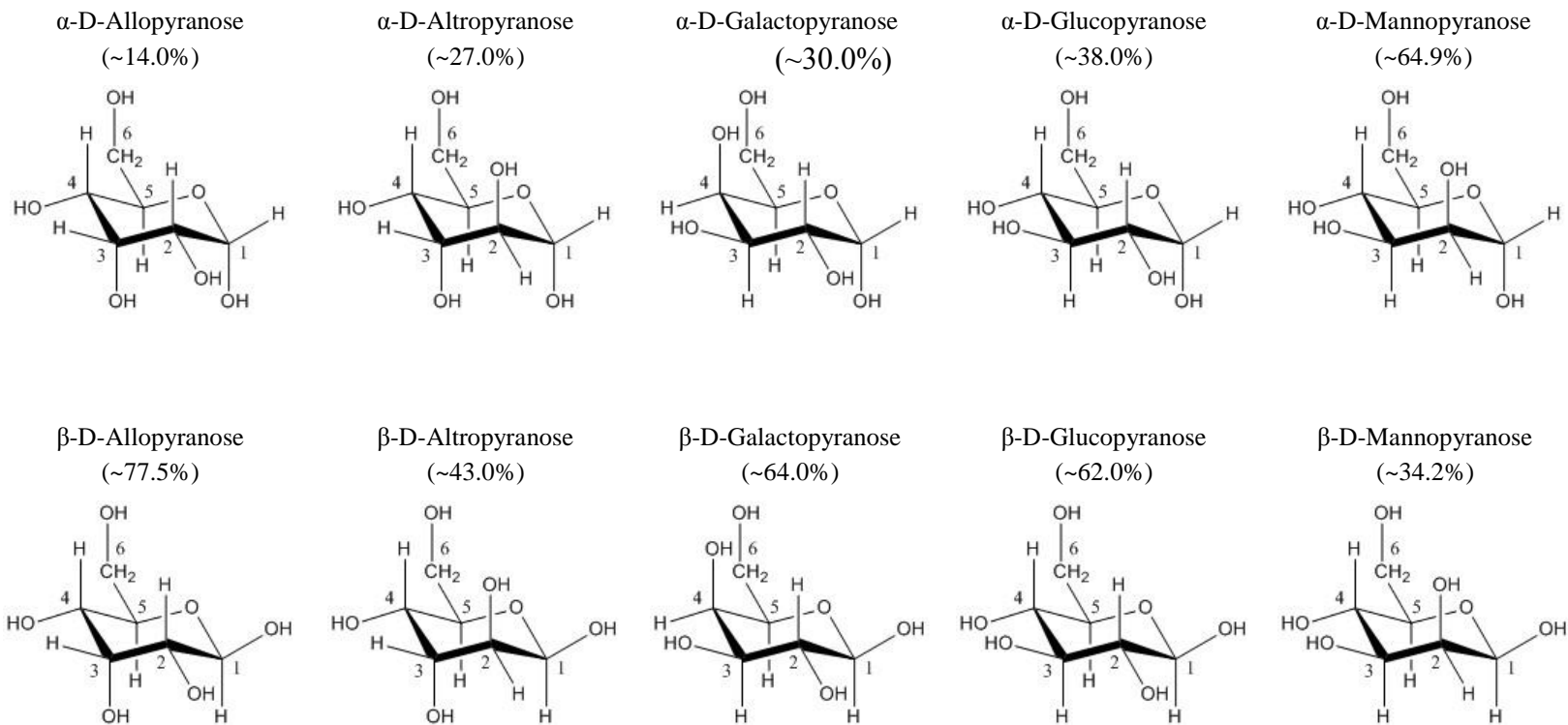


Figure 86. Reeves projections (in the  ${}^4C_1$  conformation) of the five D-aldopyranoses for structural comparison.

As stated, the partitioning among conformations of each isomeric form is also necessary to understand the dihedral angles relating the adjacent hydroxyl groups and hydrogen atoms within D-aldohexoses and D-aldopentoses. There at least 14 specific conformations possible with the pyranose ring, as reviewed by Shallenberger [56, pp. 124-128]; Note that only one of these pyranose conformations is shown in Figure 86.

- There are two chair conformations. The first is the  ${}^4C_1$ , which has the ring's ether oxygen above and carbon 3 below the plane made by carbons 1, 2, 4, and 5. The second is the  ${}^1C_4$ , which has the ring's ether oxygen below and carbon 3 above the plane made by carbons 1, 2, 4, and 5.
- There are six boat conformations, which are B1, 1B, B2, 2B, B3, and 3B.
- There are also six skewed-boat and half-chair conformations possible for pyranose rings.

Seshadri and Westmoreland [3] only considered three conformations of glucopyranose. These conformations were  ${}^4C_1$ ,  ${}^1C_4$ , and 3B, which they named the "chair," "inverse chair," and "boat," respectively. (They estimated rates for various furanoses, but they did not consider the different possible conformations of furanose rings.) While the conformations are well described, no data has been found for how the five structural isomers partition among their many possible conformations.

Tables 32 through 36 show Newman projections of the  $\alpha$ - and  $\beta$ -pyranose forms of D-allose, D-altrose, D-glucose, D-galactose, and D-mannose, respectively in their chair ( ${}^4C_1$ ), inverse-chair ( ${}^1C_4$ ), and boat (3B) conformers. These Newman projections show the dihedral angles of the adjacent hydroxyl-group and hydrogen-atom substituents more explicitly than Haworth or Reeves projections.

Table 32. Newman projections show the three conformations evaluated for D-allopyranose rings.

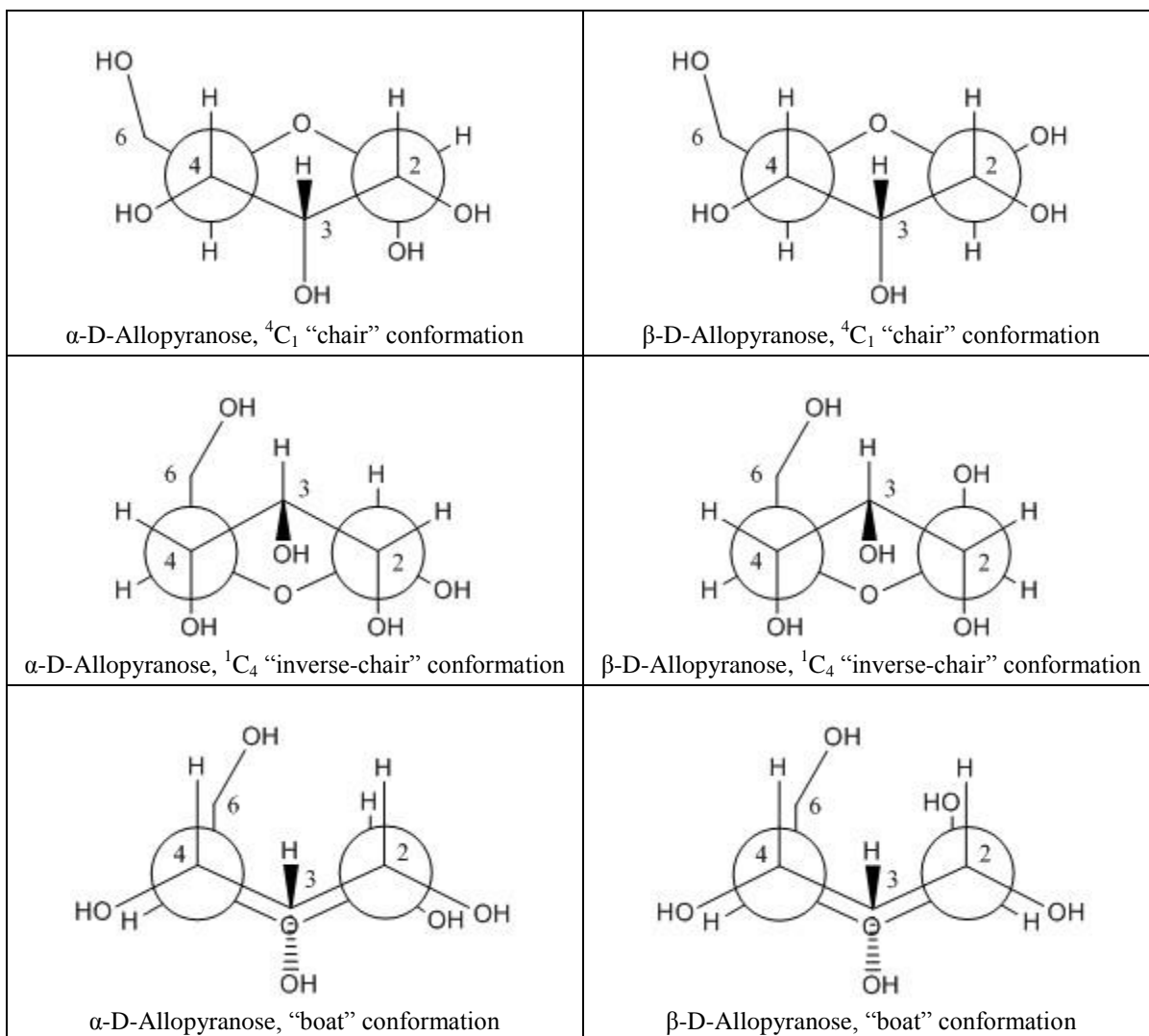


Table 33. Newman projections show the three conformations evaluated for D-altropyranose rings.

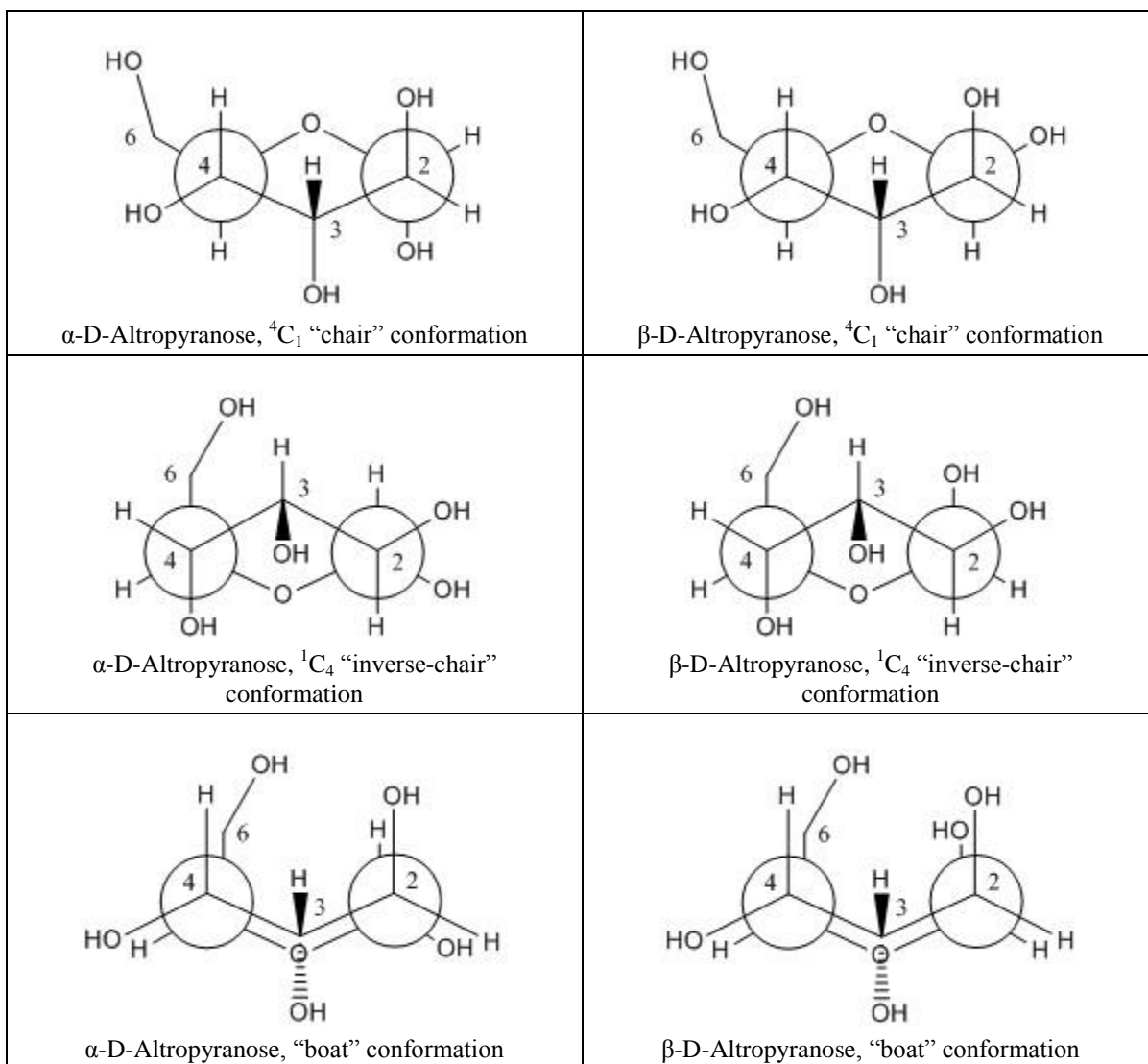


Table 34. Newman projections show the three conformations evaluated for D-glucopyranose rings.

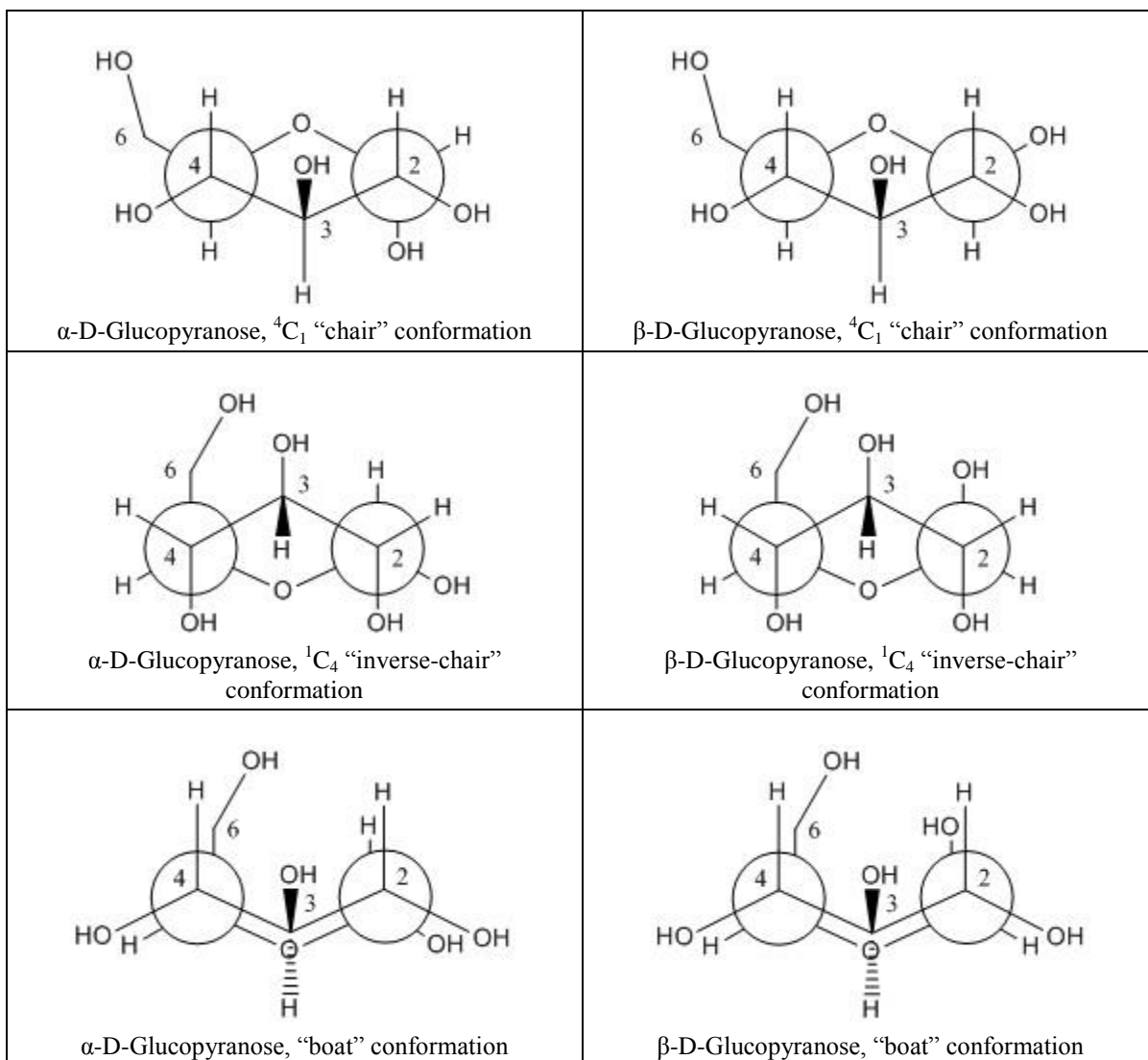


Table 35. Newman projections show the three conformations evaluated for D-galactopyranose rings.

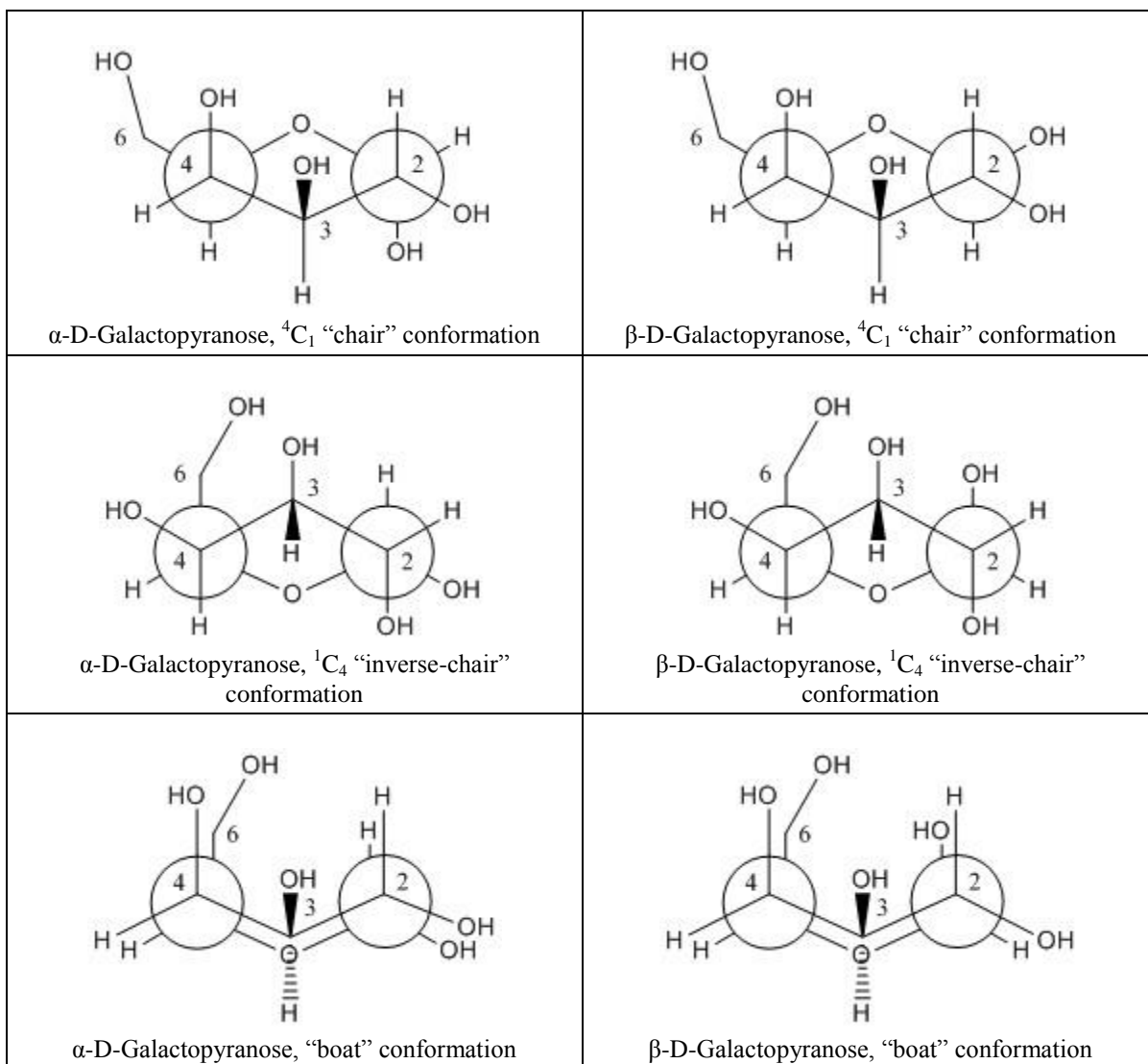
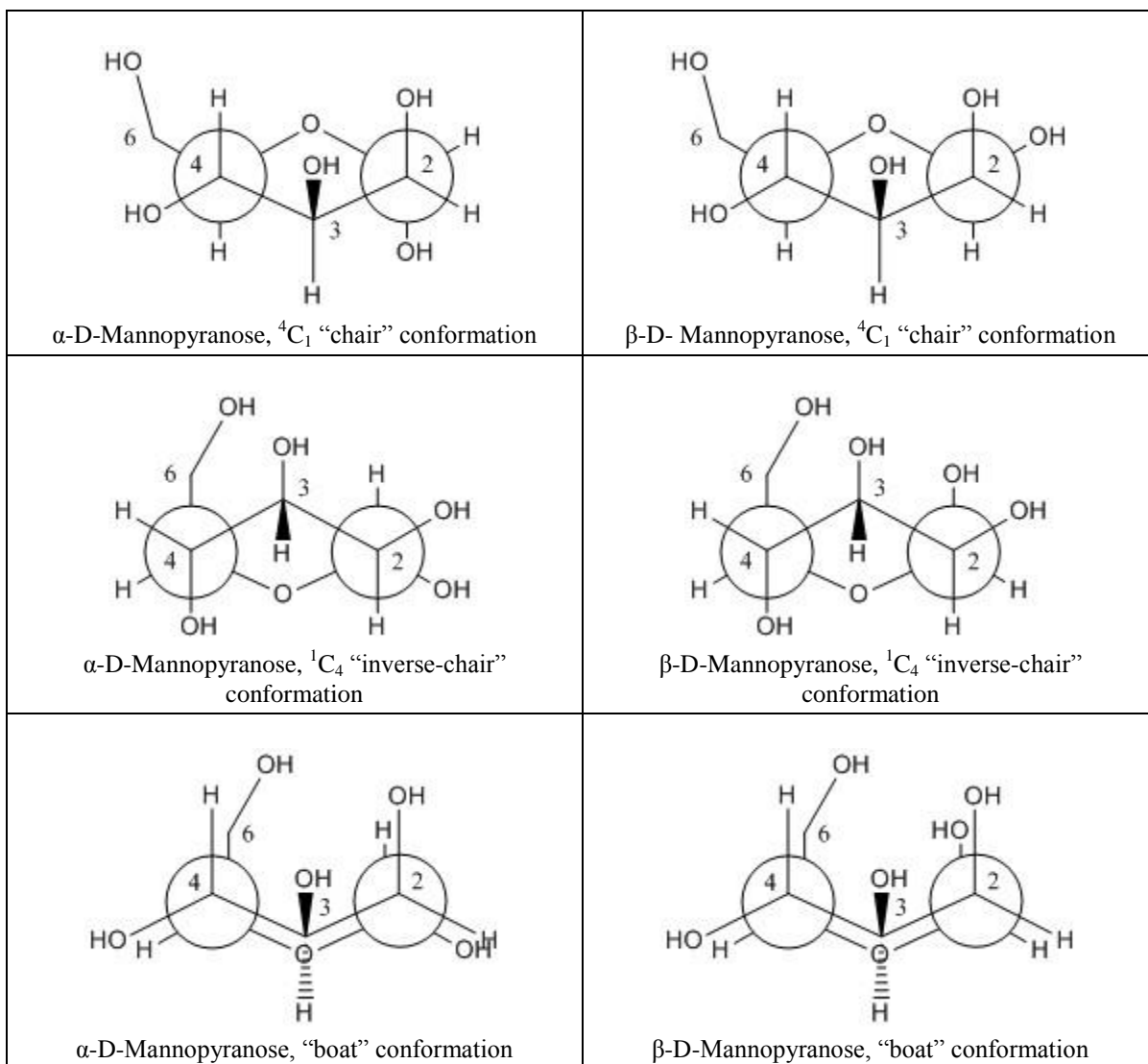


Table 36. Newman projections show the three conformations evaluated for D-mannopyranose rings.



The conformation's effect is very important for elimination reactions, and thus conformation might seriously affect the concerted-cyclic-1,2-dehydration mechanisms anticipated for pyrolyzing saccharides. Classic concerted, bimolecular eliminations ("E2 reactions") require syn-periplanar or anti-periplanar conformations. These conformations are required so that the  $sp^3$  orbitals of the substituents' breaking  $\sigma$ -bonds are parallel. Parallel  $sp^3$  bonds overlap immediately as they begin to form lone p orbitals, and overlapping p orbitals

are necessary for the forming product's  $\pi$ -bond [57, pp. 316-319]. Figures 87 and 88 show these anti-periplanar and syn-periplanar geometries for the E2 reaction applied to a generic alcohol. Newman projections are also provided here to illustrate better the anti-periplanar and syn-periplanar conformations of the reactant alcohol.

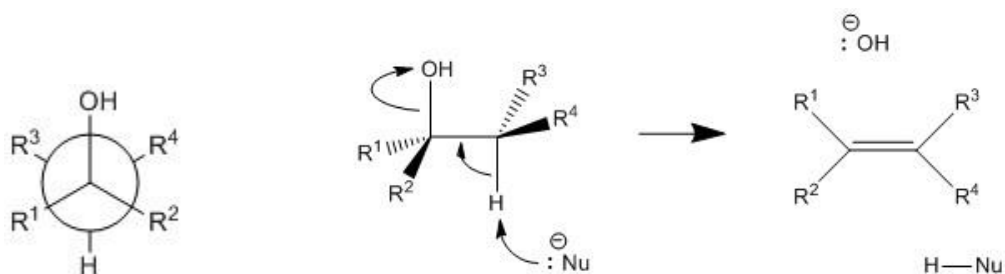


Figure 87. The Newman projection (left) for the anti-periplanar geometry in the E2 reaction (right). This E2 reaction differs from the concerted, cyclic 1,2-dehydrations due to non-cyclic nature, ionic reactants and products, and its not forming a single co-product. (After Hornback [57, pp. 316-319].)

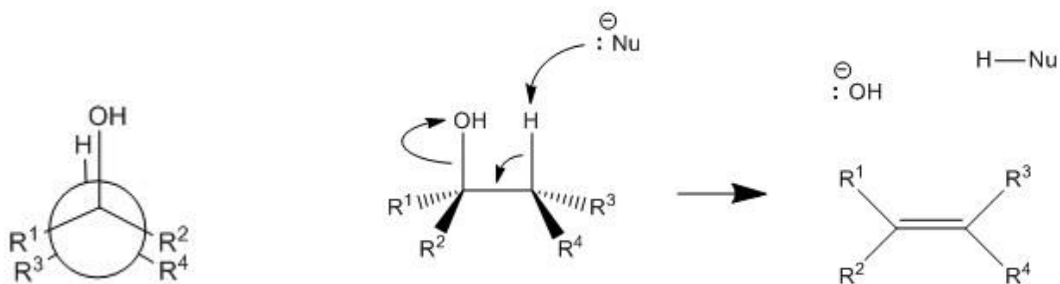


Figure 88. The Newman projection (left) for the syn-periplanar geometry in the E2 reaction (right). This E2 reaction differs from the concerted, cyclic 1,2-dehydrations due to non-cyclic nature, ionic reactants and products, and its not forming a single co-product. (After Hornback [57, pp. 316-319].)

In non-rigid molecules, the anti-periplanar conformation is preferred for E2 reactions because it lowers the transition state's torsional energy by staggering the reactant's substituent groups. Some strained cyclic molecules can prefer the syn-periplanar geometry, but cyclohexanes prefer the anti-periplanar geometry, which places the two substituents as

“trans-diaxial” [57, pp. 320-322]. The cyclohexane rings are known to change their conformations from chair to inverted chair in order for the substituents to obtain a trans-diaxial alignment. In regards to aldopyranose rings, this would first suggest that the adjacent hydrogen and hydroxyl pairs must be trans-diaxial for 1,2-dehydrations to proceed via the E2 mechanism. However, there are two important differences between the E2 mechanism and the concerted 1,2-dehydrations proposed in Section 4.5.5.

- E2 mechanisms allow the leaving-group substituent to break its bond while a separate nucleophile (hence, “bimolecular elimination”) removes a proton from the carbon adjacent to the leaving group. In other words, the leaving group does not bond with the adjacent removed proton atom to form a single co-product in addition to the main organic elimination product [57, pp. 314-323]. In contrast, the proposed concerted-cyclic-1,2-dehydration mechanisms require that the leaving group (hydroxyl group) bond with the adjacent carbon’s hydrogen atom (or bond with a hydrogen atom transferred from an assisting molecule’s hydroxyl group).
- In E2 mechanisms, often the nucleophile, leaving group, or both are ionic in nature. These ionic nucleophile reactants and leaving-group products (e.g.,  $\text{HO}^-$ ,  $\text{Br}^-$ , etc.) are possible during these classic E2 reactions because liquid solvents stabilize ionic reactants and products. In contrast, the pyrolysis environment has no mobile solvent and might preclude the presence of ionic reactants and products due to lack of solvation power.

These two differences between the classic E2 mechanism and the concerted-cyclic-1,2-dehydration mechanisms (proposed for pyrolyzing alcohols in Section 4.5.5) suggest that the anti-periplanar/trans-diaxial stereoisometric constraint of the E2 reaction in cyclohexane rings is not directly applicable to the proposed concerted, cyclic 1,2-dehydrations. In fact, the anti-periplanar/trans-diaxial geometry is unlikely for concerted, cyclic 1,2-dehydrations because it strains the cyclic transition-state geometry because bond angles are very different from common bonding angles when just four or six centers are available to accommodate the  $180^\circ$  dihedral angle. Should the removed substituent’s  $\text{sp}^3$  orbitals need to be near parallel in

order to form the product's  $\pi$ -bond, then the syn-periplanar geometry might be the only possible conformation in pyrolyzing saccharides if the concerted, cyclic 1,2-dehydration is to be operating.

The conformations of pyranose isomers force adjacent hydroxyl groups and hydrogen atoms to create a dihedral angle of  $60^\circ$  in the chair forms and  $0^\circ$  or  $120^\circ$  in the boat forms. Seshadri and Westmoreland [3] estimated the transitions between ring conformations on glucopyranose, obtaining  $5.7 \text{ kcal mol}^{-1}$  for boat to chair form and  $7.1 \text{ kcal mol}^{-1}$  for boat to inverted chair. These activation energies are small in comparison to the activation energies for dehydration, so it is expected that the glucopyranose ring configuration may easily change between chair, boat, and inverted chair during pyrolysis. This change between ring conformations is important because it allows the *quasi-cis* ring substituents to eclipse and obtain a temporary syn-periplanar conformation. With hydroxyl groups and hydrogen atoms in a temporary syn-periplanar conformation, the proposed concerted 1,2-dehydrations are compatible with the concept of overlapping orbitals when applied with the added constraint of a cyclic molecule like aldopyranoses.

A very simple method of estimating the number of hydroxyl-hydrogen pairs likely to dehydrate is counting the number of *quasi-cis* pairs. The terms *cis* and *trans* describe whether substituents are on the same or opposite sides of a plane.<sup>65</sup> These terms are modified to “*quasi-cis*” and “*quasi-trans*” for the application to the imperfect plane of cyclic saccharides because there is rarely true *cis* or *trans* geometry present in saccharides [56, pp. 51-54].

Table 37 lists each *quasi-cis* pair in both the  $\alpha$ - and  $\beta$ -anomers of D-allose, D-altrose, D-galactopyranose, D-glucopyranose, and D-mannopyranose. The total number of hydrogen-

---

<sup>65</sup> The prime example of *cis* and *trans* isomerism is with substituents about  $\pi$ -bonds, but *cis* and *trans* are also applied to  $\sigma$ -bonds. For example, *cis* and *trans* are employed to describe whether but-2-ene has its two methyl groups in a syn-periplanar (*cis*) geometry or a anti-periplanar (*trans*) geometry. *Cis* and *trans* may also be used to describe if two adjacent chlorine atoms in 1,2-dichlorocyclohexane are on the same side or opposite sides of the plane created by the cyclohexane quasi ring.

hydroxyl *quasi-cis* pairs are summed for each compound. (Their  $^4C_1$  Reeves projections in Figure 86 were used to determine these pairs.) Each *quasi-cis* pair is described by progressing around the pyranose ring from carbon 1 to carbon 6. Because there are two sides of the ring's quasi plane, one circuit is taken around the ring marking the substituents below the plane and one circuit is taken around the ring marking the substituents above the plane. This procedure is performed to compare the total hydrogen-hydroxyl *quasi-cis* pairs favorable for a 1,2-dehydration for each compound.

Having a set of five pyranoses which each have a unique combination of *quasi-cis* pairs led to a hypothesized difference in reactivity: The concerted 1,2-dehydration should be most rapid in molecules with the highest number of *quasi-cis* pairs of hydrogen atoms and hydroxyl groups. Of course the real mass-loss would be caused by both dehydration as well as other volatile-forming reactions like 1,6-bicyclic formation, but the 1,6-bicyclic formation should be similar among all five D-aldohexoses. Therefore, mass-loss should be more rapid in the compound with the most *quasi-cis* pairs of hydrogen atoms and hydroxyl groups.

Table 37. Comparison of *quasi-cis* hydrogen-hydroxyl pairs present in five D-aldohexoses viewed in their  ${}^4C_1$  Reeves projection.

Pyranose Form	Carbon-Carbon Pair	<i>Quasi-cis</i> Pairs Below ${}^4C_1$ Plane	Carbon-Carbon Bond Location	<i>Quasi-cis</i> Pairs Above ${}^4C_1$ Plane
D-Allopyranose	C1-C2	$\alpha$ anomer: OH-to-OH $\beta$ anomer: H-to-OH	C1-C2	$\alpha$ anomer: H-to-H $\beta$ anomer: OH-to-H
	C2-C3	OH-to-OH	C2-C3	H-to-H
	C3-C4	OH-to-OH	C3-C4	H-to-H
	C4-C5	OH-to-H	C4-C5	H-to-CH <sub>2</sub> OH
	C5-C6	Free rotation: (1) H-to-OH (2) H-to-H	N/A	
	Total <i>quasi-cis</i> OH-to-H Pairs in molecule	$\alpha$ anomer: 2 $\beta$ anomer: 4		
D-Altropyranose	C1-C2	$\alpha$ anomer: OH-to-H $\beta$ anomer: H-to-H	C1-C2	$\alpha$ anomer: H-to-OH $\beta$ anomer: OH-to-OH
	C2-C3	H-to-OH	C2-C3	OH-to-H
	C3-C4	OH-to-OH	C3-C4	H-to-H
	C4-C5	OH-to-H	C4-C5	H-to-CH <sub>2</sub> OH
	C5-C6	Free rotation: (1) H-to-OH (2) H-to-H	N/A	
	Total <i>quasi-cis</i> OH-to-H Pairs in molecule	$\alpha$ anomer: 6 $\beta$ anomer: 4		

Table 38, continued. Comparing of *quasi-cis* hydrogen-hydroxyl pairs present in five D-aldohexoses viewed in their  ${}^4C_1$  Reeves projection.

Pyranose Form	Carbon-Carbon Pair	<i>Quasi-cis</i> Pairs Below ${}^4C_1$ Plane	Carbon-Carbon Bond Location	<i>Quasi-cis</i> Pairs Above ${}^4C_1$ Plane
D-Galactopyranose	C1-C2	$\alpha$ anomer: OH-to-OH $\beta$ anomer: H-to-OH	C1-C2	$\alpha$ anomer: H-to-H $\beta$ anomer: OH-to-H
	C2-C3	OH-to-H	C2-C3	H-to-OH
	C3-C4	H-to-H	C3-C4	OH-to-OH
	C4-C5	H-to-H	C4-C5	OH-to-CH <sub>2</sub> OH
	C5-C6	Free rotation: (1) H-to-OH (2) H-to-H	N/A	
	Total <i>quasi-cis</i> OH-to-H Pairs in molecule	$\alpha$ anomer: 3 $\beta$ anomer: 5		
D-Glucopyranose	C1-C2	$\alpha$ anomer: OH-to-OH $\beta$ anomer: H-to-OH	C1-C2	$\alpha$ anomer: H-to-H $\beta$ anomer: OH-to-H
	C2-C3	OH-to-H	C2-C3	H-to-OH
	C3-C4	H-to-OH	C3-C4	OH-to-H
	C4-C5	OH-to-H	C4-C5	H-to-CH <sub>2</sub> OH
	C5-C6	Free rotation: (1) H-to-OH (2) H-to-H	N/A	
	Total <i>quasi-cis</i> OH-to-H Pairs in molecule	$\alpha$ anomer: 6 $\beta$ anomer: 8		
D-Mannopyranose	C1-C2	$\alpha$ anomer: OH-to-H $\beta$ anomer: H-to-H	C1-C2	$\alpha$ anomer: H-to-OH $\beta$ anomer: OH-to-OH
	C2-C3	H-to-H	C2-C3	OH-to-OH
	C3-C4	H-to-OH	C3-C4	OH-to-H
	C4-C5	OH-to-H	C4-C5	H-to-CH <sub>2</sub> OH
	C5-C6	Free rotation: (1) H-to-OH (2) H-to-H	N/A	
	Total <i>quasi-cis</i> OH-to-H Pairs in molecule	$\alpha$ anomer: 6 $\beta$ anomer: 4		

This comparison showed that D-glucopyranose has the most *quasi-cis* pairs, suggesting that D-glucopyranose should have the fastest rate of mass-loss. However, the thermogravimetric results of the D-aldohexoses show that D-glucose had the slowest mass loss in terms of requiring the highest temperatures at which the maximum mass-loss points occurred. However, at the first maximum and the mid-stage minimum, D-glucose had the fastest rate of mass loss. Meanwhile D-allose had the fewest *quasi-cis* pairs, and yet it did not have its first-stage mass loss at the lowest temperature of the D-aldohexoses. The fact that the number of *quasi-cis* pairs does not appear to correlate well with the temperatures of maximum mass loss or the rates of mass loss at these maximums appears to disprove this hypothesis for locating likely dehydration pairs.

A more precise way of estimating the number of hydroxyl-hydrogen pairs likely to dehydrate is counting the number of axial-axial pairs of adjacent hydroxyl groups and hydrogen atoms. This method seemed likely to be more successful because it ensures syn-periplanar geometry of the adjacent hydroxyl group and hydrogen atom, as is thought to be necessary for concerted elimination reactions like E2. Tables 39 through 43 describe the geometry of each pair of adjacent hydroxyl group and hydrogen atom present in the pyranose forms of D-allose, D-altrose, D-glucose, D-galactose, and D-mannose.

In the  ${}^4C_1$  chair conformation, there are no syn-periplanar pairs of adjacent substituents for D-allose, D-altrose, D-glucopyranose, D-galactopyranose, or D-mannopyranose. However, there are different numbers of anti-periplanar pairs among the isomers and anomers.

- $\alpha$ -D-allopyranose has three anti-periplanar pairs, while  $\beta$ -D-allopyranose has two anti-periplanar pairs.
- $\alpha$ -D-altropyranose has no anti-periplanar pair, while  $\beta$ -D-altropyranose has one anti-periplanar pair.
- $\alpha$ -D-glucopyranose one anti-periplanar pair, while  $\beta$ -D-glucopyranose has no anti-periplanar pairs.

- $\alpha$ -D-galactopyranose has three anti-periplanar pairs, while  $\beta$ -D-galactopyranose has two anti-periplanar pairs.
- $\alpha$ -D-mannopyranose has one anti-periplanar pair, while  $\beta$ -D-mannopyranose has two anti-periplanar pairs.

However, the number of anti-periplanar pairs of adjacent hydroxyl groups and hydrogen atoms created no correlations with either reaction rate or temperature for the first-stage maximum, mid-stage minimum, or second-stage maximum mass losses.

Table 39. The specific arrangements of adjacent H-OH pairs for carbons 1 through 5 of D-allopyranose.

Structural Isomer	Conformation	Anomer	Axial-Axial H-OH Pairs		Axial-Equatorial H-OH Pairs		Equatorial-Equatorial H-OH Pairs	
			Syn-Periplanar H-OH Pairs [Locations (Quantity)]	Anti-Periplanar H-OH Pairs [Locations (Quantity)]	Axial-H-Equatorial-OH Pairs (60°-Dihedral) [Locations (Quantity)]	Equatorial-H-Axial-OH Pairs (60°-Dihedral) [Locations (Quantity)]	Syn-Periplanar H-OH Pairs [Locations (Quantity)]	60°-Dihedral H-OH Pairs [Locations (Quantity)]
D-Allopyranose	<sup>4</sup> C <sub>1</sub> Chair (O above and C3 below the C1-C2-C4-C5 plane)	α	0	3 [C1-C2 (1), C2-C3 (1), C3-C4 (1)]	0	0	0	3 [C1-C2 (1), C2-C3 (1), C3-C4 (1)]
		β	0	2 [C2-C3 (1), C3-C4 (1)]	2 [C1-C2 (2)]	0	0	2 [C2-C3 (1), C3-C4 (1)]
	<sup>1</sup> C <sub>4</sub> Inverse Chair (O below and C3 above the C1-C2-C4-C5 plane)	α	0	3 [C1-C2 (1), C2-C3 (1), C3-C4 (1)]	0	0	0	3 [C1-C2 (1), C2-C3 (1), C3-C4 (1)]
		β	0	2 [C2-C3 (1), C3-C4 (1)]	0	3 [C1-C2 (2), C4-C5 (1)]	0	2 [C2-C3 (1), C3-C4 (1)]
	Boat (O and C3 below the C1-C2-C4-C5 plane)	α	0	2* [C2-C3 (1), C3-C4 (1)]	2* [C1-C2 (2)]	0	1 [C4-C5 (1)]	2 [C2-C3 (1), C3-C4 (1)]
		β	1 [C1-C2 (1)]	2* [C2-C3 (1), C3-C4 (1)]	0	0	2 [C1-C2 (1), C4-C5 (1)]	2 [C2-C3 (1), C3-C4 (1)]

\* The boat conformation does not have a true "axial" direction, as these substituents are not parallel in all three spatial dimensions.

Table 40. The specific arrangements of adjacent H-OH pairs for carbons 1 through 5 of D-altropyranose.

Structural Isomer	Conformation	Anomer	Axial-Axial H-OH Pairs		Axial-Equatorial H-OH Pairs		Equatorial-Equatorial H-OH Pairs	
			Syn-Periplanar H-OH Pairs [Locations (Quantity)]	Anti-Periplanar H-OH Pairs [Locations (Quantity)]	Axial-H-Equatorial-OH (60°-Dihedral) Pairs [Locations (Quantity)]	Equatorial-H-Axial-OH (60°-Dihedral) Pairs [Locations (Quantity)]	Syn-Periplanar H-OH Pairs [Locations (Quantity)]	60°-Dihedral H-OH Pairs [Locations (Quantity)]
D-Altropyranose	<sup>4</sup> C <sub>1</sub> Chair (O above and C3 below the C1-C2-C4-C5 plane)	α	0	0	1 [C4-C5 (1)]	4 [C1-C2 (2), C2-C3 (2)]	0	1 [C3-C4 (1)]
		β	0	1 [C1-C2 (1)]	1 [C4-C5 (1)]	2 [C2-C3 (2)]	0	2 [C1-C2 (1), C3-C4 (1)]
	<sup>1</sup> C <sub>4</sub> Inverse Chair (O below and C3 above the C1-C2-C4-C5 plane)	α	0	1 [C3-C4 (1)]	4 [C1-C2 (2), [C2-C3 (2)]	0	0	1 [C3-C4 (1)]
		β	0	2 [C1-C2 (1), C3-C4 (1)]	2 [C2-C3 (2)]	0	0	2 [C1-C2 (1), C3-C4 (1)]
	Boat (O and C3 below the C1-C2-C4-C5 plane)	α	1* [C1-C2 (1)]	1* [C3-C4 (1)]	0	2* [C2-C3 (2)]	2 [C1-C2 (1), C4-C5 (1)]	1 [C3-C4 (1)]
		β	0	1* [C3-C4 (1)]	0	4* [C1-C2 (2), C2-C3 (2)]	1 [C4-C5 (1)]	1 [C3-C4 (1)]

\* The boat conformation does not have a true "axial" direction, as these substituents are not parallel in all three spatial dimensions.

Table 41. The specific arrangements of adjacent H-OH pairs for carbons 1 through 5 of D-galactopyranose.

Structural Isomer	Conformation	Anomer	Axial-Axial H-OH Pairs		Axial-Equatorial H-OH Pairs		Equatorial-Equatorial H-OH Pairs	
			Syn-Periplanar H-OH Pairs [Locations (Quantity)]	Anti-Periplanar H-OH Pairs [Locations (Quantity)]	Axial-H-Equatorial-OH (60°-Dihedral) Pairs [Locations (Quantity)]	Equatorial-H-Axial-OH (60°-Dihedral) Pairs [Locations (Quantity)]	Syn-Periplanar H-OH Pairs [Locations (Quantity)]	60°-Dihedral H-OH Pairs [Locations (Quantity)]
D-Galactopyranose	<sup>4</sup> C <sub>1</sub> Chair (O above and C3 below the C1-C2-C4-C5 plane)	α	0	3 [C1-C2 (1), C3-C4 (1), C4-C5 (1)]	4 [C1-C2 (2), C2-C3 (2)]	0	0	1 [C3-C4 (1)]
		β	0	2 [C3-C4 (1), C4-C5 (1)]	4 [C1-C2 (2), C2-C3 (2)]	0	0	1 [C3-C4 (1)]
	<sup>1</sup> C <sub>4</sub> Inverse Chair (O below and C3 above the C1-C2-C4-C5 plane)	α	0	2 [C1-C2 (1), C3-C4 (1)]	0	2 [C2-C3 (2)]	0	3 [C1-C2 (1), C3-C4 (1), C4-C5 (1)]
		β	0	1 [C3-C4 (1)]	0	4 [C1-C2 (2), C2-C3 (2)]	0	2 [C3-C4 (1), C4-C5 (1)]
	Boat (O and C3 below the C1-C2-C4-C5 plane)	α	0	1* [C3-C4 (1)]	2* [C2-C3 (2)]	1* [C4-C5 (1)]	0	1 [C3-C4 (1)]
		β	1* [C1-C2 (1)]	1* [C3-C4 (1)]	2* [C2-C3 (2)]	1* [C4-C5 (1)]	1 [C1-C2 (1)]	1 [C3-C4 (1)]

\* The boat conformation does not have a true “axial” direction, as these substituents are not parallel in all three spatial dimensions.

Table 42. The specific arrangements of adjacent H-OH pairs for carbons 1 through 5 of D-glucopyranose.

Structural Isomer	Conformation	Anomer	Axial-Axial H-OH Pairs		Axial-Equatorial H-OH Pairs		Equatorial-Equatorial H-OH Pairs	
			Syn-Periplanar H-OH Pairs [Locations (Quantity)]	Anti-Periplanar H-OH Pairs [Locations (Quantity)]	Axial-H-Equatorial-OH (60°-Dihedral) Pairs [Locations (Quantity)]	Equatorial-H-Axial-OH (60°- Dihedral) Pairs [Locations (Quantity)]	Syn-Periplanar H-OH Pairs [Locations (Quantity)]	60°-Dihedral H-OH Pairs [Locations (Quantity)]
D-Glucopyranose	<sup>4</sup> C <sub>1</sub> Chair (O above and C3 below the C1-C2-C4-C5 plane)	α	0	1 [C1-C2 (1)]	6 [C1-C2 (1), C2-C3 (2), C3-C4 (2), C4-C5 (1)]	0	0	1 [C1-C2 (1)]
		β	0	0	7 [C1-C2 (2), C2-C3 (2), C3-C4 (2), C4-C5 (1)]	0	0	0
	<sup>1</sup> C <sub>4</sub> Inverse Chair (O below and C3 above the C1-C2-C4-C5 plane)	α	1 [C1-C2 (1)]	0	0	6 [C1-C2 (1), C2-C3 (2), C3-C4 (2), C4-C5 (1)]	0	1 [C1-C2 (1)]
		β	0	0	0	7 [C1-C2 (2), C2-C3 (2), C3-C4 (2), C4-C5 (1)]	0	0
	Boat (O and C3 below the C1-C2-C4-C5 plane)	α	0	0	6* [C1-C2 (2), C2-C3 (2), C3-C4 (2)]	0	1 [C4-C5 (1)]	0
		β	1* [C1-C2 (1)]	0	4* [C2-C3 (2), C3-C4 (2)]	0	2 [C1-C2 (1), C4-C5 (1)]	0

\* The boat conformation does not have a true “axial” direction, as these substituents are not parallel in all three spatial dimensions.

Table 43. The specific arrangements of adjacent H-OH pairs for carbons 1 through 5 of D-mannopyranose.

Structural Isomer	Conformation	Anomer	Axial-Axial H-OH Pairs		Axial-Equatorial H-OH Pairs		Equatorial-Equatorial H-OH Pairs	
			Syn-Periplanar H-OH Pairs [Locations (Quantity)]	Anti-Periplanar H-OH Pairs [Locations (Quantity)]	Axial-H-Equatorial-OH (60°-Dihedral) Pairs [Locations (Quantity)]	Equatorial-H-Axial-OH (60°-Dihedral) Pairs [Locations (Quantity)]	Syn-Periplanar H-OH Pairs [Locations (Quantity)]	60°-Dihedral H-OH Pairs [Locations (Quantity)]
D-Mannopyranose	<sup>4</sup> C <sub>1</sub> Chair (O above and C3 below the C1-C2-C4-C5 plane)	α	0	1 [C2-C3 (1)]	3 [C3-C4 (2), C4-C5 (1)]	2 [C1-C2 (2)]	0	1 [C2-C3 (1)]
		β	0	2 [C1-C2 (1), C2-C3 (1)]	3 [C3-C4 (2), C4-C5 (1)]	0	0	2 [C1-C2 (1), C2-C3 (1)]
	<sup>1</sup> C <sub>4</sub> Inverse Chair (O below and C3 above the C1-C2-C4-C5 plane)	α	0	1 [C2-C3 (1)]	2 [C1-C2 (2)]	3 [C3-C4 (2), C4-C5 (1)]	0	1 [C2-C3 (1)]
		β	0	2 [C1-C2 (1), C2-C3 (1)]	0	3 [C3-C4 (2), C4-C5 (1)]	0	2 [C1-C2 (1), C2-C3 (1)]
	Boat (O and C3 below the C1-C2-C4-C5 plane)	α	1* [C1-C2 (1)]	1* [C2-C3 (1)]	2* [C3-C4 (2)]	0	2 [C1-C2 (1), C4-C5 (1)]	1 [C2-C3 (1)]
		β	0	1* [C2-C3 (1)]	2* [C3-C4 (2)]	2* [C1-C2 (2)]	1 [C4-C5 (1)]	1 [C2-C3 (1)]

\* The boat conformation does not have a true "axial" direction, as these substituents are not parallel in all three spatial dimensions.

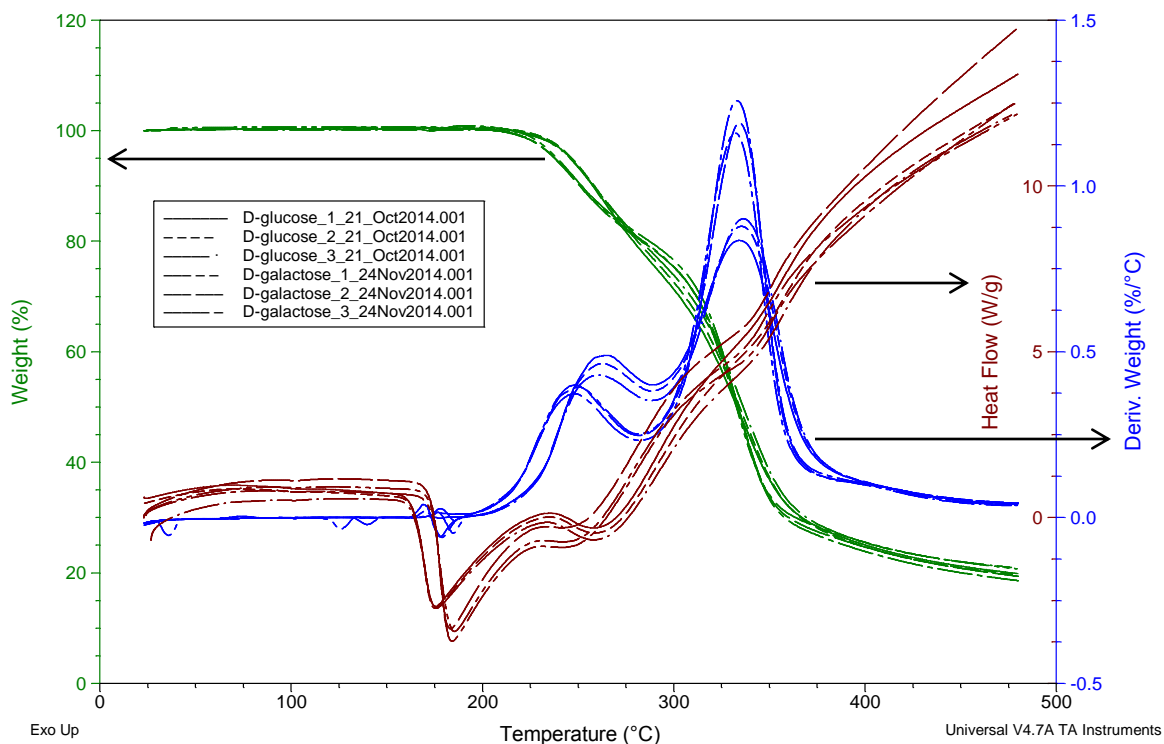


Figure 89. The derivatives of mass-vs-time show that the mass-loss onset of D-galactose leads D-glucose. In fact, both D-galactose's two peak rates of mass loss lead the two respective peak rates of mass loss for D-glucose. Heat flow suggests D-glucose melts at a lower temperature in the onset of pyrolysis for both maxima in the derivative.

### 5.6.2. *The leading explanation for two maxima in mass-loss rate*

Having two maxima in the rate of mass loss suggests that a change in reactions responsible for vapor formation occurs between the maxima. The change in vapor formation is thought to be due to the following sequence:

- A thermally favored reaction (or set of thermally favored reactions) begins. This reaction (or reaction set) causes the formation of volatile products, which causes sample mass to be reduced.

- The chemical moieties subject to these more favorable reaction(s) are consumed, leading to a decrease in reaction rate and a decrease in the rate of mass-loss.
- A second, less-thermally favored reaction (or second set of less-thermally favored reactions) begins to form vapors after the temperature increases. This second reaction (or second set of reactions) consumes a different chemical moiety than what the first, more favorable reaction (or first set of reactions) consumed.

The need for two different reactions that consume different chemical moieties available in the reactant molecule depends upon one main assumption: Without consumption and exhaustion of a favored reactive moiety, the total rate of mass loss should only increase with increasing sample temperature.

### ***5.6.3. Comparison between D-aldohexoses and D-alditols***

The comparisons of D-glucitol vs D-glucose and D-mannitol vs D-mannose show four key points:

- The aldoexitols have a higher onset temperature for mass loss than aldohexoses.
- The aldoexitols pyrolyze with just one, sharp mass-loss stage while the aldohexoses pyrolyze with two mass-loss stages.
- The single mass-loss stage of the aldoexitols has a much higher rate of mass loss than either of the two mass-loss stages of the aldohexoses.
- Practically no char is formed from aldoexitols.

These four key points are highlighted in Figures 90 and 91.

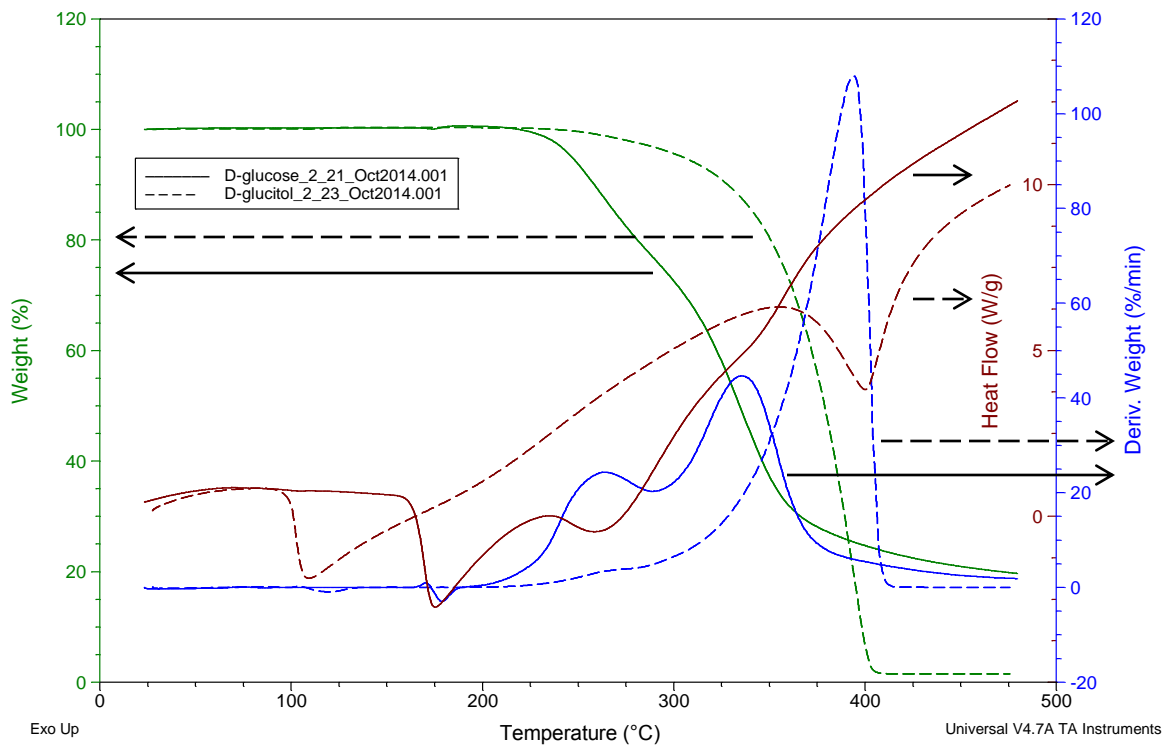


Figure 90. The comparison of D-glucose and D-glucitol at  $50^{\circ}\text{C min}^{-1}$ .

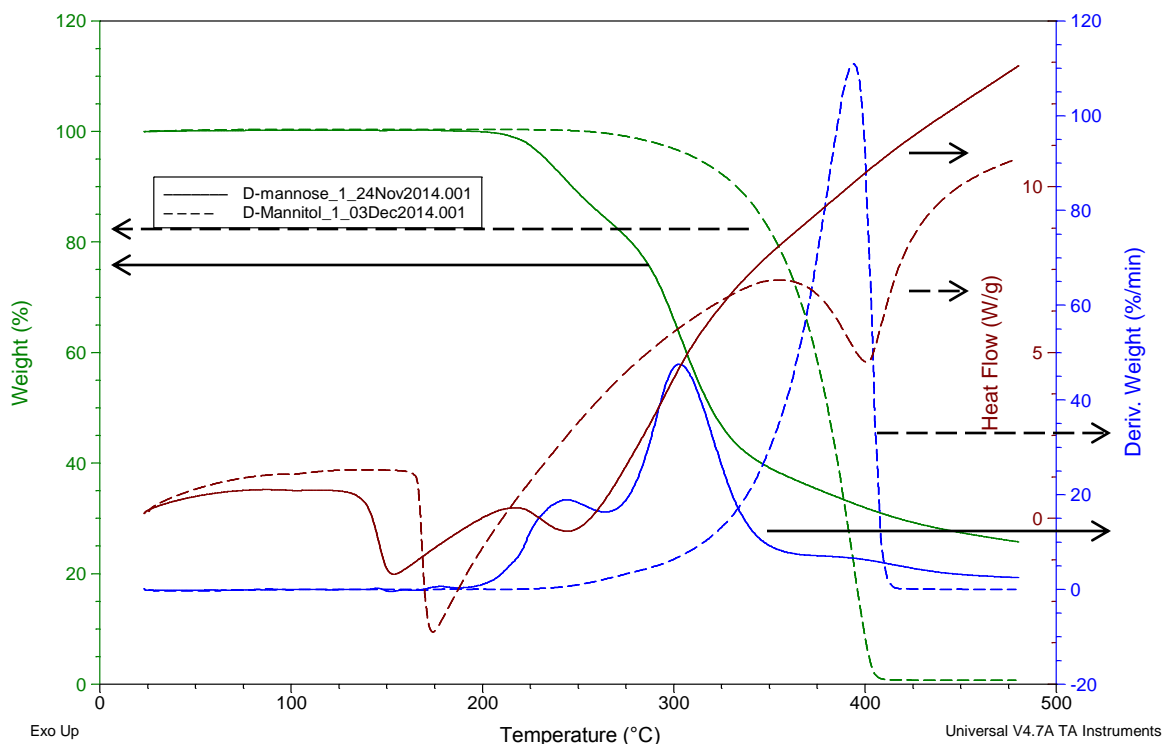


Figure 91. The comparison of D-mannose and D-mannitol at  $50^{\circ}\text{C min}^{-1}$ .

These four key differences in mass-loss behavior between aldohexoses and aldohexitols were also observed to occur between an aldopentose and its respective aldopentitol. TGA experiments by Räsänen et al. [60] showed that D-arabinitol pyrolyzed differently than D-arabinose when heating from 25 to  $700^{\circ}\text{C}$  at  $2^{\circ}\text{C min}^{-1}$  in nitrogen. Because both an aldopentose and two aldohexoses exhibit these four differences between their respective alditols, these mass-loss differences are likely not due to not the number of carbons present but are instead likely due to the nature of alcohol, carbonyl, and ether functional groups on non-volatile molecules.

The five- and six-carbon alditols pyrolyze so differently than their respective aldoses is due to their selectivity to volatile pyrolysis products. Aldopentoses and aldohexoses form char, and this char is invariably composed of bimolecular-reaction products that lack vapor

pressure. Often char is hypothesized to form via dehydration polymerization reactions, with levoglucosan in particular forming a polysaccharide-like product [50]. Alditols must fragment carbon-carbon bonds in a manner which forms almost entirely volatile products, preventing the polymerization of saccharide-like products such as levoglucosan or other pyranose and furanose rings.

In addition to TGA/DSC experiments obtaining mass-loss data, initial product identification was performed for D-glucitol by Pyroprobe®-GC-MS experiments. Its pyrolysis products were scanned specifically for levoglucosan (1,6-anhydro- $\beta$ -D-glucopyranose), and small peaks of levoglucosan were obtained. The observation of 1,6-anhydro- $\beta$ -D-glucopyranose among these products provided experimental support for three suggested reactions:

- Alcohol groups dehydrogenate in pyrolysis conditions, as it was shown in Chapter 4. While diols and the triol exhibited dehydration to a larger extent than dehydrogenation, some dehydrogenation could be expected. Of the six alcohols which could undergo dehydrogenation, carbons 1 and 6 should capture a fraction of these potential dehydrogenations. If such dehydrogenations were to occur, then some D-glucitol would dehydrogenate to acyclic D-glucose (dehydrogenation of carbon 1) and some would dehydrogenate to acyclic L-gulose (dehydrogenation of carbon 6).
- Second, it was also suggested by Sanders et al. [61] and Seshadri and Westmoreland [3] that D-glucose can interconvert between cyclic and acyclic forms during pyrolysis. Of the D-glucose formed upon any dehydrogenations, a fraction of it should cyclize to D-glucopyranose.
- Third, the most energetically favored pyrolysis reaction for  $\beta$ -D-glucopyranose is the formation of 1,6-dianhydro- $\beta$ -D-glucopyranose from  $\beta$ -D-glucopyranose according to the simulations of Seshadri and Westmoreland [3].

Should these three reactions all be valid, then D-glucitol should form a small quantity of 1,6-dianhydro- $\beta$ -D-glucopyranose upon pyrolysis by dehydrogenation at carbon 1 or 6,

followed by cyclization to a pyranose ring, and finally formation of levoglucosan by a 1,6-bicyclic formation. The observation of levoglucosan from D-glucitol pyrolysis provided some support for these three reactions being possible, although this levoglucosan observation is not proof of these three specific reactions because it does not “rule out” other pathways.

#### 5.6.4. Comparison of 2-deoxy-glucose to D-glucose

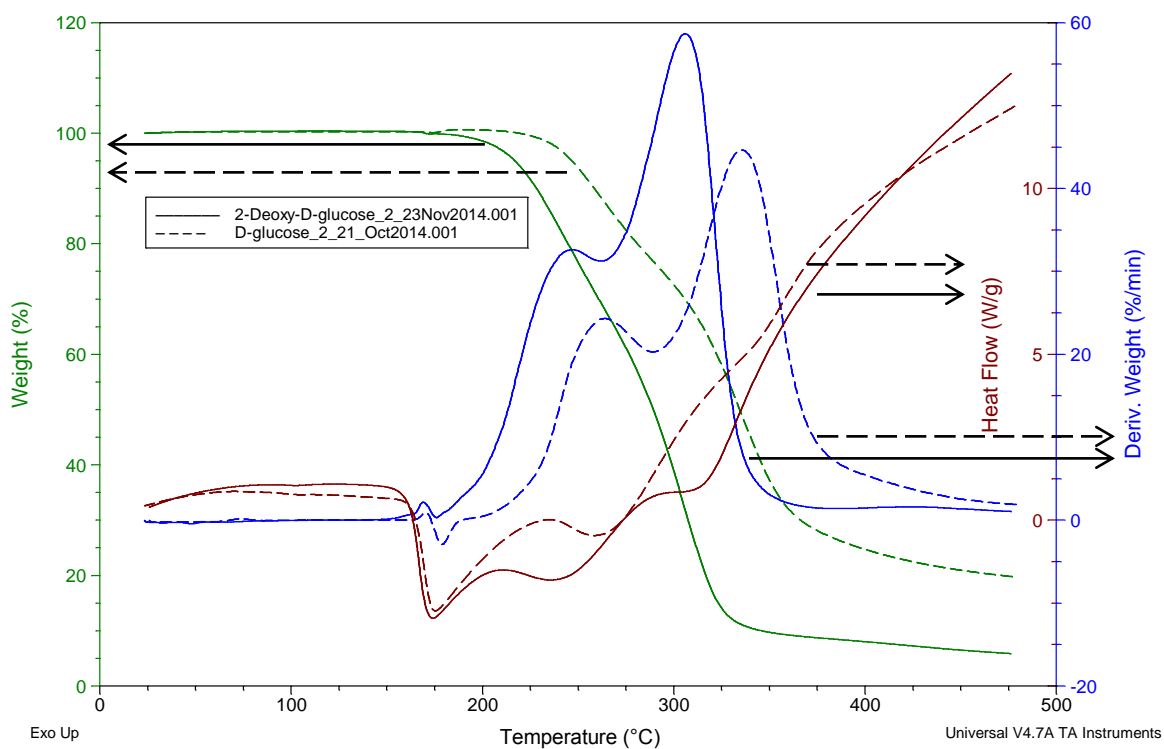


Figure 92. The comparison of one D-glucose pyrolysis experiment to one 2-deoxy-D-glucose experiment at  $50^{\circ}\text{C min}^{-1}$ .

2-Deoxy-D-glucose is obtained by replacing the hydroxyl group of D-glucose’s carbon 2 with a hydrogen atom. This replacement eliminates several reactions expected to take place on D-glucose.

- It eliminates two specific 1,2-dehydrations:
  - Dehydration of H from carbon 1 and OH from C2
  - Dehydration of H from carbon 3 and OH from C2
- It eliminates the cyclic Grob fragmentation from occurring on carbons 2, 3, and 4 by eliminating that 1,3-diol system.

Importantly, replacing the hydroxyl group on carbon 2 with a hydrogen atom does not eliminate the ability to form the bicyclic levoglucosan analog, which is a vital reaction for glucose and cellulose.

The comparison of their thermograms (Figure 92) shows that the elimination of the hydroxyl group on carbon 2, and the likely elimination of a 1,2-dehydration pathway, did not prevent the presence of two stages of mass loss. This result suggests that 1,2-dehydration at carbons 1 and 2 and 2 and 3 is not a major contributor to a stage of mass loss.

Interestingly, 2-deoxy-glucose leaves 5.87% of the original mass at 476°C while D-glucose leaves 19.7%. The drastic difference in char yields suggests that 1,2-dehydration at carbons 1 and 2 and 2 and 3 could be a major contributor to char precursors.

#### ***5.6.5. Comparison between D-aldopentoses and D-aldohexoses***

Comparing D-glucopyranose to D-xylopyranose allows a specific combination of changes to the possible reaction set. Replacing D-glucopyranose's CH<sub>2</sub>OH group of carbon 5 with a hydrogen atom gives the structure of D-xylopyranose (Figure 93). The removal of D-glucopyranose's CH<sub>2</sub>OH substituent from carbon 5 eliminates several important reaction possibilities:

- It eliminates the cyclic Grob fragmentation for carbons 4, 5, and 6 because there is no longer a 1,3-diol system.
- It eliminates a concerted 1,2-dehydration mechanism for carbons 5 and 6 because there are no adjacent hydrogen atom and hydroxyl group on carbons 5 and 6, respectively.

- It eliminates the ability to form a 1,6-anhydropyranose through any unimolecular reaction.

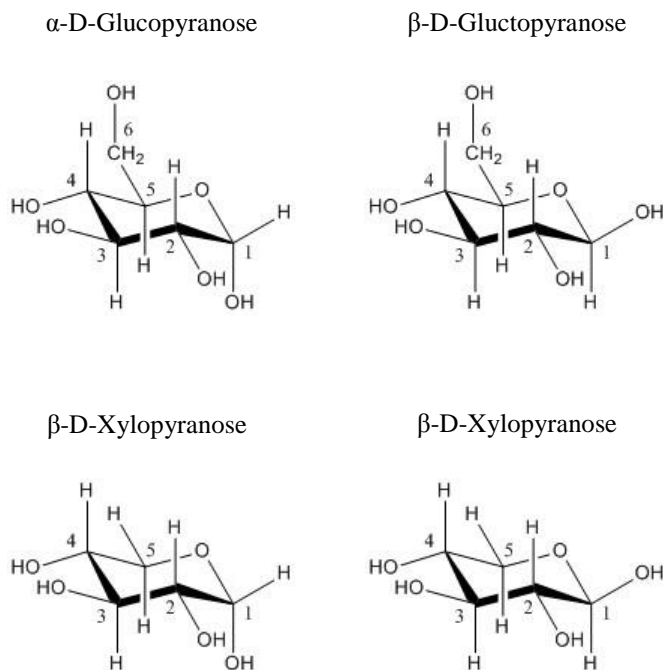


Figure 93. Reeves projections in the  ${}^4C_1$  conformation of D-glucopyranose and D-xylopyranose for structural comparison.

Observing two stages of mass loss in D-xylose and D-arabinose was imperative to learning more about D-glucose and D-glucose-based materials like cellobiose and cellulose.

Initially, the two stages of mass loss seen in the D-aldohexoses and cellobiose was hypothesized to be due to the formation of levoglucosan as the first mass-loss stage and 1,2-dehydrations and/or carbon-carbon fragmentations as the second mass-loss stage. This hypothesis was based upon how levoglucosan formation reactions are more energetically

favorable than the other reactions based upon computational-quantum-chemistry (CQC) simulations [3], [1], [2].

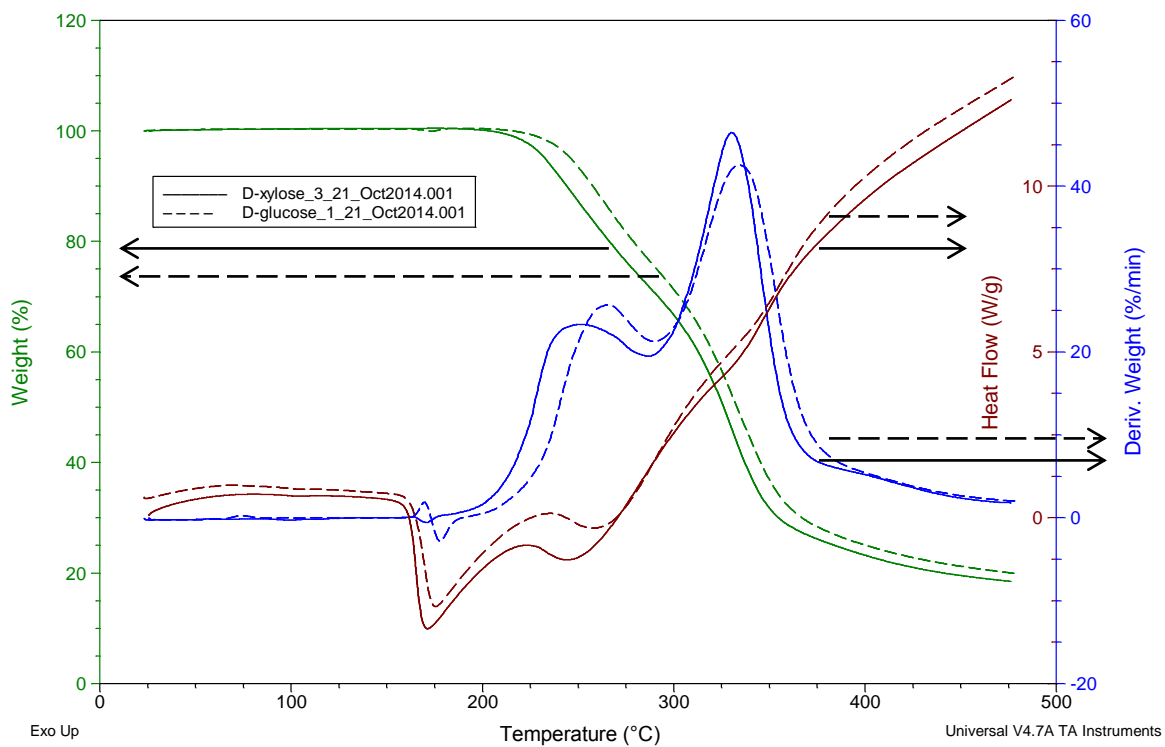


Figure 94. The two-stage mass-loss phenomena is seen with both D-glucose and D-xylose, suggesting the formation of levoglucosan is not responsible for the initial mass-loss phase in D-glucose.

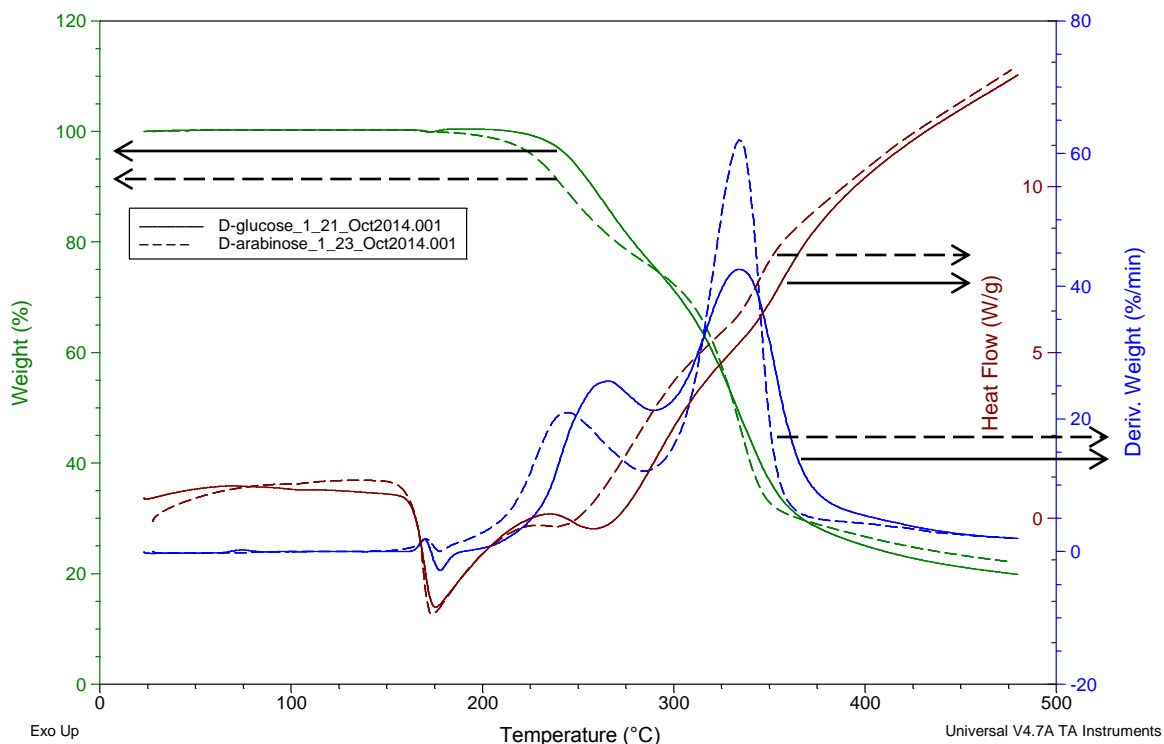


Figure 95. The two-stage mass-loss phenomena is seen with both D-glucose and D-arabinose, suggesting the formation of levoglucosan is not responsible for the initial mass-loss phase in D-glucose.

The comparison of D-glucose to D-xylose is uncommon in the pyrolysis literature, even though such a comparison brings vital information to the understanding of saccharide and polysaccharide pyrolysis. One particularly important area is the formation of a 1,6-bicyclic. Levoglucosan forms from D-glucopyranose by forming the bicyclic link C6-O6-C1 or C6-O1-C1 across its pyranose ring. D-xylopyranose cannot form levoglucosan through this pathway because it has no carbon 6.<sup>66</sup> Patwardhan et al. [48] used cellulose to help

---

<sup>66</sup> Levoglucosan cannot form from any pentose by any unimolecular mechanism because pentoses ( $C_5H_{10}O_5$ ) don't have enough carbon atoms to make an anhydrohexose ( $C_6H_{10}O_5$ ) like levoglucosan.

understand hemicellulose but did not use their observations of hemicellulose to help understand cellulose.

#### **5.6.6. Comparison between enantiomers and implication for comparing D-galactose to 6-deoxy-D-galactose comparisons**

Replacing D-galactose's hydroxyl group on carbon 6 with a hydrogen atom gives the structure of 6-deoxy-D-galactose. With the assumption that D-galactose pyrolyzes in essentially the same fashion<sup>67</sup> as L-galactose, then 6-deoxy-L-galactose is obtained by replacing D-galactose's hydroxyl group at carbon 6 with a hydrogen atom. This replacement of carbon 6's hydroxyl group with a hydrogen atom eliminates several important potential reactions.

- It eliminates the cyclic Grob fragmentation for carbons 4, 5, and 6 by eliminating the 1,3-diol.
- It eliminates the concerted 1,2-dehydration for carbons 5 and 6 due to eliminating the hydroxyl group on carbon 6.
- It eliminates the ability to form a 1,6-anhydropyranose through anticipated dehydration reaction [3].

A comparison was made between D-arabinose and L-arabinose specifically to determine the effect of reversing each stereochemical center in a molecule. This finding is important for the ability to compare 6-deoxy-L-galactose to D-galactose in a way which suggests only one effective structural change was responsible for any differences in reaction behavior.

The logic is as follows.

---

<sup>67</sup> "Essentially the same fashion" implies that the only difference in pyrolysis behavior between enantiomeric reactants is obtaining enantiomeric products.

- If D-arabinose and L-arabinose pyrolyze identically in terms of mass-loss and heat-flow behavior, then perhaps all enantiomers, including D-galactose and L-galactose, may pyrolyze identically in terms of mass-loss and heat-flow behavior.
- If D-galactose and L-galactose pyrolyze identically in terms of mass-loss and heat-flow behavior, then 6-deoxy-L-galactose may be compared to D-galactose as if the replacement of carbon 6's hydroxyl group with a hydrogen atom is the only difference in molecular structure between them.
- If the replacement of carbon 6's hydroxyl group with a hydrogen atom is the only difference in molecular structure, then any differences in reaction behavior can be attributed solely to this structural difference.

Figure 96 shows a comparison of three pyrolyses of D-arabinose and three pyrolyses of L-arabinose. Their thermogravimetric behaviors is almost identical, and this lends credibility to the assumption of how D-galactose and L-galactose would have identical thermogravimetric behavior. With this first comparison it appears reasonable to compare 6-deoxy-L-galactose to D-galactose as though they have only one effective structural change.

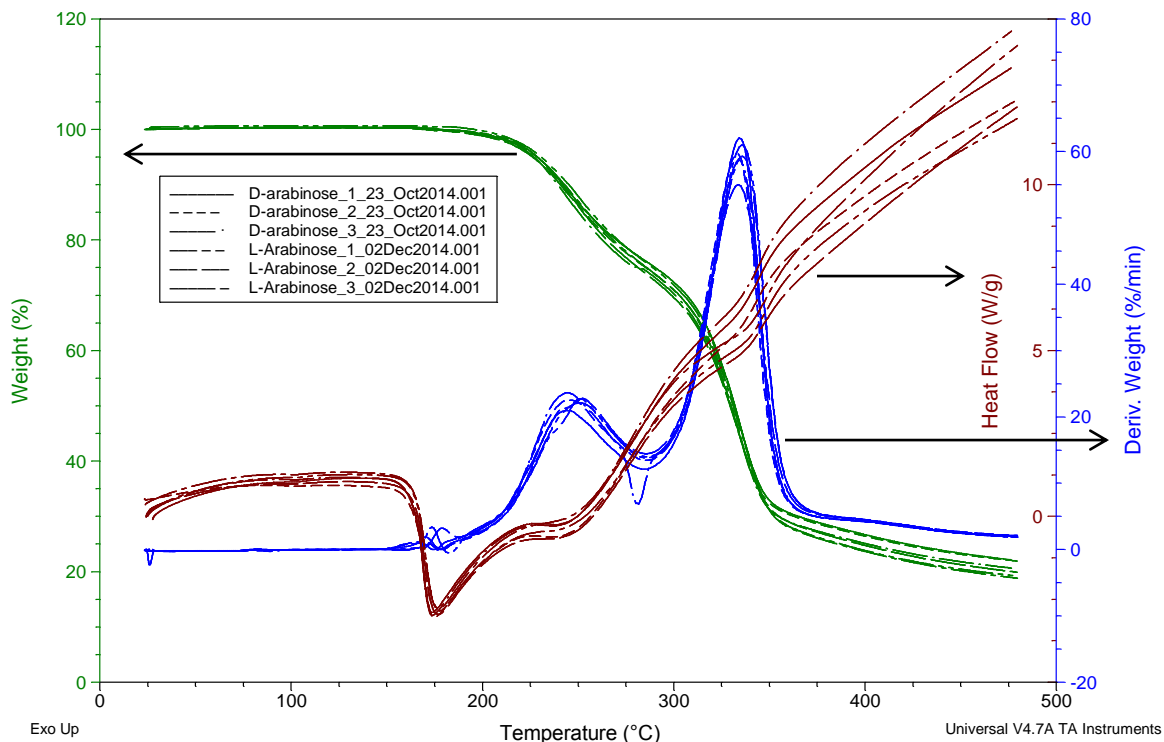


Figure 96. The mass and heat-flow signals of three D-arabinose and three L-arabinose experiments at  $50^{\circ}\text{C min}^{-1}$ .

Figure 97 shows the comparison of the thermogravimetric behavior of D-galactose and 6-deoxy-L-galactose. Both of these materials show the two-stage mass-loss behavior, although the first stage has a significantly higher mass-loss rate in 6-deoxy-L-galactose (“L-fucose”). The higher rate of mass loss during this first stage with the 6-deoxy-L-galactose suggests that a 1,6-bicyclic formation suggested by Seshadri and Westmoreland [3] is certainly not a major contributor to the first-stage reactions of the aldohexoses. In addition, the very similar temperature dependence and rates of mass loss during the second stage suggests that decomposition of a 1,6-bicyclic is not responsible for the second stage in other D-aldohexoses.

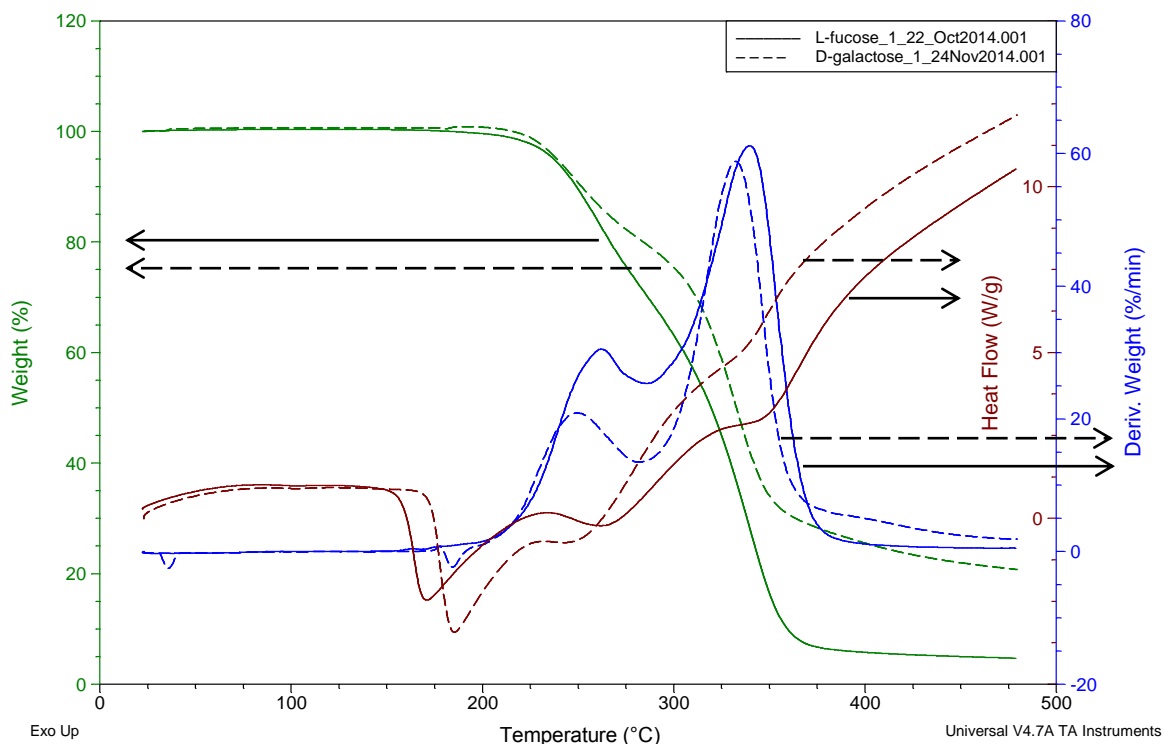


Figure 97. The comparison of D-galactose and L-fucose (6-deoxy-L-galactose).

### 5.6.7. Comparison of D-trehalose dihydrate and D-cellobiose

Perhaps the outcome most directly applicable to polymerized D-glucose is the comparison between D-trehalose dihydrate and D-cellobiose. These two materials are both dimers composed of anhydroglucopyranose units, but they differ by the position of their glycosidic bond. D-cellobiose has a  $\beta(1-4)$  linkage, while D-trehalose dihydrate has a  $\alpha(1-1)$  glycosidic linkage. The importance of this difference is that D-trehalose keeps both of its anhydroglucopyranose units as non-reducing sugars, while D-cellobiose will always have one of its anhydroglucopyranose units as a reducing sugar. D-Cellobiose, with half of its glucopyranose units being a reducing sugar, is seen as an intermediate step between D-glucose, which is entirely a reducing sugar, and cellulose, which has only one reducing sugar at one of its two terminal chain ends. D-Trehalose dihydrate provides vital information on the

pyrolysis behavior of a D-glucopyranose dimer without ability to exhibit an acyclic glucose unit.

Importantly, D-trehalose dihydrate showed only one stage of (reactive) mass loss<sup>68</sup>, while D-cellobiose showed two stages. The fact that other D-aldohexoses, D-aldopentoses, and even the deoxysugars pyrolyze with two mass-loss stages while cellulose pyrolyzes with just one mass-loss stage led to a hypothesis that acyclic isomers were responsible for the first stage of mass loss. This hypothesis appears very questionable due to how an initial experiment of xylan also showed two stages of mass loss (Figure 85). However, the comparison to xylan is very questionable because its purity is not confirmed, and even pure xylan has a variable structure in regards to branching moieties.

---

<sup>68</sup> D-Trehalose dehydrate shows multiple stages of mass loss, but the mass-loss phases below 200°C are only due to the release of the hydrated water.

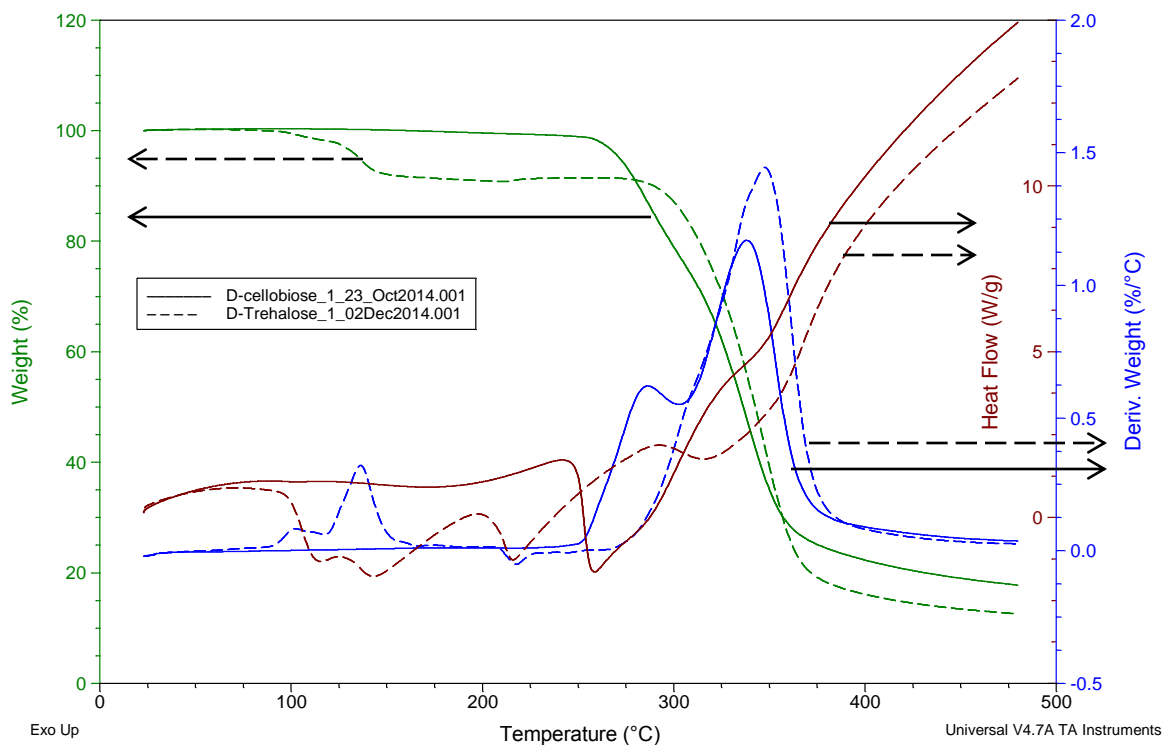


Figure 98. The comparison of D-trehalose dihydrate to cellobiose.

### 5.6.8. Recommended future research

A method for effective separation and accurate identification of glucopyranose-like materials is needed because GC-MS provides unreliable identifications for compounds vital to the results of Pyroprobe® experiments. There are two fundamental reasons for this problem of unreliable identifications.

- Glucopyranose-like analytes have very low volatilities, causing them either to fail to elute at all or create very broad, tailing peaks.
  - Non-volatile compounds, like the D-aldohexoses, are simply incapable of eluting in GC.

- When very polar compounds do manage to elute, often they elute as broad peaks. Broad peaks make the spectral matching more difficult due to poor signal-to-noise ratios.
- Glucopyranose-like analytes have complex fragmentation spectra. These complex fragmentation spectra lead to poor spectral matches, making the confidence of these spectral suggestions very low and often not repeatable for identical experiments. (Poor spectral matches are especially problematic when these complex fragmentation patterns are combined with co-elution of analytes.) As an excellent example, Pyroprobe®-GC-MS experiments for D-xylose and 6-deoxy-L-galactose (“L-fucose”) were not reproducible in terms of the peak identifications, as several different identifications were provided for major analyte peaks seen in replicate experiments. Strangely, one of the small peaks in these chromatograms was suggested to be levoglucosan. Producing levoglucosan from 6-deoxy-L-galactose is unexpected due to 6-deoxy-L-galactose having no hydroxyl group bonded to its carbon 6. Producing levoglucosan from D-xylose is especially unexpected due to D-xylose having no carbon 6 at all. These levoglucosan matches are very likely to be spectral misidentifications. These peaks could have provided very important insight to reaction pathways, but these analytes with complex and similar fragmentation spectra (and low volatility) are simply not suited for analysis by GC-MS.

Two different methods are highly recommended for identifying highly polar compounds like glucopyranose-like model compounds.

- Silylation followed by GC-MS.
- LC-MS (or LC combined with other detection methods)

Silylation is a derivatization technique that replaces the very polar hydroxyl groups with silyl ethers. Such a change drastically increases volatility and has been used to analyze saccharide materials in GC. The problem with silylation, or any other derivatization technique, is that there must be a way to understand the new fragmentation patterns of the

silylated molecule. In addition, analytes with multiple hydroxyl groups might silylate incompletely, leaving a fraction as partially silylated and fraction as fully silylated. These partial conversions must be well understood and predictable, or else the silylation method will not be capable of identifying unknown compounds.

LC is very attractive as a method of separating and detecting not only glucopyranose-like compounds, but also the oligomers of anhydroglucopyranose thought to be vital intermediates in cellulose breakdown.

### **5.7. Conclusions**

Glucopyranose-like model compounds were pyrolyzed in a TGA/DSC at  $50^{\circ}\text{C min}^{-1}$ . These model compounds were selected due to differences in their abilities to react via three highly anticipated mechanisms.

- 1,6-bicyclic formation (to levoglucosan or other 1,6-anhydroxyranoses)
- 1,2-dehydrogenation
- 1,2-dehydrations

Two stages of mass loss (two maximums in the rate of mass loss) were observed for many but not all of these model compounds. The materials exhibiting two mass-loss stages include all of the monosaccharide materials (five aldohexoses, two ketohexoses, and three aldopentoses), both deoxyaldohexoses, D-cellobiose, and xylan. Those exhibiting only one mass-loss stage were only the alditols, D-trehalose dihydrate, and cellulose. The important impact of these observations is that the presence of two stages of mass loss is not likely due to a combination of 1,6-bicyclic-forming reactions and less-favorable 1,2-dehydration reactions. These two reaction types are thought to be vital for cellulose pyrolysis, and so further understanding of how to measure these reactions independently is still crucial.

### ***5.8. Special Acknowledgements***

Were it not for the outgoing and generous nature of Dennis McOwen, William Kish, and Andrew Loder, most of the glucopyranose-like model compounds would not have been identified for use. These three fellow students graciously offered to share a few compounds more commonly used in pyrolysis experiments (e.g., D-galactose, D-mannose, dextran). However, while in their laboratories to pick up the initially targeted compounds, many rare saccharide materials were observed. These compounds like D-glucitol, D-mannitol, 2-deoxy-D-glucose, and 6-deoxy-L-galactose are rarely mentioned in saccharide-chemistry tutorials, and they do not seem to be mentioned in the cellulose-pyrolysis literature. By investigating these compounds' structures, the concept of using many more glucopyranose-like model compounds was conceived. Without the generous help of these three students, this chapter would merely be a repeat of common experiments with D-glucose, cellobiose, and cellulose.

## CHAPTER 6. RECOMMENDATIONS

### *6.1. PIQR-QMS experiments are needed for more alcohols and ethers*

The pulse-injected quartz reactor coupled to a quadrupole mass spectrometer (PIQR-QMS) proved to be a very powerful tool in determining the reactivity of volatile materials. The direct coupling to MSD (i.e., no GC separation) allowed it to characterize the pulse quality and residence time of the reactant.

This system is much more amenable to data meant for obtaining kinetic rates than the PIDSSR:

- The direct injection to QMS (i.e., no GC separation) allows it to characterize the reactant pulse for residence-time estimates.
- The reactor tube is quartz, which is much more trusted than the proprietary inert coatings of the PIDSSR.
- The furnace and reactor tube are capable of 1000°C, which allows much more experimental conditions than the PIDSSR maximum temperature of 400°C.
- The purge-gas flow in the PIQR can be controlled independently of any injection-gas flow or analytical instrument, and therefore the reactor purge-gas flow can be optimized for experiments without compromising quality of other factors of the system.

By modifying the PIQR-QMS to have heated sample-feed and reactor-effluent lines, the PIQR-QMS can operate with less volatile materials like diols and triols.

### *6.2. Evaluate the Frontier Pyrolyzer for simpler experiments to match TGA/DSC experiments*

The Pyroprobe® 5200 micropyrolyzer has two problems which negatively affect key pyrolysis experiments like the “cumulative Pyroprobe® experiments.” These problems are

(1) the pyrolysis vapors likely pass through a cold spot in or near the interface, and (2) the sample material remains in the interface until it returns to its rest/loading temperature. The combination of these two problems results in contamination of subsequent experiments and poor material balances. These problems will be discussed in detail for a more thorough understanding of the experimental limits of the Pyroprobe® 5200 instrument. It is highly recommended to evaluate the EGA/PY-3030D and PY-3030S model micropyrolyzers built by Frontier Laboratories, Ltd., as these are based upon a very different design which likely eliminates the contamination and material-balance problems.

The first problem is a likely cold spot in or near the interface. Any deposited vapor will reduce the observed product quantity in the GC-MS analysis and will also contaminate subsequent Pyroprobe® experiments. This deposition-and-contamination issue became obvious when switching between sample materials while running “cumulative Pyroprobe® experiments,” which were designed to approach the slower TGA/DSC heating rates and sample all product vapors from the beginning to the final temperature. (These experiments used only the Pyroprobe®’s interface as a heat source, and not the filament. However, using the filament would not likely prevent deposition.) A set of experiments with cellulose was performed, followed by a set of experiments with L-fucose. Levoglucosan was observed in the products resulting from both cellulose and L-fucose, but this product was highly unexpected to form from L-fucose. It was hypothesized that levoglucosan deposited in the apparatus during cellulose experiments and contaminated the vapor stream during the subsequent L-fucose experiments. This contamination was confirmed by two tests. First, the Pyroprobe® was operated with no sample tube in the interface and a levoglucosan peak was observed in the resulting chromatogram. Second, the GC method was performed with no pyrolysis method operating in the Pyroprobe®, and the resulting chromatogram showed no peaks. The Pyroprobe®’s interface was “baked out” at 325°C for an hour, and its valve enclosure and transfer-line were taken to 300°C for all new experiments, but the contamination persisted in several more chromatograms of pyrolyzing no sample.

(Deposition had occurred even though the Pyroprobe®'s valve oven and transfer line were kept at 300°C. This temperature was sufficient for significant transfer of levoglucosan for many previous Pyroprobe® experiments. In addition, levoglucosan was observed to elute from polar GC columns at roughly 225°C and evaporate to completion from the TGA/DSC at roughly 288°C.)

There is very likely a cold spot in or near the interface which allows the deposition and intermittent, incomplete release of low-volatility products. This assumption is based upon two items. (1) The observation that levoglucosan is only seen when the interface is heated. (2) The assumption that the steady-state temperatures of the valve oven and transfer line should continuously desorb the deposited vapors into the continuously flowing carrier gas. These desorbing vapors would accumulate in the GC inlet and form peaks in the next chromatogram, even in the chromatograms resulting from no method run in the Pyroprobe®. Only when the Pyroprobe® method is run and the interface temperature is cycled do these compounds create peaks in the resulting chromatograms.

The second problem, which is how the sample remains in the interface until the interface cools to its rest temperature, is an inherent design feature of the Pyroprobe® 5200 (and 5150). The Pyroprobe® will switch its internal 8-port valve at the end of the interface's final temperature duration, causing the GC carrier gas to bypass the interface and no longer carry evolving vapors to the GC inlet. Because the sample remains at reactive temperatures (>250°C) for close to a minute after the end of the interface final temperature duration, the weight lost from the sample tube will be greater than the weight of vapors actually sent to the GC inlet. It is also assumed that the sample remaining in the interface as it cools exacerbates the deposition of low-volatility products, which may continue to evolve as the sample cools to a non-reactive temperature. The only way to eliminate the "continued pyrolysis" and deposition is to pyrolyze the sample fully to a constant weight before ending the interface final temperature duration, but "cumulative Pyroprobe® experiments" preclude doing so.

As mentioned, it is recommended to thoroughly evaluate the EGA/PY-3030D and PY-3030S model micropyrolyzers built by Frontier Laboratories, Ltd. Upon viewing their schematics in their product brochures, the Frontier Laboratories micropyrolyzers appear to have two advantages. First, there is only ~10 cm of vapor path between the reactive zone and the GC inlet, which likely reduces the risk of deposition and continued gas-phase reaction. Second, the sample can be moved in and out of the hot reactive zone, so continued solid reactions can be greatly reduced. In addition, it appears that all evolved vapors are sent to the GC inlet as there is no switching between a purge vent and the GC inlet. Making all vapors go to GC inlet will ensure the weight difference will match the quantity of analytes in the chromatogram.

### ***6.3. Operate reactors independently of GC carrier-gas flow***

The PIDSSR and Pyroprobe® reactors employ the GC carrier gas to convect reactants through and out of the reactive zones. In essence, they work by splicing a reactor in between the GC's carrier-gas flow controller and the GC's inlet. While doing so first looks like a convenient way to avoid buying mass flow controllers and sampling valves, it has a serious drawback: the reactor's flow cannot be independent of the GC's inlet flows. Making the reactor's flow dependent upon the GC inlet flows means vital reactor parameters like residence time and Reynolds number cannot be specified independently for experimental purposes without affecting the GC separation.

It is highly recommended to construct pyrolysis reactors with their own dedicated mass flow controllers and a six-port valve with sampling loop. Dedicated flow control for the reactor will ensure experimental reactor parameters will not compromise quality chromatographic analysis.

### ***6.4. Reactors should operate above atmospheric pressure***

It is also suggested that pyrolysis reactors not be spliced between the GC's carrier-gas flow control and the GC's inlet be run above atmospheric pressure. A reactor employing a

separately controlled purge gas must deliver a pulse of reaction products via a sampling loop connected via a six-port valve. To ensure flow through the sampling loop and associated transfer lines and six-port valve borings, a pressure difference must exist between the reactor and the ultimate sample-vent line. A reactor running above ambient pressure can depend upon the pressure difference between itself and the room pressure to force adequate flow through the sampling equipment. A reactor running at ambient pressure requires vacuum be applied to the sample-vent line. The vacuum pump and associated flow- and pressure-control valves must be optimized, which takes time. The low pressure reduces the density of sample vapor residing in the sample loop. The below-ambient pressure allows air to leak into the sampling system, potentially causing problems for the GC system. Leaks are easier to detect in tubes containing gases above ambient pressure.

#### ***6.5. Construct a reactor to mimic TGA/DSC heating rates but employ shorter residence times***

It appears the TGA/DSC cannot achieve a short residence time due to its inherent features. Perhaps another reactor can be constructed that can match the TGA/DSC's heating rates and sample size yet also have residence times short enough to employ a convenient material balance simplification. The TGA/DSC weight-loss and heat-flow data could be matched to the product species profile obtained by this new reactor. This reactor would use an inert purge gas independent of the GC carrier gas. This reactor would be above ambient pressure so that a vacuum pump would be unnecessary to force flow through a sample loop of a six-port valve. This six-port valve would be controlled independently of the reactor furnace so any desired reaction time interval could be sampled to GC.

There may be another benefit to this reactor. Perhaps it can be made with a very short time response, so that reaction kinetics can be determined with simpler solution techniques.

- A useful approximation to a material balance simplifies the process of obtaining kinetic parameters based upon reaction-product data in semibatch reactors. This approximation assumes the time-derivative “accumulation term” is very small

compared to the flow of products out of the reactor and the “net generation” of products. This difference in magnitudes allows the accumulation term to be neglected, and, in turn, the flow out and net generation terms are roughly equal.

- For all species other than purge gas, the “in” term will be zero.
- For non-volatile species like cellulose and char, the “out” term will be zero; accumulation will equal net generation.
- For volatile degradation products like furfural and methanal, the “out” term will not be zero; accumulation will be the sum of “out” and net generation.
- Achieving this pseudo-steady-state operation requires the species transport to the reactor outlet be very fast compared to the changes in rates of formation
- The time to re-establish steady-state concentrations at the reactor outlet must be short compared to the time interval required for a change in temperature (i.e., an appreciable change in kinetic rates of species formation).

#### ***6.6. Recognize that GCxGC cannot separate highly polar pyrolysis products***

While the GCxGC separations greatly aid in identifying more analytes than GC by reducing analyte co-elution, effective GCxGC separations require rapid and complete vaporization of analytes during each thermal-modulation cycle (See Section 3.6.7). Analytes without multiple hydroxyl groups usually vaporize quite well in the thermal modulator, provided they are not at a quantity that is flooding the analytical column. Clear evidence of GCxGC separation power is shown by resolving hydrolysis oils’ complex mixtures of hydrocarbons and ketones. Meanwhile pyrolysis of cellulose, glucose, diols, and the triol resulted in numerous highly oxygenated analytes, and GCxGC cannot separate these analytes effectively due to their inability to desorb quickly and entirely during a thermal-modulation cycle. In fact, GC was required when dealing with very polar analytes like propan-1,2-diol, propan-1,3-diol, and propan-1,2,3-triol because they failed to produce any peaks during GCxGC. However, neither GC nor GCxGC can both provide sharp analyte peaks and avoid co-eluting peaks during the separation of complex mixtures which contain very polar analytes.

### *6.7. Derivatize oxygenated functional groups to allow sharper peaks in gas chromatography*

Chromatographers often derivatize analytes containing very polar groups (e.g., carbonyls, hydroxyls, and primary and secondary amines) to enable sharper, more symmetrical, and better resolved analyte peaks during gas chromatography. Such derivatization would be very beneficial to GC-MS and GCxGC-TOFMS analyses used to study biomass and cellulose pyrolysis products because many vital compounds are very polar and produce broad peaks. Such vital carbohydrate-pyrolysis analytes routinely forming broad peaks include 2-hydroxyethanal, 2,3-dihydroxypropanal, 1,3-dihydroxypropanone, and levoglucosan. With sharper peaks, these analytes could be separated with greater resolution, resulting in more certain identifications and more accurate quantifications for any smaller-quantity analytes which would normally co-elute within these broad peaks.

In GCxGC, increased volatility would drastically reduce the co-elution due to streaking analyte peaks by promoting rapid and complete vaporization during thermal modulation. With faster vaporization, broad vertical and horizontal streaking of analyte peaks can be reduced or eliminated, greatly improving the analyses by preventing co-elution and minimizing the need for the user to “combine” streaking analyte peaks which are not automatically combined by the data-processing method.

Derivatization encompasses several changes to the polar functional groups that have “active hydrogen:”

- silylation
- acylation
- methylation

Hydroxyl groups transformed into methyl ethers or silyl ethers lose their ability to form strong hydrogen-bridge bonds, thereby increasing their volatility.

Broido, Houminer, and Patai, derivatized glucose to trimethylsilyl derivatives for analysis by gas chromatograph [62]. They used the methods outlined by Sweeley, Bentley, Makita, and Wells, 1963, which was trimethylchlorosilane and pyridine. They claim all free hydroxyl groups were converted.

Shafizadeh and Lai, derivatized products from cellobiose and trehalose by trimethylsilylation followed by GC [63]. The method of silylation was not described, so it is uncertain whether silylation was carried out in the liquid or gas phase.

#### ***6.8. Preserve and analyze hypothesized monosaccharide and oligomer cellulose-pyrolysis intermediates as volatile silylated compounds***

Scalarone et al. [63] developed *in-situ* silylation to derivatize their saccharide-pyrolysis products within a micropyrolyzer's reaction zone.<sup>69</sup> Their intended application for *in-situ* silylation was not for elucidating fundamental pyrolysis-chemistry research but rather to detect evidence of saccharide materials for the purpose of identifying saccharide materials used in artworks and artifacts. While outside the scope of the identification objectives of Scalarone et al., one may question if the silylating agent(s) significantly alter the reactions responsible for saccharide pyrolysis. On one hand, altering of the pyrolysis reactions with silylation activity would obfuscate the fundamental pyrolysis chemistry of pure cellulose and appear not useful. On the other hand, these silylation reactions may enable the detection of species otherwise impossible to detect for two reasons.

- The silylation agents may preserve important intermediate species by increasing their vapor pressures and allowing them to exit the hot pyrolysis reactor quickly enough to prevent full conversion. For example:

---

<sup>69</sup> Scalarone et al. did not refer to their silylation method as "*in-situ* silylation," but this term will be used here because the derivatization was performed in the same vessel as was used to form the pyrolysis products.

- Perhaps the structural isomers of D-glucose may be preserved upon adding a silylation agent to the pyrolyzed (or pre-pyrolyzed) material. If a rapid “freezing” of the D-glucose isomer composition is possible, then this important composition of acyclic,  $\alpha$ -pyranose,  $\beta$ -pyranose,  $\alpha$ -furanose, and  $\beta$ -furanose forms may be finally understood in non-solvent conditions.
- With the silylating agents added directly to the saccharide material before pyrolysis, would the saccharide material be silylated before pyrolysis even began? Without the presence of hydroxyl groups, some reactions may proceed quite differently. For example, intermolecular attractions holding adjacent cellulose chains together may be reduced or eliminated, causing a more amorphous phase to form before pyrolysis.

While reviewing the GC-MS results of the *in-situ* silylation by Scalarone et al. [63], it was noticed that their strongest silylation reagents (hexamethyldisilazane combined with trimethylchlorosilane) allowed D-glucose to be observed in the chromatogram. D-glucose is never seen in pyrolysis gas chromatograms due to its low volatility. (In fact, usually 1,6-anhydro- $\beta$ -D-glucopyranose is the least-volatile product observed able to elute from GC, and larger anhydro-oligomers require liquid chromatography.) Glucose is considered as an important intermediate in some hypothesized reaction networks for cellulose pyrolysis. The ability for *in-situ* silylation to confirm glucose and other labile intermediate species is certainly worth investigating further.

### ***6.9. The adhesion and expansion of chars may provide vital clues to the intermolecular attractions of saccharides and polysaccharides during pyrolysis***

It was noticed that cellulose and xylan are the only saccharide materials tested during this study which appear not to form molten phases in the TGA/DSC. All other materials tested, from D-glucose to amylopectin, show chars which appear like black, solidified liquids. Why does this happen? Is there something about differences in intermolecular attractions? Perhaps cellulose is more heavily attracted to itself than monomers and other D-glucose polymer chains?

***6.10. Experimental evidence of reactive intermediates or transition states can guide iterative computational evaluations of elementary chemistry***

One technique to determine elementary chemistry involves using theory-based kinetic rates in a reactor model to compare predicted reactor performance to performance data obtained from physical experiments. The elementary-reaction networks are hypothesized, then theory is used to estimate Arrhenius parameters for each reaction in the network. If the hypothesized elementary reaction network causes the reactor model to correctly predict the final products obtained by physical experiments, then the elementary-reaction network might accurately describe the “real” reaction phenomena. If the hypothesized elementary-reaction network causes the reactor model to predict the final products obtained by physical experiments incorrectly, then the hypothesized elementary-reaction network does not accurately describe the “real” reaction phenomena. Inaccurate elementary-reaction networks must be modified and retested in the reactor model. This solution process can proceed in an iterative fashion, shown by the algorithm in Figure 99.

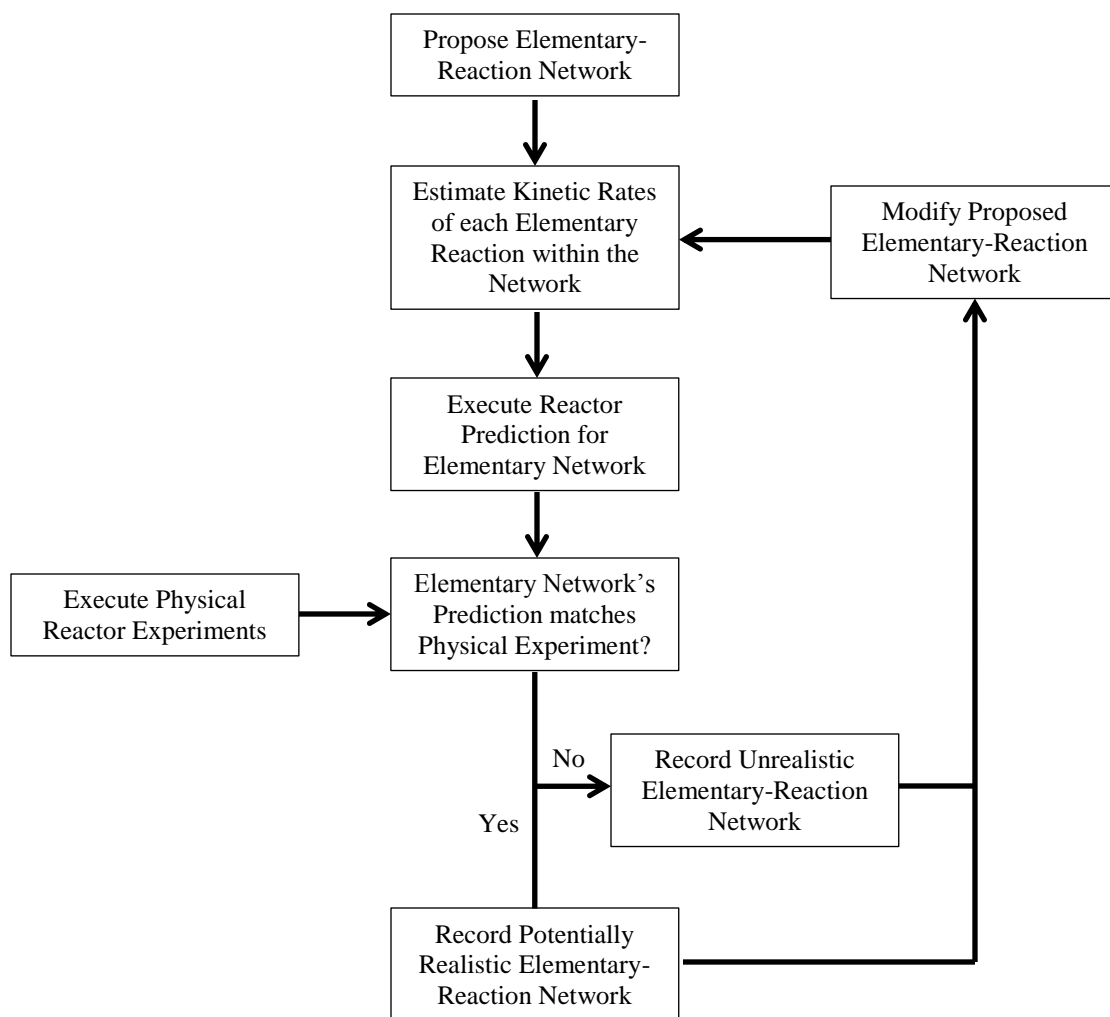


Figure 99. The iterative method of determining elementary chemistry based upon comparing a reactor model with theory-based rates to performance data from a physical reactor.

This iterative “performance-comparison method” of determining chemistry can be very useful, but it requires very advanced capabilities in order to be successful. A short list describes several required skills and tools which cannot be overlooked.

- The elementary-reaction networks must be modified properly so this iterative solution method converges. There is no guarantee that new, arbitrarily chosen elementary reaction networks will cause more accurate reactor-performance predictions.

- The theory-based kinetic rates must be predicted accurately and precisely for each of the elementary reactions. Any inaccuracy and imprecision within these theory-based kinetic-rate estimates will obscure the elementary reaction network's impact upon the accuracy and precision of the reactor predictions.
- The (physical) experimental reactor must be modeled accurately and precisely. The reactor modeling requires solving the conservation equations for momentum, energy, and mass, which are a system of partial differential equations (PDEs). Careful and clever design of experimental reactors can minimize the complexity of the conservation equations, potentially simplifying them to ordinary differential equations (ODEs) or even algebraic equations.
  - There must be zero degrees of freedom remaining in the resulting reactor-performance equations so the reactor's effluent composition can be solved as a function of known variables: the solution requires knowing every thermophysical, transport, and kinetic-rate term.
  - There must be a numerical solution technique capable of solving the reactor-performance equations with the given computational resources. Solving large sets of stiff PDEs may require specialized tools and expertise in computational fluid dynamics (CFD). PDE and CFD skills are especially important for multi-phase, many-species reactions like what occur during cellulose pyrolysis.
- If there are multiple solutions, then there must be a way to select the most appropriate solution. It is possible that several different elementary reaction networks may provide reactor predictions within the accuracy and precision stated to claim that a reaction network describes the "real" reaction phenomena.

The last complication is described in *Chemistry and Chemical Engineering of Catalytic Processes* by Katzer in a chapter titled "Chemical kinetics. The first step to reaction modeling and reaction engineering" [64]. Katzer explains the importance of elementary chemistry but warns that an accurate kinetic model does not necessarily mean the "real" mechanism has been found:

“In many cases the expressions for reaction kinetics can be derived from a knowledge of the elementary steps involved in a chemical reaction and the rate-determining step. Whenever it is possible to derive a kinetic expression in this manner, it should be done because the expression should give the best fit to a full range of kinetic data, give constants with physical meaning, and allow confident extrapolation beyond the regions in which data were available for parameter estimation. Similarly since different reaction mechanisms with different rate-determining steps give different kinetic expressions, it is possible to use chemical kinetics to eliminate potential reaction mechanisms and rate-determining steps. However, if a given reaction mechanism and rate-determining step produces a kinetic expression that fits the observed data well, it does not prove that the mechanism is correct, only that it is one of possibly several mechanisms that could be operative.” [64]

Some excellent studies on cellulose pyrolysis involve this method of matching predicted reactor performance to experimental reactor data. This iterative procedure can benefit from gathering (physical) experimental data which proves the presence or absence of key intermediates or transition states. These data can guide researchers to focus on computationally evaluating the most valid elementary reaction networks. Eliminating invalid elementary reaction networks can save precious research resources (e.g., research scientists’ time, allotted time on computer servers for theory-based rate estimation and CFD solutions), which is especially important because this performance-comparison method isn’t guaranteed to converge upon the “real” reactions within a certain number of iterations.

The work and recommendations in this dissertation focused upon providing experimental data for key intermediates and transition states.

- The deuterated experiments described in Section 4.5.2 were meant to provide evidence for the presence or absence of specific bimolecular dehydrogenation reactions.

- The recommendation to use electron paramagnetic resonance (EPR) was meant to provide evidence for the presence or absence of radical intermediates.
- The D-glucose-like model compounds were meant to provide evidence of whether
  - acyclic aldohexoses can rearrange to produce levoglucosan and
  - five-carbon species can rearrange to produce levoglucosan.

### ***6.11. Increase research on the catalytic chemistry of inorganic salts on cellulose-pyrolysis products***

Sections 1.2 and 1.3 justified spending research resources upon learning cellulose pyrolysis with the following basic premise: Cellulose is a major component of biomass, and therefore a better understanding of cellulose-pyrolysis chemistry will better enable the manufacture of renewable organic chemicals from biomass. However, if the ultimate goal is making renewable organic chemicals from biomass, then it should be a concern that three facts are well established.

- Biomass will always contain various forms of inorganic salts.
- Industrial processes do not remove all of these inorganic salts prior to pyrolytic steps.
- These inorganic salts in biomass can profoundly affect the products obtained from cellulose pyrolysis [21].

Many researchers seek the elementary chemistry of pure-cellulose pyrolysis as a foundation on which they can then add the catalytic effects of inorganic salts. This attitude appears as “crawl-before-you-walk” advice, assuming that determining the catalytic effects of inorganic salts depends upon first knowing the non-catalytic chemistry of pure-cellulose pyrolysis. But perhaps the inorganic salt’s catalytic reactions are competing with the non-catalytic reactions of cellulose pyrolysis; i.e., the catalytic and non-catalytic reactions may occur in parallel and not (entirely) in series. If these reactions are in parallel, then why are the reactions of pure-cellulose pyrolysis necessary to obtain first? Especially if biomass will always contain some quantity of inorganic salts, and these inorganic salts will not be removed prior to pyrolysis, then why is it wise to first evaluate the salt-free, non-catalytic

form of cellulose pyrolysis? Perhaps a larger fraction of research resources should be spent instead upon elementary chemistry of catalysis by inorganic-salts upon the products inherently made by cellulose pyrolysis? Such basic experiments would be drastically simpler to analyze than common cellulose pyrolysis experiments due to the reduction in product complexity. Consider the execution and analysis of two types of experiments.

- Pyrolyze cellulose, then separate, identify, and quantify the many pyrolysis products. Try to assemble the large elementary reaction network based upon these many products.
- React a pure stream of a cellulose-pyrolysis product (e.g., pure 2-hydroxyethanal or pure 1-hydroxypropanone) over a specific inorganic salt, then separate, identify, and quantify far fewer products. Try to assemble the elementary catalysis network based upon several products.

## CHAPTER 7. CONCLUSIONS

Model compounds were pyrolyzed to help understand the reaction network of cellulose pyrolysis. Cellulose and many D-glucose-based model compounds like cellobiose, cyclodextrin, and starches have been investigated thoroughly, but investigations with these model compounds are insufficient to improve the complex reaction phenomena involved in cellulose pyrolysis.

In this work, model-compound sets were not selected to simply mimic cellulose's repeating  $\beta$ -D-anhydroglucopyranose unit. Instead, model-compound sets were assembled to be similar to cellulose's repeating  $\beta$ -D-anhydroglucopyranose unit but provide specific differences between members' molecular structures. These structural differences were kept as simple as possible so that differences between their pyrolysis behavior could be attributed largely to a single structural difference. There were two main sets of model compounds:

- Alcohols
- Saccharides and saccharide-like molecules

There were four main ways of describing structural differences among members of these two main groups:

- Substitute hydroxyl groups for hydrogen atoms and vice-versa.
- Substitute methyl groups for hydrogen atoms and vice-versa.
- Change the hydroxyl-group stereochemistry (only for saccharides and saccharide-like molecules).
- Hydrogenate the carbonyl to an alcohol and vice-versa.

Attributing the differences in pyrolysis behavior to the presence of specific functional groups expands the knowledge of cellulose pyrolysis in ways not possible with testing only cellulose and closely related D-glucose dimers, oligomers, and polymers.

Several observations were made with the alcohols group by using a pulse-injected gas-phase reactor operating at 200-400°C:

- Primary and secondary monols preferentially dehydrogenated to their respective aldehyde and ketone.
- Primary and secondary monols dehydrated to a very small extent.
- Tertiary monols dehydrate and show no dehydrogenation.
- Products of carbon-carbon fragmentation were either undetected or provided only trace product quantities for all monols, with the exception being 5-hydroxymethylfurfural, which deformed to a significant degree.
- Diols and triols dehydrogenated, dehydrated, and fragmented carbon-carbon bonds.
- Phenol provided no reaction products.
- Almost no products of condensation were observed.

Concerted mechanisms were proposed for dehydrogenation and dehydration and four- and six-center cyclic transition states were evaluated.

The set of saccharide and saccharide-like model compounds were tested by TGA/DSC for their mass-loss and heat-flow behavior, where a focus was identifying the cause of two separated maxima in the mass-loss rates that occurred for many but not all model compounds. Comparisons among members of this model-compound set revealed that the cause of two separate mass-loss maxima are not due to any of the following structural aspects of reactants:

- The stereochemistry of hydroxyl groups on a pentose or hexose
- The saccharide being an aldose versus a ketose
- The presence of a carbon 6 (i.e., pentose vs. hexose)
- The presence of a hydroxyl group on carbon 6 (i.e., a 6-deoxy-hexose)
- The presence of a hydroxyl group on carbon 2 (i.e., a 2-deoxy-hexose)
- The saccharide being dimerized or polymerized

Likewise, the two-stage mass-loss is not due to the combination of 1,6-bicyclic formation and dehydration activity favored at different temperatures. However, a single maximum occurred in the mass-loss rate when the structural differences in reactants could be described by

- Hydrogenating the sugar to a sugar alcohol
- Dimerizing D-glucose with an  $\alpha(1-1)$  glycosydic bond
- Polymerizing D-glucose with  $\beta(1-4)$  glycosydic bonds

Attributing these reaction phenomena to specific structural features allows researchers to conceive new methods of investigating biomass pyrolysis given the ubiquitous nature of alcohols and saccharide-like units throughout biomass. It is hoped that this new insight will be used not simply for research aimed at making reactor predictions for conventional cellulose pyrolysis, but also to inspire researchers to modify the reaction networks of cellulose pyrolysis with new concepts like co-reagents and catalysts. Augmenting cellulose's inherent reaction network appears to be the only way to make desirable products; limiting the process to the inherent pyrolysis reaction network will only allow formation of the same bio-oil types currently made with typical pyrolysis processes.

Additionally, GCxGC was used extensively for part of this work, and some important findings are shared. Most importantly, tabulated McReynolds constants provide precise descriptions of the interaction types available to stationary-phase materials, but selecting stationary phases based solely upon these McReynolds constants did not ensure orthogonal separations in GCxGC.

## REFERENCES

- M. R. Nimlos, S. J. Blanksby, X. Qian, M. E. Himmel and D. K. Johnson,  
1] "Mechanisms of Glycerol Dehydration," *Journal of Physical Chemistry A*, vol. 110, pp. 6145-6156, 2006.
- J. Moc, J. M. Simmie and H. J. Curran, "The elimination of water from a  
2] conformationally complex alcohol: A computational study of the gas phase dehydration of n-butanol," *Journal of Molecular Structure*, vol. 928, pp. 149-157, 2009.
- V. Seshadri and P. R. Westmoreland, "Concerted Reactions and Mechanism of  
3] Glucose Pyrolysis and Implications for Cellulose Kinetics," *J. Phys. Chem. A*, vol. 116, no. 49, p. 11997-12013, 2012.
- M.-K. Bahng, C. Mukarakate, D. J. Robichaud and M. R. Nimlos, "Current  
4] technologies for analysis of biomass thermochemical processing: A review," *Analytica Chimica Acta*, vol. 651, pp. 117-138, 2009.
- R. J. Evans and T. A. Milne, "Molecular Characterization of the Pyrolysis of  
5] Biomass. 1. Fundamentals," *Energy & Fuels*, vol. 1, no. 2, pp. 124-137, 1987.
- S. Czernik and A. V. Bridgwater, "Overview of Applications of Biomass Fast  
6] Pyrolysis Oil," *Energy & Fuels*, vol. 18, pp. 590-598, 2004.
- A. V. Bridgwater, "Catalysis in thermal biomass conversion," *Applied Catalysis*  
7] *A: General*, vol. 116, pp. 5-47, 1994.
- P. M. Mortensen, J.-D. Grunwaldt, P. A. Jensen, K. G. Knudsen and A. D.  
8] Jensen, "A review of catalytic upgrading of bio-oil to engine fuels," *Applied Catalysis A: General*, vol. 407, pp. 1-19, 2011.

D. Dayton, J. Carpenter, J. Farmer, B. Turk and R. Gupta, "Biomass  
9] Hydropyrolysis in a Pressurized Fluidized Bed Reactor," *Energy & Fuels*, vol. 27, no. 7,  
pp. 3778-3785, 2013.

T. R. Carlson, T. P. Vispute and G. W. Huber, "Green Gasoline by Catalytic Fast  
10] Pyrolysis of Solid Biomass Derived Compounds," *ChemSusChem*, vol. 1, pp. 397-400,  
2008.

T. R. Carlson, J. Jae, Y.-C. Lin, G. A. Tompsett and G. W. Huber, "Catalytic fast  
11] pyrolysis of glucose with HZSM-5: The combined homogeneous and heterogeneous  
reactions," *Journal of Catalysis*, vol. 270, pp. 110-124, 2010.

P. J. Dauenhauer, J. L. Colby, C. M. Balonek, W. J. Suszynski and L. D.  
12] Schmidt, "Reactive boiling of cellulose for integrated catalysis through an intermediate  
liquid," *Green Chemistry*, vol. 11, pp. 1555-1561, 2009.

P. Christou and H. Klee, Eds., *Handbook of Plant Biotechnology*, vol. 2, West  
13] Sussex: John Wiley & Sons, 2004.

D. Kretschmann, J. Winandy, C. Clausen, M. Wiemann, R. Bergman, R. Rowell,  
14] J. Zerbe, J. Beecher, R. White, D. McKeever and J. Howard, "Wood," in *Kirk-Othmer  
Encyclopedia of Chemical Technology*, John Wiley & Sons, Inc., 2007.

A. D. French, N. R. Bertoniere, R. M. Bertoniere, H. Chanzy, D. Gray, K.  
15] Hattori and W. Glasser, "Cellulose," in *Kirk-Othmer Encyclopedia of Chemical  
Technology*, John Wiley & Sons, Inc., 2003.

J. M. J. Antal and G. Várhegyi, "Cellulose Pyrolysis Kinetics: The Current State  
16] of Knowledge," *Industrial & Engineering Chemistry Research*, vol. 34, pp. 703-717,  
1995.

W. Wilczewski, "Growing U.S. HGL production spurs petrochemical industry investment," Energy Information Agency, 29 January 2015. [Online]. Available: <http://www.eia.gov/todayinenergy/detail.cfm?id=19771#>. [Accessed 4 February 2015].

G. Várhegyi, E. Jakab and J. M. J. Antal, "Is the Broido-Shafizadeh Model For Cellulose Pyrolysis True?," *Energy & Fuels*, vol. 8, pp. 1345-1352, 1994.

J. Lédé, "Cellulose pyrolysis kinetics: An historical review on the existence and role of intermediate active cellulose," *Journal of Analytical and Applied Pyrolysis*, vol. 94, pp. 17-32, 2012.

M. Grønli, M. J. Antal, Jr and G. Várhegyi, "A Round-Robin Study of Cellulose Pyrolysis Kinetics by Thermogravimetry," *Industrial & Engineering Chemistry Research*, vol. 38, pp. 2238-2244, 1999.

P. R. Patwardhan, J. A. Satrio, R. C. Brown and B. H. Shanks, "Influence of inorganic salts on the primary pyrolysis products of cellulose," *Bioresource Technology*, vol. 101, pp. 4646-4655, 2010.

F. Ronsse, D. Dalluge, W. Prins and R. Brown, "Optimization of platinum filament micropyrolyzer for studying primary decomposition in cellulose pyrolysis," *Journal of Analytical and Applied Pyrolysis*, vol. 95, pp. 247-256, 2012.

J. B. Paine III, Y. B. Pithawalla, J. D. Naworal and C. E. Thomas, Jr., "Carbohydrate pyrolysis mechanisms from isotopic labeling Part 1: The pyrolysis of glycerin: Discovery of competing fragmentation mechanisms affording acetaldehyde and formaldehyde and the implications for carbohydrate pyrolysis," *Journal of Analytical and Applied Pyrolysis*, vol. 80, pp. 297-311, 2007.

J. B. Paine III, Y. B. Pithawalla and J. D. Naworal, "Carbohydrate pyrolysis mechanisms from isotopic labeling Part 2: The pyrolysis of D-glucose: General

24] disconnective analysis and the formation of C1 and C2 carbonyl compounds by electrocyclic fragmentation mechanisms," *Journal of Analytical and Applied Pyrolysis*, vol. 82, pp. 10-41, 2008.

J. B. Paine III, Y. B. Pithawalla and J. D. Naworal, "Carbohydrate pyrolysis mechanisms from isotopic labeling Part 3. The Pyrolysis of D-glucose: Formation of C3 and C4 carbonyl compounds and a cyclopentenedione isomer by electrocyclic fragmentation mechanisms," *Journal of Analytical and Applied Pyrolysis*, vol. 82, pp. 42-69, 2008.

J. B. Paine III, Y. B. Pithawalla and J. D. Naworal, "Carbohydrate pyrolysis mechanisms from isotopic labeling Part 4. The pyrolysis of D-glucose: The formation of furans," *Journal of Analytical and Applied Pyrolysis*, vol. 83, pp. 37-63, 2008.

M. S. Mettler, S. H. Mushrif, A. D. Paulsen, A. D. Javadekar, D. G. Vlachos and P. J. Dauenhauer, "Revealing pyrolysis chemistry for biofuels production: Conversion of cellulose to furans and small oxygenates," *Energy & Environmental Science*, vol. 5, pp. 5414-5424, 2012.

Y. Lin, J. Cho, G. A. Tompsett, P. R. Westmoreland and G. W. Huber, "Kinetics and Mechanism of Cellulose Pyrolysis," *Journal of Physical Chemistry C*, vol. 113, pp. 20097-20107, 2009.

A. Fullana, J. A. Contreras, R. C. Striebich and S. S. Sidhu, "Multidimensional GC/MS analysis of pyrolytic oils," *Journal of Analytical and Applied Pyrolysis*, vol. 74, no. 1-2, pp. 315-326, 2005.

W. Bertsch, *Multidimensional Gas Chromatography*, John Wiley & Sons, Ltd., 2006.

H.-J. de Geus and J. de Boer, "Multidimensionality in gas chromatography,"

31] *Trends in Analytical Chemistry*, vol. 15, no. 5, pp. 168-178, 1996.

J. H. Marsman, J. Wildschut, F. Mahfud and H. J. Heeres, "Identification of  
32] components in fast pyrolysis oil and upgraded products by comprehensive two-dimensional gas chromatography and flame ionisation detection," *Journal of Chromatography A*, vol. 1150, pp. 21-27, 2007.

J. Dalluge, J. Beens and U. A. T. Brinkman, "Comprehensive two-dimensional  
33] gas chromatography: a powerful and versatile analytical tool," *Journal of Chromatography A*, vol. 1000, no. 1-2, pp. 69-108, 2003.

J. B. Phillips and J. Xu, "Comprehensive multi-dimensional gas  
34] chromatography," *Journal of Chromatography A*, vol. 703, pp. 327-334, 1995.

C. J. Venkatramani, J. Xu and J. B. Phillips, "Separation Orthogonality in  
35] Temperature-Programmed Comprehensive Two-Dimensional Gas Chromatography," *Analytical Chemistry*, vol. 68, pp. 1486-1492, 1996.

H. Rotzsche, *Stationary Phases in Gas Chromatography*, New York City:  
36] Elsevier Science Publishing Company, Inc., 1991.

R. Kaliszan, *Structure and Retention in Chromatography: A Chemometric  
37] Approach*, Harwood Academic Publishers, 1997.

E. F. Barry and R. L. Grob, *Columns for Gas Chromatography: Performance and  
38] Selection*, Hoboken, NJ: John Wiley & Sons, Inc., 2007.

J. H. Marsman, J. Wildschut, P. Evers, S. de Koning and H. J. Heeres,  
39] "Identification and classification of components in flash pyrolysis oil and hydrodeoxygenated oils by two-dimensional gas chromatography and time-of-flight

mass spectrometry," *Journal of Chromatography A*, vol. 1188, pp. 17-25, 2008.

LECO Corporation, *Light Crude Oil Fingerprinting from Six Different Global Regions Using GCxGC-TOFMS with Structural Classifications to Compare Functional Group Differences*, St. Joseph, Michigan: LECO Corporation, 2013.

Restek Corporation, *GCxGC Contour Plot of Riser Pipe Oil in 2010 Gulf Oil Spill (Rxi®-17Sil MS and Rxi®-1ms)*, Bellefonte, PA: Restek Corporation.

B. Omais, M. Courtiade, N. Charon, S. Esnault and T. Didier, "Reversal of elution order in a single second dimension by changing the first column nature in comprehensive two-dimensional gas chromatography," *Journal of Chromatography A*, vol. 1255, pp. 196-201, 2012.

B. Omais, M. Courtiade, N. Charon, J. Ponthus and D. Thiébaud, "Considerations on Orthogonality duality in Comprehensive Two-Dimensional Gas Chromatography," *Analytical Chemistry*, vol. 83, pp. 7550-7554, 2011.

D. Ryan, R. Shellie, P. Tranchida, A. Casilli, L. Mondello and P. Marriott, "Analysis of roasted coffee bean volatiles by using comprehensive two-dimensional gas chromatography-time-of-flight mass spectrometry," *Journal of Chromatography A*, vol. 1054, pp. 57-65, 2004.

S. D. Johanningsmeier and R. F. McFeeters, "Detection of Volatiles Spoilage Metabolites in Fermented Cucumbers Using Nontargeted, Comprehensive 2-Dimensional Gas Chromatography-Time-of-Flight Mass Spectrometry (GCxGC-TOFMS)," *Journal of Food Science*, vol. 76, pp. 168-177, 2011.

T. Herring, Interviewee, *Personal Communication (Restek Corporation)*. [Interview]. 22 January 2015.

P. R. Patwardhan, J. A. Satrio, R. C. Brown and B. H. Shanks, "Product  
47] distribution from fast pyrolysis of glucose-based carbohydrates," *Journal of Analytical and Applied Pyrolysis*, vol. 86, pp. 323-330, 2009.

P. R. Patwardhan, R. C. Brown and B. H. Shanks, "Product Distribution from the  
48] Fast Pyrolysis of Hemicellulose," *ChemSusChem*, vol. 4, pp. 636-643, 2011.

P. R. Patwardhan, D. L. Dalluge, B. H. Shanks and R. C. Brown, "Distinguishing  
49] primary and secondary reactions of cellulose pyrolysis," *Bioresource Technology*, vol. 102, pp. 5265-5269, 2011.

T. Hosoya, H. Kawamoto and S. Saka, "Different pyrolytic pathways of  
50] levoglucosan in vapor- and liquid/solid-phases," *Journal of Analytical and Applied Pyrolysis*, vol. 83, pp. 64-70, 2008.

M. R. Nimlos, S. J. Blanksby, G. B. Ellison and R. J. Evans, "Enhancement of  
51] 1,2-dehydration of alcohols by alkali cations and protons: a model for dehydration of carbohydrates," *Journal of Analytical and Applied Pyrolysis*, vol. 66, pp. 3-27, 2003.

M. Zhang, Z. Geng and Y. Yu, "Density Functional Theory (DFT) Study on the  
52] Dehydration of Cellulose," *Energy & Fuels*, vol. 25, pp. 2664-2670, 2011.

A. D. Pouwels, G. B. Eijkel, P. W. Arisz and J. J. Boon, "Evidence for  
53] Oligomers in Pyrolysates of Microcrystalline Cellulose," *Journal of Analytical and Applied Pyrolysis*, vol. 15, pp. 71-84, 1989.

I. Pastorova, P. W. Arisz and J. J. Boon, "Preservation of D-glucose-  
54] oligosaccharides in cellulose chars," *Carbohydrate Research*, vol. 248, pp. 151-165, 1993.

P. M. Collins and R. J. Ferrier, *Monosaccharides: Their Chemistry and Their*

55] Roles in Natural Products, West Sussex: John Wiley & Sons, 1995.

R. S. Shallenberger, Advanced Sugar Chemistry: Principles of Sugar  
56] Stereochemistry, Westport, Connecticut: The AVI Publishing Company, Inc., 1982.

J. M. Hornback, Organic Chemistry, Belmont, CA: Thomson Brooks/Cole, 2006.  
57]

D. E. Levy and P. Fügedi, The Organic Chemistry of Sugars, D. E. Levy and P.  
58] Fügedi, Eds., CRC Press, 2006.

R. H. Horton, L. A. Moran, K. G. Scrimgeour, M. D. Perry and J. D. Rawn,  
59] Principles of Biochemistry, 4 ed., Upper Saddle River, New Jersey: Pearson Education,  
Inc., 2006.

U. Räisänen, I. Pitkänen, H. Halttunen and M. Hurttä, "Formation of the Main  
60] Degradation Compounds from Arabinose, Xylose, Mannose and Arabinitol During  
Pyrolysis," *Journal of Thermal Analysis and Calorimetry*, vol. 72, pp. 481-488, 2003.

E. B. Sanders, A. I. Goldsmith and J. I. Seeman, "A model that distinguishes the  
61] pyrolysis of D-glucose, D-fructose, and sucrose from that of cellulose. Application to  
the understanding of cigarette smoke formation," *Journal of Analytical and Applied  
Pyrolysis*, vol. 66, pp. 29-50, 2003.

A. Broido, Y. Houminer and S. Patai, "Pyrolytic Reactions of Carbohydrates.  
62] Part I. Mutarotation of Molten D-Glucose," *Journal of the Chemical Society B: Physical  
Organic*, pp. 411-414, 1966.

D. Scalarone, O. Chiantore and C. Riedo, "Gas chromatographic/mass  
63] spectrometric analysis of on-line pyrolysis-silylation products of monosaccharides,"

*Journal of Analytical and Applied Pyrolysis*, vol. 83, pp. 157-164, 2008.

J. R. Katzer, "Chemical kinetics. The first step to reaction modeling and reaction  
64] engineering," in *Chemistry and Chemical Engineering of Catalytic Processes*, R. Prins  
and G. C. A. Schuit, Eds., Germantown, Maryland: Sijthoff & Noordhoff, 1980, pp. 3-  
48.

P. Tomasik, Ed., *Chemical and Functional Properties of Food Saccharides*, CRC  
65] Press LLC, 2004.

D. D. Stokke, Q. Wu and G. Han, *Introduction to Wood and Natural Fiber  
66] Composites*, John Wiley & Sons, Ltd, 2014.

J.-L. Wertz, O. Bédué and J. P. Mercier, *Cellulose Science and Technology*,  
67] Boca Raton: CRC Press, 2010.

P. Zugenmaier, *Crystalline Cellulose and Derivatives*, Springer, 2008.  
68]

A. V. Bridgwater, "Upgrading Biomass Fast Pyrolysis Liquids," *Environmental  
69] Progress & Sustainable Energy*, vol. 31, pp. 261-268, 2012.

A. Demirbas and G. Arin, "An Overview of Biomass Pyrolysis," *Energy  
70] Sources*, vol. 24, pp. 471-482, 2002.

D. C. Elliott, "Historical Developments in Hydroprocessing Bio-oils," *Energy &  
71] Fuels*, vol. 21, pp. 1792-1815, 2007.

J. B. Phillips and J. Beens, "Review: Comprehensive two-dimensional gas  
72] chromatography: a hyphenated method with strong coupling between two dimensions,"

*Journal of Chromatography A*, vol. 856, pp. 331-347, 1999.

M. Weinstein and A. Broido, "Pyrolysis-Crystallinity Relationships in  
73] Cellulose," *Combustion Science and Technology*, vol. 1, pp. 287-292, 1970.

J. Wildschut, F. H. Mahfud, R. H. Venderbosch and H. J. Heeres,  
74] "Hydrotreatment of Fast Pyrolysis Oil Using Heterogeneous Noble-Metal Catalysts,"  
*Industrial & Engineering Chemistry Research*, vol. 48, pp. 10324-10334, 2009.

M. J. Antal, Jr., H. L. Friedman and F. E. Rogers, "Kinetics of Cellulose  
75] Pyrolysis in Nitrogen and Steam," *Combustion Science and Technology*, vol. 21, pp.  
141-152, 1980.

A. R. Ardiyanti, S. A. Khromova, R. H. Verderbosch, V. A. Yakovlev, I. V.  
76] Melian-Cabrera and H. J. Heeres, "Catalytic hydrotreatment of fast pyrolysis oil using  
bimetallic Ni-Cu catalysts on various supports," *Applied Catalysis A: General*, vol. 449,  
pp. 121-130, 2012.

R. S. Assary and L. A. Curtiss, "Thermochemistry and Reaction Barriers for the  
77] Formation of Levoglucosenone from Cellobiose," *ChemCatChem*, vol. 4, pp. 200-205,  
2012.

A. V. Bridgwater, "Production of high grade fuels and chemicals from catalytic  
78] pyrolysis of biomass," *Catalysis Today*, vol. 29, pp. 285-295, 1996.

L. J. Broadbelt, S. M. Stark and M. T. Klein, "Computer Generated Pyrolysis  
79] Modeling: On-the-Fly Generation of Species, Reactions, and Rates," *Industrial &  
Engineering Chemistry Research*, vol. 33, pp. 790-799, 1994.

C. S. Callam, S. J. Singer, T. L. Lowary and C. M. Hadad, "Computational  
Analysis of the Potential Energy Surfaces of Glycerol in the Gas and Aqueous Phases:

80] Effects of Level of Theory, Basis Set, and Solvation on Strongly Intramolecularly Hydrogen-Bonded Systems," *Journal of the American Chemical Society*, vol. 123, pp. 11743-11754, 2001.

R. Bentley, C. C. Sweeley, M. Makita and W. W. Wells, "Gas Chromatography  
81] of Sugars and Other Polyhydroxy Compounds," *Biochemical and Biophysical Research Communications*, vol. 11, no. 1, pp. 14-18, 1963.

D. Klemm, B. Philipp, T. Heinze, U. Heinze and W. Wagenknecht,  
82] *Comprehensive Cellulose Chemistry Volume 1: Fundamentals and Analytical Methods*, Wiley-VCH, 1998.